Characterisation of Phosphodiesterase 11 in *Drosophila melanogaster*

A thesis submitted for the degree of

Doctor of Philosophy at the University of Glasgow

By

Andrew Finlayson

Division of Molecular Genetics

Institute of Biomedical and Life Sciences

University of Glasgow

Glasgow

G11 6NU

UK

January 2010

The research reported within this thesis is my own work except where otherwise stated, and has not been submitted for any other degree

Andrew Finlayson

Abstract

The PDE 11 family of dual specificity phosphodiesterases was first identified in 2000, and has not been well characterised, although mutations in the gene have been linked to multiple disorders, including major depressive disorder, and cancer. *Dm*PDE11 is a dual specificity phosphodiesterase, which shows 96% similarity with the catalytic domain of *Hs*PDE11A, and around 40% similarity along the length of the protein. The focus of this project was to characterise this important enzyme using the model organism *Drosophila melanogaster*. The resources available to *Drosophila* researchers are unrivalled, and include a sequenced genome, unparalleled transgenic technology, of which stocks are freely available, and Homophila, a database of human disease genes and their *Drosophila* orthologues. *Drosophila* is genetically tractable to an extent not seen in any other multicellular organisms. The genetic dissection of gene function in *Drosophila* has allowed the identification and characterisation of numerous cell signalling genes. For example, mutations to *Dunce* were shown to affect olfactory learning. This allowed the identification and cloning of the mammalian *dnc* homologue PDE4. cAMP (and cGMP) were subsequently shown to modulate learning and memory in mammals.

The 5.8 kb expressed sequence tag (EST) SD13096 had previously been shown to contain sequence present in the incomplete PDE11 RA ESTs previously released by Flybase, but also incorporating a 5' UTR, and an in-frame start codon within two novel 5' exons. A Northern blot of *Dm*PDE11 RA produced one band of approximately 5.8kb; as this matches the size of the *Dm*PDE11 RA ORF, was accepted that SD13096 encodes the entire PDE11 RA ORF (Day, unpublished). Expression of this EST in S2 cells revealed that the construct produced a protein of the accepted size, and the protein localised to the cytoplasm. However, PDE assays of S2 cell lysate revealed that the enzyme did not appear to encode an enzyme with either cA- or cG-PDE activity.

*Dm*PDE11 RA was replaced on Flybase by the new isoforms *Dm*PDE11 RB and *Dm*PDE11 RC, which had two key changes to the RA isoform. Both new isoforms had different N termini, sharing a second exon, with distinct first exons. Furthermore, exon 11 of the RA exon is not present in the newly predicted isoforms. These new isoforms were verified by reverse transcriptase- polymerase chain reaction analysis. In the course of this verification, two further novel isoforms were identified, which shared the novel N termini with the RB and RC isoforms, but include a novel exon/exon boundary within the original exon 19, which results in a truncated isoform. As such the four isoforms were named

*Dm*PDE11 RB long, *Dm*PDE11 RB short, *Dm*PDE11 RC long, and *Dm*PDE11 RC short. The open reading frames of these isoforms were cloned from *Drosophila* cDNA using high-fidelity DNA polymerase and sequenced for fidelity. The open reading frames were tagged with YFP, and this tag was used to verify expression of these isoforms. Each isoform expressed a protein of the predicted size when expressed in *Drosophila*. *Dm*PDE11 B and C proteins show distinct localisation in the Malpighian tubule, where the long and short isoforms of each isoform display indistinguishable localisations. *Dm*PDE11 B localises to the apical and basolateral membranes, and *Dm*PDE11 C localises to an unknown organelle, or to vesicles. All 4 isoforms were verified as dual specificity cA- and cG- PDEs.

The previous finding (Day, unpublished) that *Dm*PDE11 co-immunoprecipitates with cGMP dependent protein kinase activity, and that cGMP dependent protein kinases co-immunoprecipitate with cG-PDE activity, and thus that cG-PDE(s) interact with at least one cGMP dependent protein kinase, directly or indirectly, was investigated. *Dm*PDE11 C long and short were co-transfected in Schneider 2 cells with the cGKs DG1, DG2P1 and DG2P2. Co-immunoprecipitation of these showed that both the long and short isoforms of *Dm*PDE11 C interact with every cGK screened. Time did not permit the application of this protocol to screen *Dm*PDE11 B interaction with the cGKs. Whether this interaction is direct or indirect was screened by peptide array. Peptide arrays were generated representing the sequence of *Dm*PDE11, DG1, and DG2, and proteins were generated fusing fragments of these proteins with HIS_6 and Glutathione-S-Transferase tags. These were expressed in *E. coli*, and verified by western blotting. HIS_6 tagged protein expression was shown to be of higher quality, and was thus affinity purified, and used to overlay and probe the peptide arrays for putative direct interactions. When the PDE11 array was overlaid with tagged protein representing the C terminal half of DG1, and the N and C terminal halves of DG2, a putative direct interaction was identified between DG1 and PDE11 on two separate regions of the PDE11 array, which both fell within the sequence of PDE11 represented by the Middle-HIS_6 fragment. As such, this was used to probe the PDE11 array. A reciprocal putative interaction was identified on three regions of the DG1 array, representing sequence in both DG1N-HIS_6 and DG1C-HIS_6 fragments. Unfortunately, although DG1-HIS_6 was verified by western blotting at the analytical stage, attempts to affinity purify the protein failed. Time did not permit the probing of the array with DG1N-GST fusion protein, and so further putative interaction sites on PDE11 may remain. The generation of alanine substitution arrays, and subsequent mutagenesis analysis with yeast two hybrid or co-immunoprecipitation would be necessary to confirm this direct

protein-protein interaction as *bona-fide*. The investigation into a putative direct interaction between PDE11 and DG2 did not yield conclusive data, and so further investigation is required.

The role of *Dm*PDE11 in immunity was investigated by the use of *Dm*PDE11 RNAi and deletion lines. The *Dm*PDE11 deletion line showed a qualitative reduction in survival in individual survival assays, but when these data were merged a significant decrease in survival compared to controls was seen. However, fly numbers did not permit the inclusion of all of the necessary controls, and so these assays should be repeated with these. However, upon immune challenge, progeny from a *Dm*PDE11 RNAi (line 9) x Act5c (a ubiquitous GAL4 driver line) cross did not show a decrease in survival compared to parental lines.

Transgenic *Drosophila* expressing *H. sapiens* PDE11A3 were generated. The protein localised to the nucleus at low levels of protein; increased expression led to nuclear exclusion, and localisation to the basolateral and especially apical membranes, with cytosolic localisation also.

The work has provided the tools needed to further research PDE11. The implication of this gene as a tumour suppressor gene, and its role in other processes, means that it is of the utmost importance that this enzyme is further characterised.

Abbreviations

AEQ	aequorin
AKAP	A kinase anchoring protein
APS	ammonium persulphate
ATP	adenosine triphosphate
BLAST	basic local alignment search tool
bp	base pairs
BSA	bovine serum albumin
C-	carboxy-
Ca^{2+}	calcium
$[Ca^{2+}]$	calcium concentration
$[Ca^{2+}]_i$	intracellular calcium concentration
CNG	cyclic nucleotide gated (channel)
CREB	cyclic AMP response element binding protein
cAMP	adenosine 3'-5' cyclic monophosphate
cDNA	complementary DNA
cGK	cGMP-dependent kinase
cGMP	guanosine 3'-5' cyclic monophosphate
cN	cyclic nucleotide
cNMP	cyclic nucleotide monophosphate
cN-PDE	cyclic nucleotide phosphodiesterase
DAG	diacylglycerol
DAPI	4,6-diamidino-2-phenylindole, dilactate
DMF	dimethylformamide
DMSO	dimethylsulfoxide
DNA	deoxyribonucleic acid
DTT	dithiothreitol
dATP	2' deoxyadenosine triphosphate

dCTP	2’ deoxycytosine triphosphate
dGTP	2’ deoxyguanosine triphosphate
dNTP	2’ deoxy (nucleotide) triphosphate
dTTP	2’ deoxythymidine triphosphate
dUTP	2’ deoxyuridine triphosphate
EDTA	ethylenediamine tetra acetic acid
EGTA	ethylene glycol bis tetracetic acid
ER	endoplasmic reticulum
EST	expressed sequence tag
EtBr	ethidium bromide
FCS	foetal calf serum
g	gram
g	centrifugal force equal to gravitational acceleration
GFP	green fluorescent protein
G-protein	guanine nucleotide-binding protein
GPCR	G-protein-coupled receptor
GST	glutathione-S-transferase
GTP	guanosine triphosphate
h	hours
HEPES	N-((2-hydroxylethyl) piperazine-N’-(2-ethanesulphonic acid))
HRP	horseradish peroxidase
IBMX	3-isobutyl-1-methylxanthine
ICC	immunocytochemistry
IP_3	inositol 1,4,5-trisphosphate
IP_3R	inositol 1,4,5-trisphosphate receptor
IPTG	isopropyl □-D-thiogalactoside
Kb	kilobases
kDa	kiloDaltons

lacZ	β-galactosidase
M	molar
MBSU	Molecular Biology Support Unit
mg	milligram
min	minutes
ml	millilitre
mm	millimetre
mM	millimolar
Mn^{2+}	manganese
mRNA	messenger RNA
N-	amino-
NO	nitric oxide
NOS	nitric oxide synthase
ng	nanograms
nm	nanometre
nM	nanomolar
OD	optical density
ORF	open reading frame
PAGE	polyacrylamide gel electrophoresis
PBS	phosphate buffered saline
PBT	PBS, Triton X-100
PCR	polymerase chain reaction
PDE	phosphodiesterase
PIP_2	phosphatidylinositol 4,5-bisphosphate
PKA	cyclic AMP-dependent protein kinase
PKC	protein kinase C
PLC	phospholipase C
rGC	receptor guanylate cyclase

RNA	ribonucleic acid
RNAi	RNA interference
RNAse	ribonuclease
RT	room temperature
RT-PCR	reverse transcriptase polymerase chain reaction
s	second
SDS	sodium dodecyl sulphate
S.E.M.	standard error of the mean
sGC	soluble guanylate cyclase
TAP	tandem affinity purification
TBS	tris buffered saline
TE	tris-EDTA
TEMED	N,N,N',N'-tetramethylethylenediamine
Tris	2-amino-2-(hydroxymethyl)-1,3-propanediol
U	unit
UAS	upstream activating sequence
UTR	untranslated region
UV	ultraviolet
X-gal	5-bromo-4-chloro-3-indolyl-□-D-galactopyranoside
µg	microgram
µl	microlitre
µM	micromolar
°C	degrees Celsius

One and three amino acid codes:

A	Ala	Alanine	N	Asn	Asparagine
C	Cys	Cysteine	P	Pro	Proline
D	Asp	Aspartic acid	Q	Gln	Glutamine
E	Glu	Glutamic acid	R	Arg	Arginine
F	Phe	Phenylalanine	S	Ser	Serine
G	Gly	Glycine	T	Thr	Threonine
H	His	Histidine	V	Val	Valine
I	Ile	Isoleucine	W	Trp	Tryptophan
K	Lys	Lysine	Y	Tyr	Tyrosine
L	Leu	Leucine	*	Stop	
M	Met	Methionine			

Table of Contents

Index of figures

Chapter 1

Figure

Chapter 2

Figure

Chapter 3

Figure

Chapter 4

Figure

Chapter 5

Figure

Chapter 6

Figure

Chapter 7

Figure

Chapter 8

Figure

Appendix

Figure

Index of tables

Chapter 1

Table

Chapter 2

Table

Chapter 3

Table

Chapter 4

Table

Chapter 6

Table

Chapter 7

Table

Chapter 8

Table

Acknowledgements

Firstly I must thank Shireen and Julian, who as well as directing my work and providing great advice when needed, helped me through the most difficult time of my life. For that, thank you. To Selim, getting a paper's never been so enjoyable, nor so educational. Many thanks. To my advisors Miles and Ian, thank you for invaluable advice. Next, to all the lab members, thanks for making these years not only rewarding but enjoyable! And where help has been given, many thanks. Next thanks go to my mum, who helped me get here by supporting my decisions, and being a great mum, and finally my dad, without whom I wouldn't be where I am today. Which is rushing to get a thesis finished! This one's for you.

Chapter 1

Introduction

1.1 Summary of Cyclic Nucleotide Signalling

The cyclic nucleotides adenosine 3',5'-cyclic monophosphate (cAMP) and guanosine 3',5'-cyclic monophosphate (cGMP) are second messengers that play important roles in virtually all cell types (Beavo and Brunton, 2002). Since the purification and characterisation of cAMP in 1957 as a second messenger for adrenaline (Rall et al., 1957; Sutherland and Rall, 1957; Wosilait and Sutherland, 1957), the enzymes responsible for the generation of cAMP, adenylate cyclase (Sutherland et al., 1962), and for the hydrolysis of cAMP to the inactive 5'AMP, phosphodiesterase (PDE) (Butcher and Sutherland, 1962), were rapidly identified. Following this, however, it took more than a decade to identify the main downstream effector enzyme, cAMP-dependant protein kinase (PKA) (Walsh et al., 1968b), and a further three decades to identify EPAC, or guanine nucleotide exchange factor directly activated by cAMP (de Rooij et al., 1998). cGMP was discovered in rat urine in 1963 (Ashman et al., 1963); it took until 1969 to identify guanylate cyclase and cGMP-PDEs (Hardman and Sutherland, 1969) cGMP dependent protein kinase (cGK) was discovered in 1970 (Kuo and Greengard, 1970). Any functional significance for cGMP besides regulation of cA-PDE activity (Beavo et al., 1971) was unknown until it was found to regulate light transduction (Miki et al., 1975). cGMP is typically present at a ten-fold lower physiological concentration than cAMP; whereas PKA, the main cAMP effector enzyme, is ubiquitous, with multiple identified targets, cGK has a more limited tissue expression profile, and, still, few identified targets (Hofmann et al., 2006). Nucleotide gated channels for both cGMP (Fesenko et al., 1985) and cAMP (Nakamura and Gold, 1987) were discovered later. Cyclic nucleotide signalling has since been shown to act as a second messenger for a great number of hormones and neurotransmitters. Mutations in cyclic nucleotide signalling genes have been shown to predispose to a number of diseases. The sheer number of genes involved – for example 21 vertebrate PDE genes – hints at a tightly spatiotemporally regulated signalling system, with multiple inputs and specific downstream effects. Indeed, five Nobel prizes later, a great deal remains to be discovered.

1.2 cAMP overview

Upon binding of a hormone or neurotransmitter to their cognate G-protein coupled receptor (GPCR), a stimulatory G protein (Gs) stimulates adenylate cyclase, which produces cAMP from ATP (Sutherland, 1962). At elevated concentrations, cAMP acts as a second messenger, effecting downstream signalling via the stimulation of PKA (Walsh et al., 1968a), CNG channels (Nakamura and Gold, 1987), and cAMP-activated guanine

nucleotide exchange factors (GEFs) (de Rooij et al., 1998; Kawasaki et al., 1998). cAMP is hydrolysed to inactive 5'AMP by cAMP-PDEs (Butcher and Sutherland, 1962) or is transported out of the cell by cyclic nucleotide transporters (Jedlitschky et al., 2000). A-kinase anchoring proteins (AKAPs) serve to bind PKA in an isoform-specific manner (Bregman et al., 1989; Bregman et al., 1991; Sarkar et al., 1984), and place these at discrete subcellular localisations, as members of protein complexes incorporating both substrates and PDEs to facilitate spatiotemporal control of cAMP signalling (Wong and Scott, 2004). cAMP signalling is summarised in figure 1.1.

Figure 1.1: The cAMP signalling system. Agonist binding to a $G\alpha_s$ coupled GPCR activates adenylate cyclase, which generates cAMP from ATP. This then acts as a second messenger, activating the downstream effectors PKA, cAMP-gated ion channels, and cAMP activated guanine nucleotide exchange factors. Intracellular cAMP concentration is reduced by hydrolysis by PDEs, and export from the cell by cyclic nucleotide transporters. AKAPs tether proteins to distinct subcellular locations. Abbreviations: GPCR = G-protein coupled receptor; GEF = Guanine nucleotide exchange factor; AKAP = A kinase anchoring protein; PKA = cAMP dependent protein kinase.

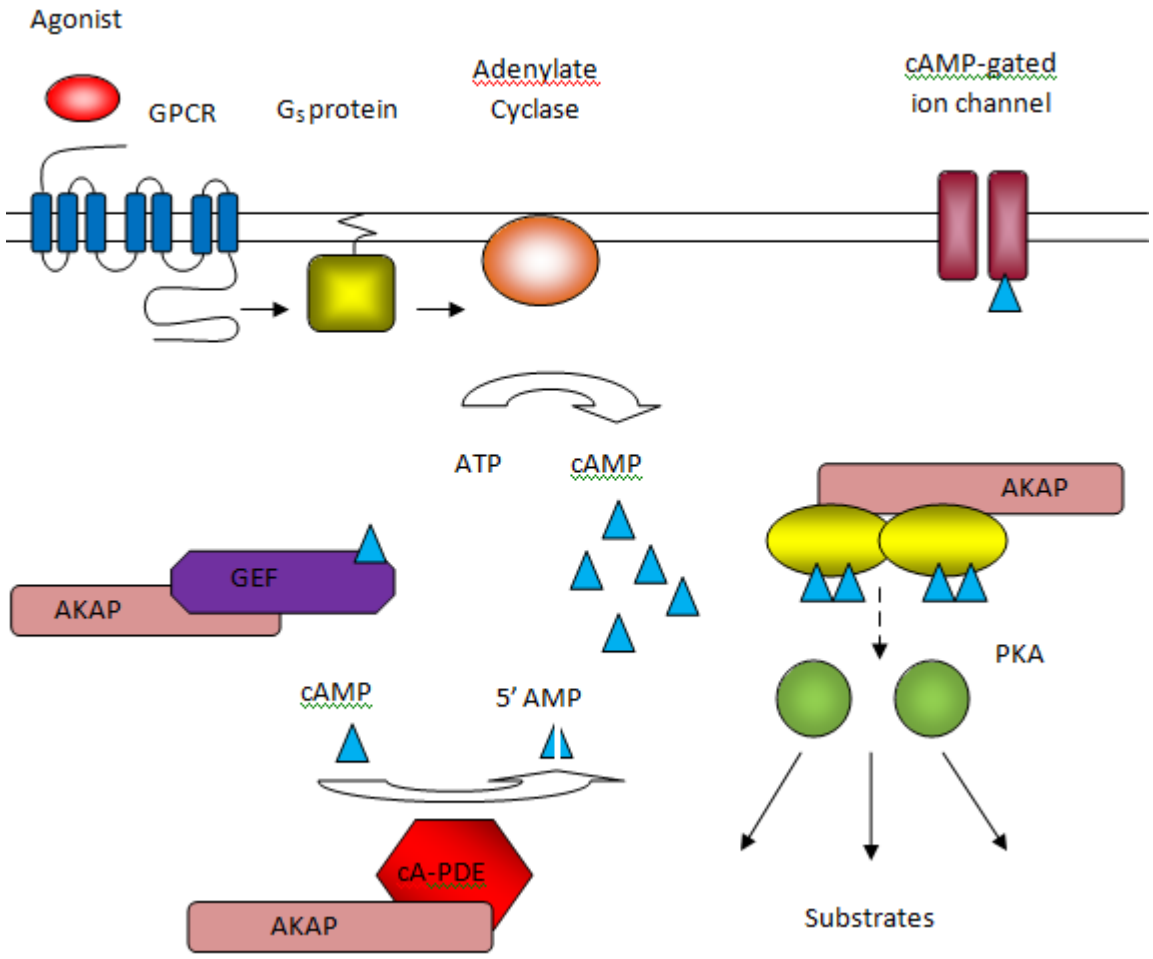

1.3 cGMP overview

cGMP is a second messenger for a number of primary messengers. cGMP is generated by guanylate cyclase from GTP. There are two types of guanylate cyclase. Receptor (also known as “transmembrane” or “particulate”) guanylate cyclase (rGC) is stimulated following the binding of a primary, extracellular messenger to its extracellular binding domain (Chinkers et al., 1989) (Schulz et al., 1989). Soluble (cytoplasmic) guanylate cyclase is stimulated via the binding of a primary messenger, but via an indirect mechanism. A primary messenger binds to a cognate GPCR, resulting in the activation of a Gq protein. This stimulates phospholipase C, which cleaves phosphatidylinositol 4,5-biphosphate (PIP_2) into diacyl glycerol (DAG) and inositol 1,4,5-triphosphate (IP_3). The increase in IP_3 stimulates IP_3 receptor (IP_3R), resulting in the release of calcium (Ca^{2+}) from internal stores. This increase in intracellular Ca^{2+} concentration in turn stimulates nitric oxide synthase (NOS), which produces nitric oxide (NO). This increase in NO stimulates soluble guanylate cyclase (sGC), which produces cGMP (Arnold et al., 1977). An atypical sGC has also been shown to be stimulated by oxygen (Gray et al., 2004; Morton, 2004). cGMP is hydrolysed to inactive 5’GMP by cGMP-PDEs (Miki et al., 1975), or is transported out of the cell by cyclic nucleotide transporters (Cropp et al., 2008; Dagger et al., 2001; Guo et al., 2003; Jedlitschky et al., 2000) . At elevated concentrations, cGMP stimulates cGK (Kuo and Greengard, 1970), CNG channels (Fesenko et al., 1985), and cAMP-PDEs (Beavo et al., 1971). cGMP signalling is summarised in figure 1.2.

Figure 1.2: The cGMP signalling system. cGMP is generated in response to a primary messenger, which either binds and activates rGC, or activates sGC via an indirect mechanism, through stimulation of a GPCR-coupled Gq protein. This stimulates phospholipase C, which cleaves phosphatidylinositol 4,5-biphosphate (PIP_2) into diacyl glycerol (DAG) and inositol 1,4,5-triphosphate (IP_3). The increase in IP_3 stimulates IP_3 receptor (IP_3R), resulting in the release of Ca^{2+} from internal stores. This increase in $[Ca^{2+}]_{cyt}$ in turn stimulates nitric oxide synthase (NOS), which produces nitric oxide (NO). This increase in NO stimulates sGC, which produces cGMP. This then acts as a second messenger, activating the downstream effectors cGK and cGMP-gated ion channels. Intracellular cGMP concentration is reduced by hydrolysis by PDEs, and export from the cell. GPCR = G-protein coupled receptor; NOS = Nitric oxide synthase; NO = Nitric oxide; sGC = Soluble guanylate cyclase; rGC = Receptor guanylate cyclase; cGK = Cyclic GMP-dependent protein kinase.

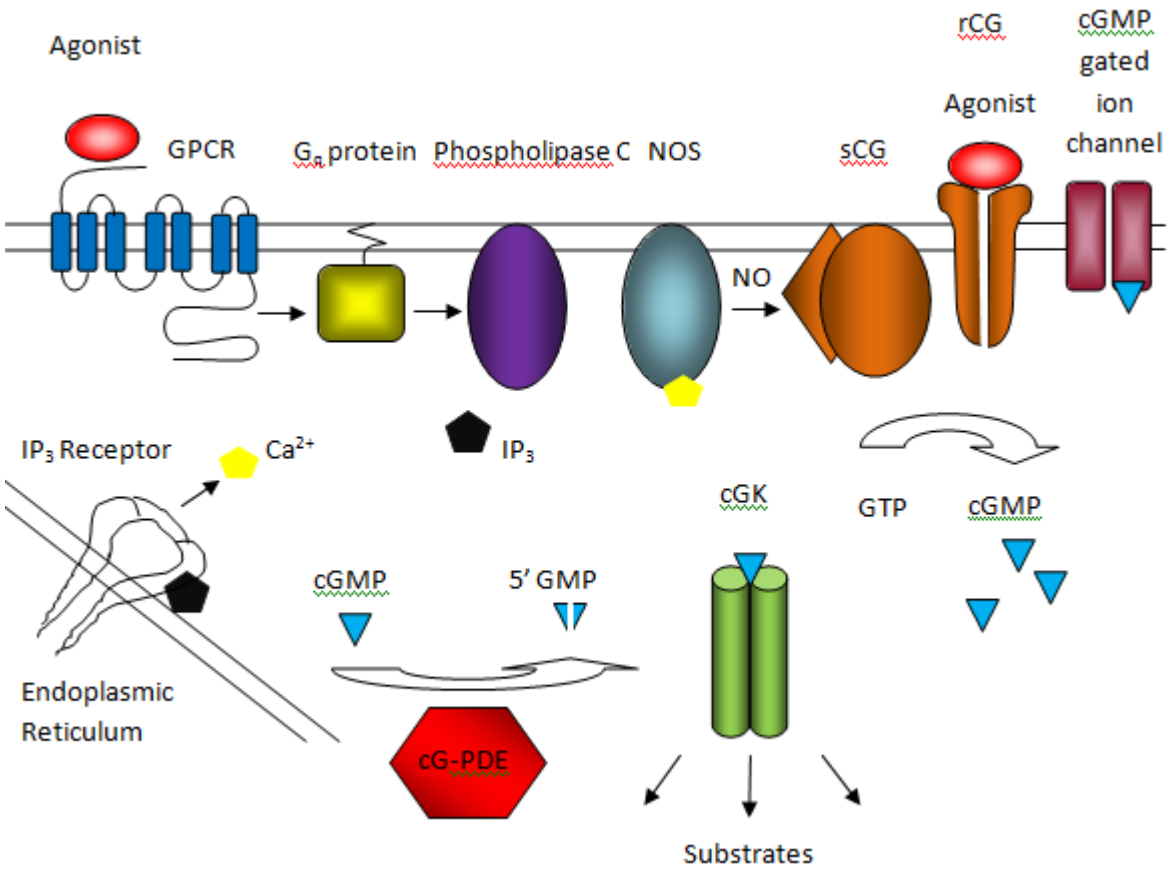

1.4 *Drosophila melanogaster* as a genetic model organism

The use of *Drosophila* as a genetic model organism was pioneered by Thomas Morgan, who was awarded a Nobel prize for his discovery of the white mutation (Morgan, 1910), and subsequent work. The benefits of *Drosophila* are well known. These include a short generation time, low cost, complex body plan, multiple physical and behavioural phenotypes, and a high relevance to mammalian systems due to high levels of homology, from gene sequence to protein function. Where *Drosophila* excels, however, is the availability of incredible genetic resources. The *Drosophila* genome has been sequenced, and the annotation is constantly updated (Adams et al., 2000). Balancer chromosomes prevent homologous recombination, and are lethal when homozygous; as they carry dominant genetic markers, stable heterozygote transgenic flies can kept as stocks for generations. The P-element, a mobile genetic element, has been instrumental in establishing *Drosophila* as an unrivalled genetic model organism. Initially used for mutagenesis, it was modified to allow enhancer trapping (O'Kane and Gehring, 1987), and later to generate transgenic flies under the control of yeast promoters and transcription factors, to deliver cell specific overexpression, or downregulation via RNAi, of a gene of choice, thus allowing the dissection of gene function at the level of cellular, tissue, and whole organism function (Figure 1.3) (Brand and Perrimon, 1993).

Figure 1.3: The GAL4/UAS binary system. A driver line carrying the yeast transcription factor GAL4 downstream of an endogenous promoter showing tissue specific expression of interest is used to drive expression of a transgene ("gene X") under the control of a UAS (Upstream Activation Sequence) GAL4 responsive promoter, in a tissue specific manner. Adapted from (Dow and Davies, 2003b).

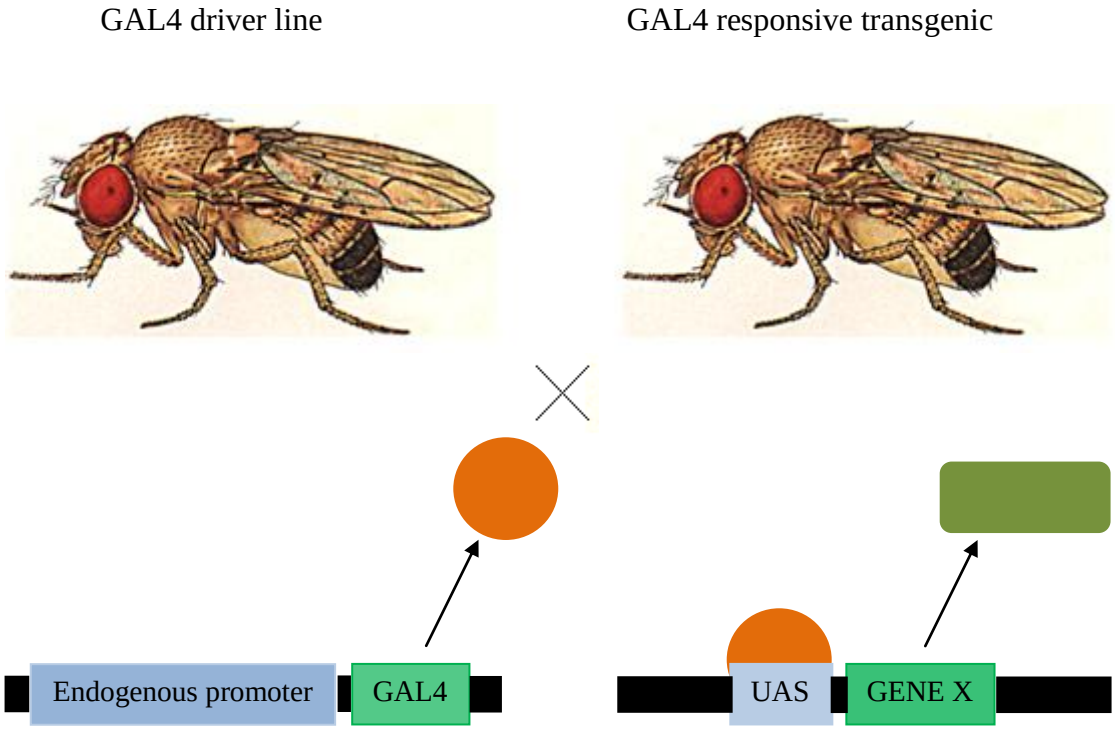

Genetic manipulation at the cellular level with the aim of understanding entire tissues has been termed integrative physiology (Dow and Davies, 2003b). The vast complexity and high levels of redundancy within mammalian cyclic nucleotide signalling networks leads to difficulties in the understanding of these pathways. *Drosophila melanogaster* has fewer signalling components in a typical signalling network, yet homologues within these pathways frequently perform the same tasks. With reduced redundancy comes clearer phenotypes; coupled with *Drosophila* genetics, e.g., cell-specific up- or down-regulation of a protein of interest, the elucidation of function is achievable where in mammalian systems it may not be.

1.5 cGMP signalling in *Drosophila*

cGMP signalling has been the focus of intense research for several decades. Individual components of the cGMP signalling pathway have mostly been identified by work in cell culture systems. Understanding of the role of cGMP signalling in physiology has been

advanced through the use of two main model organisms, mouse and fruit fly. Mouse deletion and transgenic models have greatly extended understanding of cGMP signalling. NOS isoforms have been attributed roles through the use of NOS knockouts (Mashimo and Goyal, 1999) and transgenics (Mungrue et al., 2003), as have natriuretic peptide (ANP) receptors (transmembrane guanylate cyclases) (Lopez et al., 1997). The use of mouse cGK deletion models led to the identification of several cGK substrates (Hofmann et al., 2006). The many advantages of *Drosophila*, discussed above, have led to novel discoveries in cGMP signalling. cGMP has been shown to affect learning and memory in larval (Osborne et al., 1997) and adult (Pereira and Sokolowski, 1993) *Drosophila*. cGMP was subsequently shown to have a role in learning and memory in mammals (Kleppisch and Feil, 2009; Prickaerts et al., 2002).

1.5.1 *Dm* NOS

Nitric oxide synthase is a membrane bound enzyme that generates nitric oxide in response to a rise in cytosolic Ca^{2+}, which is generated in response to an extracellular hormone or neurotransmitter binding to a cognate Gq-coupled GPCR. Activation of the Gq protein leads to the stimulation of phospholipase C, a membrane bound enzyme that cleaves phosphatidylinositol 4,5-biphosphate (PIP_2) into diacyl glycerol (DAG) and inositol 1,4,5-triphosphate (IP_3). The increase in IP_3 stimulates IP_3 receptor (IP_3R), resulting in the release of Ca^{2+} from internal stores, typically the endoplasmic reticulum. (Regulski et al., 2004; Regulski and Tully, 1995). In turn, this increase in NO stimulates sGC, which produces cGMP (Arnold et al., 1977). *Drosophila* contains one NOS gene, *dNOS*, which has 10 transcripts (NOS RA-RJ), encoding 6 novel polypeptides (http://flybase.org/reports/FBgn0011676.html). *dNOS* shows closest homology with vertebrate neuronal NOS (NOS1) (Davies, 2000; Regulski and Tully, 1995). Generation of a null allele leads to embryonic and larval lethality (Regulski et al., 2004). Overexpression affects behaviour, where flies demonstrate a reduction in motility (Broderick et al., 2003). NO has also been shown to modulate Malpighian tubule function. *dNOS* is expressed in principal cells, and increases fluid secretion in response to the neuropeptides capa-1 and capa-2 by the stimulation of cGMP production via sGC (Davies et al., 1997). NOS also has a role in immunity; activation leads to the production of immune peptides in the fat body (Foley and O'Farrell, 2003), the canonical immune tissue of the fly, and also in the Malpighian tubule, a tissue also of great importance to fly immunity (Davies and Dow,

2009; McGettigan et al., 2005). *dNOS* has been shown to play vital roles in imaginal disc development, regulation of organ growth, negative regulation of DNA replication and cell proliferation (Kuzin et al., 1996), synaptogenesis and nervous system development (Bicker, 2005), and the defence response (http://flybase.org/reports/FBgn0011676.html). Not all of these are necessarily modulated by the cGMP signalling pathway, but this array of processes clearly underlies the importance of cGMP signalling in *Drosophila*.

1.5.2 *Dm* soluble guanylate cyclase

Soluble (cytoplasmic) guanylate cyclase generates cGMP from GTP in response to NO (Arnold et al., 1977). *Drosophila* sGC exists as a heterodimer, composed of an alpha (guanylate cyclase α-subunit at 99B/ Gycα99B) and a beta (guanylate cyclase β-subunit at 100B/Gycβ100B) subunit, which generates cGMP upon NO binding (Stone and Marletta, 1996). A homodimer composed of two beta2 subunits was subsequently shown to bind NO and produce cGMP (Koglin et al., 2001). Gyc-88E, Gyc-89Da, and Gyc-89Db encode atypical guanylate cyclase subunits, which probably form Gyc-88E/89Da and Gyc-88E/89Db heterodimers *in vivo* (Morton et al., 2005). Gyc-88E also forms active homodimers. All atypical subunits were shown to generate cGMP under anoxic conditions (Morton, 2004), which suggests a potential role in feeding behaviour (Vermehren et al., 2006). Gyc-89Da and Gyc-89Db express in neurons responsible for adult eclosion and ecdysis respectively (Morton et al., 2008). *Drosophila* and mammalian sGCs are highly similar, showing similar structure and enzymatic properties (Shah and Hyde, 1995). A soluble GC hypomorph displays altered photoreceptor development, which can be phenocopied by inhibiting *dNOS* (Gibbs et al., 2001). sGC and NOS have been shown to regulate vesicle release at the larval neuromuscular junction (Wildemann and Bicker, 1999).

1.5.3 *Dm* Receptor guanylate cyclase

Receptor guanylate cyclase generates cGMP from GTP following the binding of a primary, extracellular messenger to its extracellular binding domain (Schulz et al., 1989). There are at least 7 receptor/receptor like guanylate cyclases encoded by the *Drosophila* genome (Davies, 2006). These are not well characterised, with no identified ligands. However, they share high sequence similarity with mammalian transmembrane guanylate cyclases. They have been linked to a number of phenotypes in *Drosophila*. Gyc32E is involved in

oogenisis and egg chamber development (Malva et al., 1994). Gyc76C has been shown to mediate semaphorin-1a (Sema-1a)-plexin A repulsive axon guidance of motor axons (Ayoob et al., 2004). A unique rGC was identified in *Drosophila* that is inhibited by O_2, CO, and NO, and appears to function as an oxygen sensor (Huang et al., 2007). Flyatlas reveals that multiple rGCs are expressed in the Malpighian tubule (Chintapalli et al., 2007), and in situ hybridisation has localised expression to the main fluid secreting segment of the tubule (Guo, 2007), suggesting a role in fluid secretion.

1.5.4 *Dm* Cyclic nucleotide gated channels

Cyclic nucleotide gated channels are tetrameric proteins that bind cyclic nucleotides under conditions of increased intracellular cyclic nucleotide concentration, which facilitates the permeation of extracellular cations, and thus the depolarisation of the plasma membrane. There are at least four CNG channel genes in *Drosophila* (Littleton and Ganetzky, 2000). *Cng* is expressed in eye and antenna, and forms a cGMP sensitive homomeric channel (Baumann et al., 1994). *Cng*-like is expressed in neuronal cells and in the mushroom bodies, and is a homologue of the mammalian CNG channel beta subunit. It does not form functional monomeric channels (Miyazu et al., 2000). *CG3536*, and *CG17922* both encode CNG channels although very little is known about them.

cGMP has been shown to stimulate Ca^{2+} influx into the tubule, which expresses *cng*, in a verapamil sensitive manner. As verapamil can be used as a CNG channel blocker, this suggests that cGMP gated ion channels modulate fluid secretion via Ca^{2+} signalling (MacPherson et al., 2001).

1.5.5 Cyclic nucleotide transport in *Drosophila*

Drosophila has contributed to the understanding of cyclic nucleotide transport, and the Malpighian tubule has been the tissue of choice in this area of study. Cyclic nucleotides are transported across the Malpighian tubule (Riegel et al., 1998). PDE6 has been found to regulate cGMP transport across the Malpighian tubule (Day et al., 2006); targeted overexpression in tubule principal cells completely ablates the process, whereas knockdown in principal cells significantly increases transport. This is the first demonstration of a direct role played by a PDE in cyclic nucleotide efflux. White, a

member of the ATP binding cassette G2 (ABC G2) transporter family, has classically been used as an eye colour marker in *Drosophila*. It was shown to participate in vesicular transepethilial transport of cGMP in the Malpighian tubule; the same study demonstrated that cyclic nucleotide transport is performed by the ABC G2 subfamily in *Drosophila*, and not the ABC C transporter subfamily as in mammals (Evans et al., 2008).

1.5.6 *Dm* cGKs

There are two *Drosophila* cGMP-dependent protein kinase genes; *dg1*, and *dg2 (foraging* or *for)*, which has eleven transcripts, *forRA* - *forRK*. DG2P1 and DG2P2 are the catalytically active isoforms (MacPherson et al., 2004b). DG2 shares 64% sequence identity with its nearest homologue in mammals, bovine lung cGK, with 75% sequence identity to the catalytic domain, and 64% to the cGMP binding domain. cGK is a holoenzyme, which is active as a homodimer (Gamm et al., 1995), and is maintained in a catalytically inactive state by a pseudosubstrate-like regulatory region located in the N terminus of the enzyme. At an elevated concentration of cGMP, the regulatory region is displaced, and the enzyme becomes enzymatically active. DG1 is a dimer, (Foster et al., 1996) whilst DG2 purifies as a dimer under gel filtration (MacPherson, 2004). Malpighian tubules express *dg1,* and the four main transcripts of *dg2, P1-P4.* cGKs show differential localisation in the Malpighian tubule. DG1 is localised to the cytosol and to the basolateral membrane. DG2P1 is localised to the apical and basolateral membranes, whereas DG2P2 is localised to the apical membrane. cGK activity is high in tubules, where the cGKs play distinct roles in the modulation of fluid transport in the Malpighian tubule. When overexpressed in tubule principal cells, DG1 increased fluid secretion in response to exogenous cGMP, which is transported into the tubule via cyclic nucleotide transporters (Riegel, 1998). DG2P2 overexpression, on the other hand, increased the fluid secretion response to capa-1 (MacPherson et al., 2004b). A naturally occurring polymorphism in *dg2* has been shown to determine the food search pattern employed by larval *Drosophila* (de Belle et al., 1989), where rovers (for^R) travel further to find food than the sitter (for^S) isoform (Pereira and Sokolowski, 1993). It was shown that as well as a 10% reduction in catalytic activity, the sitter isoform shows a slight reduction in transcript and protein levels (Osborne et al., 1997). The for^S and for^R isoforms were further characterised using the Malpighian tubule, where the polymorphism did not affect cGK activity, but rather the sitter polymorphism was shown to slightly increase the cGMP-PDE activity of an

unidentified PDE, with the result of lowering cGMP content (MacPherson et al., 2004a). As capa-1 neuropeptide increases fluid transport via cGMP, it follows that fluid transport of the Malpighian tubules from a *forS* background shows hypersensitivity to exogenously applied Capa-1 (MacPherson et al., 2004a) and cGMP (Dow and Davies, 2003b).

1.5.7 *Dm* PDEs

A cytogenic analysis of the *Drosophila* genome for regions that increase cAMP-PDE and cGMP-PDE activity when duplicated yielded four such regions; two of which, 3D3 / 3D4 and 90E-91B, increased cAMP-PDE activity in fly extracts when duplicated; the other two, 5D-9C and 88C-91B, increased cGMP-PDE activity in fly extracts when duplicated (Kiger and Golanty, 1977). Biochemical analysis of *Drosophila* extracts showed cAMP specific/Form II, and dual specificity (cAMP and cGMP) specific/Form I PDE activity (Davis and Kiger, 1980). *Dunce* (*dnc*) was identified in a screen for mutants in learning (Dudai et al., 1976) , and was later characterised as having Form II (cAMP) PDE activity, and mapped to 3D4 (Byers et al., 1981). The form I PDE was characterised as Ca^{2+} dependent, whereas the form II PDE was shown to be unaffected by Ca^{2+}, which suggested that the neurological defects seen in *dnc* mutants were linked directly to defects in cAMP-PDE activity, as opposed to cAMP mediated Ca^{2+} influx in presynaptic transmission (Byers et al., 1981). Work on several *dnc* mutants showed aberrant cAMP metabolism (Davis and Kiger, 1981), and molecular analysis of the enzyme verified the *dnc* gene as encoding a cAMP-PDE (Chen et al., 1986). This lead to the identification of mammalian PDE4 in rat (Colicelli et al., 1989; Davis et al., 1989; Swinnen et al., 1989) and subsequently the human PDE4 family (Conti et al., 2003). Following the discovery of *dunce*, it took several years for the cloning and characterisation for the other *Drosophila* PDEs to occur.

There are 11 mammalian PDE families encoded by 21 genes, which in total yields over 100 novel proteins. These have been grouped into 11 families, to reflect a shared sequence similarity, nucleotide specificity, regulatory properties, and inhibitory profile. Such a diverse array of proteins all responsible for degrading cyclic nucleotides allows for tight control and shaping of these signals, and contributes to the incredible specificity that these signalling events display (Beavo and Brunton, 2002). These all share a highly conserved catalytic domain, which contain a metal binding motif ($HX_{21-23}HX_3D/E$) (Charbonneau et al., 1986), the identification of which allowed homologous PDEase domains to be

identified, and the corresponding 11 phosphodiesterase gene families to be cloned. Mammalian PDE sequences were used to screen the Berkeley *Drosophila* Genome Project database (http://flybase.net/) for *Drosophila* PDE orthologues. Positive hits were then screened for the $HX_{21-23}HX_3D/E$ cyclic nucleotide motif. This analysis revealed that *Drosophila* contains orthologues to mammalian PDE1 (*CG14940*), PDE4 (*CG32498*), PDE6 (*CG8279*), PDE8 (*CG5411*), PDE9 (*CG32648*) and PDE11 (*CG10231*) (Day et al., 2005). These were also identified in a separate study (Morton and Hudson, 2002). Other than *Dunce* (Qiu, 1991), these PDEs were cloned and verified by Day et al, 2005. PDEs in *Drosophila* show widespread expression (Chintapalli et al., 2007; Day et al., 2005), underlying their importance.

1.6 *Drosophila* PDEs share biochemical, pharmacological, and structural characteristics with their mammalian orthologues

Analysis of *Drosophila* PDEs reveals a high degree of homology with respect to specificity, and the presence and arrangement of conserved domains (table 1.1).

Table 1.1: *Drosophila* contains homologues to PDE1, 4, 6, 8, 9, and 11. *Drosophila* PDEs show a high degree of homology with respect to specificity, and the presence and arrangement of conserved domains. From (Day et al., 2005).

Vertebrate PDEs	Specificity	Domains	*Drosophila* PDEs	Specificity	Domains
PDE 1	Dual spec	CaM binding	PDE 1	Dual spec	CaM binding
PDE 4	cA-PDE	UCR	Dunce	cA-PDE	-
PDE 6	cG-PDE	GAF	PDE 6	cG-PDE	GAF
PDE 8	cA-PDE	REC, PAS	PDE 8	unknown	REC, PAS
PDE 9	cG-PDE	-	PDE 9	unknown	GAF
PDE 11	Dual spec	GAF	PDE 11	Dual spec	GAF

When compared to their mammalian homologues, a high level of sequence similarity/identity was found in the catalytic domains (69-96%), with generally over 50% similarity over the length of the protein (table 1.2).

Table 1.2: A comparison of *Drosophila* and mammalian PDEs. *Drosophila* PDEs display high levels of homology with their mammalian homologues, especially within the catalytic domain. Adapted from (Day et al., 2005).

		Percentage amino acid identity (similarity)		
Gene	Human homologue	Human homologue	Catalytic domain	Predicted length of polypeptide (amino acids)
CG14940	PDE1	40 (56)	63 (79)	1818
CG8279	PDE6	28 (46)	51 (69)	1131
CG32498 transcript A	PDE4	59 (74)	79 (91)	701
CG32498 transcript B	PDE4	59 (74)	79 (91)	1209
CG32498 transcript C	PDE4	60 (76)	79 (91)	1057
CG32498 transcript D	PDE4	59 (74)	79 (91)	1068
CG32498 transcript E	PDE4	59 (74)	79 (91)	642
CG32498 transcript F	PDE4	60 (76)	79 (91)	662
CG32498 transcript G	PDE4	58 (73)	79 (91)	814
CG32498 transcript I	PDE4	59 (74)	79 (91)	1070
CG32498 transcript J	PDE4	59 (74)	79 (91)	1070
CG32498 transcript L	PDE4	61 (76)	79 (91)	521
CG32498 transcript M	PDE4	60 (74)	79 (91)	903
CG32498 transcript N	PDE4	59 (74)	79 (91)	983
CG5411 transcript A	PDE8	34 (52)	60 (79)	914
CG5411 transcript B	PDE8	35 (53)	60 (79)	904
CG5411 transcript C	PDE8	47 (66)	60 (79)	400
CG5411 transcript D	PDE8	37 (57)	60 (79)	805
CG5411 transcript E	PDE8	34 (52)	60 (79)	914
CG5411 transcript F	PDE8	23 (9 [sic])	60 (79)	400
CG32648	PDE9	26 (34)	63 (76)	2080
CG10231	PDE11	38 (55)	77 (96)	1545

1.6.1 *Dm*PDE1 (*CG14940*)

CG14940 has an ORF of 1815 nucleotides (nt), which encodes a single polypeptide of 605 amino acids (aa). *Dm*PDE1 has been shown to be a dual specificity, Ca^{2+}/calmodulin dependent PDE (Walter and Kiger, 1984). Western blotting of *CG14940* transiently transfected S2 cell lysate using an antipeptide antibody to the epitope EQAVKDAEARALAT confirmed that the gene produces a protein product of 75 kDa. Immunoprecipitation of PDE1 using this specific antisera from *Drosophila* head lysate, and subsequent PDE assays confirmed that *Dm*PDE1 is a Ca^{2+}/calmodulin sensitive dual specificity PDE, with a K_m for cAMP of 20.5 ± 1.5 μM, and a K_m for cGMP of 15.3 ± 1 μM. *Dm*PDE1 is inhibited by zaprinast at an IC_{50} of 71 ± 39 μM and by sildenafil at an IC_{50} of 1.3 ± 0.9 μM. Structurally, *Dm*PDE1 is similar to its mammalian orthologue; it shares an autoinhibitory domain at the N terminus, although it has one calmodulin binding domain, whereas mammalian PDE1 has two (figure 1.4).

Figure 1.4: Protein structure of *Dm*PDE1. *Dm*PDE1 contains an N-terminal autoinhibitory motif, and a calmodulin binding site at the N terminus. From (Day et al., 2005).

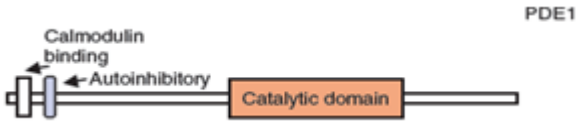

1.6.2 Dunce (*CG32498*)

The PDE best understood in *Drosophila* is *dunce* (*dnc)*, the mammalian PDE4 orthologue, a cAMP-PDE which was discovered independently in screens for mutations affecting olfactory learning and female fecundity (Byers et al., 1981). *Dnc* expresses predominantly in the neuropil of the mushroom bodies (Nighorn et al., 1991), and at lower levels in the neuropil of the nervous system, which is in agreement with its role in learning (Dauwalder and Davis, 1995). Since the identification of *dnc* involvement in olfactory learning, cAMP and cGMP have both been shown to have a role in learning and memory in mammals (Kleppisch and Feil, 2009). *Dnc* has been shown to play important roles in several additional processes. *Dnc* mutants have altered pacemaker functioning (Levine et al., 1994). Analysis of the larval neuromuscular junction in *dnc* mutants revealed a role in the plasticity of synaptic morphology (Zhong et al., 1992) and modulation of synaptic kinetics (Corfas and Dudai, 1990; Zhong and Wu, 1991). *Dnc* is involved in egg chamber and ovary development, and some *dunce* mutants are infertile (Lannutti and Schneider, 2001). Interestingly, *dnc* mutant learning, fertility and synaptic morphology phenotypes can be partially rescued by introduction of *rutabaga1*, an adenylate cyclase hypomorphic mutant, and indeed these mutations were identified in a screen for mutations that rescue the *dnc* mutant sterility phenotype (Feany, 1990; Zhong et al., 1992). *Dnc* has been biochemically characterised, with a K_m of 2.2 ± 0.5 μM for cAMP (Davis et al., 1989), and is partially inhibited by SQ20009 at 140 mM, although the IC_{50} for the compound is unknown. *Dnc* encodes 12 transcripts, resulting in 12 unique polypeptides (Qiu et al., 1991), (http://flybase.org/reports/FBgn0000479.html)

*1.6.3 Dm*PDE6 *(CG8279)*

CG8279 has an ORF of 3393 nt, which encodes a single polypeptide of 1131 aa. Western blotting of *CG8279* transiently transfected S2 cell lysate using an antipeptide antibody to the epitope HGSEDSHTPEHQRS confirmed that the gene produces a protein product of 130 kDa. Immunoprecipitation of *Dm*PDE6 using this specific antisera, and subsequent PDE assays confirmed that *Dm*PDE6 is a high K_m cG-PDE, with a K_m for cGMP of 37 ± 13 μM. PDE6 shows high sensitivity to both zaprinast and sildenafil, as it is inhibited by zaprinast at an IC_{50} of 0.65 ± 0.15 μM and by sildenafil at an IC_{50} of 0.025 ± 0.005 μM (Day et al., 2005). Interestingly, although *CG8279* has been designated as a vertebrate PDE6 homologue, it shares functional and structural characteristics with vertebrate PDE5 and PDE6, and also has high sequence similarity to PDE11 in the catalytic domain, although this is a dual specificity PDE. In common with mammalian PDE6, *Drosophila* PDE6 is prenylated via a CAAX-box prenylation motif, resulting in the recruitment of the protein to the plasma membrane, where it interacts with a prenyl binding protein (Day et al., 2008). As such, it was designated a PDE6 orthologue, although it is commonly referred to as a PDE5/6 homologue. *Dm*PDE6 has been implicated in the active transport of cGMP, as discussed above (Day et al., 2006). *Dm*PDE6 contains an N-terminal autoinhibitory motif, a consensus PKA/cGK phosphorylation site at each end of the protein, and a calmodulin binding site at the N terminus (figure 1.5).

Figure 1.5: Protein structure of *Dm*PDE6. *Dm*PDE6 contains a serine rich region at the N terminus, and a polybasic region at the C terminus, both of unknown function. There are consensus PKA/cGK phosphorylation sites at the N- and C-termini, and twin GAF domains N-terminal of the catalytic domain. The protein has a CAAX-box prenylation motif at the C terminus. From (Day et al., 2005).

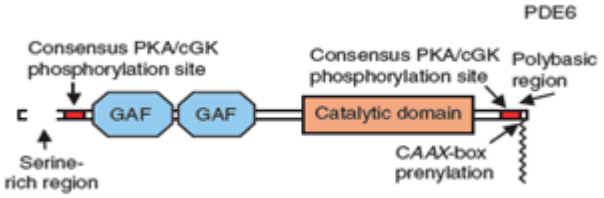

1.6.4 *Dm*PDE8 (*CG5411*)

CG5411 is a complex gene, with 5 transcripts (A-E) encoding 4 different polypeptides, where the ORFs of transcripts A and E are identical. *Dm*PDE8 has not been well characterised, although analysis of the sequence reveals that, in common with mammalian PDE8, *Dm*PDE8 contains a REC and a PAS domain to the N terminal of the catalytic domain, and an N-terminal myristoylation/palmitoylation motif (figure 1.6) (Day et al., 2005).

Figure 1.6: Protein structure of *Dm*PDE8. *Dm*PDE8 contains REC and PAS domains N-terminal of the catalytic domain, and a myristoylation/palmitoylation motif at the extreme N-terminus. From (Day et al., 2005).

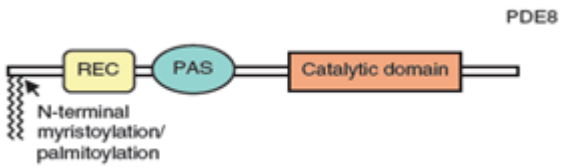

1.6.5 *Dm*PDE9 (*CG32648)*

PDE9 has not been well characterised, although the gene encoding *Dm*PDE9 resides within an area identified by Kiger and Golanty that resulted in increased cGMP-PDE activity when duplicated (Kiger et al., 1981). No ESTs are available; while the predicted polypeptide for this gene is 963 aa in length, the gene was designated a homologue of mammalian PDE9 based upon homology of 54% within the catalytic domain; outwith this region there is little homology (figure 1.7) (Day et al., 2005). As such, future research into this gene will require validation of the Flybase prediction of the gene structure.

Figure 1.7: Protein structure of *Dm*PDE9. *Dm*PDE9 contains two consensus PKA/cGK phosphorylation sites C-terminal of the catalytic domain. From (Day et al., 2005).

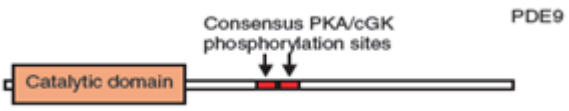

1.6.6 *Dm*PDE11 (*CG10231*)

CG10231 encodes a single ~5.8 kb transcript (*Dm*PDE11 RA) which encodes a polypeptide of 1366 aa. A full length EST clone was sequenced in order to verify *CG10231*, and northern blotting confirmed that *CG10231* produced a single transcript of ~5.8 kb. Western blotting of *CG10231* transiently transfected S2 cell lysate using an antipeptide antibody to the epitope PTSTQPSDDDNDAD confirmed that the gene produces a protein product of 100 kDa. Immunoprecipitation of PDE11 using this specific antisera from *Drosophila* head lysate, and subsequent PDE assays confirmed that *Dm*PDE11 is a dual specificity PDE, with a K_m for cAMP of 18.5 ± 1.5 μM, and a K_m for cGMP of 6 ± 2 μM. *Dm*PDE11 shares high sequence identity/similarity with mammalian PDE5, PDE6β, and PDE11A. However, the protein has highest sequence identity within the catalytic domain to PDE11A (77%), and has twin GAF domains N-terminal of the catalytic domain, a characteristic shared with the *Hs*PDE11A isoforms PDE11A3 and PDE11A4 (http://www.biochemj.org/bj/388/bj3880333add.htm). As the enzyme was shown to be a dual specificity PDE, *Dm*PDE11 was designated as a PDE11A3/PDE11A4 orthologue. Interestingly, the K_m for cGMP indicates that PDE11 has the highest affinity for cGMP of any of the *Dm*PDEs screened. PDE11 is inhibited by zaprinast at an IC_{50} of 1.6 ± 0.5 μM and by sildenafil at an IC_{50} of 0.12 ± 0.06 μM. *Dm*PDE11 has four PKA/cGK consensus phosphorylation motifs (http://www.biochemj.org/bj/388/bj3880333addhtm), suggesting that it may be a substrate of the enzyme. The enzyme contains glutamine and histidine rich regions at the N- and C-termini respectively of unknown significance (figure 1.8) (Day et al., 2005).

Figure 1.8: Protein structure of *Dm*PDE11. *Dm*PDE11 contains glutamine- and histidine-rich regions of unknown function at the N- and C-termini respectively, and has twin GAF domains to the N terminus of the catalytic domain. From (Day et al., 2005).

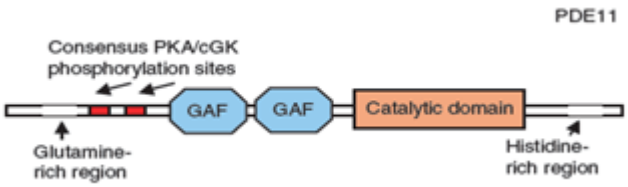

1.7 H. sapiens PDE11A

The PDE11 family of phosphodiesterases were first characterised in 2000 (Fawcett et al., 2000; Hetman et al., 2000; Yuasa et al., 2000a). *Hs*PDE11A is a dual specificity cAMP- and cGMP-PDE, with four splice variants from a single gene, each containing progressive truncations of the N terminus, with a shared C terminus containing a PDE catalytic domain; in the case of *Hs*PDE11A3, the first two exons encode novel N terminal sequence of unknown significance. The N terminus of the longest isoform – *Hs*PDE11A4 – has two PKA/cGK phosphorylation sites which reduce the EC_{50} for cGMP ~3 fold when phosphorylated (Gross-Langenhoff et al., 2008). The progressively truncated isoforms are progressively more sensitive to the inhibitors verdenafil and tadalafil and have a higher affinity for substrate. The GAF-A domain has been shown to bind cGMP, but at an EC50 outside the physiological range (Gross-Langenhoff et al., 2006). Binding of cGMP to the GAF-A domain does not stimulate catalytic activity (Matthiesen and Nielsen, 2009). The GAF-B domain is necessary for oligomerisation; *Hs*PDE11A1 forms a tetramer, while *Hs*PDE11A2-4 form dimers (Weeks et al., 2007). The structure of each *Hs*PDE11A is summarised in figure 1.9.

Figure 1.9: Protein structure of *Hs*PDE11A. *Hs*PDE11A isoforms 1-4 share a conserved C terminus containing the catalytic domain, and N termini of varying lengths, which contain complete or partial GAF domain(s). Modified from (Weeks et al., 2007).

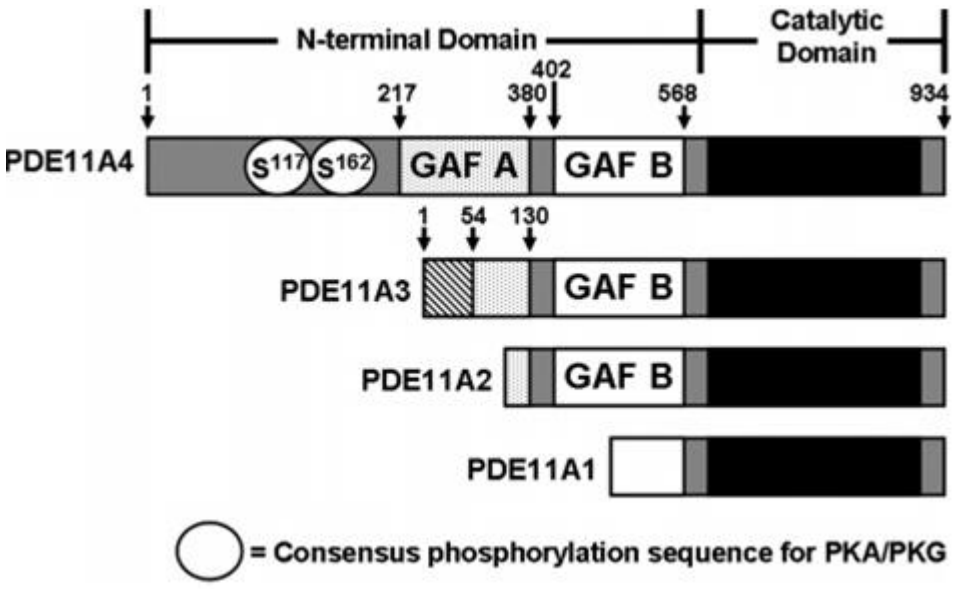

Tissue staining utilising a polyclonal antibody which recognises all four human isoforms showed expression in epithelial cells, endothelial cells, and smooth muscle cells of every tissue screened. The protein localises to the nucleus. The highest expression was found in the prostate, testis, kidney, colon, and the epidermis in the skin (D'Andrea et al., 2005). Few physiological roles for PDE11A have been identified. PDE11A3 is reported to be confined to testis in both rat and human (Yuasa et al., 2001). PDE11A has been shown to regulate spermatozoa physiology. Knockout of PDE11A renders male mice infertile (Seftel, 2005a; Seftel, 2005b). It has been linked to erectile function and premature ejaculation. Mutations to *Hs*PDE11A are frequent among patients with adrenocortical tumours (Horvath et al., 2006) and may predispose to testicular germ cell tumours (Horvath et al., 2009). Polymorphisms in *Hs*PDE11A are associated with the diagnosis of major depressive disorder (Wong et al., 2006). Taken together, there is a potential role for the PDE11A family in the central nervous system.

1.8 The characteristics of PDEs

1.8.1 Structure of the catalytic domain

All PDEs share a highly related catalytic domain, which consists of 16 alpha helices that form a cleft in which cyclic nucleotides are bound and cleaved. The core contains two metal ions, essential for function, which are tightly co-ordinated; a Zn^{2+} is bound by an aspartate and a histidine, and a Mg^{2+} is held by multiple water molecules.

1.8.2 Nucleotide specificity

Specificity to one or both cyclic nucleotides is dictated by an invariant glutamine that is proposed to form multiple hydrogen bonds with the purine ring of the cyclic nucleotide; it is the orientation of this glutamine that determines PDE specificity. Where this glutamine is free to rotate, it will bind both cAMP and cGMP; when it is hindered by its neighbouring residues it is able to bind either cGMP or cAMP (Zhang et al., 2004).

Figure 1.10: The glutamine switch. Crystal structure of PDE1B (red/C and D), PDE4D (blue/A), and PDE5A (green/B). Whereas the conserved glutamine, Q421, of PDE1B is unhindered, and thus the residue is free to rotate and thus the catalytic domain can accommodate both cAMP (C) and cGMP (D), the glutamine of PDE5A (B) and PDE4D (A) in both cases is bound in place by hydrogen bonds, and thus the glutamine is unable to rotate, resulting in cyclic nucleotide specificity (Zhang et al., 2004).

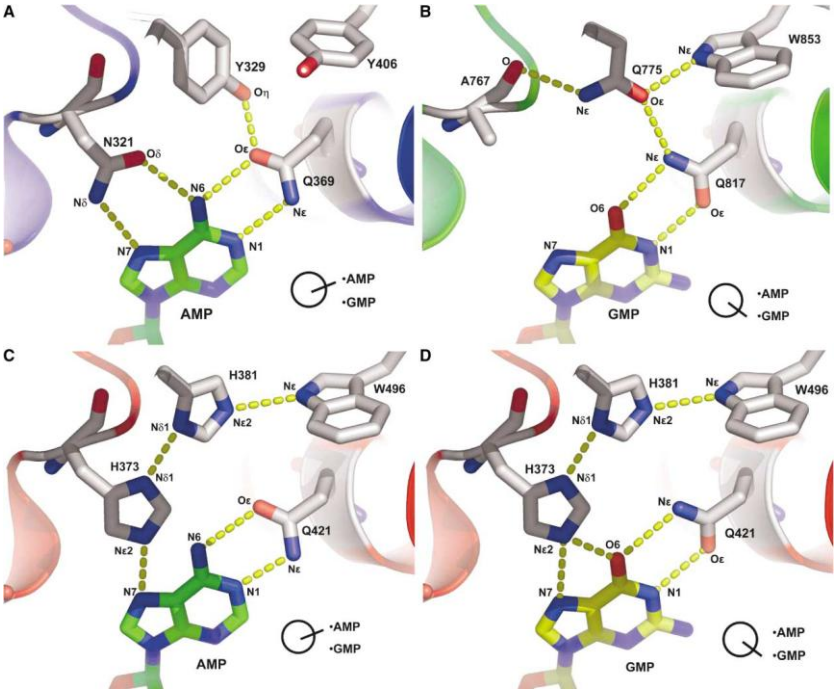

1.8.3 Regulation of PDEs

PDEs are subjected to multiple levels of regulation. Each phosphodiesterase family contains differing regulatory domains that contribute to the unique properties of each family (Beavo et al., 2007). To modulate rapid increases in cyclic nucleotide concentration, the catalytic activity of PDEs can be rapidly increased or decreased several fold (Conti and Beavo, 2007). To facilitate the localised nature of cyclic nucleotide signalling, post translational modifications or association with anchoring proteins may redirect the enzyme, for example to the cell membrane (Beavo and Brunton, 2002).

1.8.4 Cyclic nucleotide binding

GAF domains have been identified within a range of different proteins, initially cGMP-regulated PDEs, Adenylate cyclase, and the Fh1A protein, hence the acronym (Ho et al., 2000). It is a non-catalytic cyclic nucleotide binding domain, which in PDEs can modulate catalytic activity allosterically (Charbonneau et al., 1990). Studies of mammalian PDEs have shown that one or both GAF domains of PDE2, PDE5, PDE6, and PDE11 bind cGMP, and that of PDE10 binds cAMP. This can result in activation of catalytic activity, in the case of PDE2 (Martins et al., 1982) and PDE5 (Thomas et al., 1990) (Rybalkin et al., 2003). In PDE6, it has been shown to aid binding of the inhibitory γ subunit to the catalytic domain (Norton et al., 2000). In the case of PDE10 and PDE11, binding does not (directly at least) affect catalytic activity (Matthiesen and Nielsen, 2009). The binding of cGMP to the GAF domain has also been shown to modulate dimerisation in PDE2 (Martinez et al., 2002) and PDE6 (Muradov et al., 2003). Interestingly, the four isoforms of PDE11 contain four different start sites that represent a progressive truncation of the N terminus; only PDE11A4 contains two complete GAF domains, with A3, A2, and A1 each having progressively truncated GAF domains .

1.8.5 Post translational modifications of PDEs

1.8.5.1 Modulation of PDE activity by other proteins

The behaviour of phosphodiesterases can be modified through phosphorylation by cyclic nucleotide dependent kinases, and other kinases. As detailed above, DG2 has been shown to modulate an unidentified cG-PDE in Malpighian tubule (MacPherson et al., 2004a). PDE1 is stimulated by Ca/Calmodulin by up to 8 fold in mammals (Cheung, 1970) which binds sites either side of the inhibitory domains of the N terminus, likely relieving the inhibitory action of this domain (Sonnenburg et al., 1995). Calmodulin stimulates PDE1 almost 2-fold in *Drosophila* (Day et al., 2005). In mammalian systems, PDE3 has been shown to be phosphorylated by PKA (Manganiello et al., 1995), which rapidly increases catalytic activity.

The long forms of PDE4 are also known to be rapidly stimulated by PKA via phosphorylation of a crucial serine residue in the N-terminal regulatory domain (MacKenzie et al., 2002), acting as a feedback mechanism to terminate hormonal

stimulation. ERK2, a MAP kinase, phosphorylates PDE4B, C and D subfamilies in the catalytic domain, where long-form isoforms are inhibited, whereas short-form isoforms are stimulated (Baillie et al., 2000). cGK phosphorylates PDE5 when the GAF domains have bound cGMP (Thomas et al., 1990; Turko et al., 1998), to increase activity by 50-70%, and also increase the cGMP binding capacity of the GAF domain (Corbin et al., 2000). Isoform multiplicity, with the resultant sequence changes and changes to the protein's interactome that brings, may mask or remove putative phosphorylation sites, thus altering the function of these proteins.

1.8.5.2 Addition of lipids

Lipid kinases play intrinsic roles in many facets of cell signalling, trafficking proteins to the cell membrane, possibly resulting in their activation, and association with membrane based proteins or substrates and thus modifying their function (Heath et al., 2003). The catalytic subunits of PDE6 are subjected to differential prenylation at the C terminal; PDEα is modified by farnesylation, and PDEβ by geranylgeranytion (Anant et al., 1992), to ensure targeting to rod outer segment membrane (Qin and Baehr, 1994). The differential prenylation also controls binding of the inhibitory γ subunit (Cook et al., 2000). PDE8 has an N-terminal myristoylation motif, and PDE9 has an N terminal myristoylation/palmitoylation motif, although neither has been shown to occur *in vivo* within the published literature.

1.9 The use of *Drosophila* to investigate vertebrate phosphodiesterase function

Previously, *Drosophila* has been used to transgenically express vertebrate PDE genes, and these have proved functional *in vivo*. Bovine PDE5 has been overexpressed in the tubule, resulting in an increase in cGMP-PDE activity and conservation of the pharmacological characteristics of PDE5 (Broderick et al., 2004). The transgene could participate in and modulate osmoregulation, which was inhibited by sildenafil at substrate concentrations which would affect the enzyme in mammalian systems. The enzyme localised to the apical membrane, the site of fluid transport. Such physiologically relevant targeting suggests interaction with relevant signalling proteins (Broderick et al., 2004). In another example, Rat PDE4A1 increases cAMP-PDE activity in the fly when transgenically over-expressed, and can rescue cAMP-PDE levels to normal levels and beyond when expressed in a *dunce*

mutant background that displays 46% dnc cAMP-PDE activity. Furthermore, when rat PDE4A1 is expressed in this mutant background, it rescues a learning phenotype resulting from the knockdown of *dunce* activity (Dauwalder and Davis, 1995). Such functional conservation suggests that *Drosophila* and vertebrate genes originated from common ancestral genes, and as such a high degree of functional complementation still exists. That *Drosophila* and vertebrate PDE genes share functional and structural homology, yet display key differences, may allow the side by side study of PDE genes, to shed light on the function of PDEs in both areas. As such, it was decided to clone the closest orthologue to *Dm*PDE11, *Hs*PDE11A3, and to express this in fly, to allow the investigation of human PDE11A function in an *in vivo* context. The results of this investigation are presented in chapter eight.

1.10 Compartmentalisation in cyclic nucleotide signalling

A cell can transduce multiple extracellular cues simultaneously, using cAMP and cGMP as second messengers, with specific activation of target effector proteins, and resulting downstream actions. To maintain specificity, cyclic nucleotide concentration must be tightly regulated spatiotemporally. As well as the localisation of the cyclase, gene and isoform multiplicity of phosphodiesterases, and AKAPs, which modulate PDE localisation, allow the placement of PDEs with distinct subcellular localisation, which act as a "sink" to generate multiple, simultaneous intracellular domains ("pools") of elevated cyclic nucleotide concentration (Baillie, 2009). The signal transduced within these pools depends upon the effector proteins within it, and the substrates that they are directed to.

1.10.1 cAMP compartmentalised signalling

The idea the cAMP signalling may be compartmentalised was postulated as early as 1980 (Brunton et al., 1981; Hayes et al., 1980), following the discovery that within cardiac myocytes, stimulation of different adenylate-stimulatory GPCRs lead to differing physiological outputs. Advances in cAMP reporters revealed that microdomains of cAMP exist, which have distinct subcellular localisation, and show differing changes to the magnitude and duration of cAMP concentration, depending upon the upstream signal (Zaccolo and Pozzan, 2002). It was proposed that PKA is compartmentalised within these

distinct subcellular microdomains, thus allowing the phosphorylation of distinct PKA substrates, and so convey a specific signal depending upon the upstream GPCR activated (Hayes and Brunton, 1982). It was subsequently shown that PKA type I and type II are differentially tethered by A-Kinase Anchoring Proteins (AKAPs) (Di Benedetto et al., 2008). Indeed, the formation of AKAP-tethered complexes has been shown to mediate compartmentalisation at every level of cAMP signalling. Gene and isoform multiplicity of PDEs, cyclases, downstream effector proteins, and AKAPs, and the various associations between these, allow the formation of cAMP microdomains. Particular combinations of GPCRs, Gs proteins, and adenylate cyclases occupy distinct membrane localisations (Rybin et al., 2000). This allows feedback whereby PKA can phosphorylate AC to terminate the cAMP signal (Bauman et al., 2006), ensuring rapid transmission of signal, while ensuring spatiotemporal control over the cAMP signal. The formation of adenylate cyclase-AKAP-PKA complexes allows the tying of PKA-substrate association by AKAPs to the site of cAMP generation. AC activity may be modulated by serine/threonine kinases and Ca^{2+}, in addition to Gs. Combined with the subcellular targeting and association with AKAPs, this level of control ensures that microdomains may be modulated by multiple signals and proteins (Willoughby and Cooper, 2007). The formation of PKA/PDE signalling complexes allows crosstalk, where the PDE regulates local cAMP concentration, and thus PKA activity, while the kinase can modulate PDE function by phosphorylation, thus facilitating feedback. An AKAP18δ-PDE4D3/9-PKA signalling complex localised to vesicles has been shown to regulate water permeability in human renal principle cells. The water channel aquaporin 2 (AQP2) is recycled from the membrane in these vesicles. Arginine vasopressin (AVP) activates PKA, which stimulates the trafficking of vesicles containing AQP2 to the plasma membrane; thus water permeability is directly modulated by PKA activity. PKA then activates PDE4D, thus reducing local cAMP concentration inhibiting PKA activity, and stimulating the endocytosis of the AQP2 bearing vesicles (figure 1.11) (McSorley et al., 2006).

Figure 1.11: AQP2, PDE4D and PKA form an AKAP18δ mediated complex. AQP2, PDE4D, and PKA are tethered to intracellular vesicles by AKAP18δ, where PKA stimulates trafficking of the AQP2 bearing vesicle to the membrane; when at the membrane PKA phosphorylates PDE4D3/9, thus reducing localised cAMP and initiating vesicle endocytosis. From (Stefan et al., 2007).

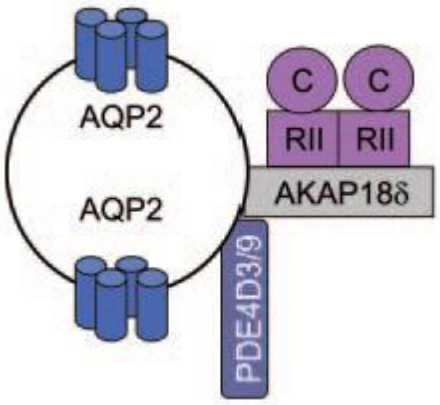

1.10.2 cGMP compartmentalised signalling

Like cAMP signalling, a cell may receive different signals that initiate a cGMP signalling event, such as a natriuretic peptide or nitric oxide, which result in distinct and perhaps simultaneous cellular responses. There is a great deal of evidence to suggest that cGMP microdomains facilitate the faithful transmission of these signals, and that this is facilitated by compartmentalisation of cGMP signalling at every level. cGK is recruited to the membrane upon binding of atrial natriuretic peptide, and directly interacts with NPRA, a type 1 ANP receptor/rGC. cGK phosphorylates the receptor, increasing the potency of the response to ANP (Airhart et al., 2003). Although both soluble and receptor guanylate cyclases exist, the terms are misleading, in that activated sGC translocates to the membrane in a Ca^{2+} concentration-dependent manner, where it is sensitised to NO stimulation (Zabel et al, 2002). NO has a very short half life, and NO is 9 times less soluble in water than in hydrophobic environments, suggesting that NO would be present in the cell in a concentration gradient highest at the membrane, and reduced in the cytosol. Thus, the modulation of sGC localisation by Ca^{2+} to bring sGC into close proximity of NOS, a membrane bound enzyme, points to a tight spatial control of cGMP signalling. The localisation of NOS itself is tightly regulated. Endothelial NOS (eNOS) is doubly acylated,

which mediates interactions with distinct caveolin isoforms in various cell types, thus dictating the localisation and activity of eNOS, and therefore the site of release of NO. These signal transducing microdomains are termed caveolae (Feron et al., 1998). In a landmark paper using a exogenously expressed CNG channel as a biosensor, by measuring cGMP-induced uptake of Ca^{2+} and Mn^{2+} in HEK cells overexpressing rGC, it was found that the "pool" of cGMP generated by rGC has stimulatory effects at the membrane, whereas cGMP generated by sGC is not accessible to membrane-localised cGMP sensing proteins (Castro et al., 2006). A similar finding was made in vascular smooth muscle cells; while stimulation of sGC led to higher cellular cGMP than stimulation of rGC, it was stimulation of rGC that resulted in the stronger CNG channel activation (Piggott et al., 2006). PDE1C and PDE5 show differing subcellular localisation across multiple cell types, and thus sample and modulate distinct pools of cGMP (Dolci et al., 2006). Inhibition of PDE2 and PDE5 has differential effects on cGMP produced by soluble and receptor GCs; PDE2 is responsible for modulating cGMP produced by rGC at the membrane, whereas PDE5 modulates cGMP generated in the cytosol by sGC, and furthermore acts as a physical barrier to prevent this pool from diffusing to the cell membrane (Castro et al., 2006). Signalling complexes have been identified in cGMP signalling, similar to those formed in cAMP signalling, which facilitate the tight spatiotemporal control of cGMP signalling events. Transmembrane conductance in enterocytes is induced by the activation of cystic fibrosis transmembrane conductance regulator (CFTR) Cl^- channels. Although both cGK type I and II can phosphorylate CFTR *in vitro*, only cGK type II can induce transmembrane conductance *in vivo*, due to its localisation at the apical membrane (Vaandrager et al., 1998). In smooth muscle cells, cGK type I forms a dimer with vimentin, with the association occurring outside of the catalytic domain at the N-terminus; this dimer then targets histone F2b, and other target peptides (MacMillan-Crow and Lincoln, 1994). cGMP-dependent protein kinase anchoring proteins (GKAPs) have been identified, which bind cGKs in the regulatory domain of the N terminus. GKAP42 serves to localise cGKIα to the Golgi apparatus of male germ cells. cGK phosphorylates GKAP42, where activation of cGKIα terminates the interaction (Yuasa et al., 2000b). GKAPs which bind cGK type II have been identified in multiple tissues (Vo et al., 1998). One such GKAP, myosin heavy chain, may facilitate cGK type II mediated smooth muscle relaxation (Lincoln et al., 1994), which is still not well understood. In platelets, a PDE5-cGK1β signalling complex is recruited to inositol 1,4,5 triphosphate receptor type 1 (IP_3R1) enriched membranes. cGK1β mediates a reduction in Ca^{2+} release from the endoplasmic reticulum by phosphorylating IP_3R1 (Schlossmann et al., 2000). cGK phosphorylates PDE5 at the ER,

causing a localised reduction in cGMP, and a subsequent inhibition of cGK activity, yet PKA does not affect PDE5 function in the cytosol (Wilson et al., 2008). Taken together, these data suggest that cGMP microdomains play a vital role in shaping signal specificity and the spatiotemporal nature of cGMP signalling events.

Understanding of cGMP signalling has been advanced by genetically encoded cGMP reporters. The first generation of FRET based cGMP reporters were generated by sandwiching PKG1α, rendered catalytically null, with the dimerisation domains removed, with differing emission-shifted green fluorescent protein at either terminus, called CGY (Sato et al., 2000) and cygnet-2 (Honda et al., 2001). Cygent-2 was used to investigate cGMP signalling in vascular smooth muscle, where natriuretic peptides induce muscular relaxation via an NO-cGMP signalling cascade. Cygnet-2 permitted the temporal characterisation of this cGMP response; it was shown that stimulation with NO, irrespective of the rate or duration of the NO release, resulted in rapid, transient cGMP "peaks", and that the kinetics of this cGMP response are controlled by the actions of soluble guanylate cyclase and PDE 5, which are not desensitised during the process, thus facilitating continuous response to NO (Cawley et al., 2007). Such a study was previously not feasible. This finding was advanced by the use of a novel, non-FRET based cGMP-indicator, where cGMP-binding domains of cGKIα and β were fused to a single GFP, named FlincGs. They found a similar, global elevation of cGMP upon application of NO to vascular smooth muscle. However, upon the application of natriuretic peptide, elevation of cGMP was limited to the sub-membrane, where inhibition of PDE5 saw global elevations (Nausch et al., 2008).

Many such advances in these sensors have been achieved, including the development of membrane permeable cynet-2 (Honda et al., 2005), which avoids the issues associated with maintaining cells in culture while transfecting the reporter, and the development of reporters with higher specificity and more rapid responsiveness, where rather than fuse whole proteins or truncates with fluorescent proteins, single cGMP-binding domains were sandwiched by CFP and YFP; constructs using cGMP binding domains from various proteins were generated, that of PDE5 was selected based on its selectivity of cGMP over cAMP, and its rapid responsiveness, and named cGES-DE5 (Nikolaev et al., 2006). Such systematic development of sensors is producing tools of increased quality (Russwurm et al., 2007), and will permit a fuller understanding of the tight spatiotemporal control cGMP signalling is evidently subjected to.

1.10.3 Cyclic nucleotide cross talk

cAMP and cGMP cross talk has been shown to widely occur in mammalian systems; further development of cGMP reporters could be used to answer whether there is overlap between cAMP and cGMP microdomains during a signalling event. Phosphorylation of PDE5 by PKA or cGK increases cG-PDE activity by 50-70%, and also increases the cGMP binding capacity of the allosteric cGMP binding sites in vitro (Corbin et al., 2000). Cyclic nucleotide cross talk occurs in PDEs; cAMP-PDE activity of PDE2 is allosterically increased by cGMP (Martins et al., 1982), whereas for PDE3, cGMP acts as a competitive inhibitor against cAMP, thus reducing cAMP-PDE activity (Shakur et al., 2001). This cGMP regulation of cAMP signalling has been shown to have several regulatory effects in cardiac cells, including a reduction in responsiveness to beta-adrenergic agonists, and the potentiation of Ca^{2+} currents (Zaccolo and Movsesian, 2007). Interestingly, cAMP and cGMP signalling often have opposing effects on cardiac function, partly due to PKA and cGK targets mediating differing physiological outputs (Shah and MacCarthy, 2000).

1.11 Immunity in *Drosophila*

Drosophila are presented with immune challenges through septic injury, and through the ingestion of infected food, termed natural infection. Whereas mammals use innate and acquired immune systems, insects use innate immunity to counter immune challenges (Janeway, 1989). *Drosophila* has informed a great deal of our knowledge towards insect immunity. There are two main types of innate immunity employed by *Drosophila*, the humeral response and the cellular response. The main humeral response is the systemic production of anti microbial peptides (AMPs), which are secreted into the hemolymph, and function to kill infectious microorganisms (Lemaitre et al., 1995). Barrier epithelia are presented with a microbial challenge when food containing microbes is ingested. The generation of ROS eliminates microbes in tissues such as the gut, trachea and Malpighian tubules (Bogdan, 2001; Ha et al., 2005). Melanisation (Nappi and Vass, 1993) and coagulation (Muta and Iwanaga, 1996) occur at the wound site to prevent further infection. The primary cellular response is performed by the haemocytes, which are responsible for phagocytosis (Meister, 2004) and also produce AMPs (Charroux and Royet, 2009; Dimarcq et al., 1997). As well as systemic production of AMPs, they are also produced in epithelial tissues (Tzou et al., 2000).

The best characterised immune response of *Drosophila* is the systemic response (Silverman and Maniatis, 2001). Pathogen detection results in the activation of the NFκB-like Toll or IMD pathways, depending upon the nature of the pathogen. Fungi and gram positive bacteria recognition occurs extracellularly, and results in the cleavage of Spaetzle by microbe-specific serine protease cascades. Cleaved Spaetzle is recognised by the toll receptor, and stimulates the production of the antimicrobial peptide drosomycin through activation of the NFκB factors Dif and Dorsal. Gram negative bacteria are recognised by peptidoglycan recognition protein (PGRP), and through activation of the NFκB homolog Relish, a transcription factor, stimulate the production of the antimicrobial peptide Diptericin. The toll and IMD pathways are summarised in figure 1.12.

Figure 1.12: The Toll and IMD pathways. Toll pathway: Gram positive bacteria and fungi induce a specific protease cascade, resulting in the proteolytic activation of C-106 Spaetzle (Spz). Upon binding of Spz, the Toll receptor forms a dimer. MyD88 interacts with Toll via TIR domains, and initiates a signalling cascade through Tube and Pelle, resulting in the activation of cactus kinase, which phosphorylates cactus, which is then targeted for degradation. This frees the transcription factor Dif, which translocates to the nucleus and initiates AMP transcription.

IMD pathway: Gram negative bacteria are recognised by PGRP-LC and –LE isoforms, which dimerise and initiate a signalling cascade through IMD, dFADD, and Dredd. Dredd can directly activate Relish by cleavage, or can signal through the IKK complex, consisting of Ird5 and Kenny; cleaved Relish translocates to the nucleus, whereupon it initiates transcription of AMPs. Diagram from (Cherry and Silverman, 2006).

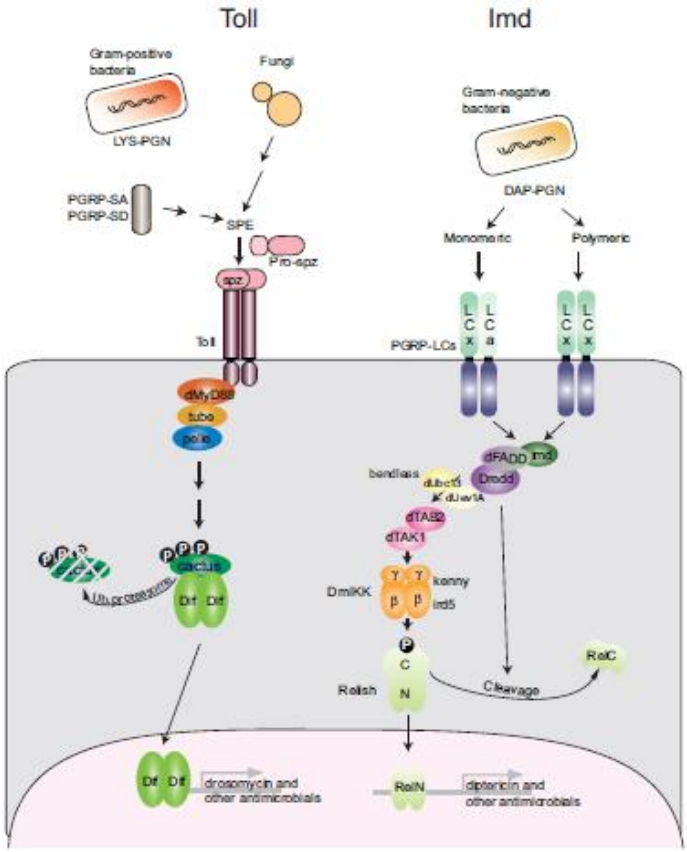

1.11.1 NO modulates innate immunity in *Drosophila*

NO has been shown to activate the IMD pathway, although the mechanism is unclear (Foley and O'Farrell, 2003). NO has been assigned an immune role as both an autocrine and a paracrine messenger (Silverman, 2003); (Foley and O'Farrell, 2003); where a tissue senses an immune challenge, NOS is upregulated, and generates NO, in order to signal to other tissues to induce an anticipatory immune reaction in distal tissues, perhaps signalling via hemocytes (Basset et al., 2000). Underlying its role in immunity, NOS is upregulated following immune challenge to the tubule (McGettigan et al., 2005).

1.11.2 The Malpighian tubule is a critical immune tissue

cGMP plays an critical role in Malpighian tubule immunity (Aitchison, 2008; Dow et al., 1994; McGettigan et al., 2005). NO has been shown to activate the IMD pathway in tubule, and transgenic upregulation of NOS in only principal cells of the Malpighian tubule leads to increased whole organism survival under immune challenge (McGettigan et al., 2005). Unpublished data, which will be discussed in the relevant results chapter, suggests a possible role for *Dm*PDE11 in immunity. This was further investigated during the course of this study, and is discussed in chapter seven.

1.12 Aims

Phosphodiesterase 11 is not well characterised, but is known to be of importance within a number of disorders. PDE11A regulates spermatozoa physiology through an unknown mechanism (Wayman et al., 2005), where inhibition of PDE11A impacts upon sperm quality (Pomara and Morelli, 2005). Certain PDE11A haplotypes are associated with major depressive disorder and affect the response to antidepressant drugs (Luo et al., 2009). Familial mutations within PDE11A may predispose to Cushing syndrome and testicular cancer (Horvath et al., 2009; Libe et al., 2008). Yet the physiological role of *Hs*PDE11 is not well understood.

As the gene model of CG34341 (*Dm*PDE11) is “weakly supported”, the ORF must be verified. Following the verification of *Dm*PDE11, the generation of genetic tools will allow the characterisation of the protein by expression in S2 cells and in *Drosophila*

melanogaster, predominantly focusing on the Malpighian tubule, as this tissue utilises cAMP and cGMP signalling (Dow and Davies, 2003a), and cGMP signalling modulates fluid secretion in the tubule (Davies et al., 1995). Previous data have suggested that *Dm*PDE11 and cGK interact; an aim is to determine the relationship between *Dm*PDE11 and the cGKs using co-immunoprecipitation and peptide arrays. The interaction of *Dm*PDE11 and cGKs may permit each to regulate the function of the other, as *Dm*PDE11 can hydrolyse cGMP (Fawcett et al., 2000), and *Hs*PDE11A4 is subject to regulation by cGK (Gross-Langenhoff et al., 2008). *Dm*PDE11 has also been implicated in immunity; an aim is to acquire further data with regards to how PDE11 might influence the immune reaction. *Hs*PDE11A will be subjected to phylogentic analysis, and the closest homologue to *Dm*PDE11 will be subject to analysis by transgenic expression in *Drosophila*, a tool that should prove valuable for future research into this important enzyme family.

Chapter 2

Materials and Methods

2.1 Drosophila melanogaster

2.1.1 Drosophila stocks

The *Drosophila melanogaster* strains used in this study and their purpose are listed in table 2.1. Lines in grey boxes were existing lab stocks, and those in darker grey were generated during this study. Those in white were supplied by Bloomington stock centre.

Table 2.1: *Drosophila melanogaster* lines used in this study

Strain	Genotype	Description and use
Oregon R	Wild type	Protein, DNA, RNA, survival assays
w^{1118} (Hazelrigg et al., 1984)	w^{1118}	Microinjection
c42 GAL4	w^{-}; +/+; c42	tubule principal cell GAL4
c42 Aequorin GAL4 (Rosay et al., 1997)	*w^{-} aeq/aeq; +/+; c42/c42*	Aequorin/GAL4 expression in principal cells; calciu
UO (Terhzaz, in prep.)	UO; +/+; +/+	tubule principal cell GAL4
Actin GAL4/CyO	w -; ActGAL4/Cyo; +/+	Ubiquitous GAL4
Actin GAL4/GFP CyO	w -; ActGAL4/GFP Cyo; +/+	Ubiquitous GAL4; non-expressors GFP
UAS-DG1	w -; +/+; UASDG1	UAS DG1 overexpressor
UAS-DG2 P1	UASDG2P1; +/+; +/+	UAS DG2 P1 overexpressor
UAS-DG2 P2	w -; UASDG2P1; +/+	UAS DG2 P2 overexpressor
UAS-PDE11 RNAi	w -; +/+; UASPDE11RNAi	UAS PDE11 RNAi
Relish E20 (Hedengren et al, 1999)	w -; +/+; $relish^{E20}$, e^{-}	homozygous relish null with ebony marker; survival a
TS10	w -; Bristle/CyO; TM2/TM6	Balancing
Ato Gal4	w -; +/+; ATO GAL4	paired DC neurons GAL4
D42 Gal4	w -; +/+; D42 GAL4	GAL4: embryogenesis: broad, larvae: motorneurons, interneurons, adult: nervous system
Appl Gal4 (Torroja et al., 1999)	appl GAL4; +/+; +/+	adult and larval neuron specific GAL4
Repo Gal4	w -; +/+; Repo Gal4/Tm3, Sb	glial cell GAL4
Sgs3 Gal4	w -; +/+; sgs3 GAL4	salivary gland GAL4
UAS-HPDE11A3 YFP	w-; Bristle/CyO; H11A3/TM6	UAS human PDE11A3 YFP Overexpressor
UAS-HPDE11A3 YFP	w-; H11A3YFP/Bristle; TM2/TM6	UAS human PDE11A3 YFP Overexpressor
UAS-HPDE11 A3	w-; Bristle/H11A3; TM2/TM6	UAS human PDE11A3 Overexpressor
UAS-HPDE11 A3	w-; 8H11/CyO; TM2/H11A3	UAS human PDE11A3 Overexpressor
11Δ121	w-; 11Δ121/CyO ; +/+	PDE11 deletion line; survival assays

Strain	Genotype	Description and use
UAS-*Dm* RB Long PDE11 YFP	w-; B11LYFP/CyO; +/+	UAS-*Dm* RB long PDE11 YFP overexpressor
UAS-*Dm* RB Long PDE11 YFP	w-; +/+; B11LYFP/Tm5	UAS-*Dm* RB long PDE11 YFP overexpressor
UAS-*Dm* RB Short PDE11 YFP	w-; +/+ ; B11SYFP/Tm5	UAS-*Dm* RB short PDE11 YFP overexpressor
UAS-*Dm* RB Short PDE11 YFP	w-; B11S YFP/CyO ; +/+	UAS-*Dm* RB short PDE11 YFP overexpressor
UAS-*Dm* RB Short PDE11 YFP	w-; B11S YFP ; +/+ ; +/+	UAS-*Dm* RB short PDE11 YFP overexpressor
UAS-*Dm* RC Long PDE11 YFP	w-; +/+ ; RCLYFP/TM5	UAS-*Dm* RC long PDE11 YFP overexpressor
UAS-*Dm* RC Long PDE11 YFP	w-; RCLYFP/CyO; +/+	UAS-*Dm* RC long PDE11 YFP overexpressor
UAS-*Dm* RC Short PDE11 YFP	w-; RCSYFP/CyO; +/+	UAS-*Dm* RC long PDE11 YFP overexpressor
UAS-*Dm* RC Short PDE11 YFP	w-; +/+; RCS/TM5	UAS-*Dm* RC short PDE11 YFP overexpressor
UAS-*Dm* RC Short PDE11 YFP	w-; RCSYFP; +/+ ; +/+	UAS-*Dm* RC short PDE11 YFP overexpressor
UAS-*Dm* RC Short PDE11	w-; +/+; RCS/TM5	UAS-*Dm* RC short PDE11 overexpressor
UAS-*Dm* RC Short PDE11	w-; RCS/CyO; +/+	UAS-*Dm* RC short PDE11 overexpressor

2.1.2 Drosophila rearing

Drosophila were raised in vials or bottles containing standard food medium (recipe in appendix), on a 12 hr: 12 hr light: dark cycle at 22-26˚C, or 18˚C when GAL4 activity proved developmentally lethal.

2.1.3 Generation of balanced transgenic flies

In order to localise P-element insertions and generate stable, balanced transgenic fly lines, homozygous transgenic flies were crossed to the TS10 balancer line (w^-; *Bl*/*CyO*; $TM2e^-$/$TM6Tb^-$), where $TM2e^-$/$TM6b^-$ is ebony. Red eyed f1 progeny were then back-crossed to TS10, and red eyed f2 progeny analysed for markers. Where flies are Bl/CyO and ebony, the insertion is on the X chromosome. Where flies are ebony, with the curly phenotype or the bristle phenotype, the insertion is on the 2nd chromosome. Where flies have the curly phenotype and the bristle phenotype, but are not ebony, the insertion is on the third chromosome. Two flies of the same balancer status were backcrossed to generate balanced transgenic flies.

2.1.4 Dissection of Drosophila tissues

Where tissue was required, 5-7 day old flies were anesthetised on ice, before dissection in sterile Schneider's medium (Invitrogen) using forceps.

2.1.5 Heat shock of Drosophila

Where transgenics were crossed to heat shock GAL4 *Drosophila*, to induce GAL4 expression and subsequently transgene expression, flies were transferred from food vials into screw top 10 ml universals, and were subjected to 3 x 30 min heat shocks in a 37˚C incubator on subsequent days. Following heat shock flies were transferred back to food vials to room temperature to recover

2.1.6 Fluid secretion assays

The diagram below shows the experimental setup used for fluid secretion assays. A dish is half filled with molten wax, which sets. A number of small depressions are made in the wax, and adjacent to these, an array of fine metal pins are arranged a half centimetre away. The dish is filled with mineral oil (Sigma), and each small depression has added to it 9 µl of a 50:50 solution of *Drosophila* saline: Schneider's solution, with a trace amount of amaranth, a red dye that allows visualisation of the bubble formed at the ureter. Drosophila Saline is made from a stock solution stored at -20˚C (7.5 mM NaCl, 20 mM KCl, 2 mM $CaCl_2$, 8.5 mM $MgCl_2$, 10.2 mM $NaHCO_3$, 4.3 mM NaH_2PO_4, 15 mM HEPES (4-(2-hydroxyethyl)-1-piperazineethanesulfonic acid, pH 7.5) by the addition of 20mM glucose. Intact Malpighian tubules are dissected from *Drosophila* as above, and are picked using a fine drawn glass rod; one end is wrapped around the metal pin, and the other is submerged in the bubble, with the ureter mid way between. Once it was established that the tubules were secreting, the secreted drops were removed from the ureter, and a timer started. Every ten minutes, the size of the drops was measured using a microscope graticule. When baseline secretion had been established, cGMP was added to the 9 µl bubble at a concentration of 10^{-3}, for a final concentration of 10^{-4}. Secreted drops were again measured every ten minutes to measure an increase in secretion rate. The process is summarised in figure 2.1.

Figure 2.1: The fluid secretion assay

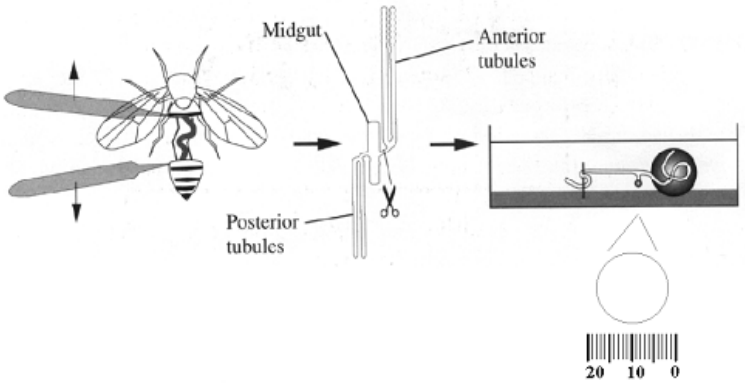

2.1.7 Microinjection

Drosophila transgenics were generated by Bestgene Inc. using the w^{1118} stain of *Drosophila melanogaster*, by co-injection of pP{UAST} and pP{D2-3} plasmids into larvae. Transgenic lines were delivered balanced, or were balanced upon arrival using the TS10 balancing line.

2.2 Escherichia coli

2.2.1 E. coli strains

Table 2.2 lists the strains of *E. coli* used in the course of this study, and their genotype.

Table 2.2: E. coli strains used in this study

Strain	Genotype
DH5a™ subcloning efficiency competent cells (Invitrogen)	F- φ80*lac*ZΔM15 Δ(*lac*ZYA-*arg*F)U169 *rec*A1 *end*A1 *hsd*R17(rk-, mk+) *pho*A *sup*E44 *thi*-1 *gyr*A96 *rel*A1 λ-
DH5a™ library efficiency competent cells (Invitrogen)	F- φ80lacZΔM15 Δ(□lacZYA-argF)U169 recA1 endA1 hsdR17(rk-, mk+) phoA supE44 thi-1 gyrA96 relA1 λ-
One Shot TOP10 competent cells (Invitrogen)	(F- mcrA, D(mrr-hsdRMS-mcrBC), f80lacZ DM15, DlacX74, recA1, deoR, araD139, D(ara-leu)7697,galU, galK, rpsL, (StrR), endA1,nupG)
BL21 pLysS competent cells (Novagen)	hsdS gal (lcIts857 ind1 Sam7 nin5 lacUV5-T7 gene 1)
XL10-gold Kan Ultracompetent cells	Tetr Δ(mcrA)183 Δ(mcrCB-hsdSMR-mrr)173 endA1 supE44 thi-1 recA1 gyrA96 relA1 lac Hte [F´ proAB lacIqZΔM15 Tn10 (Tetr) Tn5 (Kanr) Amy]

2.2.2 Plasmids

Table 2.3 lists the plasmids used in the course of this study, and their purpose.

Table 2.3: Plasmids used in this study

Plasmids used	Purpose
pP{UAST}	germline transformation of coding sequence downstream of UAS (Brand and Perrimon, 1993).
pP{D2-3}	co-transformed with pP{UAST} as transposase source
pP{YFP UAST}	germline transformation of coding sequence downstream of UAS with a C-terminal YFP tag (Kind gift of John Day)
pCR 2.1 TOPO®	TOPO® vector used for sub-cloning
pMT/V5-His-TOPO® (DES)	inducable S2 cell TOPO® expression vector
pAC V5 HIS	Constituitive S2 cell expression vector under control of actin promoter, C terminal V5 and HIS6,
pGEX-6P-1	E. Coli expression vector, fusing ORF to N-terminal GST tag
pET-28c	E. Coli expression vector, fusing ORF to N-terminal His6/thrombin/T7 tag, plus optional C-terminal His6 tag
pcDNA3.1 PDE11A3	Mammalian cell expression vector containing PDE11A3
DES PDE11 RA	DES containing PDE11 RA
DES DG1	DES containing DG1
DES DG2 P1	DES containing DG2 P1
DES DG2 P2	DES containing DG2 P2

2.2.3 Transformation of E. coli

2.2.3.1 Transformation of DH5α™ subcloning/library efficiency competent cells

Cells were thawed on ice, and aliquotted into pre-chilled 1.5 ml falcon tubes to a volume of 50 µl. 50-100 ng of plasmid or 2 µl of ligation reaction were added under sterile conditions, and gently mixed. The cells were incubated on ice for 30 min, and heat shocked for 45 s in a 42°C water bath. The tube was immediately transferred to ice, and following a 2 min recovery step, 250 µl of pre-warmed SOC broth (Invitrogen) was added. The tube

was shaken horizontally at 200 rpm at 37°C for one hour, and spread on a pre-warmed L-agar plate containing the appropriate antibiotic. The plates were incubated, inverted, overnight at 37°C.

2.2.3.2 Transformation of One Shot TOP10 competent cells

Vials of cells were thawed on ice. 2 µl of a TOPO® reaction was added under sterile conditions, gently mixed, and incubated for 30 min on ice. They were heat shocked in a 42˚C water bath for 30 s, and left on ice for 2 min. 250 µl of SOC was added, and the cells were incubated 37˚C on a flat-bed shaker for 1 hour. In the vicinity of a Bunsen burner, cells were plated at a variety of volumes on agar plates (appendix) containing an appropriate concentration and type of selective antibiotic to ensure well spread colonies. 40 µl of a 40 mg/ml X-GAL (5-bromo-4-chloro-3-indolyl-beta-D-galactopyranoside) dissolved in dimethylformamide (DMF) was added to the selective L-agar plate 30 min prior to use where blue/white selection was employed. The plates were incubated, inverted, overnight at 37°C.

2.2.3.3 Transformation of XL10-GOLD

Cells were thawed on ice, and aliquoted into pre-chilled 1.5 ml falcon tubes to a volume of 50 µl. To each tube, 2 µl of the β-Mercaptoethanol mix provided was added, and incubated on ice for 10 min, swirling gently every two min. 50 ng of plasmid or 2 µl of ligation reaction were added, and gently mixed. The cells were incubated on ice for 30 min, and heat shocked in a 42°C water bath for 30 s. The tube was immediately transferred to ice, and following a 2 min recovery step, 250 µl of pre-warmed SOC broth was added. The tube was shaken horizontally at 200 rpm at 37°C for one hour, and spread on a pre-warmed agar plate containing the appropriate antibiotic. The plates were incubated, inverted, overnight at 37°C.

2.2.4 Antibiotic usage

Selection for ampicillin resistance on L-Agar or in L-Broth was performed at 200 µg/ml, from a 100 mg/ml stock solution (w/v) in 50% H_2O, 50% ethanol which was stored at -

20°C. Selection for kanamycin resistance on L-Agar or in L-Broth was performed at 50 μg/ml from a 50 mg/ml solution (Sigma), which was stored at 4°C.

2.2.5 Selection of positive colonies

Individual colonies (white colonies where blue/white selection was employed) were picked under sterile conditions using a sterile toothpick, and added to 3-5 ml of liquid broth containing an appropriate concentration and type of selective antibiotic (1.2.4), and incubated in a flat bed shaker at 37˚C overnight. Transformants were analysed using PCR or restriction digests, detailed below.

2.2.6 Isolation of plasmid DNA

For plasmid purification, where up to 20 μg of plasmid DNA was required, the QIAprep Spin Miniprep Kit was used; where up to 100 μg of plasmid DNA was required, the QIAGEN Midi Kit was used, and where up to 500 μg of plasmid DNA was required, the QIAGEN Maxi Kit was used, following manufacturer's instructions.

2.2.7 E-Z-Prep

A 3 ml overnight culture was generated as detailed above; 1.5 ml of cells was spun down for 60 s at 13,000 x g to pellet the cells, and resuspended by vortexing in 80 μl of EZ lysis buffer (Appendix). After a 10 min incubation, a needle was used to prick a hole in the top of the eppendorf, and the sample was boiled for 1 min in a boiling water bath. Following a 2 min incubation on ice, the tube was centrifuged at 17,000 x g for 10 min. 5 μl of supernatant was used for a diagnostic digest in a total digest volume of 20 μl, and 2 μl was used for a diagnostic PCR.

2.2.8 PCR from colony

Typically one gene specific and one vector specific primers were added at 200 nM to 18 µl of ReddyMix MasterMix (Thermoprime) in a sterile PCR tube to a total of 20 µl. A colony was picked using a sterile pipette tip, and mixed into the PCR mix by pipetting. The tubes were added to a PCR block, set to the following protocol:

92°C 2 min
92°C 30 s
50-65°C 30 s } 30 cycles
72°C 30 s/kb
72°C 5 min

Samples were held at 4°C until they were run on an agarose gel.

2.2.9 Generation of a Glycerol stock

For each plasmid, 2 glycerol stocks were generated. 850 µl of overnight culture was added to a 1.8 ml Ultra Surity Cryo Vial (Alpha Labs), and 150 µl of glycerol was added. The tube was vortexed to mix, and stored at 80°C. To reanimate, the frozen stock was scraped with a sterile pipette tip, and streaked on an agar plate containing the appropriate antibiotic. A colony from this plate was picked and added to 5ml LB containing selective antibiotic to grow overnight.

2.3 Molecular protocols

2.3.1 Oligonucleotide synthesis

Oligonucleotides were synthesised by MWG biotech on a 0.01 or 0.05 µmol scale, and purified using High Purity Salt Free (HPSF) technology. Primers were assessed for quality using Matrix Assisted Laser Desorption Ionisation - Time of Flight (MALDI-TOF)

analysis. Primers were received as a lyophilised pellet, and were resuspended in distilled H_2O to generate a 100 μM stock solution, stored at -20˚C. Further dilution in distilled water to 10 μM gave working aliquots used for PCR. A list of primers used is given in the appendix.

2.3.2 Quantification of nucleic acids

Nucleic acids were quantified using a NanoDrop™ spectrophotometer ND-1000, where an OD_{260} of 1 equals 50 μg/ml of double stranded DNA, and 40 μg/ml of single stranded DNA, or RNA. The spectrophometer was zeroed with the elution buffer used. Purity was measured by the ratio of OD_{260}:OD_{280}, where a reading of >1.8 for DNA and >2.0 for RNA indicated acceptable levels of purity.

2.3.3 Polymerase Chain Reaction (PCR)

Where fidelity of amplified DNA was not a critical issue, Taq pol (NEB) was used. The reaction mix was set up according to manufacturer's instructions; 1x DNA polymerase buffer, dNTPs each at 200 μM, primers at 200 nM each, 50 ng of cDNA / 10 ng of plasmid template, 0.25 U of Taq polymerase, to a final volume of 50 μl with H_2O. Amounts of template DNA varied according to the type of DNA, and the abundance of the desired sequence within the DNA. The tubes were flicked to mix, and briefly centrifuged. Cycling was performed in thin walled 0.2 ml PCR tubes in a Hybaid OmnE, Hybaid PCR Sprint or Hybaid PCR Express-Gradient thermocycler. Cycling procedures were typically

92°C 2 min
92°C 30 s
50-65°C 30 s } 25-30 cycles
72°C 30 s/kb
72°C 5 min

Samples were then cooled to 4˚C.

2.3.4 Pfu PCR

Pfu DNA polymerase (Promega) is a thermostable enzyme which exhibits 3'→5' exonuclease activity, and was thus used for PCR reactions requiring high fidelity. The reaction mix was set up as described in the manufacturer's protocol as follows: single strength *Pfu* DNA polymerase buffer, dNTPs each at 300 μM, primers at 260 nM each, plasmid DNA template up to 10 ng, 1.25 U of *Pfu* DNA polymerase, final volume of 50 μl with H_2O. Cycling procedures were typically:

94°C 2 min

94°C 30 s
50-65°C 30 s } 25-30 cycles

72°C 2 min/kb

72°C 10 min

Samples were then cooled to 4˚C.

2.3.5 Herculase II PCR

Herculase II Fusion DNA polymerase (Stratagene) is a thermostable enzyme which exhibits 3'→5' exonuclease activity, and was thus used for PCR reactions requiring high fidelity and high yield from "difficult," e.g., GC rich template, and thus was frequently used for amplification from cDNA. The reaction mix was set up as described in the manufacturer's protocol as follows: single strength *Herculase* II DNA polymerase buffer, dNTPs each at 400 μM, primers at 250 μM each, 50-500 ng cDNA, 1 μl of *Herculase* II Fusion DNA polymerase, final volume of 50 μl with dH_2O. Cycling procedures were typically

94°C 2 min

94°C 30 s
50-65°C 30 s } 25-30 cycles

72°C 1 min/kb

72°C 10 min

Samples were then cooled to 4˚C.

For all PCRs, annealing temperatures were primer- and template-dependent; new primers were optimised by running a gradient PCR reaction across a range of annealing temperatures. The annealing temperature used gave one strong, clear band when subjected to agarose gel electrophoresis.

2.3.6 Fusion PCR

Fusion PCR was performed in three separate PCR steps. Amplification of DS fragments overlapping by ~50bp was performed with a high fidelity DNA polymerase as above. These fragments were gel purified, and used in a subsequent fusion PCR containing equimolar concentration at ≥0.7µg/50µl, with no primers, with the following PCR protocol:

92˚C, 1 min

92˚C, 30 sec
50-65˚C, 30 sec } 13 cycles

72˚C, 1min/kb

72˚C, 10 min

The product was then PCR purified, and used as a template for full length PCR at 20% of PCR volume, with primers for the extreme ends of the target DNA.

92˚C, 1 min

92˚C, 30 sec
50-65˚C, 30 sec } 30 cycles

72˚C, 1min/kb

72˚C, 10 min

PCRs were performed in a gradient PCR machine, with a spread of annealing temperatures.

2.3.7 Reverse transcription (RT) PCR

RT-PCR was performed as per the standard PCR protocol, with cDNA as the template. For cloning of an ORF, primers were designed between the ATG encoding the transcription start site, and the bases encoding the stop codon. Where the purpose of RT-PCR was to establish the presence or absence of a transcript within a tissue, primers spanning intron/exon boundaries were used, as a control against genomic contamination.

2.3.8 Quantitative PCR (Q-PCR)

2.3.8.1 Plate Setup

To quantify transcription of a gene of interest, Q-PCR was performed using DyNAmo™ SYBR® Green (Finnzymes), a 2x master mix that contains *Thermus brockianus* DNA Polymerase, SYBR Green I, a double stranded DNA binding dye, PCR buffer, 5 mM $MgCl_2$, and a dNTP mix including dUTP. Gene-specific primers were designed to amplify <500 bases across an intron-exon boundary of the gene of interest to ensure only processed mRNA would be quantified by the Q-PCR. These primers were used in a PCR to amplify a band from cDNA; if a single clean band was achieved, this was gel purified, quantified, and used as a standard in the Q-PCR. Each plate was set up on ice, using optical grade PCR strips (MJ Research, MLL-9651), and sealed with ultra-clear strip caps (MJ Research, TCS-0803). Serial 1 in 10 dilutions were performed with the purified band, to generate a

standard curve between 10^{-1} to 10^{-7} ng of template. Alongside this, two blank reactions containing 25 µl SYBR green, 25 µl H_20, and two "primer only" reactions, containing 25 µl SYBR green, 21 µl H_20, 2 µl forward primer, 2 µl reverse primer (each 0.3µM final concentration). For each cDNA condition, 25 µl SYBR green, 20 µl H_20, 2 µl forward primer, 2 µl reverse primer (each 0.3 µM final concentration), and 1 µl of cDNA, typically 500ng total, was set up, each in triplicate. To facilitate quantification against a reference gene, primers were designed against an intron-exon boundary of the ribosomal protein *rp49*, considered to have standard expression across cell types. Three biological replicates were performed on three different plates.

2.3.8.2 Q-PCR

Q-PCR strips were briefly centrifuged in a technico mini centrifuge, and added to the Opticon™ 3 thermal cycler. The following cycling protocol was followed:

Table 2.4: Q-PCR cycling protocol

Step	Temperature	Time		Function
Initial Denaturation	95˚C	10 min		Template denaturation
Denaturation	95˚C	20 s	40 cycles	
Annealing	55˚C	20 s		Determined by gradient PCR
Extension	72˚C	5 s/100bp		
Data aquisition		-		Fluorescence recorded after every cycle
Final extension	72˚C	5 min		
Melting curve	65 - 95˚C	-		Checks specificity of primers

The melting curve was analysed; where more than one clear peak was produced, either for the gene and *rp49*, data was discarded.

Data was analysed using Opticon™ 3 software, following manufacturer's instructions. Absolute quantification of gene expression was calculated by comparison of the threshold cycle C(t) of the gene to that of the standard curve generated by the gene standards of known concentration using an excel spreadsheet. Relative quantification was calculated by comparing the ratio of target gene DNA concentration to *rp49* DNA concentration. Plotted in GraphPad prism 4.0, ±SEM (where control = 1) Statistical significance determined by a 1-way ANOVA test.

2.3.9 Primer list

A list of primers used, their sequence, and their applied use are listed in table 2.5.

Table 2.5: Primers used in the course of this study.

Primer name	Sequence	Use
PDE11 RAF	ATGAAAGTGACACAGAGTGAAGAAAA	PCR of full length PDE11 RA
RCfulllengthNSF	ATGGCATCATCCCAAATA	PCR of full length PDE11
RCfulllengthNSR	TTTTTCAACCGCCATAGCG	PCR of full length PDE11
RbNtoGAFF	ATGGGCCAAGCGGCAA	truncation PDE11 cloning
RbNtoGAFR	CTCGAGCTCGTTGCAAATGT	truncation PDE11 cloning
RCNtoGAFF	ATGGCATCATCCCCAAATAA	truncation PDE11 cloning
RCNtoGAFR	CTCGAGCTCGTTGCAAATG	truncation PDE11 cloning
GafF	ATGGTGCGCACTTTGTGC	truncation PDE11 cloning
GafR	AATGGCCTTCTCGTACATGTG	truncation PDE11 cloning
CofgaflongF	ATGGTGGCAATGGCCAAG	truncation PDE11 cloning
CofGAFshortF	ATGTGGGCAATGGCCA	truncation PDE11 cloning
CofGAFshortR	CTGGGCTGGGTGGCTT	truncation PDE11 cloning
PDE11spliceBF	CCAAGCGGCAAGTATGTGTC	pUAST PDE11 cloning
PDE11spliceR	GGTGTTGTGGCGAGTTGGC	pUAST PDE11 cloning
PDE11spliceCF	CCTCAAAGGCGGATAAATACC	pUAST PDE11 cloning
dPDE11-RBORF F	ATGGGCCAAGCGGCAAGTAT	pUAST PDE11 cloning
dPDE11-RBORF	TTATTTTTCAACCGCCATAGCGG	pUAST PDE11 cloning
dPDE11-RC ORF F	ATGGCATCATCCCCAAATAA	pUAST PDE11 cloning
dPDE11-RC ORF R	TTATTTTTCAACCGCCATAGC	pUAST PDE11 cloning
Pde11ntermRcmyc	TACAGATCCTCTTCTGAGATGAGTTTTTGTT CGCAGAAGATGGCGAACGC	pUAST PDE11 cloning
Pde11nterminusR	GCAGAAGATGGCGAACGC	pUAST PDE11 cloning
Pde11CtermF	GAGGCGTTCGCCATCTTC	pUAST PDE11 cloning
dPDE11cterminusR	CTACAGATCCTCTTCTGAGATGAGTTTTTGT TCTTATTTTTCAACCGCCATAGC	pUAST PDE11 cloning
PDE11RBEcoR1F	AAAGAATTCATGGGCCAAGCGGCAAGTAT	pUAST PDE11 cloning
PDE11RBkpn1R	TTTGGTACCTTATTTTTCAACCGCCATAGCG	pUAST PDE11 cloning
Pde11rbYFPEcoR1F	GAATTCATGGGCCAAGCGGCAAGTAT	pUAST PDE11 YFP cloning
Pde11rcYFPNot1Rn	GCGGCCGCTTTTTCAACCGCCATAGCGGT	pUAST PDE11 YFP cloning
Pde11RCEcoR1F	GAGGAATTCATGGCATCATCCCCAAATAA	pUAST PDE11 cloning
Pde11RCKpn1R	GAGGGTACCTTATTTTTCAACCGCCATAGC	pUAST PDE11 cloning
Pde11RCYFPEcoR1F	GAATTCATGGCATCATCCCCAAATAAC	pUAST PDE11 YFP cloning
Pde11RCYFPNot1Rn	GCGGCCGCTTTTTCAACCGCCATAGCG	pUAST PDE11 YFP cloning
RBF72.47	ATGGGCCAAGCGGCAAGTATGTGTC	pUAST PDE11 cloning
RBR72.79	TTATTTTTCAACCGCCATAGCGGTGGC	pUAST PDE11 cloning
RCF73.39	ATGGCATCATCCCCAAATAACGCGG	pUAST PDE11 cloning
RCR72.79	TTATTTTTCAACCGCCATAGCGGTGGC	pUAST PDE11 cloning
RBNT_EcoRIF	GAATTCATGGGCCAAGCGGCAAGTA	pUAST PDE11 cloning
RCNT_EcoRIF	GAATTCATGGCATCATCCCCAAATAACG	pUAST PDE11 cloning
11NT_BglIIR	CGATTTCGCCAAAGATCTTCCA	pUAST PDE11 cloning
11CT_BglIIF	AGATCTTTGGCGAAATCGAATGC	pUAST PDE11 cloning
11CT_Kpn1R	GGTACCTTATTTTTCAACCGCCATAGCGG	pUAST PDE11 cloning
11CT_Not1NSR	GCGGCCGCTTTTTCAACCGCCATAGCGG	pUAST PDE11 cloning

Primer name	Sequence	Use
dPDE11xho1F	GCTCGAGGTGCGCACTTTG	pUAST PDE11 cloning
dPDE11xho1R	GTATCTTGTGGCACAAAGTGCGC	pUAST PDE11 cloning
dPDE11xho1F	GCTCGAGGTGCGCACTTTG	pUAST PDE11 cloning
dPDE11xho1R	GTATCTTGTGGCACAAAGTGCGC	pUAST PDE11 cloning
ShortCtermRevKpn	GGTACCTCACTGGGCTGGGTGG	pUAST PDE11 cloning
ShortCtermNSRevN	GCGGCCGCCTGGGCTGGGTGGCTTG	pUAST PDE11 cloning
RBR_3475to3492	GGCAACGTTGGAGCCATT	DmPDE11 validation
RBRgap_3475to349	TCATCATCACTGGGCTGG	DmPDE11 validation
RCF_45to63	GGCGAGACGTAAAATTGGC	DmPDE11 validation
RCR_3350to3368	CTGTTGTTGGCAACGTTGG	DmPDE11 validation
RCRgap_3344to336	ATTATCATCATCACTGGGCTG	DmPDE11 validation
Forward_3015to30	GAGCATGACTGTCTGTGATTTGT	DmPDE11 validation
dg1ntFBamHI	GATCCATGCCGCTGGAATGTTGACT	Primers for pET cloning
dg1ntFBamHI	ACGGATCCATGGCCGCTGGAATGTT	Primers for pET cloning
dg1ntRXhoI	CTCGAGTTACTTCCTGCTCTCATCGCC	Primers for pET cloning
dg1ctFEcoRI	CGAATTCGACTAGCCATGAAGCAGGCG	Primers for pET cloning
dg1ctFEcoRI	CGAATTCCTAGCCATGAAGCAGGCG	Primers for pET cloning
dg1ctRSalI	ATATATGTCGACTTAGAAATCCGCATCCCAG	Primers for pET cloning
dg2ntFEcoRI	ATTCGACGTTTCTGCTTTGATCGGC	Primers for pET cloning
dg2ntFEcoRI	TGAATTCATGCGTTTCTGCTTTGATCG	Primers for pET cloning
dg2ntRnotI	GCGGCCGCTTAGATCTGCGTCAGATCCAGAT TC	Primers for pET cloning
dg2ctFSalI	ATA TAT GTC GAC ACG CGA GAT CGT TGA CTG C	Primers for pET cloning
dg2ctFSalI	ATA TAT GTC GAC CGC GAG ATC GTT GAC TGC	Primers for pET cloning
dg2ctRNotI	GCG GCC GCT TAT TAG AAG TCC TTG TCC CAT CCA G	Primers for pET cloning
rbnNotIR	AGT TGG ATC AGC GGC CGC TTA TTG AGA TTT CTC ATA CAG CTG TGC	Primers for pET cloning
middlexhoR	AGA CCT CGA GTT AAC GAT TAT CGC GCA CGC	Primers for pET cloning
endxhoR	AGA CCT CGA GTT ATT ATT TTT CAA CCG CCA TAG C	Primers for pET cloning
rbnEcoRIFET	AGA ATT CGA GGC CAA GCG GCA AGT AT	Primers for pET cloning
rcnEcoRIFET	ATT CGA GCA TCA TCC CCA AAT AAC G	Primers for pET cloning
middleBamHIFET	ACG GAT CCG ACT GGA GAT CAA GCG GAA TCA	Primers for pET cloning
endBamHIFET	ACG GAT CCG AGA TCT GGC CGA TGT CGT G	Primers for pET cloning
modpuast_f	GAA TTC TGC CTC GAG GTT AGA TC	Modify pUAST MCS
500+puast_r	CAG GTT CAG GGG GAG GTG	Modify pUAST MCS
M13 Reverse	CAGGAAACAGCTATGAC	Sequencing primers for TOPO cloning
M13 Forward	GTAAAACGACGGCCAG	Sequencing primers for TOPO cloning

2.3.10 Automated DNA sequencing

DNA sequencing was performed at the MBSU sequencing centre of Glasgow University, using a MegaBACE1000 96 capillary sequencer, using either Big Dye (Applied Biosystems) or ET-Dye Terminator (GE Heathcare) chemistries, both based upon Sanger's dideoxy sequencing method. Construct and primers were supplies at 1 μg and 3.2 pmol

respectively. Constructs were sequenced using primers spaced by 500bp throughout the sequence to achieve 100% sequence coverage. Sequencing results were analysed using Editview 1.0 (Perkin Elmer) and MacVector software.

2.3.11 RNA extraction

For purification of RNA, the RNeasy mini kit (Qiagen) was used, following manufacturer's instructions. mRNA was prepared from either 10 whole flies, 15 heads, 30 brains, 40 Malpighian tubule pairs or 40 hindguts, dissected in Schneider's solution. Tissue was transferred to a 1.5 ml eppendorf containing 350 µl RLT buffer with 1% β-mercaptoethanol on ice, and homogenised with a pestle. Following this, the tissues were subjected to brief bursts of L2 sonication by a microson™ ultrasonic cell disruptor. Tissues other than the tubules were then centrifuged at 4˚C at 16,200 x g for 3 minutes, and the supernatant transferred to a new 1.5ml eppendorf. 350 µl 70% ethanol was added, pippetted to mix, and transferred to an RNeasy spin column. Following this, RNA was purified following manufacturer's instructions, eluted in 25 µl nuclease free water, and quantified using a NanoDrop™ spectrophotometer ND-1000 as described in 1.4.2.

2.3.12 First strand cDNA synthesis

For each amplification of cDNA performed, a further half-volume reaction was performed without superscript, and quantified for ds DNA afterwards to discount contamination. 4 µl 5x First Strand buffer, 2 µl DTT (0.1 M), 1 µl dNTP mix (10 µM each), and 1 µl oligo $DT_{12\text{-}18}$ (500 µg/ml) were added to a nuclease-free centrifuge tube, mixed, and incubated in a PCR block at 65˚C for 5 min. The tube was chilled on ice and briefly centrifuged. 1 µl/200 units of M-MLV Superscript Reverse Transcriptase, 1 µl/40 U of RNase OUT RNase inhibitor, and 1 µg RNA were added, and the mix made up to 20 µl with RNase free water. The tube was incubated in a PCR block at 42˚C for one hour; enzyme was inactivated by a further incubation at 72˚C for 15 min. cDNA was frozen at -20˚C if not used immediately. All reagents were purchased from Invitrogen.

2.3.13 Restriction digests

Digests were performed in a water bath using NEB restriction endonucleases, at the recommended concentration of enzyme, buffer and BSA. Digests were performed at the recommended temperature for that enzyme. When cloning, inserts were cloned using two different restriction sites at the 5' and 3' ends, where possible. Where double digests were performed, digests were either performed in a single reaction, or in sequential digests with PCR purification in between digests, depending on buffer compatibility. Where plasmid or insert was required for a ligation reaction, 2 – 4 µg DNA was added to a total volume of typically 80 µl, to facilitate digest loading into two agarose gel wells. Diagnostic digests were performed in 20 µl total volume with 200 µg DNA. Where plasmid was required for a ligation reaction, 1 U of alkaline phosphatase was added for the final 30 min to make the final amount of enzymes no more than 5% of total digest volume.

2.3.14 Agarose gel electrophoresis of DNA

DNA was separated by running at 100 V in a 1% agarose gel (1% agarose and 0.1 µg/ml ethidium bromide dissolved in 0.5 x TBE (appendix)), using 0.5x TBE as the electrophoresis buffer as described in (Sambrook and Russel, 2001). DNA fragment size was determined by comparison with a 1 kb ladder (Invitrogen). 6x loading dye (0.25 % (w/v) bromophenol blue, 0.25 % (w/v) xylene cyanol, 30 % (v/v) glycerol in H_20) was added to DNA samples to a final 1x concentration prior to loading.

2.3.15 Gel extraction of DNA

DNA was excised from agarose using a sterile scalpel, and purified using the QIAquick Gel Extraction Kit (Qiagen) using manufacturer's instructions.

2.3.16 PCR purification of DNA

DNA was purified from enzymatic reactions using the QIAquick PCR Purification Kit (Qiagen) using manufacturer's instructions.

2.3.17 Ligation reaction

Ligations were performed using the rapid DNA ligation kit (Roche) at a molar ratio of 6:1 insert: vector, with typically a total of 200 ng of DNA. Volume of DNA was brought to 5 µl with EB buffer, and 5 µl of T4 DNA ligation buffer was added, and mixed. To this 0.5 µl of DNA ligase was added, with thorough mixing. This reaction was left at room temperature for 30 min, and frozen at -20˚C if not used immediately.

2.3.18 TOPO cloning

Where TOPO® cloning was performed with a PCR product produced with a proofreading DNA polymerase, the PCR product was incubated at 72°C for 10 min with a non proofreading Taq pol to add A overhangs. "Half volume" reactions were used, where 2 µl of PCR product had added to it 0.5 µl of salt solution, and 0.5 µl TOPO® vector. The reaction was mixed, and left at room temperature for 5 to 30 min. Following transformation the reaction was stored at -20°C if not used immediately.

2.3.19 Modification of plasmid multiple cloning site

Where the restriction sites within a plasmid's multiple cloning site were not suitable for the insert, a new multiple cloning site was designed. Two sets of primers were designed, which represented the new multiple cloning site. These primers overlapped except for 3 bases, which were compatible with the terminal restriction sites of the plasmid's multiple cloning site; upon annealing, the primers form double stranded DNA with sticky ends. Annealing was achieved by incubating equimolar amounts of each primer at 92˚C for 2 min, then a progressively reduced annealing temperature, 65˚C for 1 min, 60˚C for 1 min, then 55˚C for 1 min. The multiple cloning site of the plasmid was removed using the appropriate restriction endonucleases, and the plasmid was subsequently treated with calf alkaline phosphatase. The double stranded DNA was then ligated into the plasmid.

2.3.20 Generation and details of DNA constructs

A list of DNA constructs generated in the course of this study are listed in table 2.6.

Table 2.6: DNA constructs generated in the course of this study

Construct	Source	Cloning method
Dm PDE11 RB EcoRI-XhoI 2.1 TOPO	PCR from cDNA	TOPO
Dm PDE11 RB XhoI-BglII 2.1 TOPO	PCR from cDNA	TOPO
Dm PDE11 RC EcoRI-BglII 2.1 TOPO	PCR from cDNA	TOPO
Dm PDE11 long C term Stop BglII-KpnI 2.1 TOPO	PCR from cDNA	TOPO
Dm PDE11 long C term No stop BglII-NotI 2.1 TOPO	PCR from cDNA	TOPO
Dm PDE11 short C term Stop BglII-KpnI 2.1 TOPO	PCR from cDNA	TOPO
Dm PDE11 short C term No stop BglII-NotI 2.1 TOPO	PCR from cDNA	Digest / ligation
PDE11RBl pP{YFP UAST}	RB EcoRI-XhoI/RB XhoI-BglII/Cl NS	Digest / ligation
PDE11RBs pP{YFP UAST}	RB EcoRI-XhoI/RB XhoI-BglII/Cs NS	Digest / ligation
PDE11RCl pP{YFP UAST}	compiled from RCN and Cl NS TOPO fragments	Digest / ligation
PDE11RCs pP{YFP UAST}	compiled from RCN and Cs NS TOPO fragments	Digest / ligation
PDE11RCs pP{UAST}	compiled from RCN and Cs S TOPO fragments	Digest / ligation
hPDE11A3 pP{UAST}	pcDNA3.1 PDE11A3	PCR w/restriction sites digeted; ligated
hPDE11A3 pP{YFP UAST}	pcDNA3.1 PDE11A3	PCR w/restriction sites digeted; ligated
PDE11RBl pAC V5 HIS	ORF from pP{UAST} construct	Digest / ligation
PDE11RBs pAC V5 HIS	ORF from pP{UAST} construct	Digest / ligation
PDE11RCl pAC V5 HIS	ORF from pP{UAST} construct	Digest / ligation
PDE11RBl pAC V5 HIS	ORF from pP{UAST} construct	Digest / ligation
pGEX-6P-1 RB N	PDE11RBl pP{YFP UAST}	PCR w/restriction sites digeted; ligated
pGEX-6P-1 RC N	PDE11RCl pP{YFP UAST}	PCR w/restriction sites digeted; ligated
pGEX-6P-1 PDE11 middle	PDE11RCl pP{YFP UAST}	PCR w/restriction sites digeted; ligated
pGEX-6P-1 long C term	PDE11RCl pP{YFP UAST}	PCR w/restriction sites digeted; ligated

Construct	Source	Cloning method
pGEX-6P-1 DG1 N	DES DG1	PCR w/restriction sites digeted; ligated
pGEX-6P-1 DG1 C	DES DG1	PCR w/restriction sites digeted; ligated
pGEX-6P-1 DG2 P1 N	DES DG2 P1	PCR w/restriction sites digeted; ligated
pGEX-6P-1 DG2 P1 C	DES DG2 P1	PCR w/restriction sites digeted; ligated
pGEX-6P-1 DG2 P2 N	DES DG2 P2	PCR w/restriction sites digeted; ligated
pGEX-6P-1 DG2 P2 C	DES DG2 P2	PCR w/restriction sites digeted; ligated
pET-28c RB N	PDE11RBl pP{YFP UAST}	PCR w/restriction sites digeted; ligated
pET-28c RC N	PDE11RCl pP{YFP UAST}	PCR w/restriction sites digeted; ligated
pET-28c PDE 11 middle	PDE11RCl pP{YFP UAST}	PCR w/restriction sites digeted; ligated
pET-28c PDE11 long C term	PDE11RCl pP{YFP UAST}	PCR w/restriction sites digeted; ligated
pET-28c DG1 N	DES DG1	PCR w/restriction sites digeted; ligated
pET-28c DG1 C	DES DG1	PCR w/restriction sites digeted; ligated
pET-28c DG2 P1 N	DES DG2 P1	PCR w/restriction sites digeted; ligated
pET-28c DG2 P1 C	DES DG2 P1	PCR w/restriction sites digeted; ligated
pET-28c DG2 P2 N	DES DG2 P2	PCR w/restriction sites digeted; ligated
pET-28c DG2 P2 C	DES DG2 P2	PCR w/restriction sites digeted; ligated
DES DG1-TAP	DES DG1	PCR; F primer w/ tap tag seq
DES DG2P1-TAP	DES DG2 P1	PCR; F primer w/ tap tag seq
DES DG2P2-TAP	DES DG2 P2	PCR; F primer w/ tap tag seq
pP{UAST} DG1-TAP	DES DG1	PCR; F primer w/ tap tag seq
pP{UAST} DG2P1-TAP	DES DG2 P1	PCR; F primer w/ tap tag seq
pP{UAST} DG2P2-TAP	DES DG2 P2	PCR; F primer w/ tap tag seq
pACT2 AD DG2 P1	DES DG2 P1	Digested PCR
pACT2 AD DG2 P2	DES DG2 P2	Digested PCR
pACT2 AD PDE11 RA	DES PDE 11 RA	Digested PCR
pGBK T7 BD DG2 P1	DES DG2 P1	Digested PCR
pGBK T7 BD DG2 P2	DES DG2 P2	Digested PCR
pGBK T7 BD PDE 11 RA	DES PDE 11 RA	Digested PCR

2.4 Schneider 2 (S2) cells

2.4.1 S2 cell maintenance

S2 cells were stored in a 28˚C incubator, in complete Schneider's *Drosophila* Medium

with 10% heat inactivated Foetal Calf Serum (FCS), and were split when they reached a density of 6 – 20 x 10^6 S2 cells/ml. Transfections were performed in a cell culture hood using sterile techniques. Stock was split into new flasks for general maintenance; transfections and selection were kept in the same flasks or plates. The S2 cells/ml of an S2 cell stock was calculated using a haemocytometer (Hawksley).

2.4.2 S2 cell transfections

For each transfection, 3 x 10^6 S2 cells/transfection were spun down in a 15 ml falcon tube at 1000 x g for 3 min, and resuspended in 800 µl of Schneider's *Drosophila* Medium (without serum). 800 µl of cells were added to each well of a 6 well plate. For each experimental condition, a total of 2 µg plasmid DNA was incubated with 10 µl Cellfectin/Cellfectin II (Invitrogen), made up to 200 µl total with Schneider's *Drosophila* Medium. This mixture was vortexed briefly, incubated for 30 min, and then added to the cells in a dropwise fashion, while swirling the plate. The plate was then incubated overnight (for Cellfectin) or for 4 hours (Cellfectin II). Cells were resuspended using a transfer pipette, added to a 1.5ml eppendorf, and spun down for 3 min at 1000 x g. The supernatant was removed, and the S2 cells were resuspended in 3 ml Schneider's *Drosophila* Medium with 10% FCS. Where DES constructs were used these were induced with $CuSO_4$ at a final concentration of 0.7 µM. Time of incubation varied depending on expression level of the plasmid, which was assessed by ICC or western blot.

2.4.3 Generation of stable S2 cell lines

Transfections were performed as above, but with the addition of an equimolar amount of pCoHygro selection vector. Stable cells were selected for using 300 µg/ml hygromycin-B, where the medium was not changed until the cells showed strong resurgence in growth.

2.4.4 Generation of an S2 cell frozen stock

S2 cells were grown to a density of 1 – 2 x 10^7 S2 cells/ml. They were centrifuged at 1000 x g, and resuspended to a density of 1.1 x 10^7 S2 cells/ml in Freezing Medium (45% conditioned complete Schneider's *Drosophila* Medium containing 10% FBS, with 45% fresh complete Schneider's *Drosophila* Medium, and 10% DMSO). 1 ml aliquots in cyrovials were placed in an insulated container, then transferred to a -80˚C freezer overnight. The vials were then stored in liquid nitrogen.

2.4.5 Initiation of S2 cell frozen stock

A frozen S2 cell stock was removed from liquid nitrogen, and thawed in a 30˚C water bath. The vial was washed with 70% ethanol, and the cells added to 5 ml room temperature complete Schneider's *Drosophila* Medium, and stored at 28˚C for 30 min. The cells were resuspended, centrifuged at 1000 x g for 3 min, and transferred to a new flask containing 5 ml Schneider's *Drosophila* Medium with 10% FCS at 28˚C until the cells reached a density of 6 x 10^6.

2.5 Immunoprecipitaions (IP)

2.5.1 Preparation of S2 cell lysates

For S2 cell transfections, each transfection was viewed under 20x magnification to assess cell membrane integrity (as a measure of survival), and resuspended using a transfer pipette. Each transfection was split into two 1.5 ml eppendorfs, and spun down for 4 min at 1000 x g. The supernatant was removed, and the cell pellets were frozen in a -80°C freezer (if there wasn't time to pre-clear overnight). When needed, these cell pellets were resuspended in a suitable volume of ice cold 3T3 lysis buffer (25mM HEPES pH 7.4, 50mM NaCl, 10% glycerol, 1% Triton X-100) containing protease inhibitor cocktail. The lysate was then sonicated on ice. Where background was apparent the buffer could be modified. 3 million S2 cells yielded ~150µg of soluble protein.

2.5.2 Preparation of Malpighian tubule lysates

For each genotype, 200 tubule pairs were dissected, and transferred to a suitable volume of ice-cold 3T3 lysis buffer with 1% (v/v) protease inhibitor cocktail. Tubules were lysed on ice, using a hand held pestle, then by brief L3 sonication. Insoluble material was pelleted by centrifugation at 18,000 x g for 10 min at 4˚C, and the supernatant transferred to a new eppendorf tube. Total protein recovered was ~30µg.

2.5.3 Preparation of whole fly lysate

For each genotype, 10 flies were anesthetized using CO_2, and transferred to a suitable volume of ice-cold 3T3 lysis buffer with 1% (v/v) protease inhibitor cocktail. Flies were lysed on ice, using a hand held pestle, then by three five second bursts of L3 sonication. Insoluble material was pelleted by centrifugation at 18,000 x g for 10 min at 4˚C, and the supernatant transferred to a new eppendorf tube. Total soluble protein recovered was ~30µg.

2.5.4 IP with rabbit serum

Where the IP was performed with a Rabbit polyclonal antibody, 50µl of pre-immune rabbit serum per ml (ideally from a pre-immune sample from the immunized rabbit) was added to each lysate, and incubated at 4°C on a rotator for ≥30 min. During this preclearing step, 10-20µl Protein A-Sepharose 4B Fast flow, from *Staphylococcus aureus* (Sigma)/IP was washed 3x in ice cold lysis buffer, and added to each lysate. The samples were incubated at 4°C on a rotator for ≥1 hour, and then spun down at 8000g. The lysate was removed and transferred to a new tube, where 20-50µl serum was added to each sample, and incubated at 4°C on a rotator for 1 hour. Pre-washed Protein A beads were added as before, and incubated at 4°C on a rotator for 1 hour. The beads were washed 3x in 750µl 3T3 lysis buffer with protease inhibitor, with the wash buffer removed as completely as possible without disturbing the pellet. The pellet was then used immediately if possible, or frozen at -80°C.

2.5.5 With Fixed state proteinA beads

Where the IP was performed with EZview Red αc-Myc Affinity Gel (Sigma), EZ View Red Protein A Affinity Gel (Sigma) was used to preclear in place of Protein A-Sepharose 4B Fast flow; serum was still used because the αc-Myc antibody is Rabbit polyclonal. Where αV5 Agarose conjugate (Sigma) was used for the IP, Protein A Agarose conjugate (Sigma) was used to preclear as above, but with no addition of serum, as the αV5 antibody is a monoclonal.

2.5.6 IP with monoclonal antibodies

Where monoclonal antibodies were used, amounts used was dictated by the recommended concentration in the accompanying protocol. A pool of monoclonal antibodies was used wherever possible, and the concentrations of each were lowered as appropriate. Antibody was added to each sample, and incubated at 4°C on a rotator for 1 hour. Pre-washed Protein A beads were added as before, and incubated at 4°C on a rotator for 1 hour. The beads were washed 3x in 750 µl 3T3 lysis buffer with 1:100 protease inhibitor, with the wash buffer removed as completely as possible without disturbing the pellet. The pellets were then used immediately if possible, or frozen at -80°C.

2.5.7 IP with antibody conjugate

Where antibody-agarose conjugates were used, the IP was performed as before, except there was no antibody incubation before the addition of the antibody-agarose conjugate.

2.6 Western blotting

2.6.1 Preparation of sample

2.6.1.1 Preparation of S2 cell lysates

For S2 cell transfections, each transfection was viewed under 20 x magnification to assess cell membrane integrity at every stage (as a measure of survival), and resuspended using a transfer pipette. Each transfection was split into two 1.5 ml eppendorfs, and spun down spun down for 4 min at 2000 rpm in a Thermo Heraeus centrifuge. The supernatant was removed, and the cell pellets were frozen in a -80°C freezer. When needed, the pellets were resuspended in IGEPAL buffer (150mM NaCl, 50mM Tris, 1% IGEPAL) containing protease inhibitor cocktail. The lysate was then sonicated on ice. An equal volume of Laemmli 2 x buffer (4% SDS, 5% β-Mercaptoethanol, 20% glycerol, 0.004% bromophenol blue, 0.125M Tris-HCl) was then added, and the samples boiled in a boiling water bath for 3 min.

2.6.2 Bradford assay

The Bradford assay was performed on a 96 well plate. Standards from 0-5 µg (typically 0 µg, 0.5 µg, 1 µg, 1.5 µg, 2 µg, 3 µg, 4 µg, 5 µg) were generated in triplicate using Bovine Serum Albumin (BSA), Fraction V (Roche) in a volume of 50 µl distilled H_20. For each protein sample, 1 µl of sample was added to 49 µl H_20 in triplicate. To each well, 200µl of a well mixed 1 in 5 dilution of Bio-rad protein assay dye reaction concentrate (Biorad) in H_20 was added. Absorbance at 590 nm was read using a plate reader; Quanta smart software was used to generate a standard curve, and from this ascertain the concentration of each protein sample.

2.6.3 Sodium Dodecyl Sulfate PolyAcrylamide Gel Electrophoresis

10 or 15 well resolving gels between 6-20% were prepared according to the size of the protein of interest, as according to (Joseph Sambrook 2001). Electrophoresis was

performed in a Biorad Miniprotean 3 Cell electrophoresis system. Samples were run at 50 V until the dye front had settled at the bottom of the stacking gel, and then at 130 V for 1 hour. Prestained Benchmark Ladder (Invitrogen) was used to determine the size of proteins.

2.6.4 Coomassie staining of PAGE gels

PAGE gels were fixed by brief treatment with 40% distilled H20, 10% acetic acid, 50% methanol on a horizontal shaker. The gel was then added to the same mix but with the addition of 0.25% by weight Coomassie Brilliant Blue R-250, and incubated for 4 hours to overnight. The gel was then washed in 67.5% distilled H_20, 7.5% acetic acid, 25% methanol on a horizontal shaker, the solution changed until excess dye was removed, and the protein bands were clear.

2.6.5 Transfer

Hybond P was incubated in methanol for 5 min, and then rinsed in distilled H_20. Western blotting was carried out according to Novex Xcell II Blot Module (Invitrogen) instructions. Transfer was carried out at 60 V for 1 hour, with ice packs to prevent overheating.

2.6.6 Ponceau S Staining

To visualise protein on the membrane, the membrane was rinsed in methanol, then washed in PBST. The membrane was then incubated for 5 min in PBST-10% (v/v) Ponceau with rocking, scanned, rinsed in methanol to remove the stain, and then washed in PBST.

2.6.7 Western blotting

The membrane was briefly rinsed with PBS with 0.1 % (v/v) Tween 20 (PBST), and blocking was performed with PBST containing 5% Marvel Milk (w/v), for three hours, or overnight at 4°C. The membrane was then rinsed in PBST. Incubation with a primary

antibody was performed in block with a suitable amount of primary antibody, for one hour. The membrane was then extensively washed for an hour with frequent changes of PBST. The membrane was then incubated with a HRP-conjugated secondary antibody in block for one hour. The membrane was then extensively washed for an hour with frequent changes of PBST. All steps were performed on a flat bed shaker.

2.6.8 Signal detection

Chemiluminescence detection was performed using the ECL™ Western Blotting analysis system (Amersham Pharmacia) following manufacturer's instructions. Equal volumes of reagent 1 and reagent 2 were mixed, and added to a sheet of Saran wrap. The filter was added protein side down, and incubated for 1 min. The membrane was then wrapped in Saran Wrap, added to a cassette, and exposed to ECL film (Amersham Pharmacia), before development in an X-OMAT film processor.

2.7 Antibody design and purification

2.7.1 Antibody design

Polyclonal antibody epitopes were designed by analysing protein sequence with Abie Pro 3.0: Peptide Antibody Design and Macvector software. 14mers showing high antigenicity were selected, and a cysteine added at the C terminal to facilitate conjugation. Putative sites were blasted against the Drosophila proteome, and any showing 5 consecutive amino acids with identity against other proteins were rejected. Antibodies were generated by PickCell Laboratories, using the Express Rabbit 28 day protocol, and subjected to ELISA testing on peptides attached to Polysorb plates. Serial dilutions of rabbit serum were applied for 2 h at rt. Specific IgGs were detected using gamma-chain specific anti-rabbit IgG-HPRO conjugate.

2.7.2 Isolation of IgG fraction from immune-serum

Antibody was purified as detailed in Day, 2005. A 'HiTrap Protein A HP' column (Amersham) was flushed with 5 ml 0.1 M glycine pH 2.5, passed through at ~2ml/min, then equilibrated with 30 ml of PBS. 5 ml of immune-serum was filtered through a 0.45 μM filter, and then syringed through the column to bind. The column was washed with 30 ml of PBS, and the IgG fraction was eluted with 17 ml of 0.1 M glycine, pH 3.0. The first 2 ml were discarded, and the subsequent 15 ml flow-through was collected in a 50 ml Falcon tube containing 1.5 ml 1 M Tris-HCl pH 8.0. The column was then washed with 5 ml 0.1 M glycine pH 2.5, and stored, sealed, containing ethanol, at 4˚C. The absorbance at 280 nm was read to confirm IgG elution, and the IgG eluate was dialysed overnight against a large volume of PBS in a Slide-A-Lyzer dialysis cassette (Pierce).

2.7.3 Preparation of affinity columns

The bottom cap was fitted to a 10 ml polypropylene column (Pierce) and the column filled with deionised water. A frit was pushed to the bottom of the column using the plunger from a disposable syringe. The water was drained by removing the end cap and 5 ml of Sulfolink slurry (Pierce) was added. When the slurry had sedimented, the slurry buffer was removed down to the surface of the gel and 2 x 25 ml of 50 mM Tris-HCl, 5 mM Na-EDTA pH 8.5 was run through the column, with the end cap replaced when the buffer reached the slurry. 1 mg of antibody-specific peptide was dissolved in 4 ml of 50 mM Tris-HCl, 5 mM Na-EDTA, and added to the column. The top cap was added, and the column subjected to rotation for 15 min at 4˚C. The column was left upright for 45 min, following which the column was drained. 15 ml of 50 mM cysteine in 50 mM Tris-HCl, 5 mM Na-EDTA was added to the column, and rotated for 15 min at 4˚C. The column was set upright and allowed to settle for 45 min. The top cap was removed and the top frit fitted just above the level of the gel. The end cap was removed and the column drained. 60 ml of 1 M NaCl was then run through the column, followed by 50 ml of PBS and then 40 ml of 0.05 % (w/v) sodium azide in PBS keeping the level above the gel. The end caps were fitted and the column stored at 4 ^{o}C until use.

2.7.4 Affinity purification of antibodies

The affinity column was brought to room temperature and the sodium azide was drained. The column was equilibrated by passing through 30 ml of PBS and the IgG fraction was passed through in 5ml batches. Next followed a wash with 30 ml of PBS and finally the antibody was eluted with 0.1 M glycine, pH 3.0. 12 x 1 ml fractions were collected into 12 x 1.5 ml Eppendorfs containing 100 μl Tris-HCl pH 8.0. To determine the yield the absorbance at 280 nm of each fraction was measured and fractions with readings greater than 0.05 were pooled and dialysed overnight against PBS with 0.01 % (w/v) sodium azide. The absorbance at 280 nm was again taken in order to ascertain the final yield using the equation:

Antibody concentration (mg/ml) = O.D 280 x 1.35 mg/ml

Aliquots of the antibodies were made and frozen at -20 ^{o}C until use.

2.7.5 Antibodies generated

The rabbit polyclonal antibodies generated during the course of this study, the epitope chosen, and any additional remarks are listed in table 2.7.

Table 2.7. Antibodies generated during the course of this study, the epitopes used.

Antibody generated	Epitope chosen	Remarks
αDG1	PKYEKDFSDKQQIKD	
αDG2	FDDYPPDPEGPPPDD	Recognises all isoforms
αPDE11	KTKTSQDQEPEEEQQ	Recognises all isoforms
αhPDE11Aa	QRQTKTKDRRFNDE	Recognises *Dm* PDE11-A3 and -A4
αhPDE11Ab	SKGEYDWNIKNHRD	PDE11-A1, -A2, -A3, -A4, -006, -202, -203, -204

2.7.6 Antibodies used in this study

A list of the antibodies used during the course of this study are shown alongside their dilution and use in table 2.8.

Table 2.8: Antibodies used in this study

Antibody used	Dilution and use
PDE11-1 rabbit polyclonal (αPQNGHGLPFGSYQH)	1: 500 (IP)
PDE11-2 rabbit polyclonal (αPTSTQPSDDDNDAD)	1: 500 (IP)
DG1 rabbit polyclonal	1: 500 (IP)
DG2 rabbit polyclonal	1: 500 (IP)
Anti-V5 (mouse monoclonal, Invitrogen)	1:1000 (immunocytochemistry), 1:5000 (western)
Anti-cMyc (mouse monoclonal, Invitrogen)	1:5000 (western)
Anti-GFP (mouse monoclonal, ZYMED)	1:1000 (western)
Alexa FluorÒ568-labelled anti-rabbit IgG H & L (goat polyclonal, Molecular Probes)	1:500 (immunocytochemistry)
Alexa FluorÒ568-labelled anti-mouse IgG H & L (goat polyclonal, Molecular Probes)	1:500 (immunocytochemistry)
HRP labelled anti-rabbit IgG H & L (donkey polyclonal, Amersham)	1:5000 (western)
HRP labelled anti-mouse IgG H & L (sheep polyclonal, Amersham)	1:5000 (western)
Anti-HIS_4 HRP-conjugated 1° antibody (mouse monoclonal, Biorad)	1:5000 (peptide array)

2.8 Immunocytochemistry on tubules

Protocol from {MacPherson, 2001}. Malpighian tubules from 10 flies were dissected in Schneider's medium and transferred to a 1.5 ml eppendorf containing 100 µl of PBS. This was aspirated with care taken not to disturb the tubules. 200 µl of fixation solution (4 % (w/v) paraformaldehyde in PBS) was then added for 30 min. The fixation solution was removed, and the tubules were washed three times in PBS for 30 min each wash, following

a single quick wash. The tubules were then permeabalised for 30 min with PBS, 0.5% triton (v/v), 0.15M NaH_2PO_4, 0.1% Sodium Azide (PBTA) (w/v), changing every 10 min. The tubules were then incubated in PBS, 0.3 % (v/v) Triton X-100, 0.5 % (w/v) BSA (PAT) for 3 h at RT. Hybridisation in 1° antibody (at an appropriate concentration in PAT) was carried out overnight at 4°C. Tubues were then washed 4 x in PAT for 2 h, and then blocked with PAT for 3 h. Incubation with 2° antibody was performed in PAT for 1 h to overnight. The tubules were washed three times with PBTA for 30 min each wash. Where nuclei staining was required, the tubules were incubated with DAPI (500 ng/ml in PBS) for 2 min, and washed three times with PBTA for 30 min each wash. Finally, the tubules were then washed 2 x 10 min in PBS. All solutions were filter sterilised using a 0.22 μm filter.

2.8.1 Mounting

Tubules were mounted in glycerol mounting medium. The tubules were incubated in 20 % glycerol in PBS for 15 min. Around 2mm of a 1ml pipette tip was cut off, and the tubules were then pippetted into a dish with 50% glycerol. Slides or glass-bottomed dishes had 80% glycerol added, and the tubules transferred to these. Where coverslips were required, they were sealed with glycerol/gelatin (Sigma).

2.9 Survival assays

2.9.1 Septic challenge with a needle

A single pellet of freeze-dried pellet of *E. coli* (Selectrol freeze-dried pellets, TCS biosciences) was added to 5 ml LB-broth, and grown overnight at 37˚C with shaking to stationary phase. *E. coli* was harvested by centrifugation, the LB-broth removed, and the pellet resuspended in a small volume of B broth. 5-7 day old flies were separated into vials containing 30 flies each. These were anaesthetised on the gas pad. A thin-bore needle (BD Microlance ™ 3, 26 G x ⅝) was dipped into the bacterial culture; the flies were stabbed just below the first abdominal turgite. Control stabbing with a sterile needle was carried out on an equal number of flies to monitor stabbing-induced death. Survival was monitored at least daily. Flies were tipped into fresh vials daily.

2.9.2 Septic challenge with microinjection

A single pellet of freeze-dried pellet of *E. coli* (Selectrol freeze-dried pellets, TCS Biosciences) was added to 5 ml LB-broth, and grown at 37˚C with shaking to an OD_{600} of 2.0. The *E. coli* was harvested by centrifugation, and resuspended in an equal volume of PBS. Flies were injected with 69 nl bacteria using a Nanoject II (Drummond Scientific) mounted to a micromanipulator. Microinjection needles (N-51-A glass capillaries) were pulled using a moving coil microelectrode puller (Campden Instruments limited). The tip of the needle was broken by touching to the flat plane of a pair of forceps, and the needle was backfilled with mineral oil prior to the uptake of bacteria. Where possible, the same needle was used for every fly. The site of injection was just below the first abdominal turgite. 30 flies/genotype were used, and transferred daily to fresh vials.

2.10 Enzymatic assays

2.10.1 $[Ca^{2+}]_i$ measurements in aequorin expressing tubules

Measurement of $[Ca^{2+}]_i$ in the Malpighian tubules was performed using transgenically expressed aequorin, following the method detailed in {Rosay, 1997}. To reconstitute intracellular aequorin, 30 tubules from 5-7 day old adults were dissected in Schneider's medium and placed in 160 μl of Schneider's solution with coelenterazine added to a final concentration of 2.5 μM. Samples were then incubated in a rack wrapped in tin foil for 3 h. Bioluminescence recordings were carried out using an LB9507 luminometer (Berthold Wallace). To monitor tubule condition and control for transients initiated by the injection process itself, samples were 'mock' injected with 25 μl of Schneider's, before injection with the appropriate agonist at the desired concentration, and bioluminescence recorded for 20 min. Tubules were then disrupted with 300 μl lysis solution (1% (v/v) Triton X-100, 100 mM $CaCl_2$); integration of total counts allowed the calculation of total aequorin levels. Ca^{2+} concentrations for each time point in an experiment were calculated by backward integration, using a program written in Perl based on work previously described by {Button, 1996}, and plotted using Excel or GraphPad prism.

2.10.2 PDE assays

PDE assays were performed as per the protocol detailed in {Day, 2005}.Samples were prepared as above, in KHEM buffer (50 mM KCl, 10 mM EGTA, 1.92 mM MgCl2, and 50 mM HEPES), containing protease inhibitor cocktail (Sigma) at a 1:100 dilution. Protein samples were added at equal concentrations to 1.5 ml eppendorfs in a total of 50 µl on ice, with two control tubes containing 50 µl KHEM buffer for each substrate concentration. A 2 x stock solution was generated by adding the appropriate amount of 3', 5'-cyclic adenosine monophosphate, or 3', 5'-cyclic guanosine monophosphate (sigma) to 20 mM Tris-Hcl, 10 mM $MgCl_2$ pH 7.4. To this solution, [^{3}H] cGMP or [^{3}H] cAMP was added at 3 µCi/ml. 50 µl of substrate was added to the protein samples, and mixed by flicking the tubes. Phosphodiesterase activity was stimulated by incubation in a 30˚C water bath for 20 min. Samples were transferred to a boiling water bath for 2 min to denature the enzyme, and were then cooled on ice. 25 µl of snake venom (diluted 1:10 from a 10 mg/ml stock solution (Sigma)) was added to each sample, the tubes flicked to mix, and transferred to the 30˚C water bath for a further 10 minutes, to remove phosphate groups from AMP or GMP. Dowex ion exchange resin (Sigma) diluted 1:1 in water was further diluted 1:2 with ethanol, and 400 µl was added to each sample. Tubes were vortexed, incubated on ice for 15 min, and vortexed again. Tubes were then subjected to centrifugation at 13,000 x g, 4˚C for 2 min, and 150 µl of supernatant was removed from each sample, and added to a fresh eppendorf containing 1 ml Ecoscint ORIGINAL scintillation fluid (National Diagnostics), with a further two "substrate" eppendorfs generated by adding 50µl substrate. Each tube was vortexed to homogeneity, and added to a beta scintillation counter set to record ^{3}H counts for 1 min / sample. Counts should not exceed 18,000 counts / min after subtraction of blanks to represent less than 20% of substrate hydrolysed.

2.10.3 Calculation of PDE activity and kinetic parameters

Specific PDE activity was calculated using the following formula:

$$A = \frac{2.61 \times \left(\frac{(C - B)}{S} \right) \times N \times 10^{12} \times \left(\frac{1000}{P} \right)}{t}$$

Where

A = specific PDE activity (pmol cGMP or cAMP/mg/min)

C = sample value (CPM)

B = blank value (CPM)

S = substrate value (CPM)

N = cAMP or cGMP in substrate (moles)

P = protein (μg)

t = time (min)

2.24 Cyclic GMP-dependent protein kinase assay

The cyclic GMP-dependent protein kinase activity of Malpighian tubules was determined by direct measurement of radiolabelled phospho-transfer to a short peptide sequence substrate, homologous to sequence of a bovine PDE 5 cGK phosphorylation site, as detailed in {MacPherson, 2004}. Approximately 400 tubules per sample were dissected and homogenised on ice in 20 μl of homogenisation buffer (20 mM Tris (pH 7.5), 250 mM sucrose, 2 mM EDTA, 100 mM NaCl, 50 mM β-mercaptoethanol, 1:100 dilution of protease inhibitor cocktail (Sigma)). The protein concentration of each sample was measured by Bradford assay, and standardised by addition of homogenisation buffer. Two stock solutions of kinase assay buffer were prepared fresh, with and without 1 μM cGMP. This comprised 20 mM Tris-HCl, pH 7.5, 1 mM EDTA, 2 mM EGTA, 10 mM magnesium acetate, 1 nM PKA inhibitor (TYADFIASGRTGRRNAI-NH_2), 20 μM ATP, 1 mM zaprinast, 1 μM sildenafil, 1 mM DTT, 0.2 μg/ml GLASS-tide (RKRSRAE, Calbiochem), 0.5-2 μl of [γ-^{32}P] ATP (370 MBq/ml, to an approximate specific activity of 4000 cpm/pmol ATP).

Reaction samples were generated by the addition of 40 µl kinase assay buffer to 5 µl (approximately 30 mg of protein) homogenised tubule sample in 500 µl eppendorfs. Two sets were generated, one with and one without cGMP in the reaction buffer. Sample blanks consisted of 40 µl reaction buffer and 5 µl homogenisation buffer. Kinase activity was stimulated by incubation for 30 min in a 30˚C block, after which 35 µl of each sample was spotted onto individual squares of P81 paper (Whatman, Maidstone, Kent) labelled with pencil, and allowed to dry on a tray with benchtop paper, facing absorbent side up under a plastic shield for 45 min. To calculate specific activity of the radiolabelled ATP at the end of the reaction, 5 µl of several random samples (representative of 1/9 total count) were spotted onto individual squares of P81 paper ('total count'), and allowed to dry as above.

The reaction samples were washed for 3 x 5 min in 75 mM phosphoric acid, then washed once for 15-20 s in ethanol and allowed to dry. All squares of paper, including the total count samples, were then transferred to scintillation vials, with the addition of 3 ml scintillation fluid and counted in a scintillation counter (Beckman, High Wycombe, UK) set to record ^{32}P for 60 s.

Specific activity of [γ-^{32}P] ATP was calculated (9 x mean c.p.m. of total count squares/[ATP] in reaction) and used to calculate protein kinase activity (pmol ATP min^{-1} μg^{-1} protein) as follows:

kinase activity = γ-^{32}P $\frac{\text{cpm (total) x 45}}{5}$ (45 initial radiation mix put in; 5 amount of

(usually 20) µM moles ATP radiation mix added to substrate paper)

0.37 mBq usually used.

= 1µL / ml

→ ½ life 14 days; double this amount/14 days

Activity = (γ-^{32}P $\frac{\text{cpm – blank cpm x 35}}{\text{Specific activity x total protein x time x 45 (assay buffer amount)}}$)

Where

C = sample counts per minute

B = blank counts per minute

V = sample volume on filter

R = reaction time in minutes

P = protein amount in μg

S = specific activity

2.11 Peptide arrays

The peptide array protocol given is based upon {Bolger, 2006}.

2.11.1 SPOT synthesis of peptides

Peptide libraries comprising amino acid 25mers were generated on a Whatman 50 cellulose membrane support by automatic SPOT synthesis using Fmoc (9-fluorenylmethyloxycorbonyl) chemistry with the Autospot Robot ASS 222 (Intavis Bioanalytical Instuments).

2.11.2 Expression of HIS_6 tagged proteins

HIS_6 tagged proteins were generated by transfection of the expression vector pET-28c (cloned with appropriate ORF) into BL21 (DE3) pLysS competent cells following manufacturer's instructions. Cells were thawed on ice, mixed, and 100 μl aliquots were generated in pre-chilled 1.5 ml culture tubes. To each tube, 1.7 μl of β-mercaptoethanol was added and mixed. 50ng of DNA was then added to each tube, and flicked to mix. Tubes were stored on ice for 10 min, and heat-shocked in a 42°C water bath for 45–50 s in a water bath. Tubes were then transferred to ice for 2 min. 900μl of (4°C) SOC medium was added to each transformation reaction, and the tubes were incubated for 60 minutes at 37°C on a horizontal shaker at 225rpm. Cells were plated on antibiotic plates, and left, inverted, at 37˚C overnight.

2.11.3 Analytical-scale growth

Individual cultures were added to 3 ml L. Broth, and grown to an OD_{600} of ≥0.6 – ≤1.0. From this 3 ml, 1 ml was removed, from which 100 µl was centrifuged at 18,000 g for 3 min and the pellet used as a non-induced control, and 900 µl were used to generate a glycerol stock as detailed in materials and methods. The remaining 2 ml culture was induced by the addition of IPTG (typically 0.1 mM) and incubated for a further 2 h with shaking at 37˚C. Two 1 ml aliquots were centrifuged at 18,000 g. One of these pelltets was lysed in IEPAL lysis buffer, and one lysed in native lysis buffer using L3 sonication, both with protease inhibitor, and lysed on ice. These were run alongside the non induced control (also lysed in IGEPAL with an identical dilution factor) on an SDS page gel, and western blotting was performed with the appropriate antibody. All conditions were individually optimised for each fusion protein.

2.11.4 Purification-scale growth

Following optimisation of the growth and induction protocol, growth was performed on a large scale to facilitate protein purification. Growth was performed as above, except the 3 ml culture was used a starter culture. From this, 100 µl was added to 50 ml L. Broth containing the appropriate antibiotic, and was incubated at 37˚C with shaking to an OD_{600} of ≥0.6 – ≤1.0. The culture was induced by the addition of IPTG (typically 0.1 mM) and incubated for a further 2 h with shaking at 37˚C. Cells were harvested by centrifugation at 3,000 x g for 5 min at 4˚C.

2.11.5 Native cell lysis

The 50 ml cell pellet was resuspended in 8 ml native lysis buffer. 8 mg lysozyme was added to the cell pellet, and incubated on ice for 30 min. Cells were lysed by L3 sonication on ice. To reduce viscosity, 10 µg/ml RNase A and 5 µg/ml DNase I (Invitrogen) were added, and mixed. Insoluble material was pelleted by centrifugation at 3,000 x g for 15 min, at 4˚C, and the supernatant used for protein purification.

2.11.6 Preparation of Ni^{2+}/NTA columns

HIS_6 tagged peptides were purified using 2 ml Ni^{2+}/NTA agarose (Invitrogen) immobilised in a disposable chromatography column, under native conditions, following manufacturer's instructions. 10 ml Ni^{2+}//NTA Columns were prepared by pipetting 1.5 ml of well-mixed resin into a 10-ml Purification Column with a frit at the bottom. The resin was allowed to settle, and the supernatant was aspirated. 6 ml distilled water was added to the column, and the resin resuspended by tapping the column. The resin was allowed to settle, and the supernatant again removed. 6 ml Native Binding Buffer (50 mM NaH_2PO_4, pH 8.0, 0.5 M NaCl) was then added to the column, and the resin resuspended by tapping the column. When the resin had settled, the supernatant was removed and the column stored at 4˚C until use.

2.11.7 Purification of HIS_6 tagged peptides

8 ml lysate was added. The column was rotated at 4˚C for 30–60 min. The resin was allowed to settle, and the supernatant aspirated, and stored for SDS-PAGE analysis. The resin was then washed with 8 ml Native Wash Buffer (50 mM NaH_2PO_4, pH 8.0, 0.5 M NaCl, 10 mM Imidazole), and allowed to settle. The supernatant was aspirated and again saved for SDS-PAGE analysis. This wash was repeated three times. The column was then clamped in a vertical position, and the bottom cap of the column was removed. The protein was eluted with 8–12 ml Native Elution Buffer (50 mM NaH_2PO_4, pH 8.0, 0.5 M NaCl, 250 mM Imidazole), which was collected in 1 ml fractions. These were analysed by SDS-PAGE, and stored at 4˚C with protease inhibitors until use.

2.11.8 Overlay experiments

The array was bathed in ethanol for 5-10 min, and equilibrated in TBST (50mM Tris, 150 mM NaCl 0.1% Tween-20 (v/v),pH 7.5) in a 10 min wash on a flat bed shaker. The array was then blocked in 5% Marvel-TBST (w/v), 0.1% Tween-20 (v/v) for two hours. After a brief rinse with TBST, recombinant HIS_6 tagged proteins were diluted at 10 μg/ml in 1% Marvel-TBST (w/v) 0.1% Tween-20 (v/v), applied to the array in a sealed bag, and incubated overnight with shaking at 4°C. Following 3 x 15 min washes with TBST, an

anti-HIS_4 HRP-conjugated 1° antibody (Biorad) was applied to the array, diluted 1:5000 in 1% block. This was incubated in a sealed bag at 4°C for two hours. Following 3x15 min washes in TBST, the array was treated with ECL as in an Immunoblot, and several different exposures were obtained.

2.11.9 Stripping arrays

Stripping buffer (0.31g DTT 2g SDS 0.75g Tris-HCl in 100ml H_20, pH 6.8) was pre-heated to 70°C and applied to the array, face up in a hybridisation tube. The arrays were bathed with rotation in a hybridisation oven set to 70°C for 30 min. The stripping buffer was removed, and the array was briefly rinsed twice, then for 2 x 10 min, in TBST. The array was then removed, dried on blue roll on the non-protein side, and stored, sealed, at 4°C; arrays were stripped and reused a maximum of 4 times. When needed for reuse, the membranes were bathed in ethanol and incubated in TBST as before.

2.12 Phylogenetic analysis

Phlogentic analysis was performed using ClustalW alignment in MacVector, using a Gonnet matrix with the default settings (open gap penalty = 10, extend gap penalty 0.1, delay divergent 40%, using end gap separation, residue specific penalties and hydrophilic penalties). A best tree phylogram was generated using neighbour joining tree building, and uncorrected “p” distance calculation. As a control bootstrap analysis (1000 repetitions) was performed.

Chapter 3

Analysis of *Dm*PDE11RA

3.1 Summary

This chapter describes the work done on the *Drosophila melanogaster* dual specificity phosphodiesterase PDE11RA. The PDE11 family was discovered in 2000. It is a dual specificity phosphodiesterase, but the *in vivo* function of the enzyme is currently not well understood. *Drosophila melanogaster* utilises cAMP and cGMP signalling to control numerous vital processes, which are well studied in the organism. As such, *Drosophila* should prove a useful tool to reveal the function *in vivo* function of PDE11.

Difficulties were encountered in proving that *Dm*PDE11RA was in fact a *bona fide* PDE, which was likely explained by Flybase release 5.2 (http://flybase.org/), which replaced the RA transcript with two newly predicted transcripts, RB and RC, as detailed in chapter four. The aims of my PhD when this enzyme was shown to be falsely predicted did not change, save the need to clone the newly predicted RB and RC isoforms, and from these repeat any necessary subcloning in order to perform subsequent experiments. As such this chapter essentially serves as a blueprint for the work done on the RB and RC transcripts, although limited time dictated that some experiments be prioritised, and other experiments were replaced because they did not appear to work, or had been superseded by alternative techniques.

3.2 Introduction

Phosphodiesterases are the only known enzyme responsible for cyclic nucleotide hydrolysis, and as such are of great importance in the modulation of cyclic nucleotide signalling. The PDE11 phosphodiesterase family is the most recently discovered of the PDEs. Discovered in 2000 (Fawcett et al., 2000a; Hetman et al., 2000; Yuasa et al., 2000b), its function is not well understood. It is a dual specificity enzyme, with four isoforms in human, and one in *Drosophila melanogaster*.

Drosophila has been used to great effect in the study of PDE4, known as dunce in *Drosophila.* Furthermore, many phenotypes in *Drosophila* have been linked to both cAMP-, and cGMP-dependent processes and enzymes. Yet until 2005, only two PDEs had been identified in *Drosophila*, PDE1, a Ca^{2+}/Calmodulin sensitive, dual specificity PDE (Walter and Kiger, 1984), and PDE 4, dunce, a cA-PDE (Davis et al., 1989). Work undertaken in the Dow/Davies lab revealed that *Drosophila* expresses six of the PDE

families; PDE 1, PDE 4, PDE6 (cG-PDE), PDE 8 (predicted cA-PDE), PDE 9 (predicted cG-PDE), and PDE11 (dual specificity PDE) (Day et al., 2005). These genes showed high sequence similarity with their mammalian counterparts, with amino acid identity ranging from 26 – 47% (34 – 66% similarity). However sequence identity in the catalytic domain was higher at 51 – 77% sequence identity (69 – 96% similarity). The lower number of PDE genes in *Drosophila* should result in lower redundancy than mammalian systems, and thus make the elucidation of function easier. These genes show widespread expression (http://www.flyatlas.org/), underlying their importance (table 3.1).

Table 3.1: Tissue expression profiles of the *Drosophila* phosphodiesterases. Data from (Chintapalli et al., 2007)

	PDE1	dunce	PDE6	PDE8	PDE9	PDE11
Tissue	Enrichment					
Brain	0	4.1	7.3	5.4	8.9	2.5
Head	0.4	1.3	2.5	1.9	4.6	1.2
Eye	0.23	1.83	0.91	1.79	6.55	3.09
Thoracicoabdominal ganglion	0	3.3	8.9	3.3	13	1.5
Salivary gland	0.06	6.07	2.23	1.45	2.96	2.53
Crop	0	0.9	0.8	2.4	2.9	1.7
Midgut	6	0.8	0.5	1.9	0.6	1.8
Tubule	1	1.5	2.1	3.7	2	1.5
Hindgut	1.8	0.7	2.1	3.5	0.8	2.7
Heart	0.9	2.37	1.34	2.36	6.21	3.14
Fat body	1.36	0.79	3.08	2.2	5.15	0.92
Ovary	0	1	0.1	0.5	0.4	1.8
Testis	0	0.2	0.1	2.9	1.8	0.4
Male accessory glands	0.5	0.8	1.4	1.5	1.6	0.7
Virgin spermatheca	1.56	0.79	4.55	0.69	7.17	0.99
Mated spermatheca	1.49	0.9	3.9	0.75	4	1.04
Adult carcass	0.6	1.6	1.3	2.3	3.9	1
Larval CNS	0.01	1.87	1.82	2.46	2.43	0.75
Larval Salivary gland	1.12	0.8	0.28	0.47	4.21	1.66
Larval midgut	6.81	0.86	0.11	1.79	2.4	0.86
Larval tubule	1.1	0.7	0.3	3.1	3.8	1.7
Larval hindgut	2.15	0.89	0.49	2.31	1.89	1.63
Larval fat body	0.2	0.5	0.3	1.1	4.5	0.7
Larval trachea	0.05	1.75	0.14	3.48	5.35	1.48
Larval carcass	0.01	3.49	2.58	3.25	0.99	0.73
S2 cells (growing)	0	1.05	0.01	6.78	3.67	2.31
Whole fly	1	1	1	1	1	1

The number of cG-PDEs represented above is reflected in the numerous processes that are modulated by cGMP in *Drosophila*. These include fluid secretion of the Malpighian tubule

(Davies et al., 1995), feeding behaviour (Osborne et al., 1997), immunity (McGettigan et al., 2005), hypoxia (Dijkers and O'Farrell, 2009), and nervous system signalling (Bicker, 1998).

3.3 *Dm*PDE11RA

CG34341 encodes *Dm*PDE11RA, a gene spanning 9kb at position 37A1 on chromosome 2 (Figure 3.1).

Figure 3.1: Ensemble CG34341/*Dm*PDE11RA gene model. http://www.ensembl.org/*Drosophila*_melanogaster/geneview?gene=CG34341. Accessed 04.03.2008.

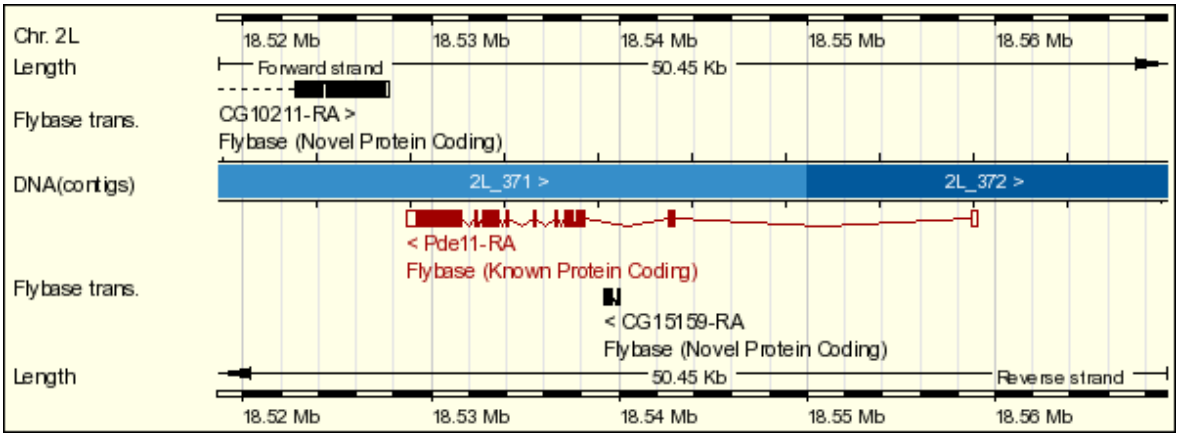

The expression profile of *Dm*PDE11 is shown in table 3.2.

Table 3.2: PDE11 expression in *Drosophila melanogaster*. Table showing enrichment of *Dm*PDE11 expression in each tissue when compared to whole fly (Chintapalli et al., 2007).

	PDE11
Tissue	
Brain	2.5
Head	1.2
Eye	3.09
Thoracicoabdominal ganglion	1.5
Salivary gland	2.53
Crop	1.7
Midgut	1.8
Tubule	1.5
Hindgut	2.7
Heart	3.14
Fat body	0.92
Ovary	1.8
Testis	0.4
Male accessory glands	0.7
Virgin spermatheca	0.99
Mated spermatheca	1.04
Adult carcass	1
Larval CNS	0.75
Larval Salivary gland	1.66
Larval midgut	0.86
Larval tubule	1.7
Larval hindgut	1.63
Larval fat body	0.7
Larval trachea	1.48
Larval carcass	0.73
S2 cells (growing)	2.31
Whole fly	1

Drosophila PDE11 shows widespread expression in the fly, with enrichment in brain, eye, salivary gland, heart, gut tissues, and Malpighian tubules (Chintapalli et al., 2007). Likewise, *H. sapiens* PDE11 shows widespread expression, and is enriched in the pituitary gland, the salivary gland, testis, liver and kidney (D'Andrea et al., 2005; Fawcett et al., 2000b).

3.3.1 The Expressed Sequence Tag SD13096 encodes the entire PDE11RA ORF

When attempts to clone the full length ORF of PDE11RA were undertaken (Day, 2005), two incomplete Expressed Sequence Tags (ESTs) were available that included sequence extending from approximately half way through the ORF through to the poly-A tail and

3’UTR. Attempts to clone the 5’ end of the gene using Reverse Transcriptase-Polymerase Chain Reaction (RT-PCR) and Rapid amplification of 5' complementary DNA ends (5’ RACE) on the available ESTs failed. The EST SD 10396 was released by the BDGP EST sequencing program concurrently with these efforts. SD 10396 is a 5.8Kb EST, containing sequence present in the previously released, incomplete *Dm*PDE11RA ESTs, but also incorporating a 5’ UTR, and an in-frame start codon within two novel 5’ exons. A Northern blot of PDE11RA produced one band of approximately 5.8kb; as the sizes matched it was accepted that SD13096 encodes the entire *Dm*PDE11RA ORF. However, expression of full-length protein in S2 cells was not achieved (Day et al., 2005).

3.3.2 *Dm*PDE11RA encodes a protein of the predicted size

*Dm*PDE11RA was sub-cloned from the full length EST SD13096 into *Drosophila* Expression System (DES) pMT/V5-His-TOPO vector in-frame with the C-terminal V5 and His tags (primers used listed in materials and methods table 2.5). Two constructs were generated; one full length and one N terminal construct extending to the end of the catalytic domain. These constructs were expressed in *Drosophila* S2 cells to verify expression (figure 3.2).

Figure 3.2: Western analysis of pMT/V5-His *Dm*PDE11RA transfected S2 cells. Lanes 1 + 2: N terminal half of *Dm*PDE11RA-V5 (expected size 95kDa) Lanes 3 + 4: Full length *Dm*PDE11RA-V5 (expected size: 173kDa). Antibody used anti-V-5 mouse monoclonal.

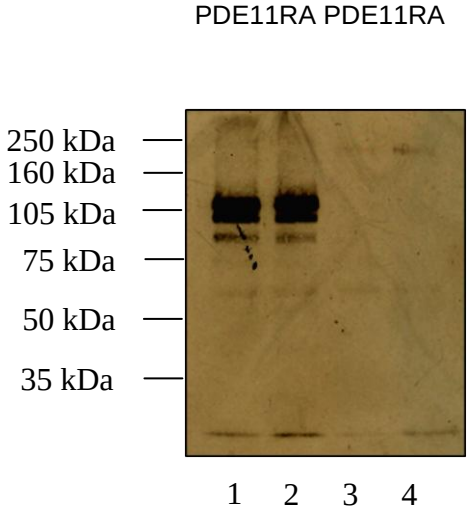

When S2 cell lysate was subjected to western analysis, the full length protein (lanes three and four), predicted to be 173kDa, showed one faint band at approximately the correct size, and an equally faint band around 60KDa, which potentially represents a breakdown product. The faintness of the band can be attributed to an extremely low transfection efficiency of less than 5%, determined by immunocytochemistry of anti-V5 antibody-probed transiently transfected S2 cells, where ≥95% of DAPI-stained cells showed no fluorescence. The N terminal construct was predicted to yield a protein of 95kDa. One band was produced at approximately this size, with two additional bands, one over 100kDa and one around 80kDa. The larger band may be explained by post translational modification, such as phosphorylation. The smaller band may be explained by an alternative in-frame start codon, 267bp into the ORF. Alternatively, as PDEs usually run to a larger size than that predicted under SDS-PAGE analysis, bands other that the largest may again represent breakdown products.

3.3.3 *Dm*PDE11RA shows cytoplasmic localisation

Full length *Dm*PDE11RA tagged with a V5 epitope tag was transiently transfected into S2 cells. These were subjected to immunocytochemistry in order to determine protein localisation (figure 3.3).

Figure 3.3: Subcellular localisation of *Dm*PDE11A-V5 in S2 cells. S2 cells were transiently transfected with pMT/V5-His *Dm*PDE11RA. Subcellular localisation of the protein was ascertained by staining with anti-V5 monoclonal antibody, TRITC secondary (Red). Nuclei were stained with DAPI (blue). Two examples of transfected cells are shown (A and B), and an untransfected cell is shown in C, where immunocytochemical techniques used were identical.

A

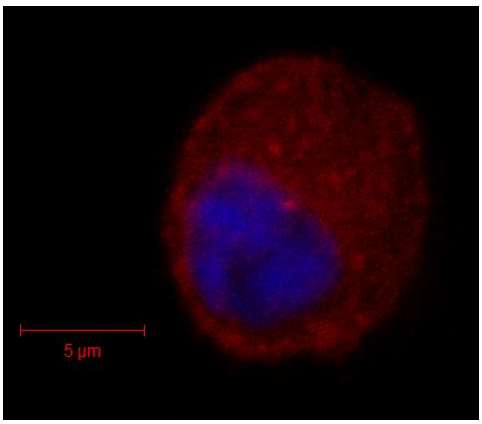

B

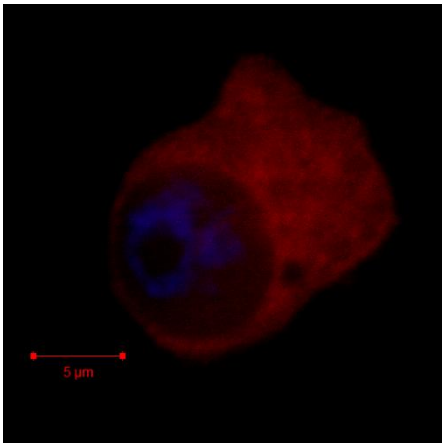

C

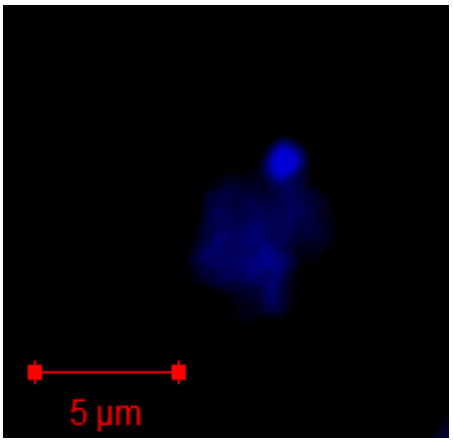

The protein showed cytosolic localisation in S2 cells. Levels of expression were judged to be low, both in terms of cellular protein level, and transfection efficiency. Untransfected cells showed no visible background expression; one such example is shown in figure 3.3C.

3.3.4 Analysis of full length *Dm*PDE11RA

Previous attempts to express full length *Dm*PDE11RA in S2 cells had not produced protein on western blots (Day et al., 2005). The catalytic domain of *Dm*PDE11 was expressed in S2 cells, and showed no cG-PDE activity above basal, and cA-PDE activity at 1, 2, and 4µM of substrate, but this activity fell at higher concentrations (Day, 2005). Following this, *Dm*PDE11 was verified as a *bona fide* dual specificity PDE by cA- and cG-PDE assays performed on immunoprecipitated *Dm*PDE11 from head lysate, using specific antisera (Day et al., 2005). This data is summarised in appendix 2. As shown above, in my hands the construct yielded expressed protein in western blots and ICC. As such, cAMP and cGMP PDE assays were performed on transiently transfected S2 cells with the full length pMT/V5-His *Dm*PDE11RA construct. Initial experiments to ascertain an effective concentration of cAMP and cGMP for use in PDE assays on *Dm*PDE11RA, and a construct expressing a truncation of *Dm*PDE11RA, from the N terminus to the end of the catalytic domain, were performed. When compared to control, *Dm*PDE11RA overexpressing S2 cells showed no significant increase in either cA-, or cG-PDE activity (data not shown).

Following this, I surmised that S2 cells may lack factors required for either the activation or stabilisation of *Dm*PDE11RA. *Dm*PDE11RA contains 4 putative cGK phosphorylation motifs. To identify whether DG2P1 or DG2P2 would either phosphorylate, thereby modulating *Dm*PDE11 function, or stabilise *Dm*PDE11 by association, I co-expressed these with *Dm*PDE11 in S2 cells, and performed cA- and cG-PDE assays (figure 3.4).

Figure 3.4: *Dm*PDE11A does not show cG- or cA-PDE activity when transiently transfected in S2 cells, and is not stimulated by DG2. cG- (A) and cA- (B) PDE assay on transiently transfected S2 cell lysate using 1μM substrate in each case. In order to aid comparison, data is expressed as % cN-PDE activity of mock transfected S2 cell, where (A) mock = 23.8 pmol cGMP/mg/min, and (B) mock = 32.4 pmol cAMP/mg/min. N=1

A

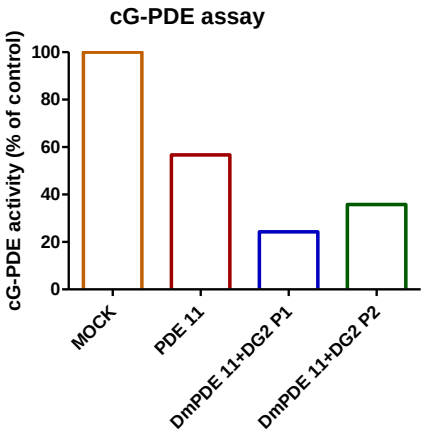

B

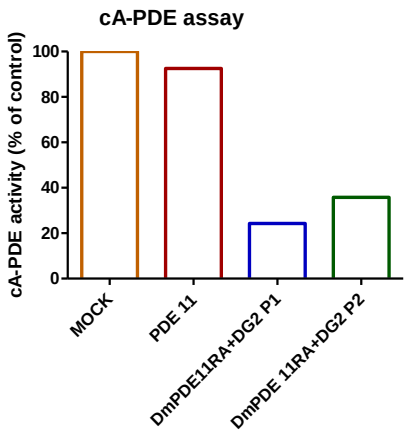

When compared to control, *Dm*PDE11RA overexpressing S2 cells showed no significant increase in either cA-, or cG-PDE activity, as found previously. Co-expression of either DG2P1 or DG2P2 with *Dm*PDE11 drastically reduced both cA- and cG-PDE activity. This data should be considered preliminary, as only one replicate was performed in either experiment, and cGK-only transfected S2 cells were not assayed. As these were only transient transfections, a large number of cells would have unaltered PDE activity. This suggests that in those cells which do express cGK, endogenous PDE activity is massively reduced, in turn suggesting that the over-expressed cGK modulates phosphodiesterase activity or protein levels. The experiment was not repeated, as it mirrors a finding in flies overexpressing DG2P1 and DG2P2 in tubule principal cells, which show a drastic reduction in endogenous PDE activity (Macpherson and Day, 2004).

3.4 C42 driven *Dm*PDE11 RNAi does not significantly affect cA-PDE activity in tubule

In order to measure the effect on cA-PDE activity in the tubule, *Dm*UAS-PDE11 RNAi (line 9), c 42, and *Dm*UAS-PDE11 RNAi (line 9)/c42 progeny were aged upon eclosion to 5-7 days, and the tubules were excised and homogenised. A cA-PDE assay was performed with 3 biological replicates, using 2 uM cAMP, and 3 μCi/ml [^{3}H] cAMP (figure 3.5).

Figure 3.5: C42 driven *Dm*PDE11 RNAi does not significantly affect cA-PDE activity in the tubule. 50 Malpighian tubules from *Dm*UAS-PDE11 RNAi (line 9), c42, and c42/*Dm*UAS-PDE11 RNAi (line 9) progeny were assayed for cA-PDE activity at 2μM cAMP in biological triplicate. Specific cA-PDE activity given in pmol cAMP/mg protein/min.

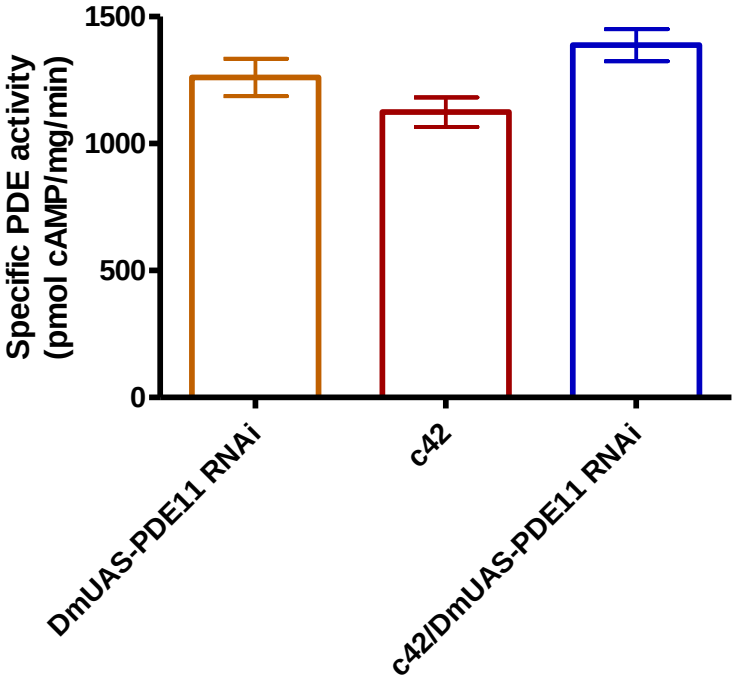

There was no significant change in cA-PDE activity between parents and progeny. Reasons for this are unknown, although 2μM is below the K_m of 18.5 ± 5.5μM ascertained from IP of head lysate. However the catalytic domain, expressed in S2 cells, only yielded cAMP-specific PDE activity at concentrations of between 1 μM and 4 μM of cAMP, hence the use of 2μM. Counts were around 15000, close to the 18000 maximum acceptable in

this assay. Repeat with higher substrate concentration (with a shorter 30°C incubation period to reduce activity and thus counts) may yield different results, and would be desirable. The complementary cG-PDE assays were not performed, as replicates of the cA-PDE assay were carried out instead with available tissue lysate.

A PDE11 deletion line (*Dm*PDE11Δ121) in our possession also gave no significant change in cA-PDE activity when midgut was excised and assayed. However cG-PDE assays revealed a large reduction when head lysate was assayed (Sebastian, 2009).

3.4.1 Transgenic tools for the study of *Dm*PDE11

3.4.1.1 Q-PCR to validate the knockdown of *Dm*PDE11 by RNAi

Two *Dm*PDE11 RNAi stocks were generated by Day, 2005, labelled *Dm*PDE11 RNAi line 1 and *Dm*PDE11 RNAi line 9. These were targeted against the same sequence, but differed in the insertion point of the pWIZ PDE11 transgene. When *Dm*PDE11 RNAi were crossed to the ubiquitous driver line Act5cGAL4, crosses were ~90% lethal at room temperature. As such knock down was validated by crossing *Dm*PDE11 RNAi with the principal cell driver c42. c42/*Dm*PDE11 RNAi line 1 progeny tubule cDNA and parental strains were subjected to Q-PCR analysis. Progeny showed a knockdown of 69% compared to parental controls (Aitcheson, 2006). However, the melting curve showed two distinct peaks, and thus two products were produced. New primers were designed, and Q-PCR was performed using c42/PDE11 RNAi (line 9) and parental strain tubule cDNA; this Q-PCR showed a knockdown of 34%, and gave a single product of the predicted size (figure 3.6 A and B).

Figure 3.6: Q-PCR to determine knock down of PDE11 RNAi (line 9). (A) Q-PCR performed on cDNA from excised tubules, using primers specific to the C-terminal of *Dm*PDE11. cDNA biological triplicate from PDE11 RNAi (line 9) parent, c42 GAL4 parent (drives expression in the principal cell of the Malpighian tubule,) and c42/PDE11 RNAi (line 9) progeny. Significance to a P value of <0.01. Analysis performed using 1-way ANOVA. (B) Melting curve for a single well/product for PDE11RNAi q-PCR: Upper melting curve (Aitcheson) shows two distinct peaks; lower melting curve relating to this Q-PCR shows a single peak and thus a single product.

A

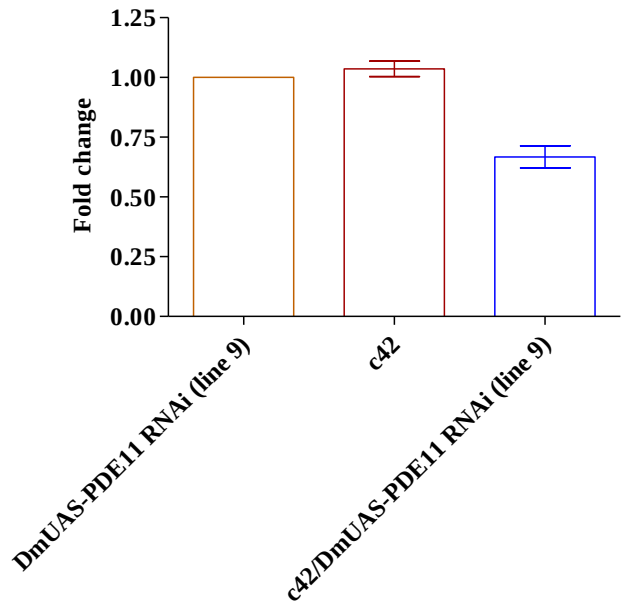

B

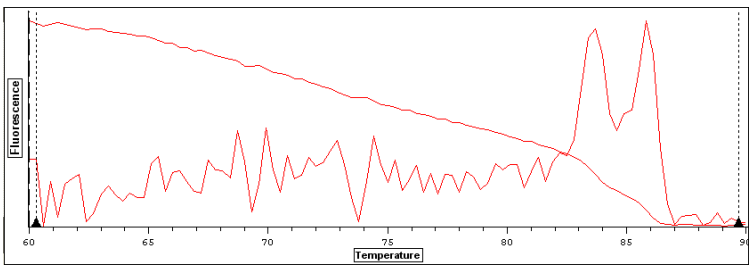

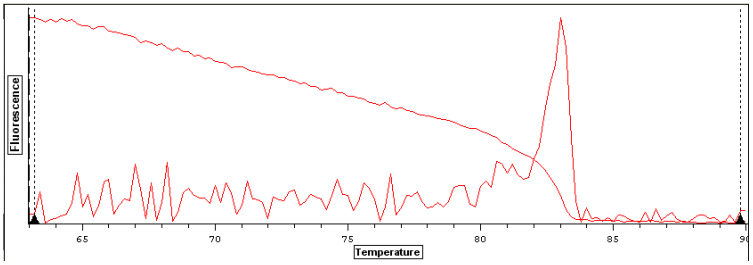

Q-PCR using the new primers for line 1 has yet to be repeated. c42 drives GAL4 expression in principal cells, yet Q-PCR of tubule cDNA will amplify *Dm*PDE11 transcripts from all cell types in the tubule. In order to determine total knockdown, Q-PCR would have to be performed on cDNA using a high level ubiquitous driver crossed to *Dm*PDE11 RNAi.

3.4.2 Phenotype screen

As mentioned above, ubiquitous knock down of *Dm*PDE11 using the pWIZ RNAi line 9 results in ~90% lethality at the larval stage when crossed to the ubiquitous driver Actin GAL4, consistent with widespread expression pattern of *Dm*PDE11. Additionally, the larvae show delayed eclosion by a day. Upon eclosion males display a green abdomen usually present in 10 day plus males. However upon dissection organs appeared normal in colour.

Following this result, PDE11 RNAi (line 9) was crossed to several tissue-specific GAL4 drivers, in order to screen for phenotypes (table 3.3).

Table 3.3: Screen for phenotypes in the progeny of PDE11 RNAi (line 9) crossed to various GAL4 driver lines. All tissue-specific Gal4 crosses did not show any obvious phenotypes

Driver	Expression pattern	Phenotype?
Ato Gal4	paired DC neurons	x
D42 Gal4	embryogenesis: broad, larvae: motorneurons,	x
	interneurons, adult: nervous system	
Appl Gal4	neuron specific	x
Repo Gal4	glial cell expression	x
Sgs3 Gal4	salivary gland expression	x

None of these crosses yielded visible phenotypes, and all eclosed normally.

3.5 *Dm*PDE11 doesn't affect osmoregulation

*Dm*UAS-PDE11 RNAi (line 9) flies were crossed with c42 GAL4, and Malpighian tubules from *Dm*UAS-PDE11 RNAi (line 9) parents, and c42/*Dm*UAS-PDE11 RNAi (line 9) progeny were assayed for secretion induced by a final concentration of 10^{-5} M exogenous cGMP, as detailed in materials and methods. No change was seen between either the basal or stimulated fluid secretion rate of Malpighian tubules from c42 and c42/*Dm*UAS-PDE11RNAi (line 9) flies (figure 3.7). The data represents the pooling of three datasets.

Figure 3.7: Fluid secretion assay. The basal fluid secretion rate of intact Malpighian tubules was measured for 30 minutes, whereupon the tubules were stimulated with 10^{-5} cGMP (final concentration, time point of addition represented by arrow), and the secretion rate measured for a further 30 minutes. Tubules from *Dm*UAS-PDE11 RNAi (line 9) parental line, and from c42/*Dm*UAS-PDE11 RNAi (line 9) progeny showed no difference in fluid secretion. Error bars represent SEM.

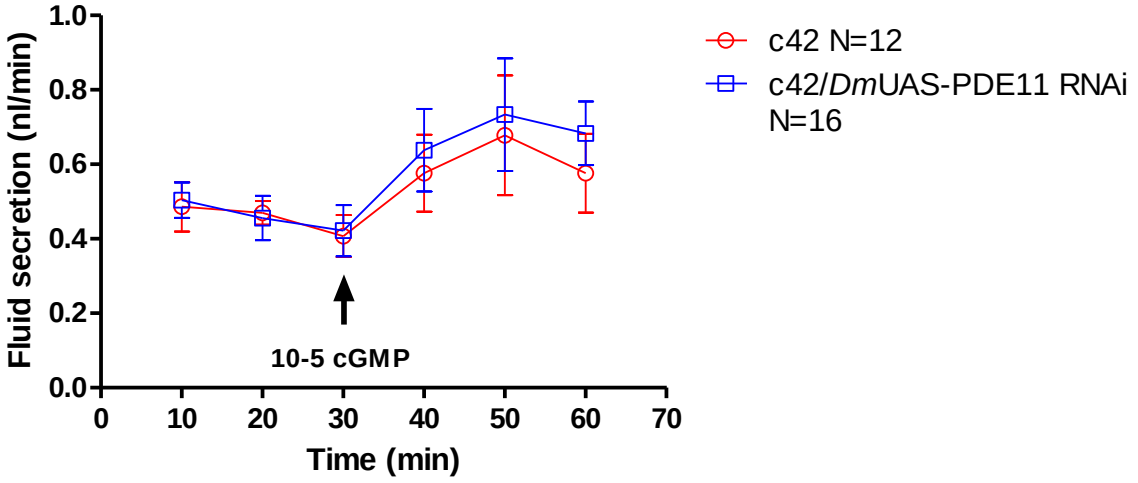

3.6 Calcium signalling

The Malpighian tubule utilises cGMP, cAMP and calcium signalling, (Davies and Day, 2006) and there is cross talk between these signalling pathways (Arnold et al., 1977; Valeyev et al., 2009; Walter and Kiger, 1984). The nitrigergic peptide capa-1 induces a rise in $[Ca^{2+}]_i$, and stimulates NO production and thus cGMP production in the Malpighian tubule, when applied exogenously (Kean et al., 2002). To determine whether *Dm*PDE11 affects this process in the tubule, *Dm*UAS-PDE11 RNAi flies were crossed with c42 GAL4-aequorin flies, which express a luminescent calcium reporting transgene in tubule principal cells. The Malpighian tubules of these flies were excised, and the calcium transients induced by capa-1 peptide were measured in a luminometer (figure 3.8), as described in materials and methods.

Figure 3.8: Capa-1 induced $[Ca^{2+}]_i$ transients are not affected by a reduction in *Dm*PDE11 levels. A: In order to measure capa-1-induced $[Ca^{2+}]_i$ transients, 30 tubule pairs from c42 aequorin (c42 aeq) and c42 aequorin/*Dm*PDE11 RNAi (line 9) (c42 aeq/*Dm*UAS-PDE11 RNAi (line 9) flies were treated with 10^{-7} M capa-1 peptide (arrow). Each trace represents the average of four replicates. **B:** Basal $[Ca^{2+}]$ levels for each genotype were calculated from the data point 1 min pre-stimulation with capa-1. Measurement of the secondary peak was taken from the data point four min post-stimulation with capa-1. Results expressed as mean nM $[Ca^{2+}]_i$, where N=4 for each genotype. Basal $[Ca^{2+}]_i$, the primary response peak, and the secondary response peak were not significantly different when analysed with an unpaired T-Test.

A

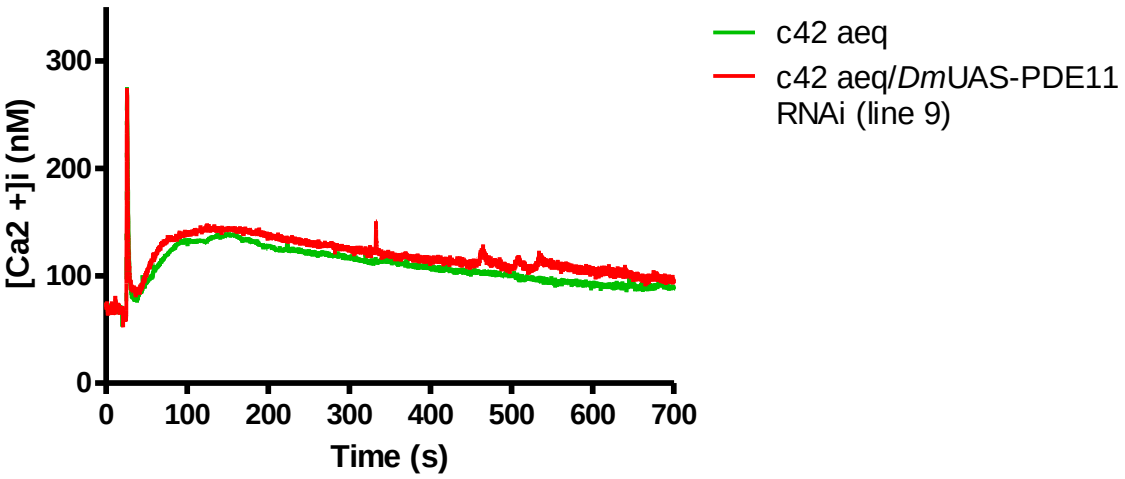

B

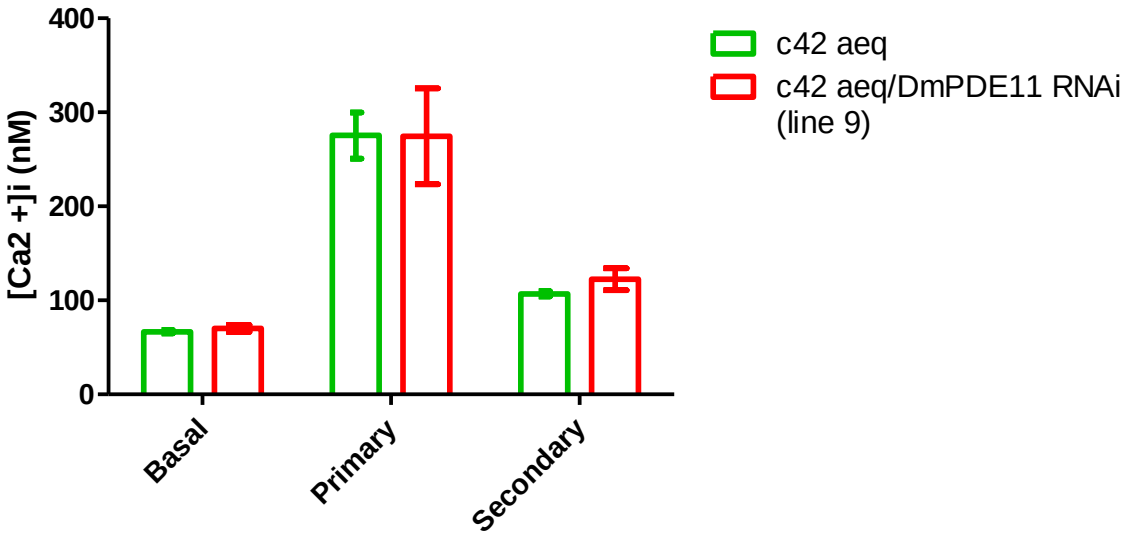

The basal $[Ca^{2+}]_i$, primary response peak, and secondary response peak of c42 aequorin and c42 aequorin/*Dm*PDE11 RNAi (line 9) Malpighian tubules were compared using an unpaired T-test. There was no significant difference between any of these. This suggests that *Dm*PDE11 does not modulate capa-1 induced $[Ca^{2+}]_i$ transients in the Malpighian tubule.

3.7 *Dm*PDE11A and DG2 colocalise in S2 cells

3.7.1 Individual transfections

In order to determine subcellular localisation, S2 cells were transiently transfected with *Dm*PDE11RA tagged with a V5 epitope, or one of the cGKs DG2P1 or DG2P2, tagged with a c-Myc epitope. Subcellular localisation was determined for *Dm*PDE11RA with an anti-V5 antibody (red) (figure 3.9), and for DG2P1 and DG2P2, where anti-c-Myc antibody was used (green) (figure 3.10). Nuclei were stained with DAPI (blue).

Figure 3.9: Confocal image of S2 cells transfected with V5-*Dm*PDE11 (red). Subcellular localisation ascertained by staining with anti-V5 monoclonal antibody, TRITC secondary Nuclei were stained with DAPI (blue).

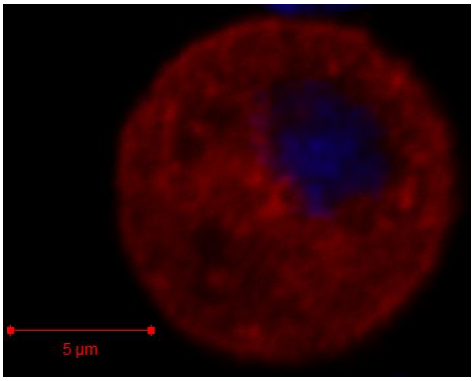

Figure 3.10: Confocal images of S2 cells transfected with c-Myc-DG2P1 (green), and c-Myc-DG2P2 (green). Subcellular localisation ascertained by staining with anti-c-Myc monoclonal antibody, TRITC secondary (green). Nuclei were stained with DAPI (blue). Untransfected cells showed no background immunofluorescence; nuclei of untransfected cells are visible in both pictures.

c-Myc-DG2P1 c-Myc-DG2P2

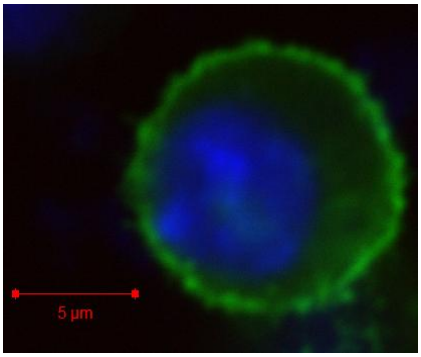

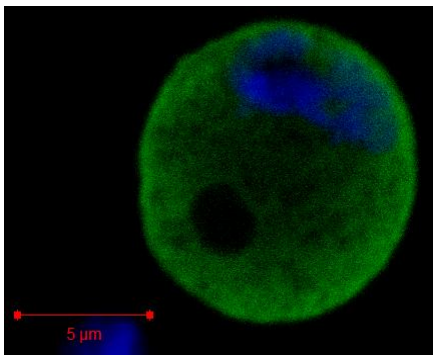

In agreement with published data (MacPherson et al., 2004b), c-Myc-DG2P1 localised predominantly to the membrane in S2 cells. Published images of DG2P2 are of V5-tagged DG2P2, stained with anti-V5 monoclonal antibody and also a vertebrate anti-cGK antibody, anti-cGKI, from (Markert et al., 1995). Images with anti-V5 antibody show solely localisation to the membrane, while those stained with anti-cGKI rabbit polyclonal antibody also showed localisation within the cytosol, stronger towards the membrane. The DG2P2 construct in my possession was tagged with c-Myc. Staining with an anti-c-Myc antibody produced similar staining to the published anti-cGKI stained images,

predominantly showing localisation to the membrane, with staining in the cytosol, stronger towards the membrane. This may be a characteristic of the antibody; however, untransfected cells show no background staining. The c-Myc tag may alter protein localisation; however the tag is one amino acid smaller than the V5 tag used in Macpherson et al, 2004, and so this is doubtful. A third alternative, and perhaps the most likely, is that conditions in those images using anti-c-Myc and anti-cGKI antibodies were more sensitive, and so fluorescence was detected that was not detected in anti-V5 images. Polyclonal antibodies designed against a novel epitope were unfortunately not delivered on time to test untagged DG2P2.

3.7.2 Co-transfections

It was reasoned that as *Dm*PDE11 will affect cGK activity, the proteins may colocalise so that *Dm*PDE11 samples the same pools of cGMP. S2 cells were transiently co-transfected with *Dm*PDE11RA tagged with a V5 epitope, and either DG2P1 or DG2P2, tagged with a c-Myc epitope.

3.7.2.1 PDE11RA and DG2P1 colocalise in S2 cells

In order to screen for co-localisation, V5-*Dm*PDE11RA and c-Myc-DG2P1 were transiently transfected in S2 cells, and the subcellular localisation of the proteins determined by immunohistochemistry (figure 3.11).

Figure 3.11: An S2 cell expressing c-Myc-DG2P1 and V5-*Dm*PDE11A. Confocal images of V5-*Dm*PDE11A (red) co-transfected with c-Myc-DG2P1 (green). V5-*Dm*PDE11A subcellular localisation ascertained by staining with anti-V5 monoclonal antibody, TRITC secondary. c-Myc-DG2P1 subcellular localisation ascertained with anti-c-Myc monoclonal antibody, FITC secondary (green). Nuclei were stained with DAPI (blue)

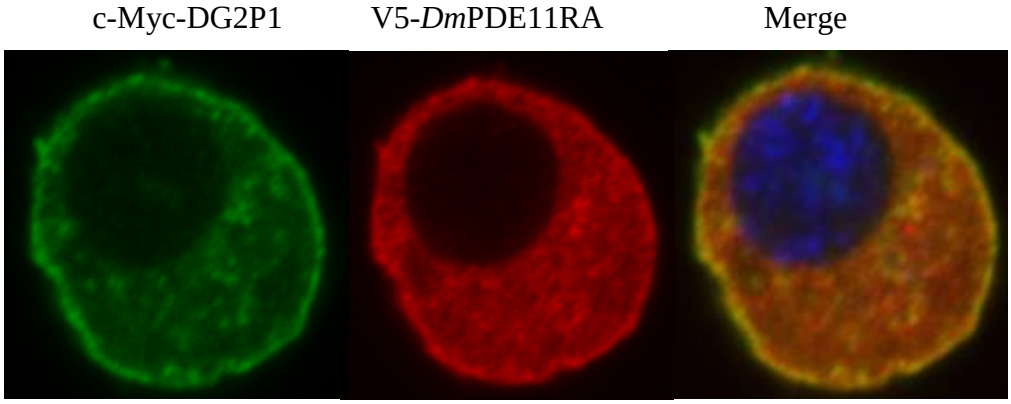

When co-transfected, V5-*Dm*PDE11RA and c-Myc-DG2P1 show a large degree of co-localisation in S2 cells. The distribution of each changes; V5-*Dm*PDE11A shows an association with the membrane, and c-Myc-DG2P1 shows an increase in cytoplasmic localisation compared to the single transfections in figure 3.12.

3.7.2.2 *Dm*PDE11A and DG2P2 colocalise in S2 cells

In order to screen for co-localisation, V5-*Dm*PDE11RA and c-Myc-DG2P2 were transiently transfected in S2 cells, and the subcellular localisation of the proteins determined by immunohistochemistry (figure 3.12).

Figure 3.12: An S2 cell expressing c-Myc-DG2P2 and V5-*Dm*PDE11A. Confocal images of V5-*Dm*PDE11A (red) co-transfected with c-Myc-DG2P2 (green). V5-*Dm*PDE11A subcellular localisation ascertained by staining with anti-V5 monoclonal antibody, TRITC secondary. c-Myc-DG2P2 subcellular localisation ascertained with anti-c-Myc monoclonal antibody, FITC secondary (green). Nuclei were stained with DAPI (blue). Merge shows two additional nuclei from untransfected cells.

c-Myc-DG2P2 V5-*Dm*PDE11RA Merge

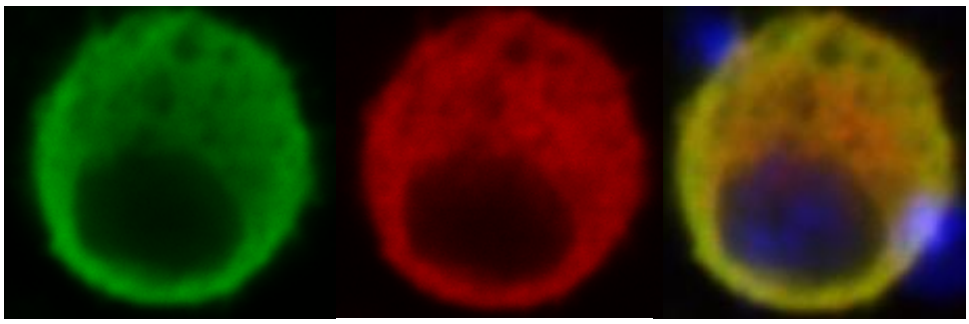

Figure 3.14 shows that V5-*Dm*PDE11RA and c-Myc-DG2P2 show a large degree of co-localisation in S2 cells. There are multiple areas in the cytosol where both proteins are excluded. These could be an unknown form of vesicle, or endosomes. As both proteins show a cytoplasmic localisation, however, this does not suggest that either protein modulates the localisation of the other.

3.8 Projects undertaken that were halted when the new *Dm*PDE11 sequence predictions were released

As the *Dm*PDE11RA gene model was replaced with two newly predicted isoforms in Flybase release 5.2, several constructs and projects were postponed until the gene model could be investigated and postponed. Subsequently, the data presented in chapter 4 led to the verification of the new gene model, and the cancelation of these projects. Details of these are found in appendix 1.

3.9 Generation of transgenic *Dm*PDE11RA flies

In order to generate *Dm*PDE11RA overexpressing *Drosophila*, the ORF was sub-cloned into the pP{UAST} vector. Two constructs were generated, one with a stop codon, and one with without, in order to fuse *Dm*PDE11RA in-frame with YFP. The inserts were sequenced for fidelity (data not shown); generation of the flies was postponed until *Dm*PDE11RA could be validated as a *bona fide* PDE. In the same week Flybase 5.2 was released; as above, the data presented in chapter 4 verified the new gene model and rendered the constructs invalid.

3.10 Discussion

The 5.8 kb expressed sequence tag (EST) SD13096 had previously been shown to contain sequence present in the incomplete PDE11RA ESTs previously released by Flybase, but also incorporating a 5' UTR, and an in-frame start codon within two novel 5' exons. A Northern blot of *Dm*PDE11RA produced one band of approximately 5.8kb; as this matches the size of the *Dm*PDE11RA ORF, was accepted that SD13096 encodes the entire PDE11RA ORF (Day). Expression of this EST in S2 cells revealed that the construct produced a protein of the accepted size, and that the protein localised to the cytoplasm, as is the case for several cA- and cG-PDEs (Omori and Kotera, 2007).

A screen for phenotypes, whereby UAS-*Dm*PDE11 RNAi (line 9) flies were crossed to various GAL4 driver lines, and the progeny screened for phenotypes. Eclosed flies appeared normal, other than flies crossed to Act-5c GAL4, which had a green tint to their abdomen. The flies were dissected, but the tissue responsible was not identified.

Calcium signalling is modulated by cGMP (Schlossmann et al., 2000), and in Malpighian tubules capa-1 and capa-2 stimulate fluid transport via calcium and cGMP signalling pathways (Davies et al., 1995; Kean et al., 2002), where the entry of extracellular calcium is permitted by the activation of a cyclic nucleotide gated channel, *cng*, where cGMP enhances cytosolic calcium and increases fluid transport (MacPherson et al., 2001). cAMP and calcium signalling networks display extensive crosstalk in non-excitable cells, where each modulates the spatiotemporal dynamics of the other (Bruce et al., 2003; Valeyev et al., 2009). As *Dm*PDE11 is a dual specificity PDE, it was hypothesised that the protein

may exert a modulatory effect on tubule calcium signalling in response to capa-1. Thus, the protein's role in calcium signalling was investigated by stimulating aequorin expressing Malpighian tubules from c42 aequorin, and c42 aequorin/*Dm*UAS-PDE11 RNAi (line 9) flies with capa-1, and measuring the calcium response to the neuropeptide. The basal $[Ca^{2+}]_i$, primary response peak, and secondary response peak were compared between the two genotypes using an unpaired T-test, where neither were found to be significantly different. This suggests that *Dm*PDE11 does not modulate the $[Ca^{2+}]_i$ response to capa-1 in the Malpighian tubule.

PDEs are responsible for the hydrolysis of cyclic nucleotides, which subsequently affects the activity of cyclic nucleotide-responsive effector proteins (Beavo et al., 2007). cGKs, in turn, have been shown to modulate the catalytic activity of PDE11A4 and PDE5A, two PDEs capable of hydrolysing cGMP, through phosphorylation (Corbin et al., 2000; Gross-Langenhoff et al., 2008; Turko et al., 1998; Yuasa et al., 2000a), thus providing a feedback loop facilitating a reduction in the activity of the activated cGKs. The co-localisation of PDE5 and PKG1β has previously been shown to play an important physiological role, where PDE5 has been shown to localise to the ER in a PKG1β signalling complex responsible for the cGMP mediated inhibition of IP_3R dependent Ca^{2+} release in platelets, where PKG1β phosphorylates and activates PDE5, thus initiating a negative feedback loop. This co-localisation appears to result from both proteins interacting with IP_3R and not a direct interaction (Wilson et al., 2008). Thus, the subcellular localisation of *Dm*PDE11 and DG2 were characterised and compared in S2 cells. Co-expression of V5 tagged *Dm*PDE11, and c-Myc tagged DG2 P1 and P2 showed that the two co-localise. DG2P1 shows a stronger presence in the cytosol when co-expressed with *Dm*PDE11A, which shows an association with the membrane in doubly transfected cells.

Attempts to identify *Dm*PDE11RA as a *bona-fide* PDE were made using two methods; cA- and cG-PDE assays on S2 cell transiently transfected with *Dm*PDE11RA, and a cA-PDE assay of the parents and progeny of a *Dm*UAS-PDE11 RNAi (line 9) x c42 cross, as *Dm*PDE11 is upregulated in the Malpighian tubule 1.5 times (http://www.flyatlas.org/). *Dm*PDE11A did not yield any cA- or cG-PDE activity when expressed in S2 cells. With the rationale that DG2 has been shown to modulate cG-PDE activity in the tubule (MacPherson et al., 2004a), and that DG2 may therefore modulate *Dm*PDE11 activity, *Dm*PDE11 was co-expressed in S2 cells with DG2P1 or DG2P2, and the lysate use to perform cA- and cG-PDE assays. Although these were only performed as N=1, again, no increase in cA- or cG-PDE activity was seen in *Dm*PDE11 transfected cells. Furthermore,

where *Dm*PDE11 was co-transfected with DG2P1 and DG2P2, a reduction in PDE activity was seen. This mirrors an unpublished observation by MacPherson and Day.

In order to determine if a knock-down in *Dm*PDE11 transcript levels and therefore protein levels affected PDE activity in the tubule, *Dm*UAS-PDE11 RNAi (line 9) were crossed to c42, and the Malpighian tubules of parent and progeny subjected to a cA-PDE assay. No difference in cA-PDE activity was seen. However, it may be that the concentration of cAMP used was such that other cA-PDEs expressed in the tubule may have dwarfed the contribution of *Dm*PDE11 to total PDE activity, and so no difference was seen. As such, it is desirable that this assay be repeated at higher cAMP concentration, and also that the assay be performed for cG-PDE activity.

The significance of the Flybase 5.2 release is discussed in chapter four.

Chapter 4

Identification and cloning of *Dm*PDE11RB long, *Dm*PDE11RB short, *Dm*PDE11RC long, and *Dm*PDE11RC short

4.1 Summary

The *Dm*PDE11RA isoform was replaced in the Flybase 5.2 release by two newly predicted isoforms; *Dm*PDE11RB and *Dm*PDE11RC (http://fb2007_01.flybase.org/reports/FBgn0085370.html). Both are similar, but not identical isoforms to the RA transcript. There are two key differences between *Dm*PDE11RA and the two newly predicted isoforms. Firstly, the first two exons of *Dm*PDE11RA were predicted to be incorrect, and these exons were newly predicted to be 5' UTR within the *Dm*PDE11RB transcript. *Dm*PDE11 RB and RC each have novel N termini encoded by alternate first exons, and share a second exon not present in *Dm*PDE11RA. Secondly, exon 11 within the *Dm*PDE11RA transcript was also predicted as false, and is not present in the *Dm*PDE11RB or *Dm*PDE11RC isoforms. Analysis of transiently transfected S2 cells expressing V5-tagged *Dm*PDE11RA had shown that the protein displayed no discernable cA- or c-PDE activity, and showed low levels of expression. As such, it was probable that *Dm*PDE11RA was not a bona fide PDE.

The evidence rank supporting *Dm*PDE11 RB and RC on Flybase is "weakly supported"; i.e., they are predictions backed by sequencing of end sequenced cDNA clones (or ESTs) around 500 bases long, and computational prediction. The length of supporting ESTs prohibit their use in cloning. As both *Dm*PDE11 RB and RC were still rated as "weakly predicted", updating the RA ORF by cloning the novel N-termini, and the region around exon 11, and sub-cloning these into the *Dm*PDE11RA transcript using endogenous restriction sites was not pursued, as only PCR of the entire ORF would guarantee that the isoforms were *bona fide*, and the Flybase predictions correct. Prior to cloning these isoforms, they were confirmed as being transcribed by three methods; comparison of predicted exons with a head and Malpighian tubule EST database not used in the Flybase sequence analysis, sequencing of RT-PCRs from cDNA from multiple tissues, and diagnostic RT-PCRs, where multiple exons were amplified, and analysed by agarose gel electrophoresis and sequencing.

Each isoform was amplified in fragments using a high-fidelity DNA polymerase from brain or hindgut cDNA, sequenced for fidelity, and ligated together utilising endogenous restriction sites to yield a full length open reading frame. Sequencing of RT-PCR amplified ORF fragments revealed a novel exon/exon splice site in the C-terminus not predicted by Flybase; the novel exon encodes 4 amino acids followed by a stop codon 1kb from the stop codon of the "long" C terminus, and thus a truncated protein. RT-PCR analysis revealed

that both the B and C isoforms have both a long and a short isoform, thus yielding two additional novel ORFs. Polyclonal antibodies previously raised against sequence from *Dm*PDE11RA target the long isoforms only, in an area with no sequence changes. The pWIZ RNAi construct targeted against *Dm*PDE11RA utilises sequence from an unchanged region, shared by all four isoforms.

Transgenic *Drosophila* expressing the four *Dm*PDE11 isoforms were generated, and the proteins verified by western blotting. The B and C isoforms showed differential subcellular localisation in the Malpighian tubule, where the long and short isoforms of *Dm*PDE11B localised to the apical and basolateral membranes, and the long and short isoforms of *Dm*PDE11C localised to unidentified organelles or vesicles.

Over-expression of *Dm*PDE11 C long or short in S2 cells failed to yield an increase in cA- or cG-PDE activity. However, when ubiquitously overexpressed in fly, immunoprecipitated, and subjected to PDE assays, YFP tagged *Dm*PDE11B long and short and C long and short display cA- and cG-PDE activity, and thus are *bona fide* dual specificity phosphodiesterases.

4.2 Introduction

Previous attempts to transiently transfect S2 cells with *Dm*PDE11RA failed to generate expressed protein (Day). Although further attempts to express V5 tagged *Dm*PDE11RA yielded expression of a protein of the expected size, the protein was expressed at low levels, and displayed unusually low transfection efficiency. Attempts to verify that *Dm*PDE11RA was a *bona fide* phosphodiesterase through PDE assays yielded no cA- or cG-PDE activity above background (as detailed in chapter 3). Previously, PDE assays on the sub-cloned catalytic domain yielded slight cA-PDE activity (Day).

It was thought that perhaps *Dm*PDE11 needed some unknown binding partner to facilitate PDE activity; thus S2 cells co-transfected with PDE11 and DG2 were subjected to PDE assays; again, these yielded no significant activity, and indeed cGK/PDE11RA co-transfected S2 cell lysate demonstrated lower PDE activity than untransfected cells (summarised in chapter three).

4.2.1 Flybase 5.2 replaces *Dm*PDE11RA with *Dm*PDE11RB and *Dm*PDE11RC

In the Flybase 5.2 genome annotation release of August of 2007, *Dm*PDE11RA was replaced with two newly predicted transcripts, *Dm*PDE11 RB and RC (figure 4.1). Ensemble was updated accordingly in March 2008.

Figure 4.1: *Dm*PDE11 RB and RC. Diagram representing the initial transcript, mRNA, and cDNAs of the *Dm*PDE11 isoforms. From http://flybase.bio.indiana.edu/reports/FBgn0085370.html.

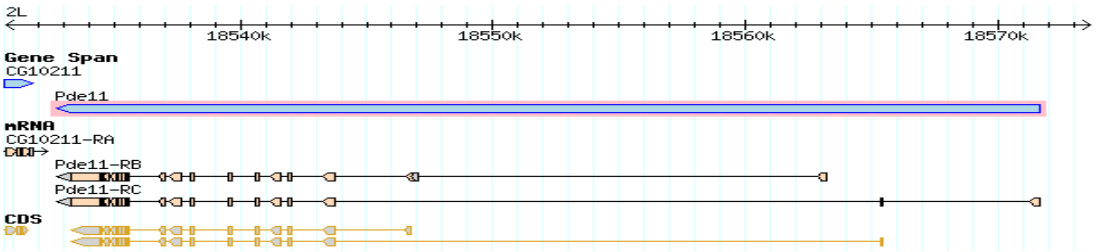

The Flybase 5.2 predictions for *Dm*PDE11 RB and RC were still based on computational prediction, and a number of incomplete cDNAs (or ESTs). The prediction was still classed as "very weak". This may explain why Ensemble kept their prediction as RA until March 2008. However, several aspects of the research detailed in chapter 3 led me to believe that *Dm*PDE11RA was incorrectly predicted. The enzyme provided no PDE activity above baseline when expressed in S2 cells. Whereas transient expression of the N terminus of PDE11RA in S2 cells gave robust expression, expression levels of transiently transfected full length protein were much lower. Furthermore, the protein showed a classical "non-specific" cytoplasmic localisation. Thus, validation of the newly predicted isoforms was undertaken. The 5639 bp *Dm*PDE11RB transcript contains 17 exons, and encodes a protein product of 1451 residues. The 5238 bp *Dm*PDE11RC transcript contains 17 exons, and encodes a protein product of 1407 residues. Both encode similar, but not identical protein products to the RA transcript.

4.2.2 Comparison between *Dm*PDE11RB and *Dm*PDE11RA

The predicted first two exons of *Dm*PDE11RA were predicted to be incorrect, and replaced in the RB transcript, which contains two alternate exons at the 5' end (figure 4.2).

Figure 4.2: Transcript structure of *Dm*PDE11RA and *Dm*PDE11RB. Kb figure refers to the breadth of sequence localisation within chromosome 2L. White = UTR, Red = exon.

RA

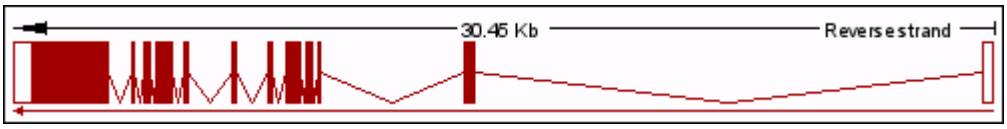

RB

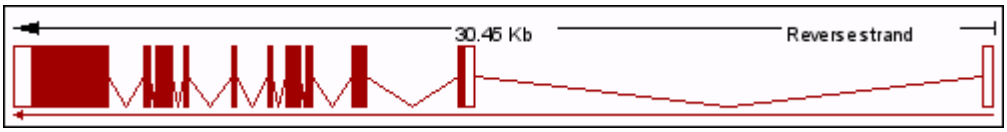

A further difference between RB and RA is the omission of the 78 bp exon 11 of RA from the RB transcript. The RB ORF remains in-frame so that 26 amino acids are removed from this site but the amino acids following this are unaffected (figure 4.3).

Figure 4.3: ClustalW alignment of *Dm*PDE11RA and *Dm*PDE11RB. Sequences of *Dm*PDE11RA and *Dm*PDE11RB were aligned using ClustalW, which revealed a 78bp deletion within the RB ORF present in the predicted RA ORF.

```
                    2310       2320       2330       2340       2350       2360       2370       2380       2390       2400
dPDE11-RB ORF       AATGGCCAAGCAGAGTGTCACCCTGGAGGTGCTCAGCTACCACGCATCGGCCACCATGGACGAGGCTCATCGACTGCGG--------------------
dmpde11 ra orf      AATGGCCAAGCAGAGTGTCACCCTGGAGGTGCTCAGCTACCACGCATCGGCCACCATGGACGAGGCTCATCGACTGCGGAAACAGAAACAGCAGCAACAA
                    ********************************************************************************

                    2410       2420       2430       2440       2450       2460       2470       2480       2490       2500
dPDE11-RB ORF       ------------------------------------------------------------CGCCTTCGAGTGCCTTCAGCTGTACACTTTCGACTGCATGACT
dmpde11 ra orf      GCTGTCGGCCTAAGGCAAGCTCCTCTGTCCCTGCCCCCGCGTAAAAAGCTTCAACGTCGCCTTCGAGTGCCTTCAGCTGTACACTTTCGACTGCATGACT
                                                                           ********************************************
```

This deletion corresponds to exon 11 of RA. This sequence is located between the GAF domains and the catalytic domain. This deletion aside, the C termini of the two isoforms

are identical. As such, *Dm*PDE11B still contains twin GAF domains, and a dual specificity PDase domain.

4.2.3 Comparison between *Dm*PDE11RC and *Dm*PDE11RA

*Dm*PDE11RC has a unique N-terminus, consisting of two novel exons not present in *Dm*PDE11RA, the second of which is shared with *Dm*PDE11RB (figure 4.4).

Figure 4.4: Transcript structure of *Dm*PDE11RA and *Dm*PDE11RC. Kb figure refers to the breadth of sequence localisation within chromosome 2L. White = UTR, Red = exon.

RA

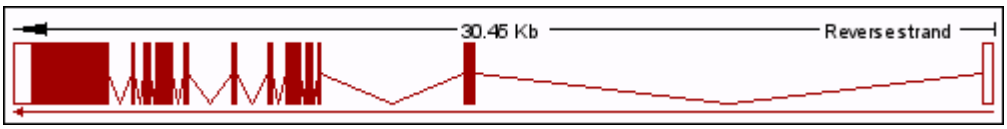

RC

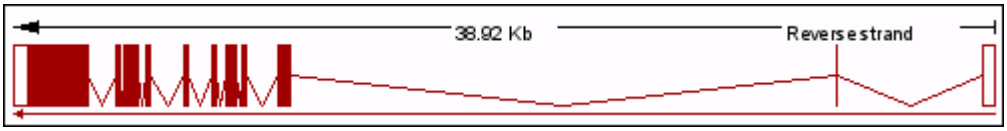

Exon 11 of *Dm*PDE11RA is also not present in *Dm*PDE11RC. As such, the only difference between *Dm*PDE11RB and *Dm*PDE11RC is the first exon.

4.2.4 Verification of the newly predicted isoforms

4.2.4.1 Analysis of Expressed Sequence Tag traces

The RB and RC transcripts were predicted through a combination of EST sequencing and computational prediction. I analysed Solexa Illumina EST sequencing runs from poly-A primed mRNA generated from head and Malpighian tubule RNA (Dow and Wang, 2009), using a CLC genomics workbench suite (CLC Genomics Workbench 3.7., CLC Bio) which allowed the further screening of predicted exons in the EST library. These ESTs were not used in the Flybase sequence analysis. EST sequencing traces of 50 base pairs, unless representative of repeat genomic sequence over-represented in the genome, should

only be found in one genomic location. The genomic region of *CG34341* was "overlaid" with the EST traces using a CLC genomics workbench suite, and the putative start sites and exons of the transcripts were validated by comparison with EST coverage. Tubule EST reads are shown.

The sequence originally designated as RA exons 1 and 2 and is now designated as RB 5' UTR. Within this region there are four ESTs, and significant areas are not represented (figure 4.5).

Figure 4.5: 50bp reads representing the 5' UTR of the PDE11 transcript *Dm*PDE11RB. Yellow band represents translated region. Green band represents UTR. Purple highlighted sequence shows previously predicted start site for *Dm*PDE11RA.

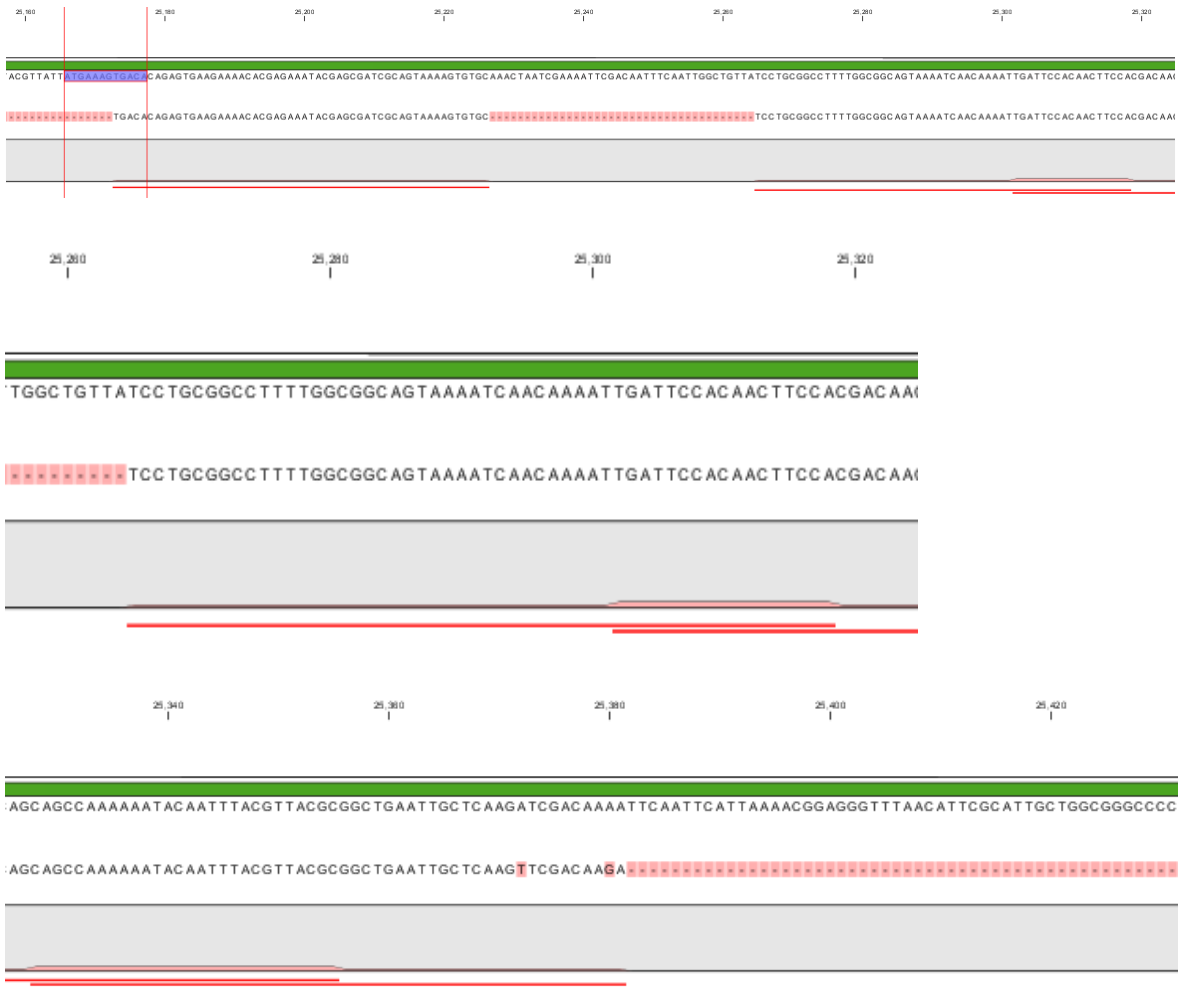

Of prime importance was the verification of the newly predicted *Dm*PDE11RB and *Dm*PDE11RC N termini. These are represented in the ESTs gathered (figure 4.6 and 4.7).

Figure 4.6: 50bp read representing first exon of *Dm*PDE11RB with start codon (ATGGGCCAAGCGGCA...). Yellow band represents translated region. Green band represents 5' UTR.

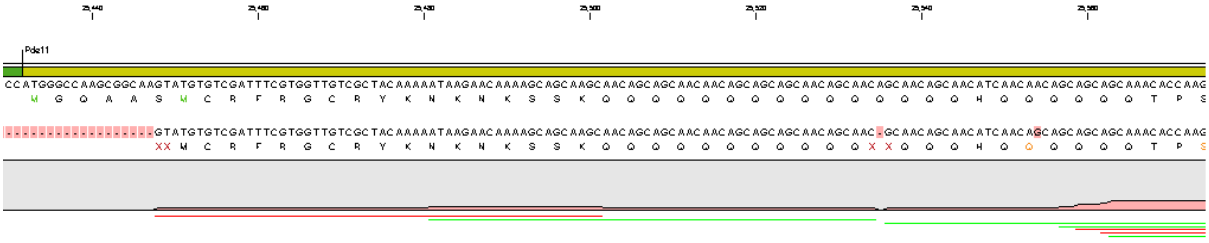

Figure 4.7: 50bp read representing first exon of *Dm*PDE11RC with start codon (ATGGCATCATCCCCA...). Yellow band represents translated region. Green band represents 5' UTR.

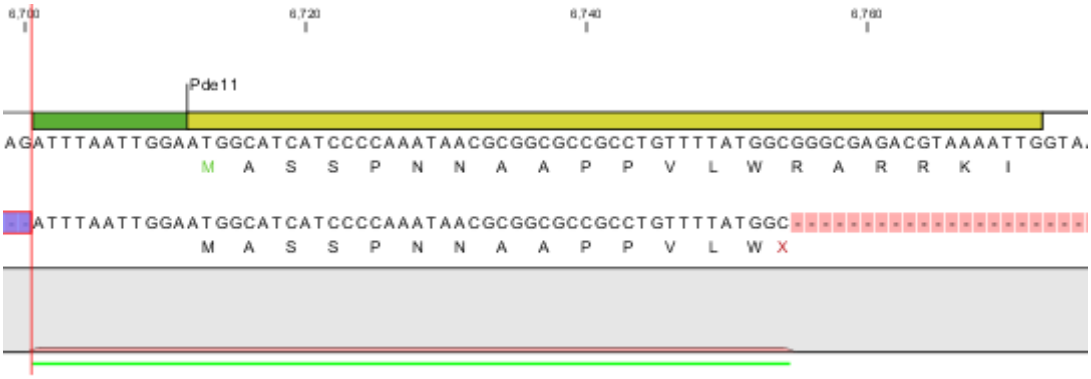

The presence of these novel N termini in these sequencing runs supports the Flybase prediction. The second, shared exon is also represented within the EST database (figure 4.8).

Figure 4.8: 50bp read representing second exon of *Dm*PDE11RB and RC. Yellow band represents translated region.

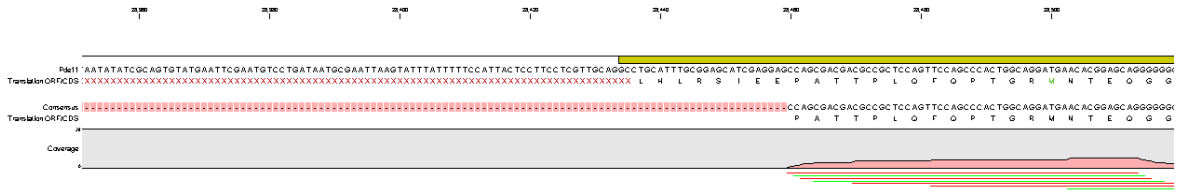

The coverage of these exons in the Solexa Illumina EST sequencing runs, as well as those used in the Flybase prediction, suggests strongly that the newly predicted N termini of the RB and RC isoforms are correct.

4.3 Amplification and further verification of *Dm*PDE11 RB and RC

4.3.1 Amplifying *Dm*PDE11 RB and RC from cDNA

Flyatlas, a database of whole fly and tissue specific expression levels of every known *Drosophila* gene (Chintapalli et al., 2007), shows the highest enrichment for *Dm*PDE11 transcript compared to whole fly in brain and hindgut (table 4.1)

Table 4.1: Tissue expression profile of *Dm*PDE11. mRNA signal: abundance of transcript in each tissue. Enrichment: compared to whole fly (Chintapalli et al., 2007).

Tissue	mRNA Signal	Enrichment
Brain	268 ± 9	2.5
Head	132 ± 10	1.2
Eye	327 ± 37	3.09
Thoracicoabdominal ganglion	154 ± 11	1.5
Salivary gland	268 ± 1	2.53
Crop	176 ± 7	1.7
Midgut	188 ± 8	1.8
Tubule	161 ± 7	1.5
Hindgut	285 ± 11	2.7
Heart	332 ± 13	3.14
Fat body	98 ± 7	0.92
Ovary	192 ± 2	1.8
Testis	39 ± 2	0.4
Male accessory glands	77 ± 4	0.7
Virgin spermatheca	105 ± 10	0.99
Mated spermatheca	110 ± 7	1.04
Adult carcass	102 ± 8	1
Larval CNS	79 ± 2	0.75
Larval Salivary gland	176 ± 13	1.66
Larval midgut	91 ± 8	0.86
Larval tubule	180 ± 7	1.7
Larval hindgut	172 ± 9	1.63
Larval fat body	73 ± 4	0.7
Larval trachea	156 ± 16	1.48
Larval carcass	77 ± 9	0.73
S2 cells (growing)	245 ± 9	2.31
Whole fly	106 ± 11	

The probes used in the *Drosophila* Fly Atlas did not differentiate between RB and RC. It was shown by Day and Sebastian that both isoforms are expressed in hindgut and head, as shown in appendix 3. As both isoforms are expressed in these tissues, cDNA was generated from dissected brain (as this showed enrichment over head) and hindgut, and this cDNA used to clone the ORFs, as full length ESTs were not available.

4.4 Cloning of *Dm*PDE11RB and RC

4.4.1 PCR of full length ORFs

The newly predicted *Dm*PDE11 RB and RC mRNA coding regions (ORFs) are 4365bp and 4224bp in size respectively. Attempts to clone the entire ORFs failed, despite attempts

with non-proofreading DNA polymerase, and with Platinum Taq DNA polymerase high fidelity (Invitrogen), an enzyme supposedly capable of amplifying up to 20kb, adding weight to Sambrook's description of manufacturer's claims towards their proprietary *Taq* polymerases as "indefatigably optimistic" (Sambrook and Russell, 2001). As with all cloning from cDNA in this chapter, a gradient PCR, with a wide spread of annealing temperatures, was used. Every variable; primer concentration, $MgCl^{2+}$ concentration, cDNA type and concentration, and cycle number, were altered, but to no avail.

4.4.2 Fusion PCR

Fusion PCR is a method of amplifying two or more fragments of DNA, and subsequently fusing these fragments into one long DNA molecule (Shevchuk et al., 2004). This involves three PCR steps. The first amplifies the fragments, using primers that result in two (or more) products with a 21 bp "overlap" homologous region; these fragments are gel purified. The subsequent two steps fuse these fragments. An initial 13 cycles are performed without primers, during which the region of homology essentially acts as a primer, and generates a full length dsDNA template from the newly fused fragments. Following this, the product of the previous fusion step is DNA purified and used as a template; a PCR with primers for the extreme 5' and 3' ends of the gene, (PCRs were performed with two sets of primers, either with incorporated restriction sites to facilitate cloning, or without), and an extended extension step (to reflect the increase in size of the template) should yield full-length fusion product.

The N termini of RB and RC, and the conserved C terminus, were amplified with a 21bp overlap, as one clean band in each case. Equimolar amounts of these were used in the fusion PCR. When the products were separated by gel electrophoresis, strong, non-specific bands were obtained, and when a combined annealing/extension PCR program still yielded these bands the approach was abandoned (data not shown).

4.4.3 Sub cloning of *Dm*PDE11 using endogenous restriction sites

As amplification of the full length ORF failed, a multi-step cloning strategy was planned. Analysis of *Dm*PDE11 RB and RC sequence for endogenous restriction sites showed a BglII site around midway through the two ORFs.

This pointed towards a two stage cloning strategy; amplify the two unique N termini of RB and RC, and the single shared C terminus with these incorporating the endogenous BglII site, adding unique restriction sites at the N and C terminals, and clone these sequentially into a compatible multiple cloning site. As RB and RC have unique N termini, differing forward primers were designed to amplify these. Reverse primers for the common C terminal were designed with and without a stop codon. These fragments could then be ligated together to yield a full-length ORF, both YFP-tagged and untagged, following verification by sequencing (figure 4.9).

Figure 4.9: Cloning strategy for *Dm*PDE11

Step 1: Primers are designed to amplify the N and C terminal halves of RB and RC, extending just past the endogenous BglII site. The C terminal half of RB and RC are identical. Restriction sites, not present within the ORF, corresponding to sites in pUAST MCS are incorporated at the N and C terminal ends of RB and RC. The C terminal was amplified with and without a stop codon to facilitate in frame fusion with a YFP tag.

Step 2: TOPO clone the fragments, and sequence them to screen for fidelity

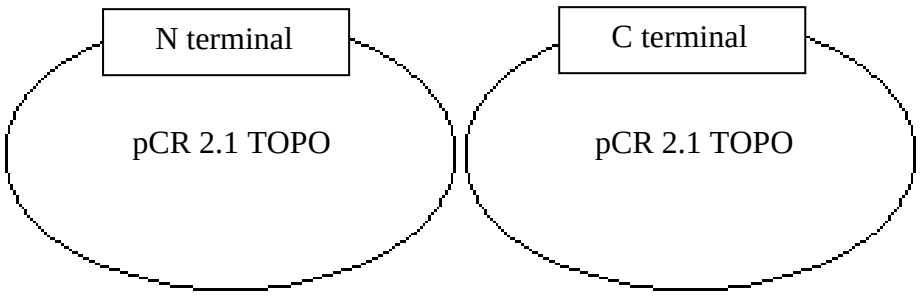

Step 3: Digest the N and C terminal ends, and ligate sequentially into digested, MCS-modified pUAST

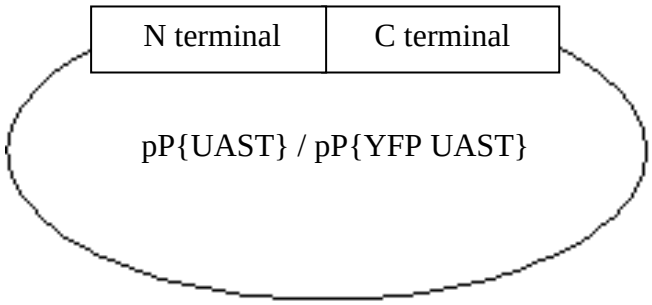

Step 4: Screen colonies for full length PDE11 RB and RC inserted into pUAST and pUAST-YFP.

All PCRs were performed with Herculase II DNA polymerase, following manufacturer's instructions. For all PCRs at least three TOPO cloned inserts were sent for sequencing.

4.4.3.1 Amplification of *Dm*PDE11RB N terminus

The BglII site is 2654bp into the RB ORF. Although the fragment would amplify with standard DNA polymerase, using proofreading DNA polymerase, the N terminus of RB did not amplify despite extensive attempts to optimise the protocol, including primer redesign without a 5' EcoRI addition. Fortuitously, a Xho I site exists half way through this N terminal fragment, and so the N terminus was amplified in two fragments. These fragments overlapped so that the primers did not contain a Xho I site, as a control. The EcoRI – XhoI fragment, and the XhoI to BglII fragment were amplified, sub-cloned into pCR TOPO 2.1 vector, and verified by PCR and restriction analysis. They were then sequenced for fidelity.

4.4.3.2 Amplification of *Dm*PDE11RC N terminus

Using proofreading DNA polymerase, the N terminus of *Dm*PDE11RC amplified as a single clean band of the predicted size. This band was sub cloned into the TOPO 2.1 vector, verified by PCR and restriction analysis, and sequenced for fidelity.

4.4.3.3 Amplification of the conserved *Dm*PDE11 C terminus

The C terminus was amplified using two different reverse primers, one with a stop codon, incorporating a KpnI restriction site, and one without a stop codon, with a NotI restriction site, to facilitate in-frame fusion to a YFP tag. With either reverse primer, PCR of the C terminus of *Dm*PDE11 yielded two fragments, one of the predicted size, and one that ran approximately 50bp smaller (figure 4.10). Both were gel purified, TOPO-cloned using pCR TOPO 2.1 vector, verified by PCR and restriction analysis, and sent for sequencing.

Figure 4.10: The *Dm*PDE11 C terminus amplifies as a doublet. Two PCR fragments of the *Dm*PDE11 C terminus, produced using proofreading PCR polymerase, BglII C term forward and KpnI reverse primers, and tubule cDNA. Fragments were separated by agarose gel electrophoresis. Band size identified using 1kb ladder.

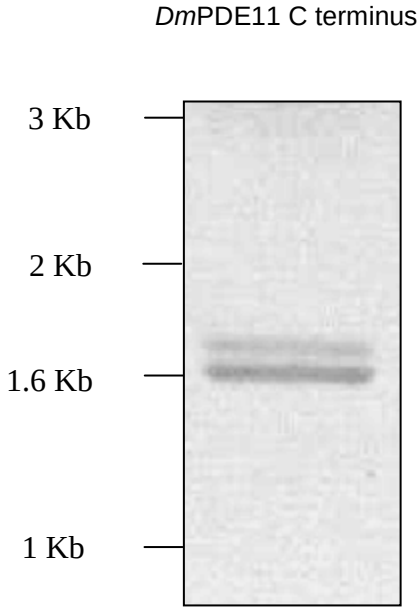

Sequencing of these fragments showed that the smaller band contained a novel exon/exon boundary, not predicted by Flybase, which results in 4 novel amino acids followed by a novel stop codon 1kb from the C-terminus, and thus a truncated protein (figure 4.11).

Figure 4.11: Truncated *Dm*PDE11 transcript. Sequencing of two *Dm*PDE11 C terminal PCRs from cDNA, showing a novel intron/exon boundary. * denotes matching sequence

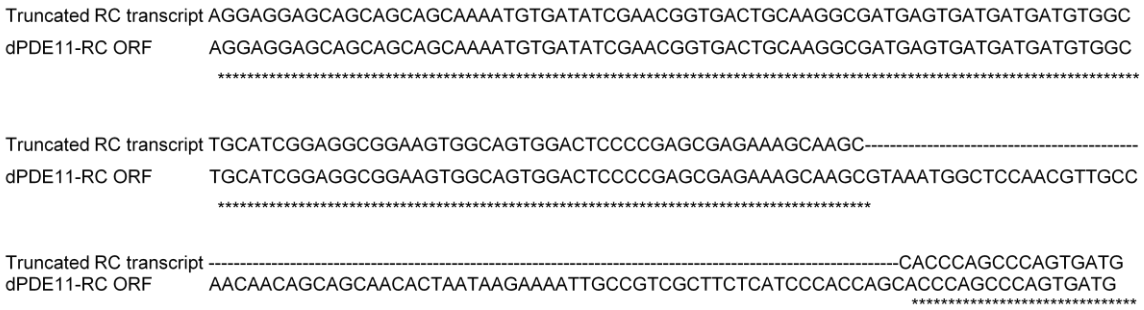

When the C terminal, amplified with no stop codon, was TOPO cloned in-frame with a V5 tag, and expressed in S2 cells, western blot of cell lysate gave bands of the predicted size. The transfer was "dirty," and so although bands were visible on the exposed film, when scanned the bands were no longer visible, and so the data is not shown.

4.4.4 RT-PCR to verify long and short isoforms

With two possible N termini, and two C termini, the question of how many isoforms exist *in vivo* arose. RT-PCR was performed in order to determine which combinations of N termini and C termini were represented in transcripts. Primers were designed in the unique B and C termini, as close to the novel exon/exon boundary as possible. Two reverse primers were generated, one within the originally predicted exon/exon boundary, and one within the novel exon/exon boundary within the short C terminus (figure 4.12). These primers were designed to generate products of ~3.5 kb.

Figure 4.12: *Dm*PDE11 transcript verification strategy. Primers were designed to confirm the presence of long and short full length isoforms. Forward primers were designed in regions of sequence specific to the B and C isoforms, and reverse primers were designed to either represent the originally predicted exon/exon boundary of the long isoform, or to represent the newly discovered exon/exon boundary of the short isoform.

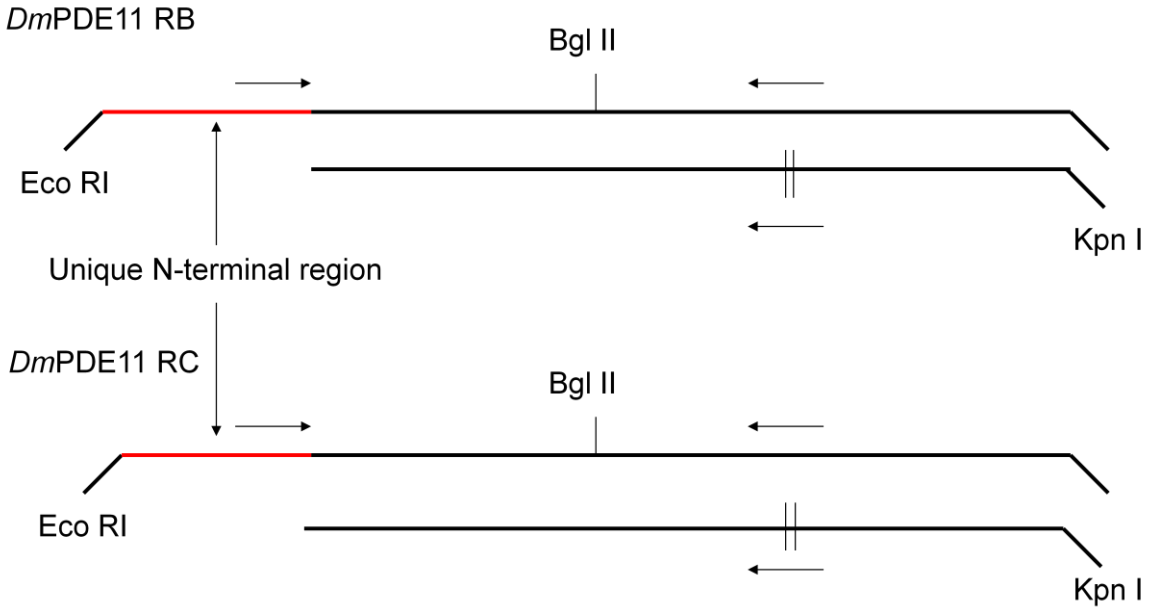

These primers were used in PCRs of hindgut cDNA, and the PCRs run on an agarose gel (figure 4.13).

Figure 4.13: Verification of *Dm*PDE11RB and RC. Forward primers specific to the N-termini of *Dm*PDE11-RB and –RC isoforms (RBF and RCF respectively) were used alongside reverse primers designed to amplify the originally predicted exon/exon boundary of the long isoform (REV), or to amplify the newly discovered exon/exon boundary of the short isoform (GAP) from hindgut cDNA. Band size identified using 1kb ladder.

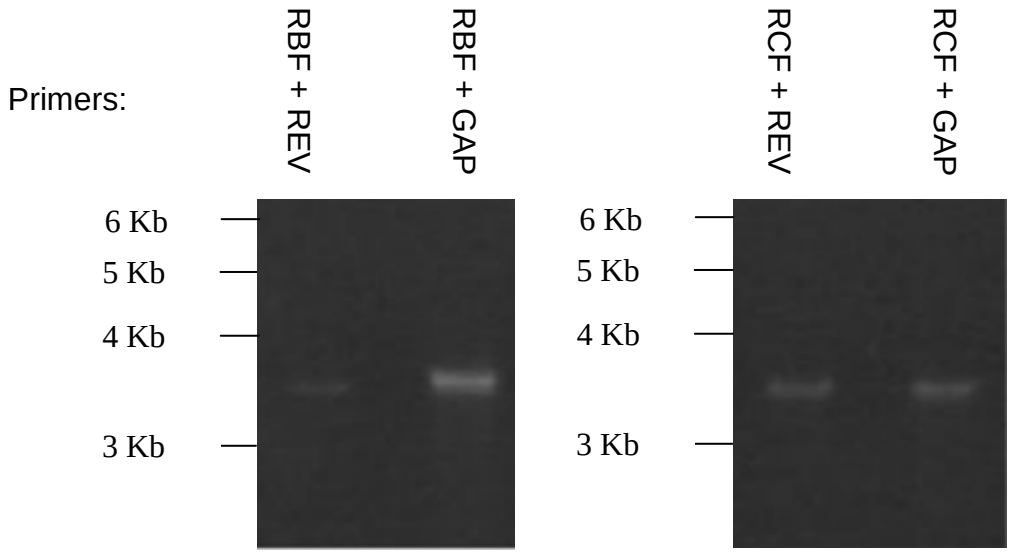

Bands of the expected size (~3.5kb) were produced for both *Dm*PDE11 RB and RC using both the reverse primer within the originally predicted exon/exon boundary, and one within the novel exon/exon boundary within the short C terminus. Thus, both *Dm*PDE11-RB and -RC were found to have a full length and a truncated isoform, and as such these were designated *Dm*PDE11RB long, *Dm*PDE11RB short, *Dm*PDE11RC long, and *Dm*PDE11RC short. The features of these proteins are summarised in figure 4.14.

Figure 4.14: The four *Dm*PDE11 isoforms. Antibody epitope refers to the polyclonal rabbit antibody generated for *Dm*PDE11RA.

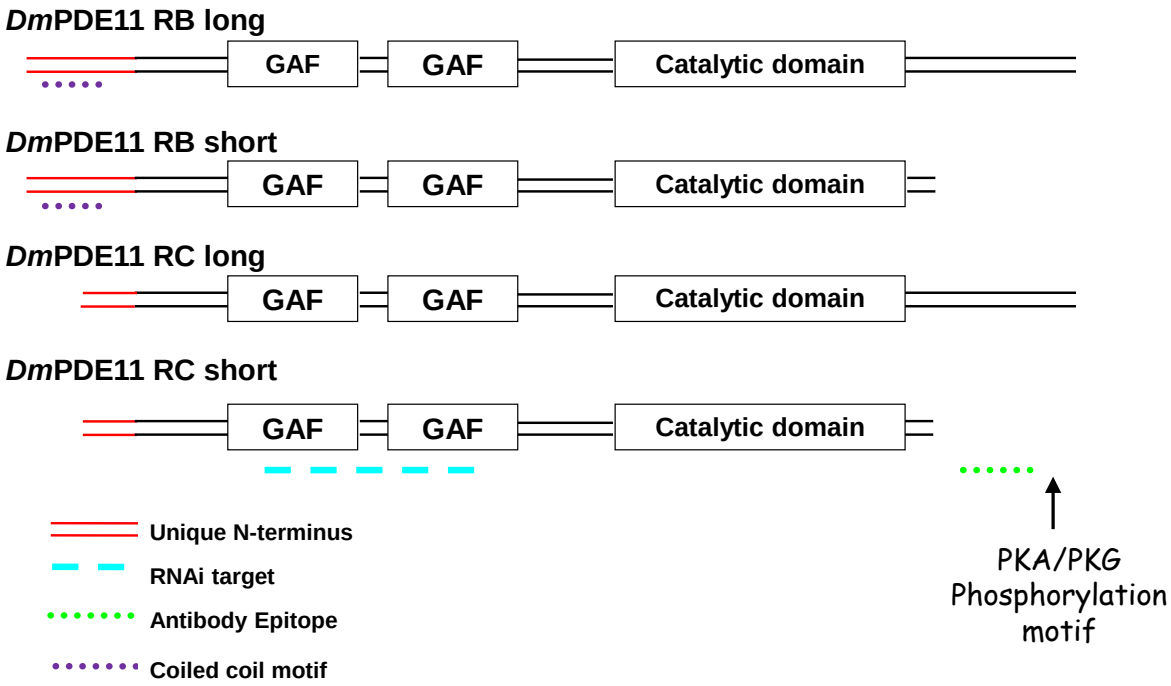

GAF: cGMP-binding phosphodiesterase, Anabaena adenylyl cyclase, and Escherichia coli FhlA domain

These isoforms share a "core" area containing twin GAF domains, and a dual specificity PDEase domain (Attwood et al., 2003; Bateman et al., 2004; Letunic et al., 2006). The novel N termini are of low homology when compared to *Hs*PDE11A, as is the long C terminus. The novel N terminus of *Dm*PDE11B is predicted to contain a coiled coil motif when analysed with the COILS program (Lupas, 1997; Lupas et al., 1991).

4.5 Generation of *Dm*PDE11 transgenic flies

Due to time constraints, it was reasoned that I should generate the four verified *Dm*PDE11 transgenic flies while concurrently assaying for cA- or cG-PDE activity in S2 cells. As PDE assays on S2 cell over-expressed PDE11RA and catalytic domain had shown no significant PDE activity, but anti-*Dm*PDE11 immunoprecipitate of whole fly lysate yields significant cA- and cG-PDE activity, it was reasoned that expression in whole fly may be needed to verify one way or the other, as the catalytic domain remains unchanged in terms of sequence. As such, if the S2 cell PDE assays were unsuccessful, PDE assays on *Dm*PDE11 overexpressing whole fly could be performed.

4.5.1 Cloning of *Dm*PDE11 ORFs into pUAST

4.5.1.1 Cloning of *Dm*PDE11RC long and short

Attempts to ligate the N and C termini of RC into pUAST simultaneously failed, and as such these were cloned sequentially. The long and short C terminals (with a stop codon) were cloned into pUAST first. pUAST-YFP was a kind gift from John Day; the long and short C terminals (without a stop codon) were cloned into this construct in frame with the C-terminal YFP tag. The N terminus of RC was then cloned into these constructs in order to generate full length ORFs. pUAST-*Dm*PDE11RC-YFP long and short, and pUAST-*Dm*PDE11RC short were generated, however, despite numerous attempts, the N terminus did not sub-clone into pUAST-Cterm long, and so pUAST-*Dm*PDE11RC long could not be generated. Were untagged *Dm*PDE11RC long required, it could be generated by PCR using pUAST-*Dm*PDE11-YFP long as a template, with a stop codon incorporated into the reverse primer.

4.5.1.2 Generation of modpUAST

The order of restriction sites of *Dm*PDE11RB, 5' → 3', is EcoRI-XhoI-BglII-NotI/KpnI. Numerous vectors were checked for an EcoRI-XhoI-BglII order in the MCS to facilitate sequential cloning, but none were found. The multiple cloning site of pUAST has restriction sites in the order of EcoRI-BglII-NotI-EagI-XhoI-KpnI-XbaI. As this would not permit sequential sub-cloning of the EcoRI-XhoI, XhoI-BglII, and BglII–KpnI/NotI TOPO cloned fragments, the MCS of pUAST was modified. This was achieved by the generation of two overlapping primers representing the sequence of the desired MCS; the overlap

facilitated the formation of “sticky ends” when then two were incubated together, and ligated into doubly digested pUAST (materials and methods 1.3.19). The forward primer was coupled to a reverse primer 500bp into pP{UAST}, and this primer set was used to screen for successful recombinants (figure 4.15).

Figure 4.15: Screen for successful mod pP{UAST} recombinants. PCR screening of modified pP{UAST} yielded a successful recombinant (lane 10, indicated by an arrow).

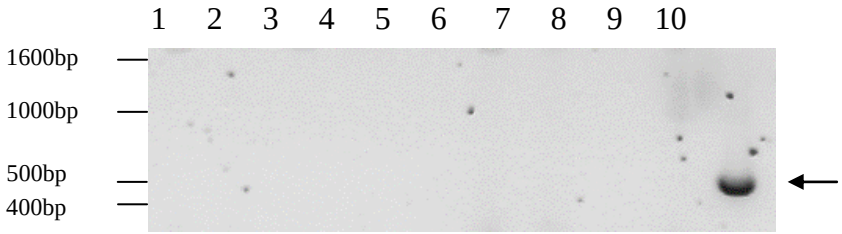

When this recombinant pP{UAST} was identified (lane 10), *Dm*PDE11RB was subcloned into it in the order BglII–KpnI/NotI, XhoI-BglII, then EcoRI-XhoI. However, the EcoRI site was found to be mutated, and so the EcoRI-XhoI fragment was sub-cloned into the N terminus of pP{UAST} PDE11RC. However, frustratingly the EcoRI-XhoI fragment would not ligate into the untagged PDE11 RC long or short constructs, and so only *Dm*PDE11RB long-YFP and *Dm*PDE11RB short-YFP could be generated. Were untagged constructs required, these could be generated by PCR of the entire ORF, with a stop codon incorporated into the reverse primer.

4.5.2 Cloning of ORFs into pAc5.1/V5-HIS C

The above ORFs were sub-cloned into pAc5.1/V5-HIS C, an S2 expression system that does not require induction with $CuSO_4$, as it was considered a possibility that $CuSO_4$ may displace the Zn ion at the active site of the PDE, rendering it catalytically null, or resulting in the mis-folding of the protein. An experiment to check this, where untransfected S2 cells, one treated with the concentration of $CuSO_4$ used to induce expression using DES vectors, and an “uninduced” control, showed a marked reduction (~13%) in PDE activity where the cells were exposed to $CuSO_4$, although this was N=1 and would need to be repeated at N=3 to verify the finding.

4.6 Verification of protein size

YFP tagged *Dm*PDE11 flies were crossed to the GAL4 driver line heat shock GAL4 (HSG4), which drives GAL4 expression ubiquitously in response to a 37˚C heat shock. Fly lysate was subjected to western blot analysis. Protein size was verified by western blotting using an anti-GFP antibody which recognised YFP. YFP tagged *Dm*PDE11B long and B short were immunoprecipitated from whole fly lysate alongside HSG4 control, and subjected to western blot analysis (figure 4.16).

Figure 4.16: Analysis of YFP-tagged *Dm*PDE11B. YFP-*Dm*PDE11B long and YFP-*Dm*PDE11B short flies were crossed to the ubiquitous driver line heat shock GAL4 (HSG4), and gene expression induced by 3 x 20 min heat shocks. Protein sizes were identified by western blot analysis, where YFP-tagged proteins were identified using αGFP monoclonal (that recognises YFP) primary, αmouse Cy3-coupled secondary, and band size was calculated using ImageQuantTL software (GE Healthcare).shown is the. Lane 1. Fly lysate HSG4 2: Fly lysate YFP-*Dm*PDE11RBL/HSG4 3. Fly lysate YFP-*Dm*PDE11RBS/HSG4. Expected sizes YFP-*Dm*PDE11B long: 187.9, YFP-*Dm*PDE11B short: 157.0 kDa.

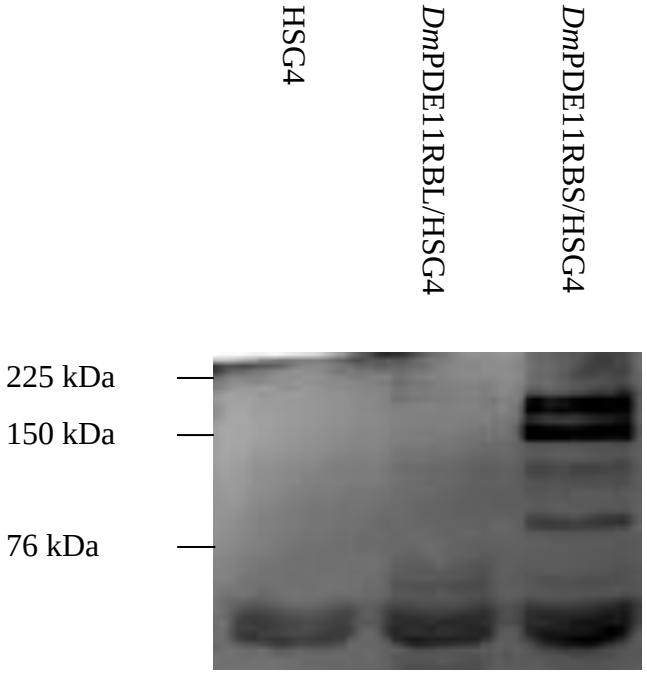

Expected band sizes for YFP-tagged *Dm*PDE11B long and short are 187.9 kDa and 157.0 kDa respectively. Analysis of band sizes for YFP-tagged *Dm*PDE11B long using ImageQuantTL software identifies a novel band at 186.2 kDa, in close agreement with the predicted protein size of 187.9 kDa, and a band at 164.6 kDa. Analysis of band sizes for YFP-tagged *Dm*PDE11B short identifies a novel band at 159.2 kDa, again in close agreement with the predicted protein size of 157.0 kDa, and two further novel bands at 121.0 kDa and 55 kDa. Three bands were present in the HSG4 negative control lane (one ~85 kDa and two ≤30kDa), and so were identified as non-specific bands.

Fly lysate from YFP tagged *Dm*PDE11C long and Canton S control were subjected to western blot analysis (figure 4.17).

Figure 4.17: Analysis of YFP-tagged *Dm*PDE11C long. YFP-*Dm*PDE11C long and YFP-*Dm*PDE11C short flies were crossed to the ubiquitous driver line heat shock GAL4 (HSG4), and gene expression induced by 3 x 20 min heat shocks. Protein sizes were identified by western blot analysis, where YFP-tagged proteins were identified using αGFP monoclonal (that recognises YFP) primary, αmouse HRP-coupled secondary, and band size was calculated by comparison with Benchmark prestained protein ladder. Intervening lanes deleted in Paint program, and lanes moved together. Lane 1. Fly lysate Canton S 2: Fly lysate YFP-*Dm*PDE11RCL/HSG4. Expected protein size YFP-*Dm*PDE11C long: 182.6 kDa.

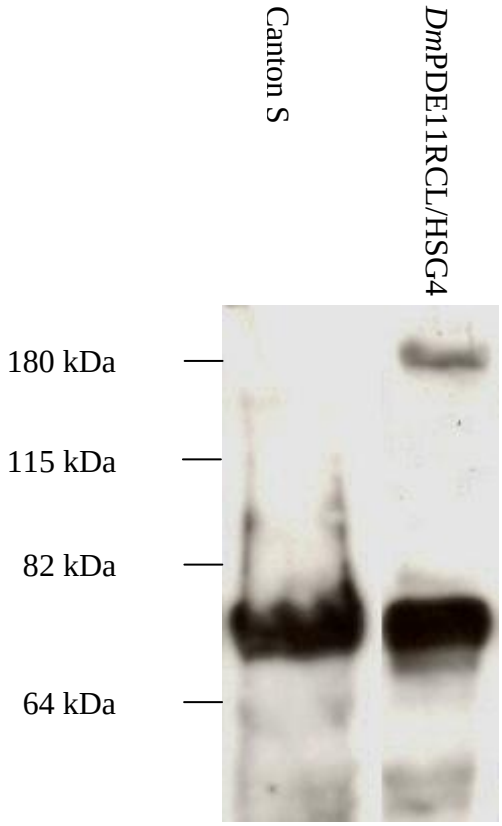

YFP-tagged *Dm*PDE11C long is predicted to be 182.6 kDa. When expressed in fly, the protein runs to ~180 kDa, in close agreement with the predicted protein size of 182.6 kDa. A band of ~70 kDa was present in the Canton S negative control lane, and so was identified as a non-specific band.

YFP tagged *Dm*PDE11C short was immunoprecipitated from whole fly lysate alongside HSG4 control, and subjected to western blot analysis (figure 4.18).

Figure 4.18: Analysis of YFP-tagged *Dm*PDE11C short. YFP-*Dm*PDE11C long and YFP-*Dm*PDE11C short flies were crossed to the ubiquitous driver line heat shock GAL4 (HSG4), and gene expression induced by 3 x 20 min heat shocks. Protein sizes were identified by western blot analysis, where YFP-tagged proteins were identified using αGFP monoclonal (that recognises YFP), and band size was calculated using ImageQuantTL software (GE Healthcare). Lane 1. Fly lysate HSG4 2: Fly lysate YFP-*Dm*PDE11RBL/HSG4 3. Fly lysate YFP-*Dm*PDE11RBS/HSG4. Expected protein size *Dm*PDE11C short 151.7 kDa.

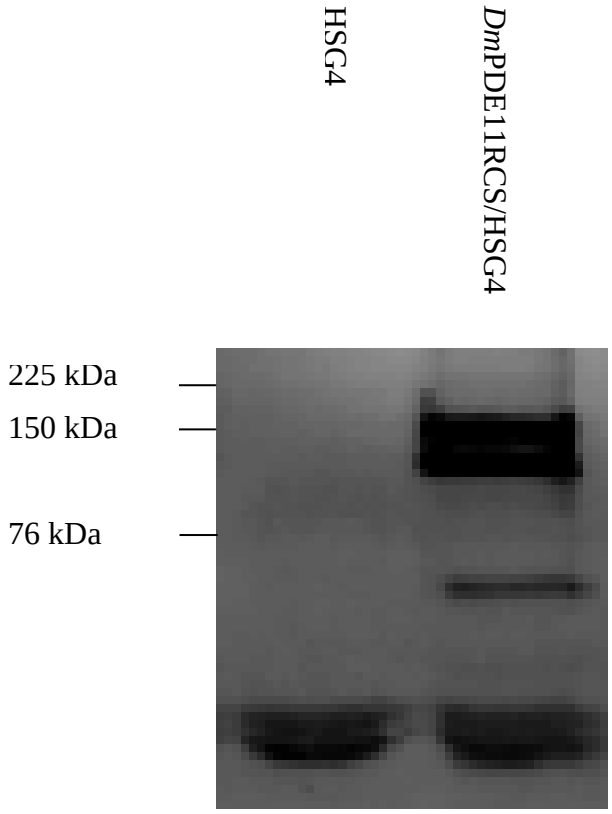

YFP-tagged *Dm*PDE11C short is predicted to be 151.7 kDa. Analysis of the two novel bands in the *Dm*PDE11C short lane identifies one band of 149.0 kDa, in close agreement with the predicted protein size, and two further bands of 112.7 kDa and 54.2 kDa. Two

bands were present in the HSG4 negative control lane of ≤30kDa, and so were identified as non-specific bands.

4.7 Verification of phosphodiesterase activity

S2 cells were transfected with *Dm*PDE11RC long (untagged and YFP tagged) and RC short (untagged, V5 tagged, and YFP tagged). cA-PDE assays were performed on S2 cell lysate, with concentrations of 5 µM and 10 µM cAMP. None of these constructs gave a significant increase in PDE activity at either concentration (figure 4.19).

Figure 4.19: *Dm*PDE11RC does not yield cA-PDE activity when expressed in S2 cells. cA-PDE assay on transiently transfected S2 cell lysate using 5 µM substrate (A) and 10 µM substrate (B). In order to aid comparison, data is expressed as % cA-PDE activity of mock transfected S2 cell, where for A, mock = 142.1 pmol cAMP/mg/min (SEM ±14.61), and for B mock = 90.23 pmol cAMP/mg/min (SEM ±10.12). N=≤3 biological replicates, except for *Dm*PDE11RCs V5 and *Dm*PDE11RCs stop, where N=2 biological replicates.

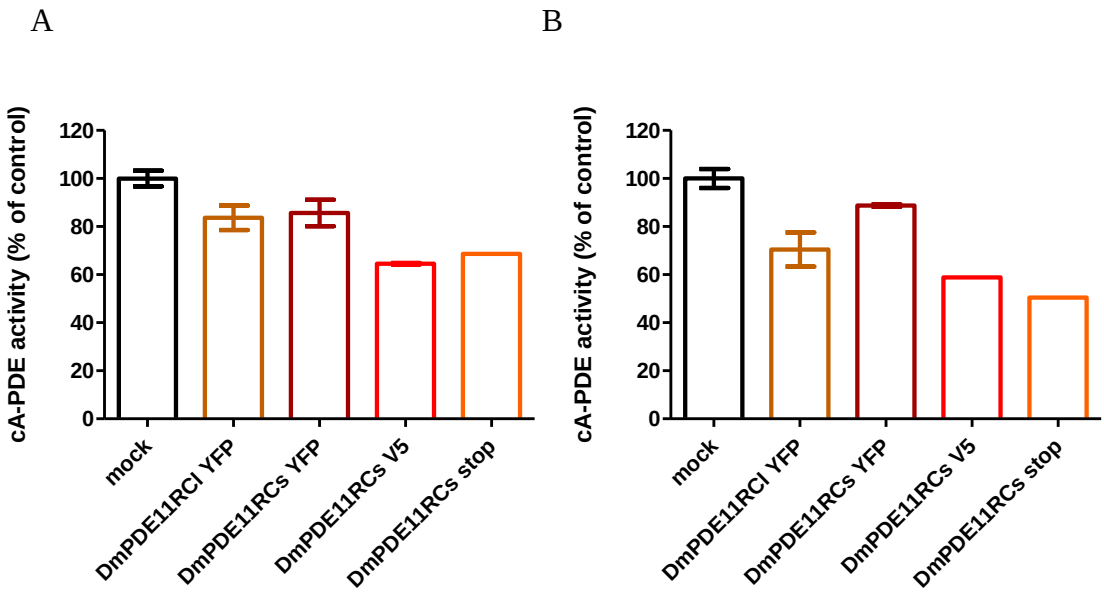

Indeed, where *Dm*PDE11RC constructs were transfected this resulted in a significantly (analysis with one-way anova) lower level of cA-PDE activity compared to untransfected control. Reasons for this are unknown; perhaps the protein acts as a catalytically null dominant negative in S2 cells. A smaller cAMP/min/mg value for the 10µM assay mock control may have been due to unusually high blank readings. PDE assays using

immunoprecipitate (IP) with an anti-*Dm*PDE11 polyclonal antibody against whole-fly yields a Km of 6±2µM for cGMP, and 18.5±5.5µM for cAMP, as published in Day et al, 2005. Thus, *Dm*PDE11 is a dual specificity cAMP- and cGMP-PDE. It is notable that *Dm*PDE8, when transiently expressed in S2 cells and subjected to PDE assays, also fails to yield measurable PDE activity (Day, 2005). Furthermore, when aligned with the catalytic domain of other *Drosophila* PDEs, the sequence showed a very high sequence similarity, with only one amino acid change within this region, with the same change in *Dm*PDE6 catalytic domain (figure 4.20). A cG-PDE, this has been shown to display cG-PDE activity in S2 cells.

Figure 4.20: ClustalW alignment of *Drosophila* PDE catalytic domains with their human homologues. This region is invariant between the RA, and RB/RC isoforms of *Dm*PDE 11 (From Day et al, 2005)

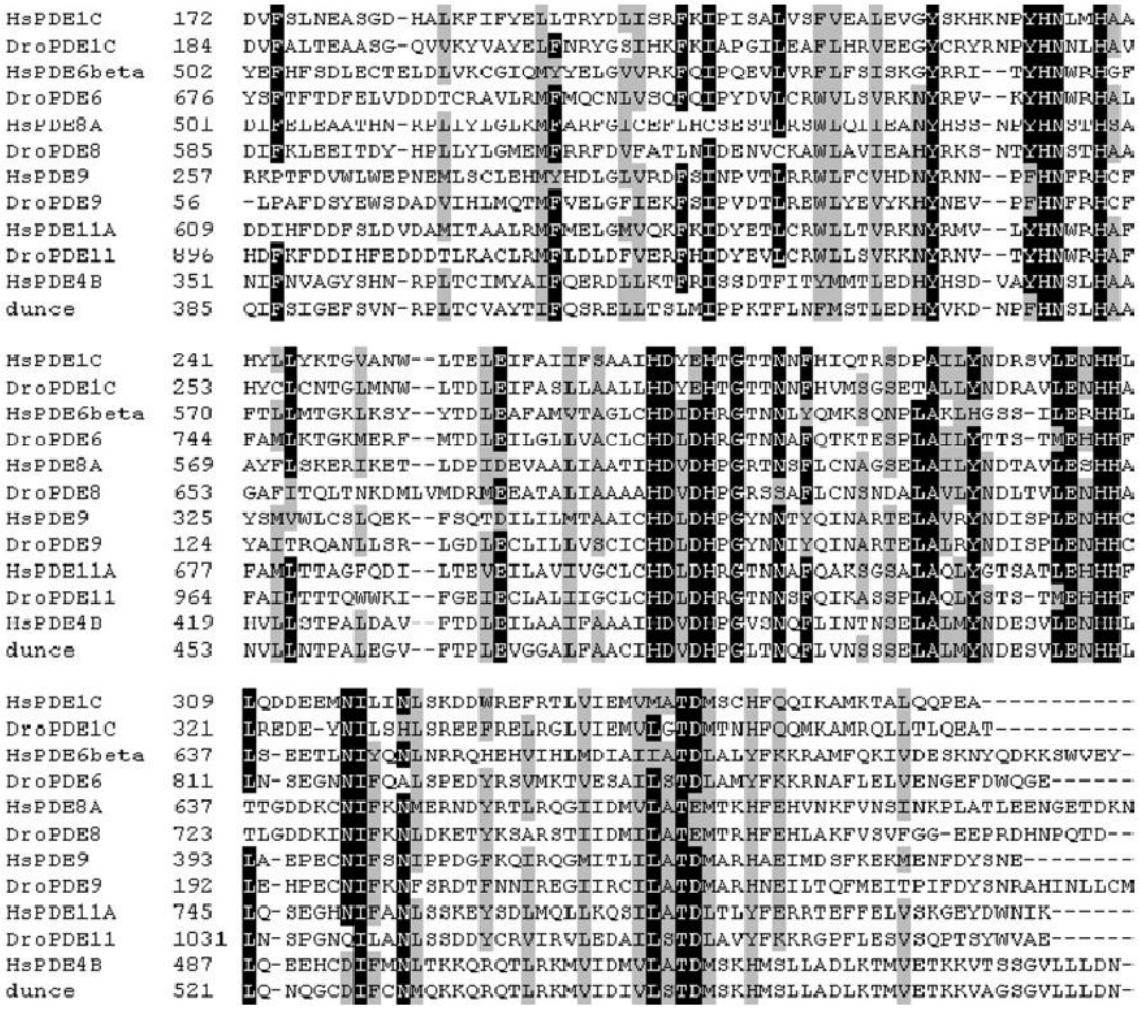

As such it was decided to send the pP{UAST} constructs for injection, and with the generated transgenic flies to perform PDE assays on fly lysate. Indeed, analysis of the protein by western blot does suggest that the enzyme may be subjected to a post-translational modification when expressed in fly, which may affect its activity. As such, YFP-tagged *Dm*PDE11RB and RC expressing flies were crossed to heat shock GAL4 flies to ubiquitously induce expression of the transgene. The protein was immunoprecipitated, and the immunoprecipitate used to assay cA- and cG-PDE activity of the protein (figures 4.21 and 4.22).

Figure 4.21: YFP tagged *Dm*PDE11RB long, RB short, RC long, and RC short yield significant cA-PDE activity when transgenically expressed in *Drosophila*. cA-PDE assay on αYFP immunoprecipitated PDE from transgenic whole fly lysate using 10 μM substrate. Data expressed as pmol cAMP hydrolysed/IP/min. Assay performed in biological triplicate. Data statistically significant between parental control and PDE-expressing progeny to P<0.0001 (Student's unpaired T test). Error bars show SEM.

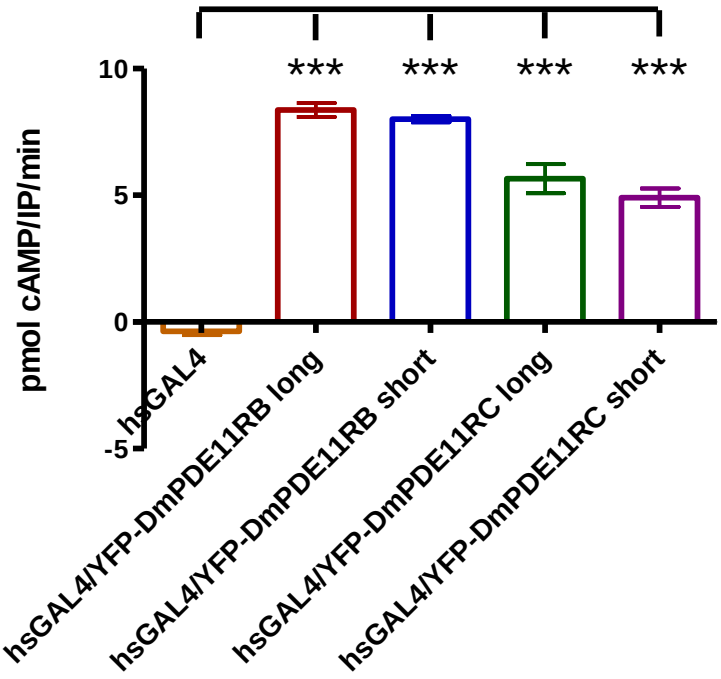

Figure 4.22: YFP tagged *Dm*PDE11RB long, RB short, RC long, and RC short yield cG-PDE activity when transgenically expressed in *Drosophila*. cG-PDE assay on αYFP immunoprecipitated PDE from transgenic whole fly lysate using 10 μM substrate. Data expressed as pmol cGMP hydrolysed/IP/min. Assay performed in biological duplicate. Error bars show SEM.

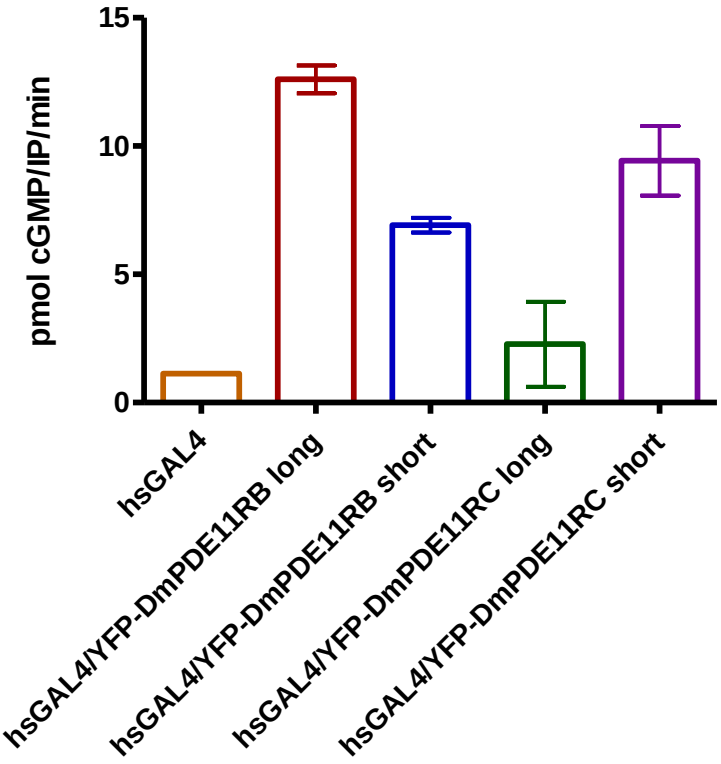

Each YFP tagged PDE11 isoform showed a significant increase in cAMP-PDE activity compared to heat shock GAL4 parental control (figure 4.21). As the cGMP-PDE assays were performed in biological duplicate, statistics cannot be performed, however B long, B short, and C short gave an increase in cGMP-PDE activity compared to heat shock GAL4 control.

4.8 Implications of the *Dm*PDE11 sequence change

A concern was that tools designed around the sequence of *Dm*PDE11RA would become redundant with the prediction of the RB and RC isoforms. The epitope used to raise anti-*Dm*PDE11 polyclonal rabbit antibodies is unchanged in the long isoforms, but is not present in the short isoforms. The published western blot shows one clear band (Day,

2005); it may be that the RB and RC long isoforms run so close together as to be indistinguishable on a western blot.

The RNAi (pWIZ) construct was targeted against an area conserved between all 4 isoforms, which remains unchanged between RA, and RB and RC. Thus it should knock-down all four isoforms. Furthermore the primers used in the PDE11RA Q-PCR also amplified a region present in all 4 isoforms, and as such, remains valid, as no single region would allow Q-PCR against a single isoform, as Q-PCR with primers designed against sequence specific to *Dm*PDE11RB or RC would amplify sequence from both long and short isoforms.

Flyatlas was produced using the *Drosophila* genome 2 array, which contains 14 probes against *Dm*PDE11-RA (Affymetrix nettafx analysis center). These probes hybridised between 4529 and 5049bp of the ORF. Again, this range of sequence remains unchanged between *Dm*PDE11RA and both RB and RC transcripts, and thus these probes hybridise to, but do not differentiate between, RB long, RB short, RC long and RC short.

4.9 Confocal microscopy of *Dm*PDE11

Transgenic *Drosophila* were crossed to heat shock GAL4 flies, the tubules dissected and fixed, and images obtained by immunocytochemistry (figures 4.23-4.27).

Figure 4.23: RB long YFP single plane. Tubules from *Dm*PDE11RB long/HSG4 flies were fixed and visualised by confocal microscopy.

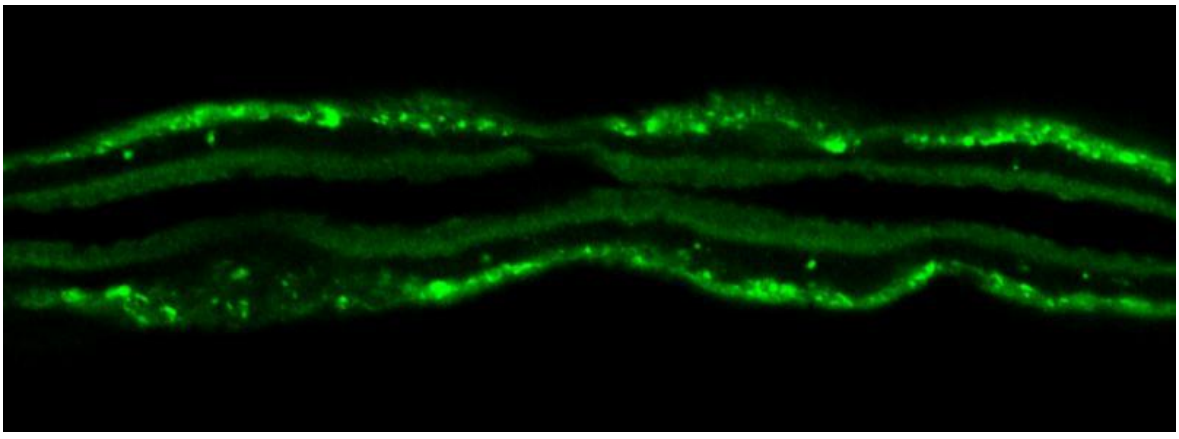

Figure 4.24: RB short YFP single plane. Tubules from *Dm*PDE11RB short/HSG4 flies were fixed and visualised by confocal microscopy.

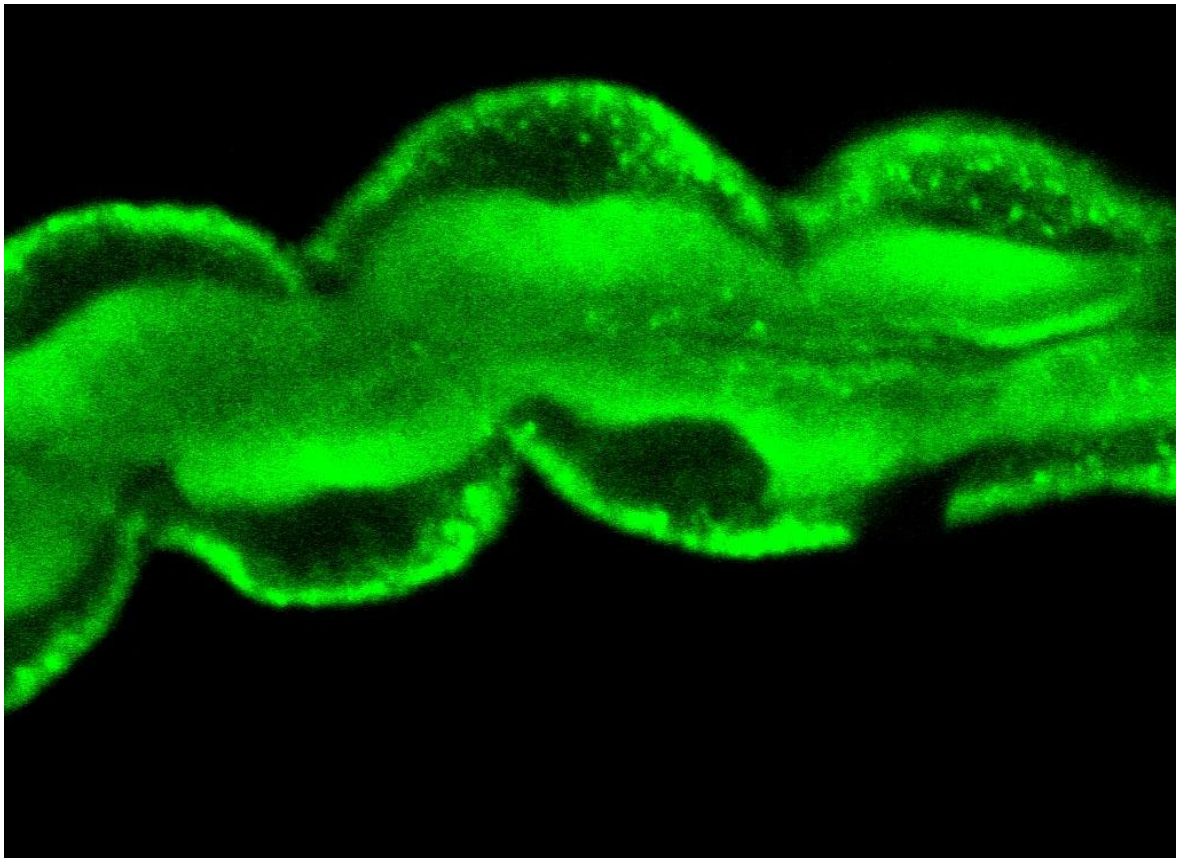

Figure 4.25: *Dm*PDE11 B long YFP projection. Tubules from *Dm*PDE11 B long/HSG4 flies were fixed, and a Z-stack obtained by confocal microscopy. Shown is a projection of this Z-stack.

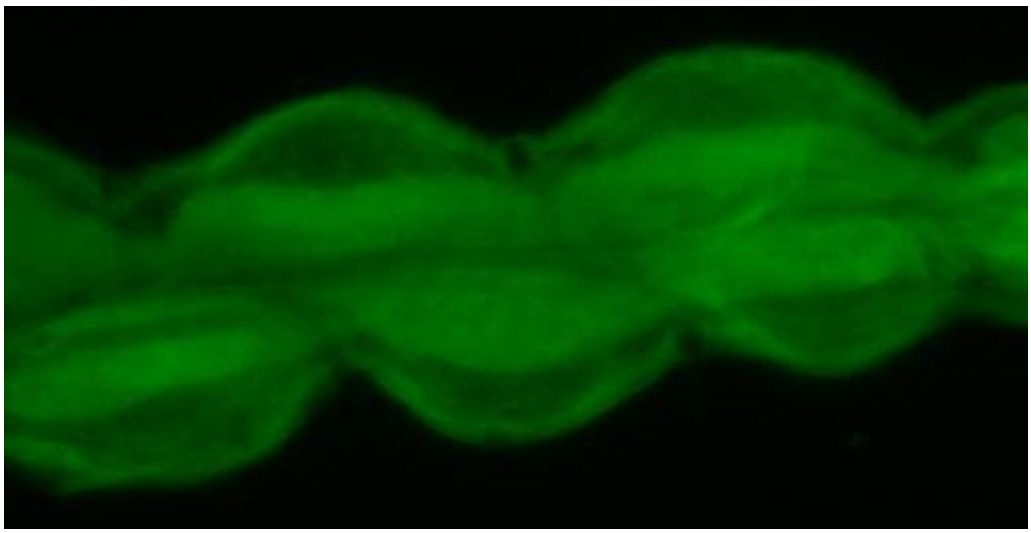

Confocal images of both *Dm*PDE11B long and short show that both proteins show similar localisation, both localising primarily to the apical and basolateral membranes of the Malpighian tubule, with lesser staining in the cytosol.

Figure 4.26: *Dm*PDE11 C long YFP single plane. Tubules from *Dm*PDE11 C long/HSG4 flies were fixed, DAPI stained, and visualised by confocal microscopy. Shown is a single cell from the main segment. *Dm*PDE11 C long YFP = green, DAPI = blue.

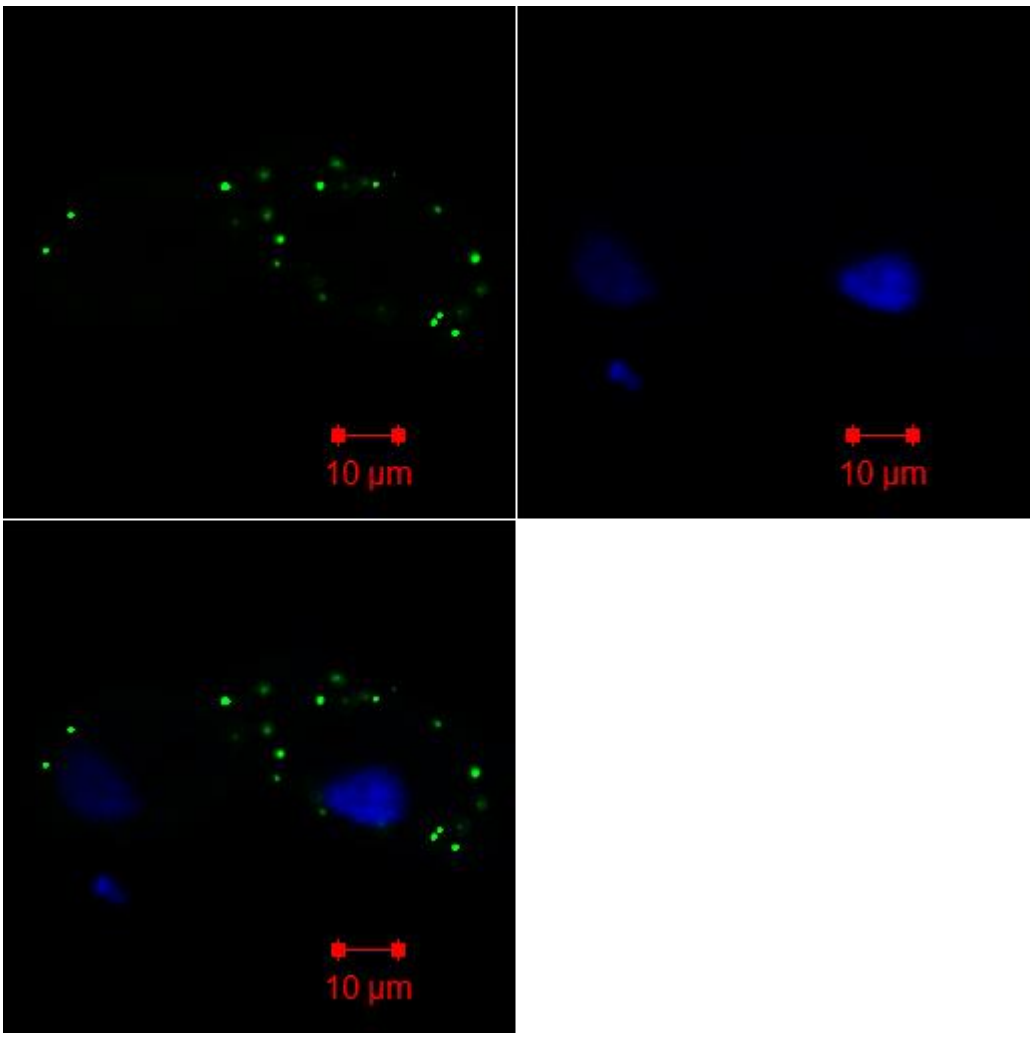

Figure 4.27: *Dm*PDE11 C short YFP single plane. Tubules from *Dm*PDE11 C short/HSG4 flies were fixed, DAPI stained, and visualised by confocal microscopy. *Dm*PDE11 C long YFP = green, DAPI = blue.

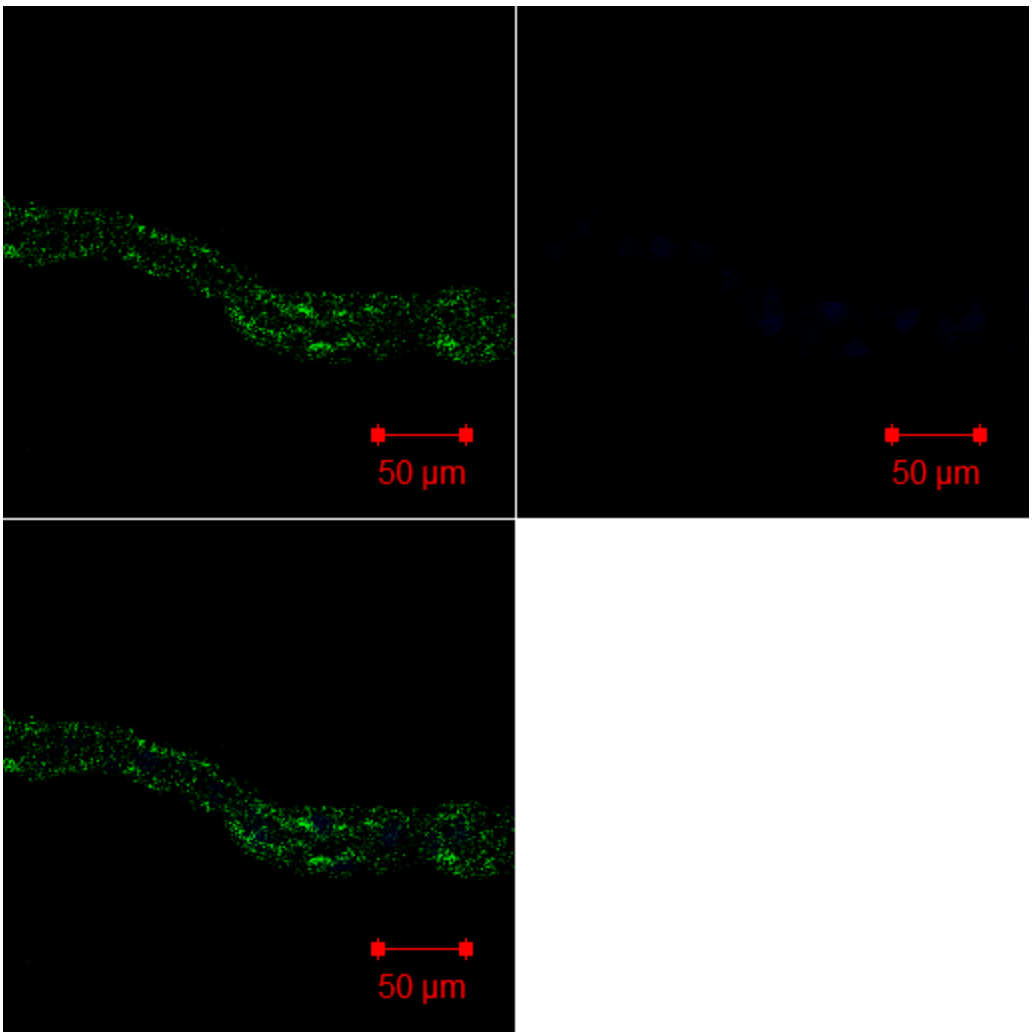

RC long and short isoforms showed indistinguishable localisation to an unidentified organelle, or perhaps vesicles. It shows no nuclear localisation.

4.10 Discussion

*Dm*PDE11RA was replaced in the Flybase 5.2 release with two novel isoforms, *Dm*PDE11RB and RC. In this chapter, these isoforms were verified as being expressed. The ORFs of these genes were cloned into S2 cell expression vectors, and pP{UAST}. Overexpression of YFP tagged *Dm*PDE11 in fly yielded proteins of the predicted size. cA-PDE assays on S2 cells transfected with *Dm*PDE11RC at 5 µM and 10 µM did not yield

cA-PDE activity above that of untransfected S2 cell control, and indeed, as PDE activity was reduced compared to control, it may be that in S2 cells transgenically expressed YFP tagged *Dm*PDE11 acts as a dominant negative, reducing endogenous PDE activity. However, when transgenically overexpressed in fly, the enzymes yield cA- and cG-PDE activity, and are thus *bona fide* dual specificity PDEs. No direct comparison can be made with PDE assays performed on αPDE11 IPs from head lysate published in (Day et al., 2005), where values were ~2.5 pmol/min/IP for cGMP, and ~6 pmol/min/IP, as the protocols of that paper and this work differ markedly; Day used 20 heads instead of 10 whole flies as starting lysate, and used the αPDE11 polyclonal antibody which targets an epitope shared by all 4 isoforms of PDE11 referred to in chapter 3 to pull down endogenous (untagged) PDE11, instead of αGFP monoclonal antibody to pull down YFP tagged overexpressors. As PDE assays on immunoprecipitate cannot give specific activity/min/mg protein, the data of figures 4.21 and 4.22 do not show whether the isoforms differ in affinity for their substrates. A dose response curve would need to be generated using overexpressed protein, in a format that allowed quantification of protein. As for the reasons that the enzymes displayed no cAMP- or cGMP-PDE activity in S2 cells, while these same enzymes displayed cAMP- and cGMP activity when transgenically overexpressed in *Drosophila*, they are unknown. It may be that a post translational modification occurs in *Drosophila* but not in S2 cells, which may be necessary to confer enzymatic activity on the protein. cNMP-PDE assays were previously performed in S2 cells on transiently transfected full length PDE1 and PDE8 (transcript A), and the catalytic domain of PDE6, 9, and 11 (Day, 2005). Of these, PDE 6 showed cGMP-PDE activity, and the catalytic domain of PDE11 showed cAMP-PDE activity, but only at substrate concentrations of between 1 - 4 μM, and did not show cGMP-PDE activity, as was the case for IP from fly head lysate. Thus, S2 cells do not appear to be a good cell choice for the heterologous study of PDE catalytic function.

The subcellular localisation of each isoform was determined by immunocytochemistry on fixed YFP tagged-*Dm*PDE11 expressing Malpighian tubules. The long and short isoforms of YFP-*Dm*PDE11B localised to the apical and basolateral membranes, with lower levels of protein in the cytosol. The unique N-terminus of *Dm*PDE11B is 64 amino acids in length, and is not predicted to be a transmembrane domain when analysed with Argos or von Heijne tests using MacVector software. It contains a polyglutamine region that falls within a region predicted to form a coiled coil structure when analysed with the Ncoils test of the protein analysis toolkit (Lupas, 1997). Coiled coils are known to reversibly mediate homo- and heteromeric protein-protein interaction (Strauss and Keller, 2008), and can

facilitate the formation of protein complexes (Langosch and Heringa, 1998). Therefore this region may facilitate the interaction of *Dm*PDE11B with an unidentified protein that tethers the PDE to the membrane. PDEs from several other families have been shown to localise to the membrane due to interaction with other proteins. PDE3 contains N-terminal hydrophobic membrane association domain, which either mediate localisation by interaction with unidentified proteins, or by functioning as a transmembrane domain (Wechsler et al., 2002). PDE4 isoforms contain differing N-termini that encode unique subcellular targeting motifs and direct novel protein-protein interactions that tether the enzymes to particular subcellular localisations. PDE4A1 contains a motif called tryptophan anchoring phosphatidic acid selective-binding domain (TAPAS-1), which permits a Ca^{2+} sensitive association with the membrane via phosphatidic acid binding (Baillie et al., 2002). PDE4D5 is recruited to the membrane due to the presence of a β-arrestin binding site in the N terminus (Bolger et al., 2006). PDE6 localises to the membrane due to its interaction with glutamic acid-rich proteins (GARPs) (Körschen et al., 1999), as well as lipid modifications to the C terminus of the catalytic subunits (Anant et al., 1992).

The long and short isoforms of YFP-*Dm*PDE11C localised to foci within the cytosol, likely within unidentified organelles, or to vesicles. As *Dm*PDE11B and C show markedly different localisation, and the only difference between these isoforms is the first exon, this sequence must encode a targeting motif. As the long and short isoforms of *Dm*PDE11B or C do not show any discernable differences in localisation, the long C terminal must have some other, unknown function, perhaps pertaining to the predicted PKA/PKG consensus phosphorylation site. The C terminus is of low homology to that of *Hs*PDE11A. As *Dm*PDE11C is YFP tagged, the identification of the unknown organelle could be identified by either co-staining of each organelle using specific antibodies, or by the crossing of these flies to proteins tagged with a different marker such as Venus or GFP that are known to localise to a particular organelle, and screening for co-localisation. YFP-*Dm*PDE11C localise to organelles similar in appearance to peroxisomes in S2 cells as reported in (Ally et al., 2009), a pattern that does not match that reported in (Southall et al., 2006) where the peroxisomes are fewer in number and larger. Regardless, the number of peroxisomes per cell in the Malpighian tubule is clearly far higher than the number of organelles per cell containing *Dm*PDE11C in the tubule, thus discounting the peroxisomes as a candidate organelle. The localisation is distinct to the staining pattern seen in Malpighian tubules when using antibodies against proteins localised to the sarcoplasmic reticulum, endoplamic reticulum, Golgi (Southall et al., 2006), and vesicles (Evans et al., 2008), and is distinct to that of lysosomes in S2 cells (Tsruya et al., 2002). Thus a survey of the literature does not

identify a candidate organelle. The localisation of other PDEs to organelles is dictated by association with anchoring proteins. PDE4A localises to numerous organella via interaction with AKAPs, for example AKAP95 (perinucleus), AKAP149 (mitochondria), AKAP 450 (Golgi) (Dodge-Kafka et al., 2008), and myeloid translocation gene (Golgi), which also confers Golgi localisation to PDE7A (Asirvatham et al., 2004). PDE4D localises to the Golgi via association with Myomegalin (Verde et al., 2001). PDE5A is localised to vesicles and also the centrosome in human myometrical cells (Dolci et al., 2006)

That the N termini of *Dm*PDE11B and C affect subcellular localisation, likely by affecting the interaction of these proteins with the proteasome, immunoprecipitation of each isoform (i.e., using specific antisera or pulling down tagged PDE) and identification of interacting proteins using mass spectrometry specific to each isoform, and subsequent characterisation of these would perhaps identify proteins showing overlapping subcellular localisation that were worthy of investigation as putative anchoring proteins.

As the short and long isoforms of *Dm*PDE11 B and C show identical subcellular localisation, the extended C-terminal of the protein does not contain a subcellular localisation sequence.

The subcellular localisation of *Drosophila* PDEs has not been widely studied. GFP tagged *Dm*PDE6 localises predominantly to the apical membrane of the Malpighian tubule, with lower intensity fluorescence at the basolateral membrane (Day et al., 2006). When bovine PDE5, a close homologue of *Dm*PDE6, is transgenically overexpressed in tubule, it too predominantly localises to the apical membrane (Broderick et al., 2004). *Dm*PDE11B localises to the basolateral and apical membranes. The presence of two *Dm*PDEs capable of hydrolysing cGMP to the membranes suggests that cGMP signalling is under tight control in the Malpighian tubule, befitting the prominent role of cGMP signalling in the tubule.

Chapter 5

A study of *Dm*PDE11/cGK interaction

5.1 Summary

Previously obtained data (Day and Sebastian) suggested that *Dm*PDE11, and other *Dm*PDEs capable of hydrolysing cGMP, interact directly or indirectly with cGKs. The *Dm* cG-PDEs PDE1, PDE6, and PDE11 co-immunoprecipitate with significant amounts of cGK activity when immunoprecipitated using specific antisera from *Drosophila* head lysate. Likewise, the cGKs DG1 and DG2 co-immunoprecipitate with significant amounts of cG-PDE activity when immunoprecipitated using specific antisera from *Drosophila* head lysate.

Co-transfection in S2 cells of *Dm*PDE11 RB long and the cGKs shows that *Dm*PDE11B long shows a high degree of co-localisation with DG1, DG2P1, and DG2P2. Furthermore, DG1 appears to mediate *Dm*PDE11B long internalisation from the membrane. *Dm*PDE11 long appears to internalise membrane-tethered DG2P1, so that DG2P1 shows increased cytosolic localisation, and localises to foci within the cytosol, mostly coinciding with those of PDE11B long.

Co-immunoprecipitation experiments were performed in S2 cells, between the long and short isoforms of *Dm*PDE11, tagged with YFP, and the cGKs, tagged with c-Myc, where cGK was immunoprecipitated with anti-c-Myc-conjugated beads, the immunoprecipitate resolved by SDS-PAGE, and immunoblotted with anti-GFP antibody which recognised YFP. YFP-tagged *Dm*PDE11C long and short was shown to co-immunoprecipitate with c-Myc tagged DG1, DG2P1, and DG2P2, where bands of the expected size were present in doubly transfected anti-c-Myc immunoprecipitates, but not for anti-c-Myc immunoprecipitates of singly-transfected YFP-tagged *Dm*PDE11C long or short, or mock transfected S2 cell lysate. No data is presented for *Dm*PDE11B-cGK interactions, as negative controls showed background staining, although this was of lower intensity that doubly-transfected S2 cells. This provides direct evidence of *Dm*PDE11 interacting with each of the cGKs, directly or indirectly, and suggests the prospect of potential cGMP signalling compartmentalisation in *Drosophila*.

5.2 Introduction

Previously obtained data summarised in appendix 4 (Day and Sebastian, unpublished data) suggested that *Dm*PDE11, and other *Dm*PDEs capable of hydrolysing cGMP, interact directly or indirectly with cGKs. This demands further investigation, as interactions between numerous cA-PDEs and PKA isoforms (mediated by AKAPs) have been shown to

dictate the specificity of cAMP signalling events, and facilitate the formation of a feedback loop where each protein may modulate the function of the other (Wong and Scott, 2004), as detailed in the introduction. Differential localisation of cGK and PDE proteins, facilitated by gene and isoform multiplicity, permits the transmission of multiple, simultaneous signalling events. Interaction of cGKs and cG-PDEs would allow cG-PDEs to modulate interacting cGK function by affecting local cGMP concentration. It has previously been shown that DG2 modulates cG-PDE activity in the Malpighian tubule (MacPherson et al., 2004a). This modulation may occur by one of several methods; by modulation of cG-PDE function through phosphorylation, by direct, non catalytic binding, either of which would be facilitated by protein-protein interaction, or by reduction of PDE transcription. Furthermore, association of cG-PDEs with the main effectors of the cGMP signalling pathway could modulate PDE and cGK localisation, thus facilitating the formation of cGMP microdomains, and altering cGK substrate specificity.

5.3 *Dm*PDE11B long and cGK co-localise in S2 cells

*Dm*PDE11 RA and DG2 displayed a large degree of co-localisation when co-transfected in S2 cells and visualised by staining with anti-tag antibodies and subsequent confocal microscopy, as detailed in chapter 3. The above immunoprecipitation data suggests that the two proteins interact, directly or indirectly. However, to interact, proteins must demonstrate subcellular localisations that at least partially overlap. Thus, S2 cells were transiently transfected with *Dm*PDE11 RB long tagged with C-terminal YFP, and one of the cGKs DG1, DG2P1, or DG2P2, each tagged with C-terminal c-Myc, and immunocytochemistry performed to ascertain subcellular localisation. To assay whether the localisation of cGK or *Dm*PDE11 is affected by the presence or absence of the other, each construct was also transfected individually.

5.3.1 Individually transfected constructs

Constructs were transfected individually to ascertain the subcellular localisation of each protein. An S2 cell expressing YFP tagged *Dm*PDE11B long is shown in figure 5.1.

Figure 5.1: Confocal image of S2 cells transfected with YFP-*DmPDE11 RB long* (green). Nuclei were stained with DAPI (blue).

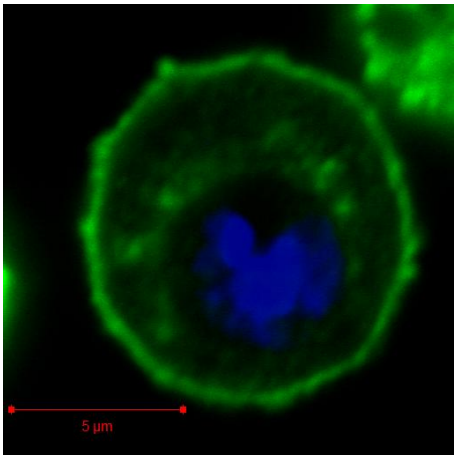

YFP tagged *Dm*PDE11B long predominantly localises to the membrane, with foci-like regions within the cytosol showing strong fluorescence, and lighter fluorescence throughout the cytosol.

Individual S2 cells expressing c-Myc tagged DG1, DG2P1, and DG2P1 are shown in figure 5.2.

Figure 5.2: Confocal images of individual S2 cells transiently transfected with c-Myc-*DG1* (A), c-Myc-*DG2P1* (B), and c-Myc-*DG2P2* (C). Subcellular localisation was ascertained by staining with anti-c-Myc monoclonal antibody, TRITC secondary (red). Nuclei were stained with DAPI (blue). Untransfected cells showed no background fluorescence (example cell visible in C).

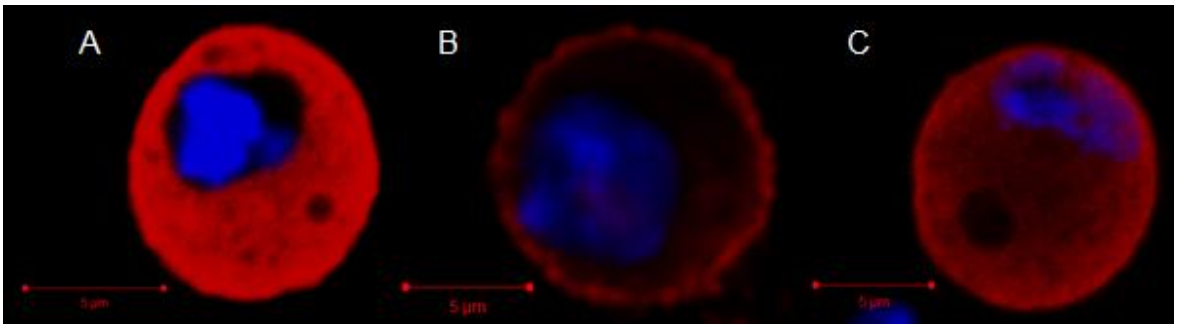

DG1 localises to the cytosol, with stronger staining towards the membrane. Published images show staining adjacent to the membrane, in common with the image above, although did not display quite as strong cytosolic staining (MacPherson et al., 2004b). The localisation of individually transfected DG2 P1 and P2 are discussed in chapter 3, but shall be repeated here. In agreement with published data (MacPherson et al., 2004b), DG2P1 localised predominantly to the membrane in S2 cells. Published images of DG2P2 are of

V5-tagged DG2P2, stained with anti-V5 monoclonal antibody and also a vertebrate anti-cGK rabbit polyclonal antibody, anti-cGKI, from (Markert et al., 1995). Images with anti-V5 antibody show solely localisation to the membrane, while those stained with anti-cGKI antibody also showed localisation within the cytosol, stronger towards the membrane. The DG2P2 construct in my possession was tagged with c-Myc. Staining with an anti-c-Myc antibody produced similar staining to the published anti-cGKI stained images, predominantly showing localisation to the membrane, with staining in the cytosol, stronger towards the membrane. This may be a characteristic of the antibody; however, untransfected cells show no background staining. The c-Myc tag may alter protein localisation; however the tag is one amino acid smaller than the V5 tag used in Macpherson et al, 2004, and so this is doubtful. A third alternative, and perhaps the most likely, is that conditions in those images using anti-c-Myc and anti-cGKI antibodies were more sensitive, and so fluorescence was detected that was not detected in anti-V5 images. Polyclonal antibodies designed against a novel epitope were unfortunately not delivered on time to test untagged DG2P2.

5.3.2 Co-transfection of c-Myc-cGK and YFP-*Dm*PDE11 RB long in S2 cells

In order to screen for co-localisation, S2 cells were co-transfected with YFP-*DmPDE11 RB long* and c-Myc-*DG1*, and the subcellular localisation of the proteins was ascertained by confocal microscopy (figure 5.3).

Figure 5.3: Confocal images of S2 cells co-transfected with YFP-*DmPDE11 RB long* (green) and c-Myc-*DG1*. Subcellular localisation of c-Myc-DG1 was ascertained by staining with anti-c-Myc monoclonal antibody, TRITC secondary (red). Nuclei were stained with DAPI (blue).

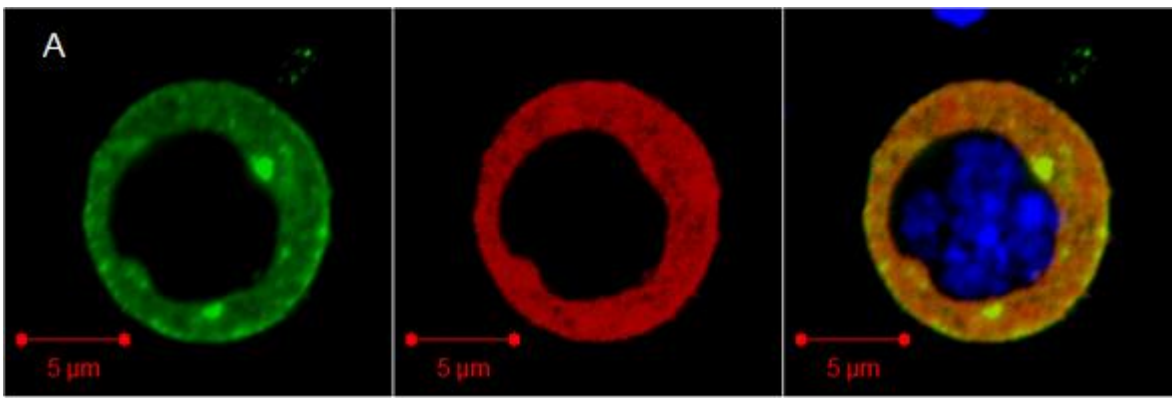

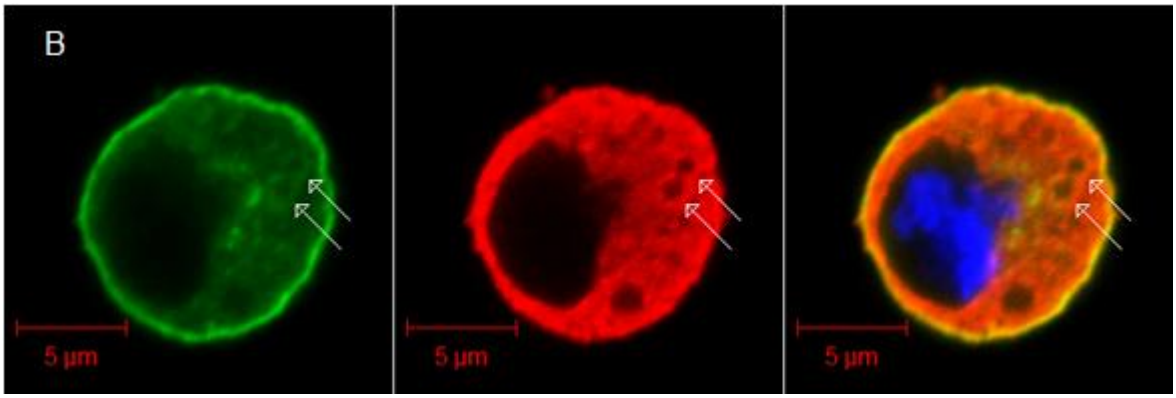

Shown are two examples of doubly transfected S2 cells; two images are shown because in some cells, YFP-DmPDEB long showed lower levels of membrane localisation when compared to S2 cells expressing YFP-B long only, suggesting that DG1 may mediate the internalisation of the protein (figure 5.5 A). This is interesting, as DG1 is not endogenously expressed in S2 cells (Chintapalli et al., 2007). In either case, the two proteins show a large degree of co-localisation within the cytosol. DG1 localisation does not appear to alter when co-expressed with *Dm*PDE11RB long. It appears that within the cytosol, (immuno)fluorescence of both proteins increases around what appear to be vacuoles, or some other organelle (figure 5.5 B, white arrows).

In order to screen for co-localisation, S2 cells were co-transfected with YFP-*DmPDE11 RB long* and c-Myc-*DG2P1*, and the subcellular localisation of the proteins was ascertained by confocal microscopy (figure 5.4).

Figure 5.4: Confocal image of an S2 cell co-transfected with YFP-*DmPDE11 RB long* (green) and c-Myc-*DG2P1*. Subcellular localisation of c-Myc-DG2P1 was ascertained by staining with anti-c-Myc monoclonal antibody, TRITC secondary (red). Nuclei were stained with DAPI (blue).

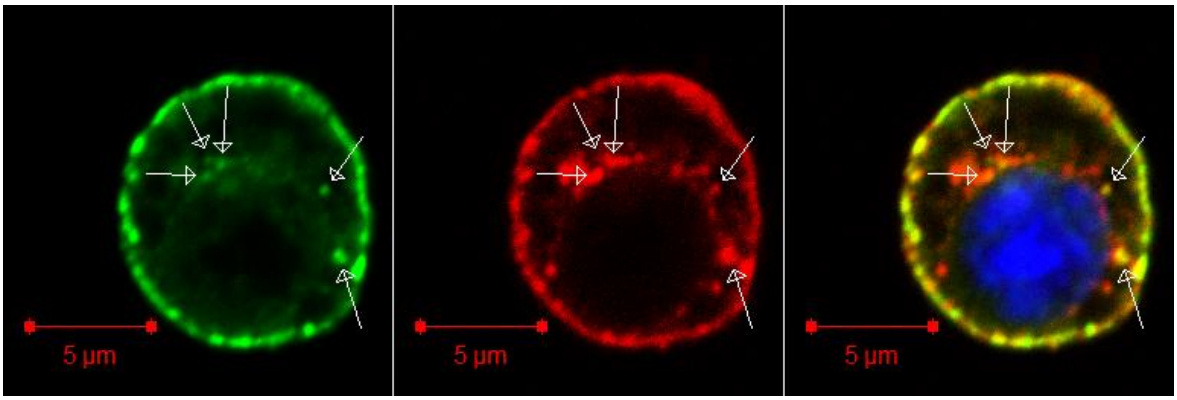

In YFP-*DmPDE11 RB long* and c-Myc-*DG2P1* co-transfected S2 cells, the proteins show a large degree of co-localisation. Localisation of DG2P1 is altered when compared to

individually transfected S2 cells, as the protein shows increased cytosolic localisation, and localises to foci within the cytosol similar to those of by PDE11B long. This finding was observed in several doubly transfected cells. The two proteins co-localise within these foci (white arrows), although DG2P1 shows localisation to additional foci that PDE11B long does not localise to. The two proteins co-localise to the membrane, where each protein has regions of increased intensity, and furthermore this variation in intensity shows a very similar pattern for the two proteins.

In order to screen for co-localisation, S2 cells were co-transfected with YFP-*DmPDE11 RB long* and c-Myc-*DG2P2*, and the subcellular localisation of the proteins was ascertained by confocal microscopy (figure 5.5).

Figure 5.5: Confocal image of an S2 cell co-transfected with YFP-*DmPDE11 RB long* (green) and c-Myc-*DG2P2*. Subcellular localisation of c-Myc-DG2P1 was ascertained by staining with anti-c-Myc monoclonal antibody, TRITC secondary (red). Nuclei were stained with DAPI (blue).

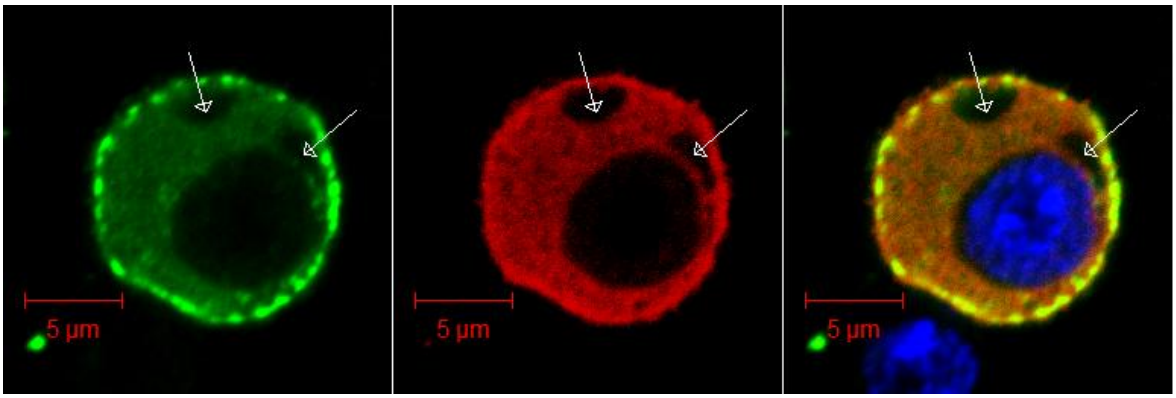

An overlay of PDE11B long and DG2P2 shows that the proteins show a large degree of co-localisation, predominantly at the membrane, although also in the cytosol. Both proteins are excluded from what appear to be vacuoles or some other organelle (white arrows). The subcellular localisation of each protein does not noticeably change between co-transfected cells and individually transfected cells.

5.4 Kinase assay from DG2 immunoprecipitate

As *Dm*PDE11 was shown to co-localise with DG2, it was reasoned that *Dm*PDE11 may affect cGK activity, and that a reduction in *Dm*PDE11 transcript levels and therefore protein levels might lead to an increase in cGK activity, due to an increase in localised [cGMP] concentration. In order to test this hypothesis, DG2 was immunoprecipitated from Malpighian tubule lysate of UAS-PDE11 RNAi (line 9), and c42/UAS-PDE11 RNAi (line

9) progeny using specific anti--DG2 antisera, and the immunoprecipitate was subjected to a kinase assay, which uses a bovine PDE5 substrate ("glasstide") to measure ATP transfer and thus levels of total kinase activity, as detailed in materials and methods (figure 5.6).

Figure 5.6: Malpighian tubules display a qualitative increase in kinase activity when PDE 11 expression is reduced in tubule principle cells via expression of a UAS-PDE11 RNAi transgene with the GAL4 driver c42. N=3 for each genotype, error bars show standard error of the mean. Statistical significance was not achieved, as determined by a two-way T-test.

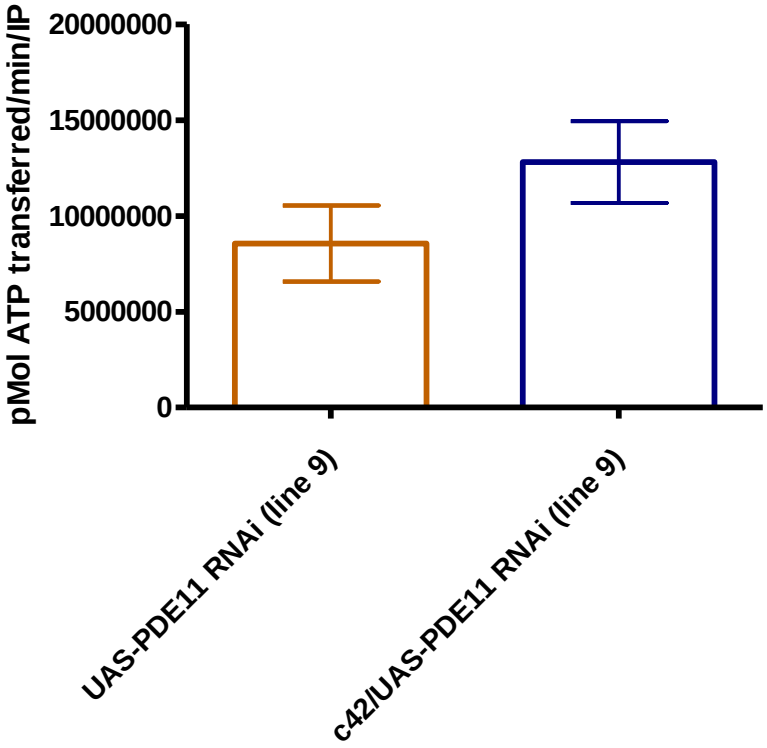

When *Dm*PDE 11 expression was reduced in Malpighian tubule principal cells, total cGMP-dependant protein kinase activity of the whole tubule was qualitatively increased, but no significant difference was seen. However, the qualitative increase suggests that further analysis would be worthwhile; kinase assays at various concentrations of cGMP for each genotype would generate two response curves, which would show whether cGK activity was affected by *Dm*PDE11 expression levels.

5.5 *Dm*PDE11 C long and short co-immunoprecipitate with DG1, DG2P1, and DG2P2

Appendix 4 shows data obtained by Day and Sebastian that provide evidence of an interaction between *Dm*PDE11 and the cGKs, although only DG2P2 has been directly identified as co-immunoprecipiting, where it was shown to associate with *Dm*PDE11 by MALDI-TOF MS analysis of *Dm*PDE11 immunoprecipitate. The interaction of these proteins was investigated using co-immunoprecipitation, where immunoprecipitation was performed of c-Myc tagged cGK, and V5- and YFP-tagged *Dm*PDE11, and the potential binding partner screened by immunoblot using anti-tag antibodies. Direct capture immunoprecipitation was employed for c-Myc and V5 tags, and indirect capture in the case of the YFP tag. That is, anti-c-Myc and –V5 antibodies were coupled to solid-state support, whereas anti-GFP (which recognise YFP) antibodies were captured using Protein-A conjugated sepharose beads. These methods are detailed in materials and methods.

5.6 Immunoprecipitation of V5-tagged *Dm*PDE11B, immunoblot of c-Myc-tagged cGK

In order to determine which cGKs interact with *Dm*PDE11B, coimmunoprecipitations were performed from the lysate of 3 x 10^6 S2 cells co-transfected with one of YFP-tagged Dm*PDE11 RB and RC long and short*, and one of c-Myc tagged *DG1*, *DG2P1*, or *DG2P2*. Additionally, 3 x 10^6 S2 cells were singly-transfected with YFP-tagged *DmPDE11 RB long and short*, and with c-Myc tagged *DG1, DG2P1, or DG2P2*, and the lysate from these used as negative controls (Figure 5.7).

Figure 5.7: Immunoprecipitation of V5-PDE11B is enhanced when co-expressed with c-Myc-cGK. S2 cells were transfected with V5-*Dm*PDE11RB long (lane 1), V5-*Dm*PDE11RB short (lane 2), V5-*Dm*PDE11RB long + c-Myc-DG1 (lane 3), V5-*Dm*PDE11RB short + c-Myc-DG1 (lane 4), V5-*Dm*PDE11RB long + c-Myc-DG2P1 (lane 5), V5-*Dm*PDE11RB short + c-Myc-DG2)1 (lane 6), V5-*Dm*PDE11RB long + c-Myc-DG2P2 (lane 7), V5-*Dm*PDE11RB short + c-Myc-DG2P2 (lane 8), c-Myc-DG1 (lane 9), c-Myc-DG2P1 (lane 10), c-Myc-DG2P2 (lane 11). Anti V5 immunoprecipitation performed with anti-V5 affinity gel (Invitrogen), blot probed with Anti c-Myc monoclonal.

The predicted sizes of these (c-Myc tag included) are: DG1 89 kDa, DG2P1 123kDa, DG2P2 85 kDa

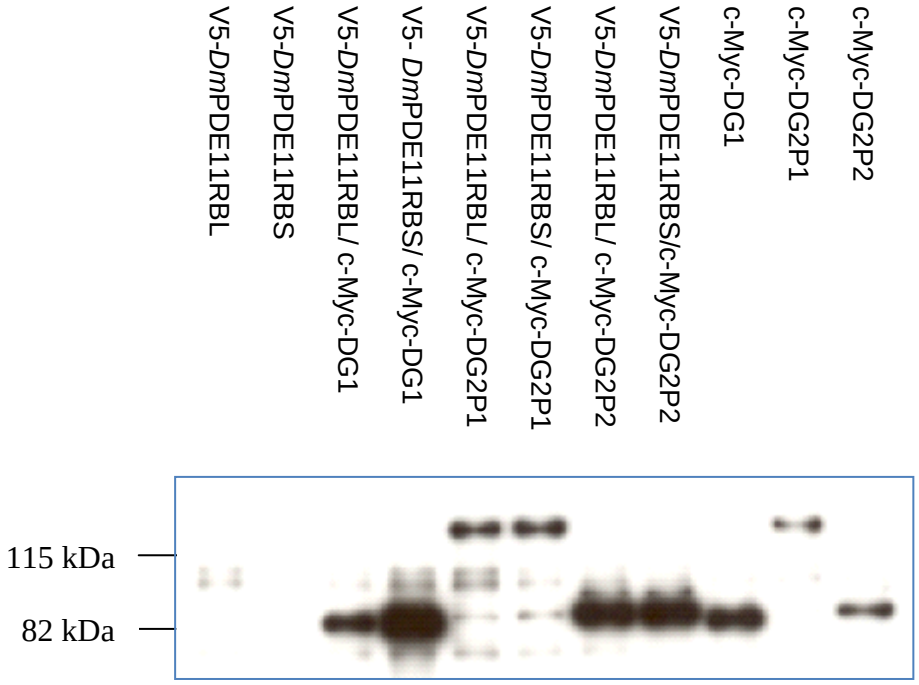

While a qualitative increase was seen in all double-transfected immunoprecipitations above negative controls (i.e., singly transfected immunoprecipitations), background was still apparent in cGK-only controls, and so the interaction could not be verified. This result was obtained several times.

5.7 c-Myc cGK immunoprecipitation, anti-YFP *Dm*PDE11 immunoblot

As a preliminary experiment to gauge conditions, without negative controls other than mock transfected S2 cells, S2 cells were co-transfected with one of c-Myc tagged *DG1*,

DG2P1, or P2, and one of YFP-tagged *DmPDE11RC long or short*. Lysates were precleared by incubation with rabbit serum (as EZview™ Red protein A affinity gel uses affinity purified anti-c-Myc rabbit polyclonal antibody), then incubated with EZview™ Red protein A affinity gel (Sigma). Supernatant was then incubated with EZview™ Red Anti-c-Myc Affinity Gel, then washed 3 x in 3T3 lysis buffer, and processed for SDS-page and immunoblotting. The figure is shown with a cropped, zoomed view of the *Dm*PDE11C long bands for clarity (figure 5.8).

Figure 5.8: YFP-*Dm*PDE11C long co-IPs with DG2. anti-YFP immunoblot of anti-c-Myc immunoprecipitated *Dm*PDE11-YFP/cGK-c-Myc overexpressing S2 cell lysate. Sample precleared in protein A beads, pulled down using 10µl anti-c-Myc proteinA beads, immunoblotted with a pool of anti-GFP monoclonal antibodies. The predicted sizes of these (tag included) are: YFP-*Dm*PDE11C long: 182 kDa, YFP-*Dm*PDE11C short: 152 kDa.

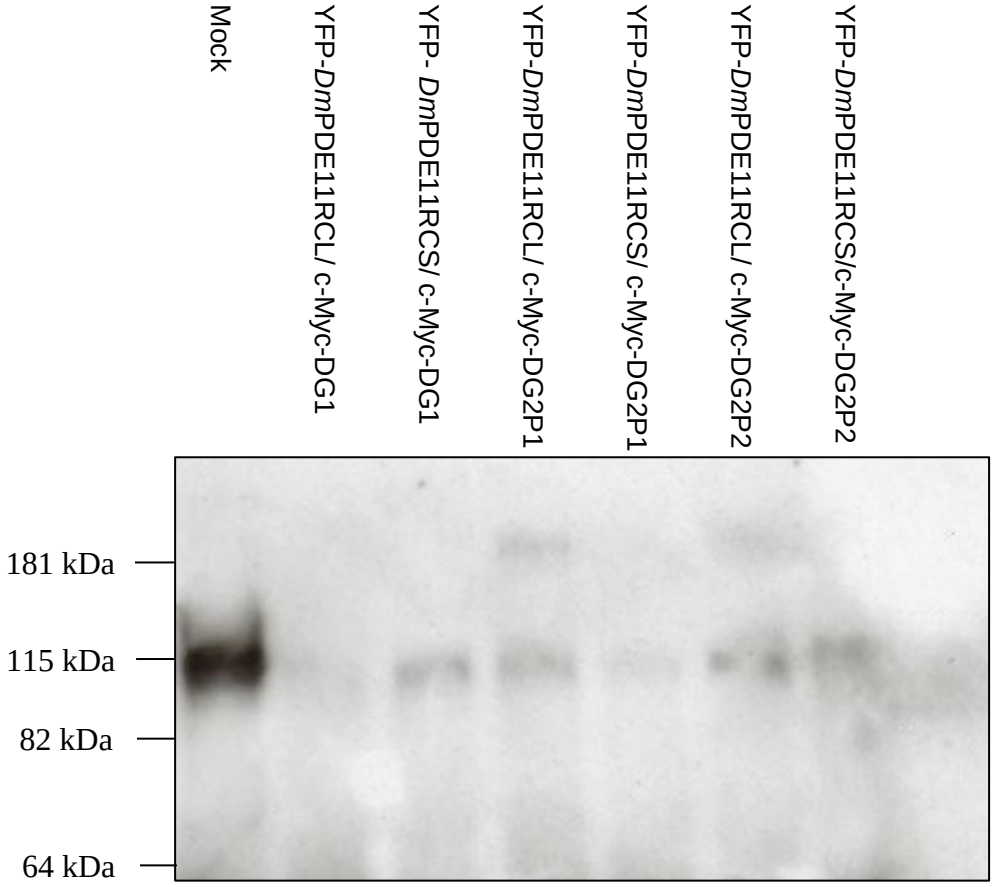

Bands of the predicted size were obtained of YFP-*Dm*PDE11C long in c-Myc DG2P1 and DG2P2/YFP-*Dm*PDE11 RC long co-transfected S2 cell immunoprecipitate. No other bands of the predicted size are visible for the other experimental conditions.

Thus, the experiment was repeated, with an aim to reduce background, while boosting the signal of those interactions not confirmed by this experiment, and including *Dm*PDE11 transfected S2 cells as further controls. To boost the signal, the concentration of S2 cell lysate used was doubled, an increased amount of antibody used, and an increased incubation time in immunoblotting were used. To reduce background binding, the amount of beads used for antibody/protein capture was halved, the % Triton-X 100 in the lysis buffer used was increased from 1% to 1.5%, and more extensive washing was performed, where the amount of wash buffer was doubled, and the three wash steps were extended to 10 min rotation at 4°C. For the immunoblot, block and wash steps were extended. The blot is shown in figure 5.9.

Figure 5.9: YFP-*Dm*PDE11C long and short co-IP with DG1 and DG2. (A) S2 cells were transiently transfected with YFP tagged *Dm*PDE11 RC long and short, both individually and in combination with c-Myc tagged DG1, DG2P1, and DG2P2. cGK was immunoprecipitated using c-Myc affinity gel, and the immunoblot was probed with αGFP antibody that recognises YFP in order to screen for co-immunoprecipitation of *Dm*PDE11C and cGK. Expected band sizes: *Dm*PDE11 RC long: 182 kDa, DmPDE11 RC short: 152kDa. (B) Control αc-Myc immunoblot of c-Myc-cGK immunoprecipitations, where an equal amount of beads were analysed by western blotting. Expected band sizes: c-Myc-DG1: 88.0 c-Myc-DG2P1: 122.5 kDa c-Myc-DG2P2: 84.5 kDa (C) Control αGFP immunoblot of equal amounts of S2 cell lysate prior to immunoprecipitation with c-Myc affinity gel. Expected band sizes: *Dm*PDE11 RC long: 182 kDa, DmPDE11 RC short: 152kDa.

A

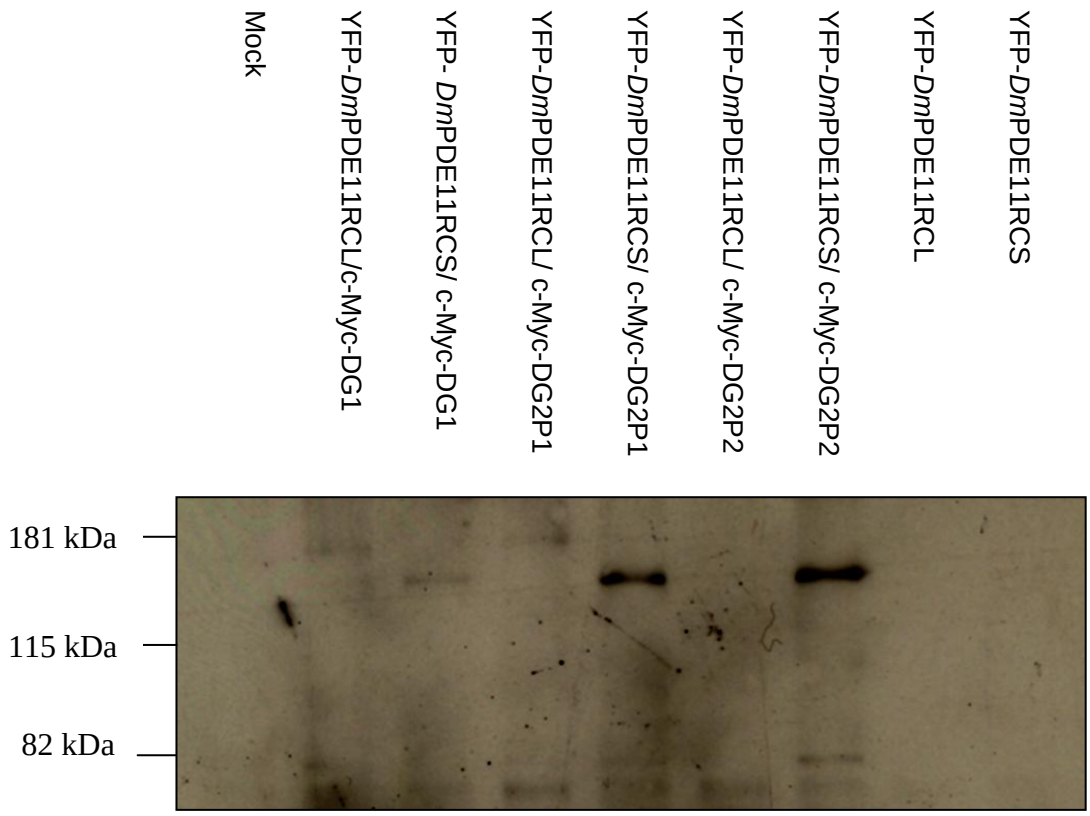

B

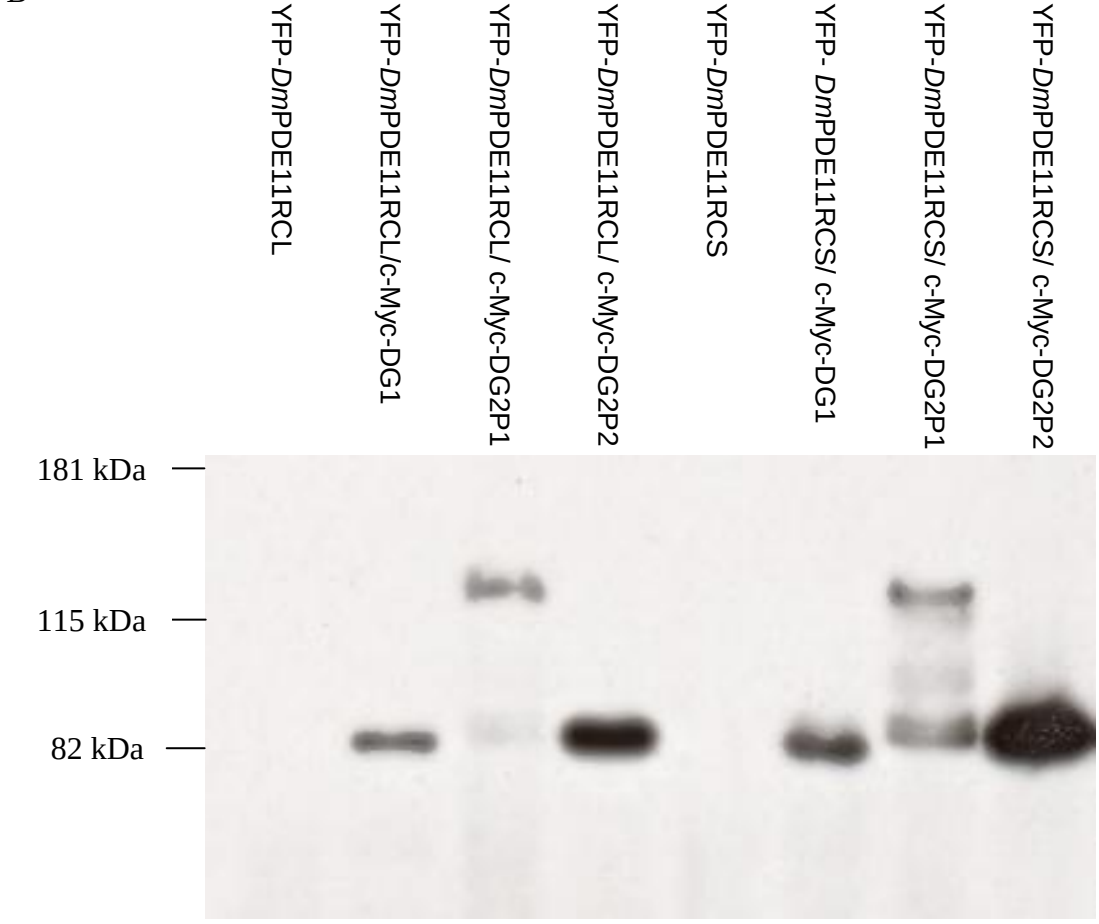
YFP-DmPDE11RCS/ c-Myc-DG2P2
YFP-DmPDE11RCS/ c-Myc-DG2P1
YFP- DmPDE11RCS/ c-Myc-DG1
YFP-DmPDE11RCS
YFP-DmPDE11RCL/ c-Myc-DG2P2
YFP-DmPDE11RCL/ c-Myc-DG2P1
YFP-DmPDE11RCL/c-Myc-DG1
YFP-DmPDE11RCL
181 kDa
115 kDa
82 kDa

C

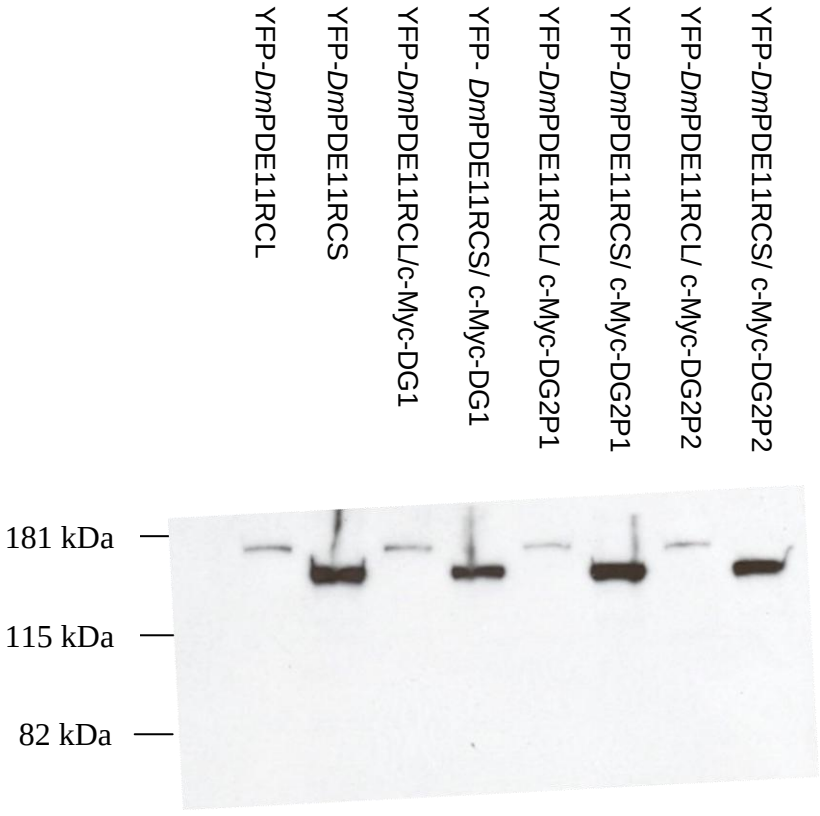
YFP-DmPDE11RCS/ c-Myc-DG2P2
YFP-DmPDE11RCL/ c-Myc-DG2P2
YFP-DmPDE11RCS/ c-Myc-DG2P1
YFP-DmPDE11RCL/ c-Myc-DG2P1
YFP- DmPDE11RCS/ c-Myc-DG1
YFP-DmPDE11RCL/c-Myc-DG1
YFP-DmPDE11RCS
YFP-DmPDE11RCL
181 kDa
115 kDa
82 kDa

This experiment yielded bands of the predicted size for all experimental conditions, bar the negative controls, and the *Dm*PDE11C long/DG2P2 immunoprecipitation which gave a band in the prior experiment. An aliquot of each cell lysate was analysed by western blotting, to ensure equal *Dm*PDE11C expression in each lysate, which was confirmed (data not shown).. The experiment should be repeated two more times, and repeated with YFP tagged *Dm*PDE11 RB long and short.

5.8 Discussion

cGMP signalling is known to be highly compartmentalised, and so the subcellular localisation of *Dm*PDE11A and DG2 were investigated in chapter 3, where *Dm*PDE11A was shown to colocalise with DG2P1 and P2 in S2 cells. As *CG34341* was now known to encode four isoforms that differ in sequence from the originally predicted *Dm*PDE11A, the c-Myc tagged cGKs *DG1*, *DG2P1*, and *DG2P2* were co-expressed with YFP-*DmPDE11RB long* in S2 cells, to see if the proteins still showed co-localisation in light of *Dm*PDE11B localising predominantly to the cell membrane, as opposed to the cytoplasmic localisation of *Dm*PDE11A. Each cGK displayed strong co-localisation with YFP-*Dm*PDE11B long. DG1 is not endogenously expressed in S2 cells (Chintapalli et al., 2007). Co-transfection of S2 cells with c-Myc-*DG1* and YFP-*DmPDE11RB long* yielded some S2 cells in which YFP-*Dm*PDE11B long showed a lower degree of membrane localisation. This could be mediated by a number of factors; direct association with the protein and sequestration to the cytosol, or modulation of localisation by phosphorylation, either of the PDE or some other substrate that then interacts with the PDE. While PKA has been shown to modulate the subcellular localisation of PDE10A by phosphorylation (Kotera et al., 2004), no examples have been shown where cGK alters the subcellular localisation of a PDE.

YFP-*Dm*PDE11B long also co-localises with c-Myc tagged DG2 P1 and P2, where the localisation of c-Myc-DG2P1 is altered, with increased cytosolic expression, in which the protein localises to foci. This increases co-localisation, as *Dm*PDE11B long also localises to the cytosol, and foci within the cytosol, although these foci do not necessarily contain both proteins.

When this experiment was performed, anti-DG1, anti-DG2, and anti-PDE11 antibodies had been designed against new epitopes, with the intention of apply these to immunocytochemistry of Malpighian tubules and other tissues to screen for co-localisation between the four *Dm*PDE11 isoforms and the cGKs *in vivo*. However, the antibodies were

produced behind the anticipated schedule, by which time my time in the laboratory had finished.

YFP tagged *Dm*PDE11B long and short isoforms in tubule localise to the apical and basolateral membranes, which overlaps with the localisation of the cGKs in tubule. DG1 localises to the basolateral membrane and the cytosol, DG2P1 localises to the apical and basolateral membranes, and DG2P2 localises to the apical membrane (MacPherson et al., 2004b). In S2 cells, *Dm*PDE11B long was shown to co-localise with DG1, DG2P1, and DG2P2. The *Dm*PDE11C isoforms localise to some unidentified organelle or vesicle, which does not overlap with the subcellular localisation of any of the cGKs in the Malpighian tubule (other than perhaps DG1, which localises to the cytosol but predominantly to the basolateral membrane). Although the co-immunoprecipitation data reported in this chapter relates to both *Dm*PDE11B and *Dm*PDE11C isoforms, if co-localisation is mediated by domains common to the B and C isoforms, it is possible that although both isoforms can potentially interact, that the *in vivo* localisation of these isoforms may dictate whether or not any interaction with the cGKs actually occur. To confirm this, immunocytochemistry of Malpighian tubules co-staining for cGK and each *Dm*PDE11 isoform would demonstrate if *in vitro* demonstrations of interactions are potentially relevant *in vivo*. Clearly, the generation of tagged cGK expressing flies would allow co-immunoprecipitation to be applied to fly. Alternatively, the availability of specific anti-cGK and anti-*Dm*PDE11 antisera would allow these to be used in immunoprecipitation; use of specific antisera against organisms and not cell systems is considered the gold standard for co-immunoprecipitation. The tubule would be a physiologically relevant tissue to use, as the cGKs have been shown to play roles in fluid secretion (MacPherson et al., 2004b), and cG-PDE function also modulates the process (MacPherson et al., 2004a). Furthermore, DG1 has a limited expression pattern, with high expression in the tubule and hindgut, and slight expression in head (and the tissues within).

Chapter 6

Investigation of the *Dm*PDE11/cGK interaction using peptide arrays

6.1 Summary

In this chapter, peptide arrays were used to investigate if the interaction between *Dm*PDE11 and the cGMP-dependent kinases is direct, and if so, identify the peptide sequence within these proteins responsible for these interactions. Peptide arrays representing the sequences of *Dm*PDE11, DG1, and DG2 were generated using an autospot robot. The open reading frames of the genes encoding of these proteins were fused in-frame into either pGEX-6P-1 or pET-28-c expression vectors in fragments to generate Glutathione-S-Transferase- (GST) or HIS_6-tagged proteins respectively. These were transformed into BL21 (DE3) cells, and expression was analysed in terms of protein size, non-proteolysis, and solubility by western blotting. In all cases, HIS_6 tagged fusion proteins were found to yield protein with more desirable characteristics, and so these were used to overlay the peptide arrays. Large scale purification was undertaken, and purified protein was then overlaid on the arrays, which were probed with HRP conjugated anti-HIS_5 antibody. These arrays were compared to negative controls, which were probed with a HIS_6 protein derived from empty pET-28-c vector, then with antibody as above. Putative direct interactions were found between DG1 and *Dm*PDE11, where three regions were identified on a DG1 peptide array that were immunoreactive when probed with a HIS_6-fused truncate of *Dm*PDE incorporating the second GAF domain and the catalytic domain. Likewise when the PDE11 array was probed with a HIS_6-fused DG1 C terminal truncate, two putative regions of interaction were found. Taken alongside the co-immunoprecipitation data presented in chapter five, this provides evidence of a direct interaction that should be verified by alanine substitution arrays, or *in vivo* work. Attempts to affinity purify DG1N-HIS_6 failed, and so the *Dm*PDE11 array was not probed with this fragment. Peptide array experiments to determine whether the interaction between DG2 and *Dm*PDE11 presented in chapter 5 is direct did not yield conclusive data, and so should be researched further.

6.2 Introduction

Chapter six describes the use of peptide arrays to investigate the interactions between the four isoforms of PDE11, and the cGKs DG1, and DG2 presented in chapter 5. Spot synthesis, the technique of synthesising multiple peptides or peptide chains simultaneously onto a membrane, was first described in 1992 (Frank, 1992). The screening of these peptide libraries with overlaid protein, metal and DNA was described the next year (Kramer et al., 1993). The process of mapping protein-protein interaction sites was validated in a paper that forms the basis for current peptide array techniques (Reineke et al., 1996). The process sees the entire sequence of a protein of interest arrayed onto a membrane by an autospot robot using F-moc chemistry in spots of 25 amino acids, 25mers, which overlap by 20 amino acids. Thus each subsequent spot represents a 5 amino acid frameshift within the sequence. These peptide arrays are probed with soluble, recombinant protein, which is tagged with a protein tag. This tag acts both as an affinity tag, which permits the affinity purification of the protein, and as an epitope tag, which allows the use of an anti-tag antibody to identify those 25mer spots which have bound, interacting protein. A primary, "antibody only" experiment identifies spots that are present as background, i.e., they are immunoreactive in the absence of overlaid protein of interest. Tagged protein of interest is then overlaid on the array, and the array probed with anti-tag antibody; immunoreactive spots not present in the initial control experiment are considered as putative sites of interaction.

In the course of this study, Glutathione-S-Transferase (GST) and HIS_6 tagged proteins were generated. The HIS_6 tag is highly suitable for use in peptide arrays, due to the availability of specific monoclonal antibodies, the small size of the tag, and thus minimal disruption of protein structure, and its reversible affinity for metal matrices, which aids in protein purification. The GST tag is larger, and so may compromise overall protein levels and structure, but acts as a solubilisation tag, which aids in the solubilisation of the protein, and thus may prevent the formation of inclusion bodies. Its affinity for glutathione allows its affinity purification, and again there are specific antibodies available. For HIS_6, negative controls are performed by overlaying an array with purified HIS_6 peptide, then immunoblotting with anti-HIS_5-HRP coupled mouse monoclonal antibody (Qiagen). GST negative controls are performed with a monoclonal anti-Glutathione-S-Transferase antibody (Sigma-Aldrich).

Like yeast two-hybrid, false positives and false negatives can occur. Expressing a fusion protein transgenically in *E. coli* can yield proteins that do not behave as they would in mammalian systems. Misfolding may occur, the protein may be unavoidably degraded during cell lysis and subsequent protein purification, or inclusion bodies may form, rendering the protein insoluble. As the tertiary structure of an individual domain may be influenced by other domains within the protein, a truncated, transgeneically expressed protein may adopt a novel structure, which may alter the protein's binding properties, which in turn may result in false positive or false negative interactions. The conformation of the spotted peptide may not be suitable to facilitate binding, or the spot may be immunoreactive in negative controls, thus masking the interaction site. The array may present epitopes that do not reside on the surface of the protein *in vivo*, which may result in false positive interactions. Despite this, the system offers an unparalleled opportunity to not only detect if a protein-protein interaction is direct, but to identify those amino acids responsible for the interaction.

Ideally, the generation of both peptide arrays and tagged recombinant protein for two potential interactors should yield reciprocal binding sites. This data can be confirmed by alanine substitution arrays, which sequentially replace each amino acid within the stretch of sequence positive for an interaction with an alanine residue, which renders the interaction null if that residue was vital for the interaction (Gibbs and Zoller, 1991; Uttamchandani et al., 2003); in this case, it is the non-immunoreactive spots that are informative.

Taken together, it is clear that any positives are considered putative, but where an array is confirmed by an alanine array, which identifies individual amino acids essential for the interaction, this knowledge can then be used to screen for any resultant phenotypes when this interaction is disrupted. This can be achieved through the generation of a protein mutated at this site, or via the generation of peptides representing this sequence, which will act as a dominant-negative when present in excess, or by generating protein mutant at this site. This can be used in co-immunoprecipitation to confirm that an interaction has been rendered null, or a transgenic animal or cell can then be subjected to a functional assay in which the mutant protein has been implicated.

6.3 Generation of peptide arrays

Peptide arrays representing the sequence of *Dm*PDE11 RB and RC, and DG1 were produced in collaboration with Dr. Alan Dunlop of the Houslay laboratory. Two arrays representing the sequence of DG2 were produced by Dr George Baillie as part of a previous collaboration with Dr Matt Macpherson.

6.4 Design of truncate fusion protein

The *E. coli* pET and pGEX expression systems will facilitate a maximum of 2kb of ORF sequence. As the *Dm*PDE11 and cGK ORFs are significantly larger than this, it was necessary to generate tagged truncates which would still incorporate entire functional domains, as protein-protein interactions can occur at the level of domain-domain interactions (DDIs) (Pawson and Nash, 2003). The amino acid sequences were analysed using InterProScan (Zdobnov and Apweiler, 2001). InterProScan uses a total of ten databases including PFAM, SMART, and PROFILE to define each functional domain within the protein (Quevillon et al., 2005). As each database gives a different prediction as to the extent of each domain, the region of truncation was determined by selecting regions that are not designated as domains by any of the tools, with the rationale that domains will not be truncated with this approach.

6.4.1 Consideration of Drosophila cGK literature

DG1 and DG2 were isolated in 1989 (Kalderon and Rubin, 1989). Phylogenetic analysis suggested that DG1 is most closely related to mammalian type II cGK, and DG2 is most closely related to mammalian type I cGK (Jarchau et al., 1994). As well as this work there are of course a number of papers focusing on these important *Drosophila* enzymes. As such there is further information pertaining to the location of domains within DG1 and DG2; indeed, the InterProScan database uses some of these domains in its analysis. A dimerisation domain is believed to reside within the amino terminal of both DG1 and DG2, but amino acid similarity with the dimerisation domain of mammalian cGK is so low that InterProScan does not predict the domain. The exact size and location is unknown in both enzymes and is thus not shown. Likewise, a regulatory domain is believed to be present in

each enzyme, but low homology prevents computational prediction of its localisation (Heil et al., 1987; Monken and Gill, 1985; Takio et al., 1984). It is believed to be directly N-terminal of the CNB domains. The bovine regulatory domain acts as a substrate analogue and binds to the catalytic domain at a lower affinity than cGMP, and thus impairs function in the absence of cGMP. However, Kalderon and Rubin believe that homology of this regulatory domain is low enough in both DG1 and DG2 that the mode of regulation may differ in *Drosophila*.

6.4.2 DG1

The amino acid sequence of DG1 was analysed using Interproscan (table 6.1).

Table 6.1: Interproscan analysis of DG1

Domain	Program	Site	
Cyclic nucleotide binding domain	PFAM	203-285	322-415
	SMART	185-299	304-428
	PROFILE	185-301	304-427
Protein kinase, core	PROFILE	457-717	
AGC Kinase, C terminal	SMART	718-768	
	PROFILE	718 - 768	

InterProScan analysis revealed a length of sequence between the twin cyclic nucleotide binding domains and the kinase domain around halfway through the protein which was not designated as a domain, and so the constructs were generated using this as the boundary. DG1 is 768 amino acids in length. The N terminal truncate is 427 amino acids in length and extends to the end of the second of the cyclic nucleotide binding (CNB) domains, and incorporates the dimerisation and regulatory domains. The C terminal truncate extends from the end of the second CNB domain to the end of the protein, thus incorporating the kinase, ATP binding domains, and the AGC (cAMP-dependent, cGMP-dependent and protein kinase C) kinase C-terminal domain, a regulatory domain conserved between a diverse range of kinases (Kannan et al., 2007; Newton, 2003) and consists of 341 amino acids (figure 6.1).

Figure 6.1: Primary structure of DG1, showing regions used to generate fusion proteins. Shaded cylinders represent domains. Drawn to scale.

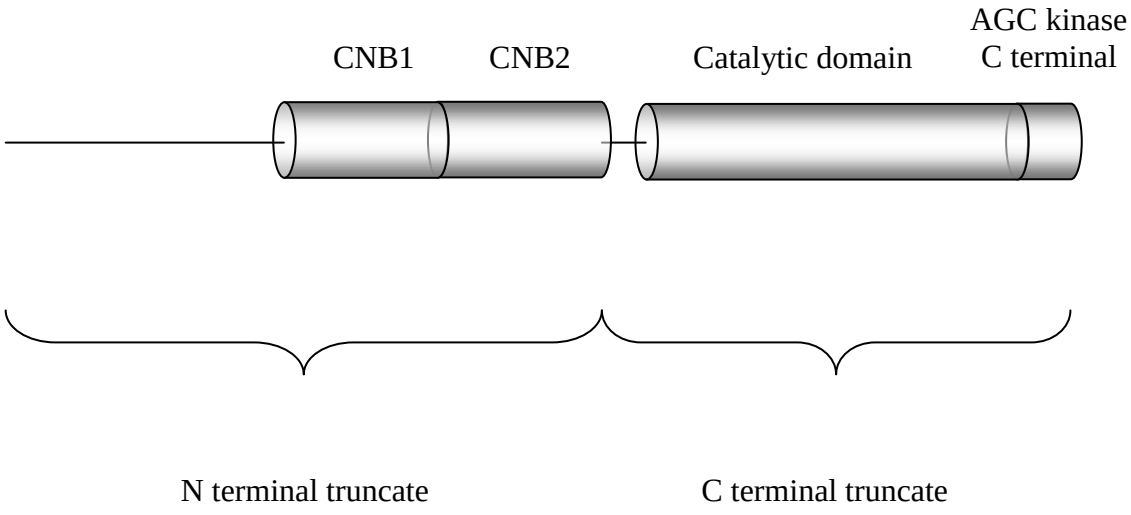

6.4.3 DG2

The amino acid sequence of DG2 was analysed using Interproscan (table 6.2).

Table 6.2: Interproscan analysis of DG2

Domain	Program	Site	
Cyclic nucleotide binding domain	PFAM	538-623	656-749
	SMART	520-636	656-749
	PROFILE	520-635	638-761
Protein kinase, core	PROFILE	777-1036	
AGC Kinase, C terminal	SMART	1037-1088	
	PROFILE	1037-1088	

DG2 P1 is 1088 amino acids in length; DG2 P2, the other active DG2 isoform in Drosophila (MacPherson et al., 2004), is a truncate of this and is represented entirely within the DG2 P1 sequence (http://flybase.org/reports/FBgn0000721.html). InterProScan analysis shows that the CNB domain starts at amino acid 520, and so this was picked as the boundary. The N terminal truncate is 519 amino acids long, and incorporates the

dimerisation and regulatory domains. The C terminal truncate is 569 amino acids long and incorporates the ATP binding, twin CNB, protein kinase, and the AGC kinase C terminal domains (figure 6.2).

Figure 6.2: Primary structure of DG2 (P1), showing regions used to generate fusion proteins. Shaded cylinders represent domains. Drawn to scale.

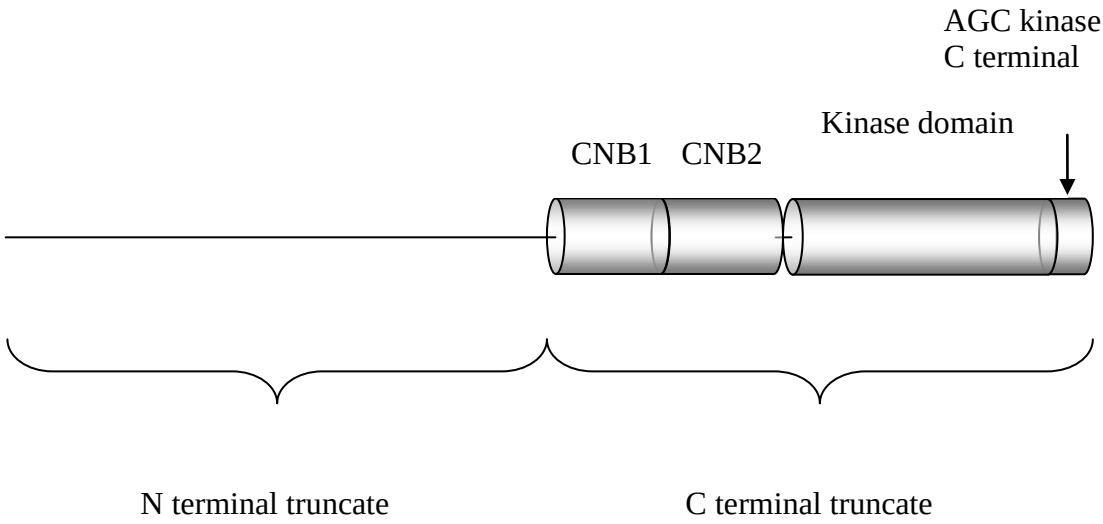

6.5 *Dm*PDE11

The amino acid sequence of *Dm*PDE11 was analysed using Interproscan (table 6.3).

Table 6.3: Interproscan analysis of *Dm*PDE11. Amino acids refer to those of *Dm*PDE11B long.

Domain	Program	Residues	
3'5'-cyclic nucleotide phosphodiesterase	PFAM	859-1097	
	PROSITE	900-911	
GAF	PFAM	419 - 572	604 - 754
	SMART	419 - 582	604 - 764

As a size of 2kb was the maximum size of insert that the *E. coli* expression vectors could facilitate, the ~4.5kb *Dm*PDE11 ORF was cloned as three fusion protein truncates.

InterProScan analysis dictated that the best three-way split would be two N terminal truncates, incorporating sequence from the unique B or C isoform N termini, until the end of the first GAF domains, and thus the B isoform N terminal fragment incorporates 582 amino acids, and the C isoform N terminal fragment incorporates 538 amino acids. The "Middle" truncate incorporates sequence ranging from the start of the second GAF domain until the end of the catalytic PDEase domain, and consists of 515 amino acids. The "End" C terminal truncate extends from the end of the catalytic domain to the end of the long C-terminus, and consists of 354 amino acids (figure 6.3).

Figure 6.3: Primary structure of *Dm*PDE11, showing regions used to generate fusion proteins. Shaded cylinders represent domains. Drawn to scale.

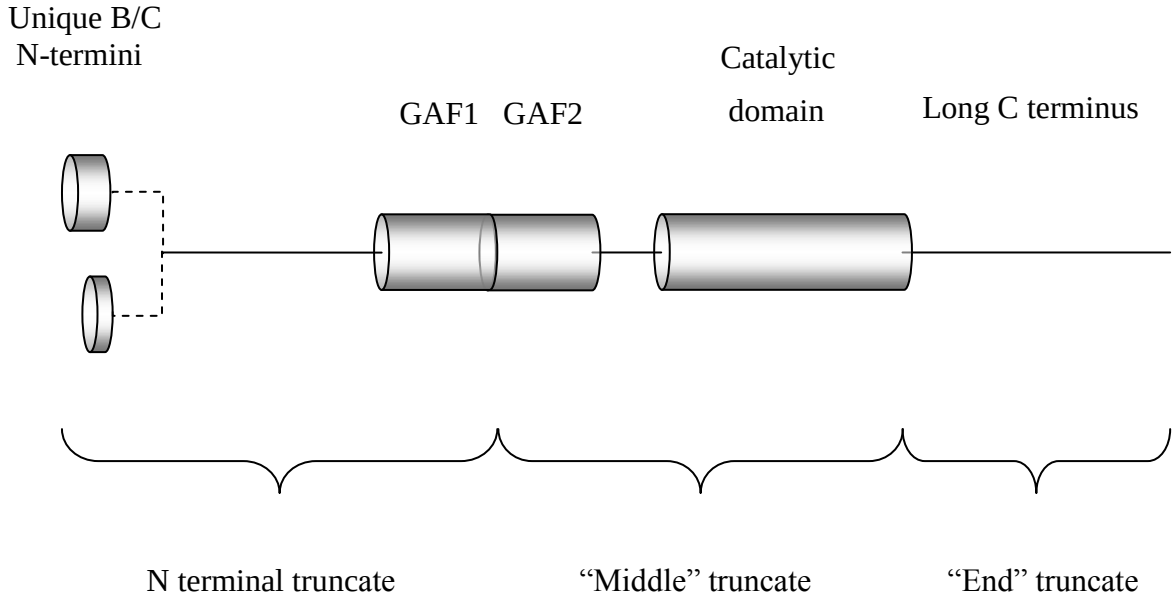

The unique sequence within the short C terminal is represented in the PDE11 peptide array; as the sequence is so short, and co-immunoprecipitations show an interaction with both the long and short isoforms, it was assumed that it would not mediate the interaction.

6.6 Cloning of ORFs into expression vectors

Primers were designed to generate *E. coli* expression constructs for all of the above truncates, using pET-28-c, a gene fusion vector with an N terminal HIS_6-thrombin-T7 tag, and pGEX-6P-1, a gene fusion vector with an N terminal Glutathione S-Transferase (GST) tag. All ORFs were amplified using proofreading DNA polymerase from previously verified plasmid DNA, with primers designed to incorporate restriction sites not present in

the ORF, but present in the multiple cloning site to permit direction cloning of the inserts. These PCR fragments were digested with the appropriate restriction enzymes, and ligated into digested expression vector. These were transformed into Stratagene Gold ultracompetent cells, and plasmid DNA was recovered from multiple colonies by miniprep and screened using both digestion and PCR analysis.

6.7 Expression of constructs

As pET and pGEX constructs were generated for each gene, it was sought to determine which of these, in each case, provided the greater amount of pure, non-degraded protein by performing small scale growth and induction to analyse by western blot. In each case, BL21 (DE3) pLysS competent cells were transformed with plasmid DNA, and a colony used to generate a 3ml culture, which was grown to an OD_{600} of $\geq 0.6 - \leq 1.0$ at 37˚C with shaking. Of 1 ml, 100µl was spun down, the pellet used as a non-induced control, and 900µl to make a glycerol stock. The remaining 2ml was induced with 0.4mM IPTG (pGEX) or 0.1mM IPTG (pET) for two hours. Two 1 ml aliquots were spun down and lysed, one in IGEPAL lysis buffer to completely solubilise the cellular protein, the other in the appropriate native lysis buffer using L3 sonication, both with protease inhibitor and lysed on ice. These were run alongside the non induced control (also lysed in IGEPAL with an identical dilution factor) on an SDS page gel, and western blotting was performed with the appropriate antibody.

Comparison between HIS_6- and GST-tagged protein lysate showed HIS_6 tagged protein showed higher levels of immunoreactivity, and lower levels of background, for which most of the GST lysates displayed high levels (data not shown). The HIS_6 protein also displayed lower levels of degradation. Although this may have been down to a poor anti-GST antibody, the HIS_6 tagged protein expression did not appear to need any modification of protocol (with the exception of the *Dm*PDE11 End fragment, which gave an equally poor yield when tagged with GST), and thus these were affinity purified using Ni-NTA columns for use with the arrays, as detailed in materials and methods.

6.8 Purification of HIS_6 protein

HIS_6 protein was purified using a Ni-NTA column as described in materials and methods. 5 µl aliquots of lysate (following application to column), wash fraction, and the 1 ml HIS_6 eluates were analysed by western blotting.

6.8.1 HIS_6

HIS_6 protein was generated by the transformation of pET-28-c vector into BL21 (DE3) pLysS competent cells, for use as a negative control. The HIS_6 protein has an expected size of ~3 kDa. Affinity purified fractions were analysed by western blotting (figure 6.4).

Figure 6.4: HIS_6 purified peptide. HIS_6 peptide, from pET-28-c vector. 14% SDS-PAGE gel. Lane 1: run-through lysate applied to column, lane 2: wash fraction, lanes 3 – 11: purified fractions. 1° antibody anti-HIS_6 mouse monoclonal HRP conjugated.

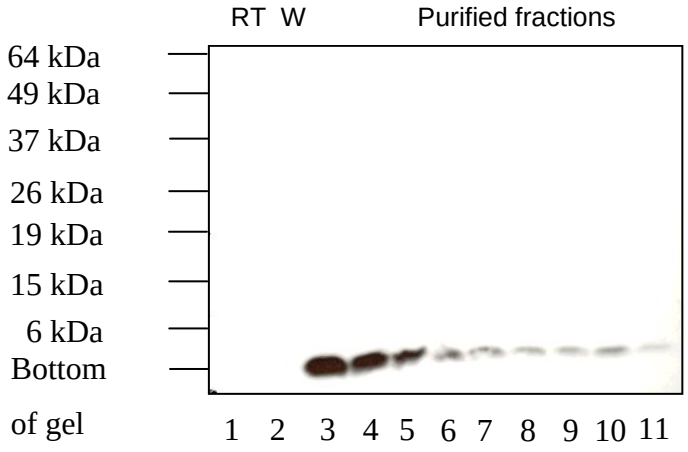

Western analysis of HIS_6 purified protein yielded a band of the predicted size, and showed no unspecific bands. The protein purified to a high concentration.

6.8.2 *Dm*PDE11BN-HIS_6

*Dm*PDE11BN-HIS_6 protein (BN-HIS_6) was generated by the transformation of *Dm*PDE11RBN-pET-28-c vector into BL21 (DE3) pLysS competent cells. BN-HIS_6

protein has an expected size of ~67 kDa. Affinity purified fractions were analysed by western blotting (figure 6.5).

Figure 6.5: BN-HIS$_6$ purified protein. 10% SDS-PAGE gel. Lane 1: run-through lysate applied to column, lane 2: wash fraction, lanes 3-10: purified fractions, lanes 11 and 12: fractions purified at a higher imidazole concentration.

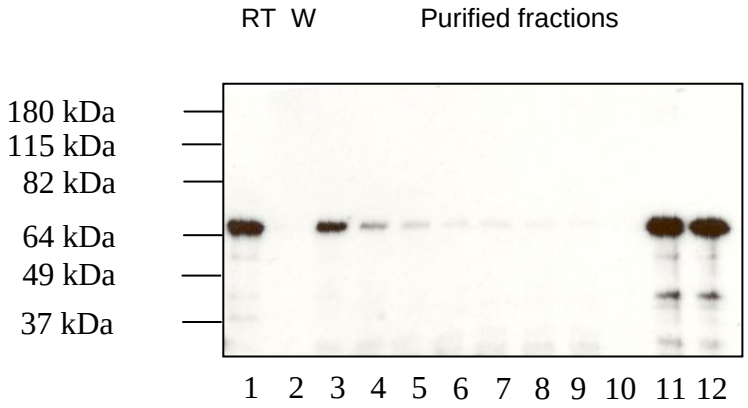

BN-HIS$_6$ purified protein was of the predicted size, recovered at a high concentration, higher in those fractions containing a high concentration of imidazole, and showed little degradation, increased in the higher imidazole elates; as such these were not used.

6.8.3 *Dm*PDE11CN-HIS$_6$

*Dm*PDE11CN-HIS6 (CN-HIS$_6$) protein was generated by the transformation of *Dm*PDE11RCN-pET-28-c vector into BL21 (DE3) pLysS competent cells. CN-HIS$_6$ protein has an expected size of ~61 kDa. Affinity purified fractions were analysed by western blotting (figure 6.6)

Figure 6.6: CN-HIS$_6$ purified protein. 10% SDS-PAGE gel. Lane 1: soluble lysate, lane 2: wash fraction, lanes 3-9: purified fractions, lanes 10 and 11: fractions purified at a higher imidazole concentration.

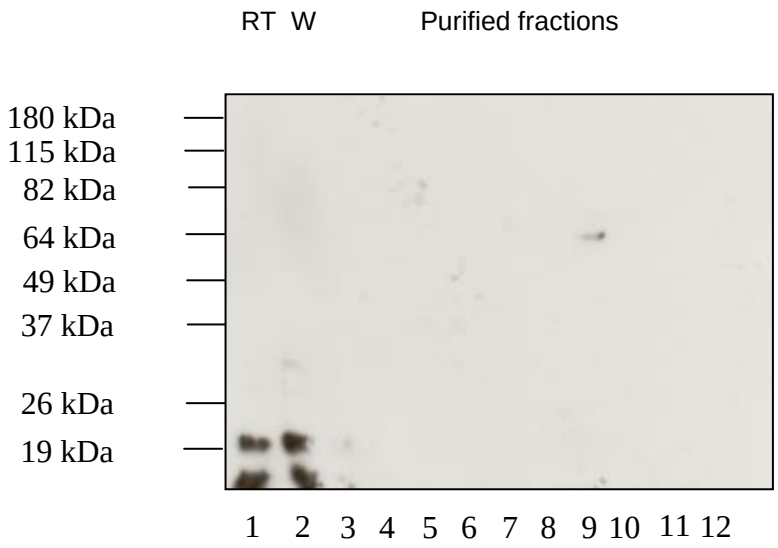

CN-HIS$_6$ purified protein was of the expected size (lane 9), was recovered at a low concentration only from those fractions eluted using a high concentration of imidazole, and showed no appreciable degradation.

6.8.4 *Dm*PDE11 Middle-HIS$_6$

*Dm*PDE11 Middle-HIS$_6$ protein was generated by the transformation of Middle-pET-28-c vector into BL21 (DE3) pLysS competent cells. Middle-HIS$_6$ protein has an expected size of ~62 kDa. Affinity purified fractions were analysed by western blotting (figure 6.7).

Figure 6.7: Middle-HIS$_6$ purified protein. 10% SDS-PAGE gel. Lane 1: soluble lysate, lane 2: wash fraction, lanes 3-9 purified fractions: lanes 10 and 11: fractions purified at a higher imidazole concentration.

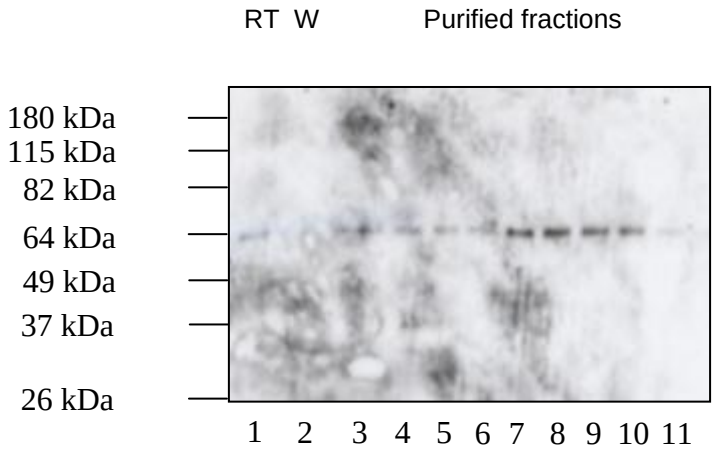

Middle-HIS$_6$ purified protein was of the expected size, and was recovered at a reasonable concentration. The protein showed no appreciable degradation.

6.8.5 End-HIS$_6$

*Dm*PDE11 End-HIS$_6$ protein was generated by the transformation of End-pET-28-c vector into BL21 (DE3) pLysS competent cells. End-HIS$_6$ protein has an expected size of 41 kDa. Affinity purified fractions were analysed by western blotting (figure 6.8).

Figure 6.8: End-HIS$_6$ purified protein. 10% SDS-PAGE gel. Lane 1: soluble lysate, lane 2: wash fraction, lanes 3-9: purified fractions, lanes 10 and 11: fractions purified at a higher imidazole concentration.

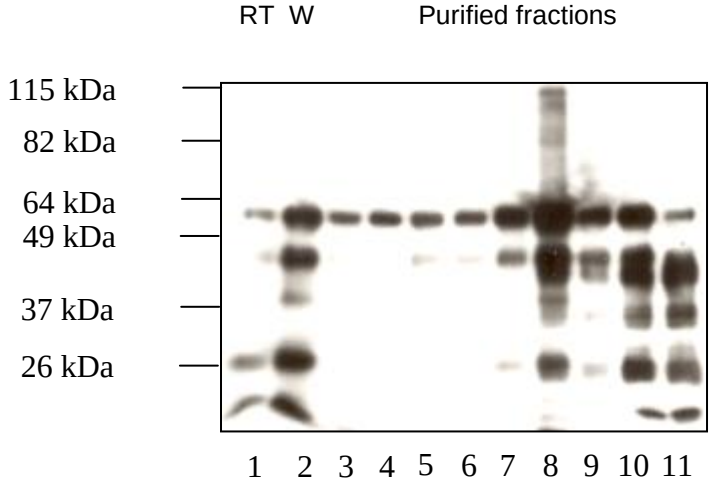

Although protein of the predicted size purified at high concentration, the protein showed high levels of degradation. Furthermore a non-specific band of ~64 kDa co-purified with the fusion protein. Subsequent to this attempt, incubation with $MgSO_4$ for 30 min prior to application to the column prevented the 64 kDa protein, which the literature suggests is the common contaminant DnaK, from co-purifying, although the immunoblot of the subsequent western blot was “dirty”; although the bands were clearly visible, the blot would not scan clearly, and so is not shown. In lanes with a higher concentration of protein, immunoreactive protein that had not migrated from the wells was present, which suggests that the protein forms inclusion bodies at high concentrations. The gel shown has two lanes with protein of the correct size, with little degradation (lanes 7 and 9); the compromised transfer showed bands equally pure without DnaK, and so these eluates were applied to the array.

6.8.6 DG1N-HIS$_6$

DG1N-HIS$_6$ protein was generated by the transformation of DG1N-pET-28-c vector into BL21 (DE3) pLysS competent cells. DG1N-HIS$_6$ yielded soluble protein of ~50 kDa at the analytical stage, yet no protein was observed in western blots of Ni-Nta column purified protein. This was despite attempts to optimise the purification protocol, by excluding imidizole from the binding buffer, using a reduced-strength wash buffer, varying the length of the binding step, and performing the purification as quickly as possible to minimise degradation (data not shown).

6.8.7 DG1C-HIS$_6$

DG1C-HIS$_6$ protein was generated by the transformation of DG1C-pET-28-c vector into BL21 (DE3) pLysS competent cells. DG1C-HIS$_6$ protein has an expected size of ~42 kDa. Purified fractions were analysed by western blotting (figure 6.9).

Figure 6.9: DG1C-HIS$_6$ purified protein. 10% SDS-PAGE gel. Lane 1: soluble lysate, lane 2: wash fraction, lanes 3-9: purified fractions, lanes 10 and 11: fractions purified at a higher imidazole concentration.

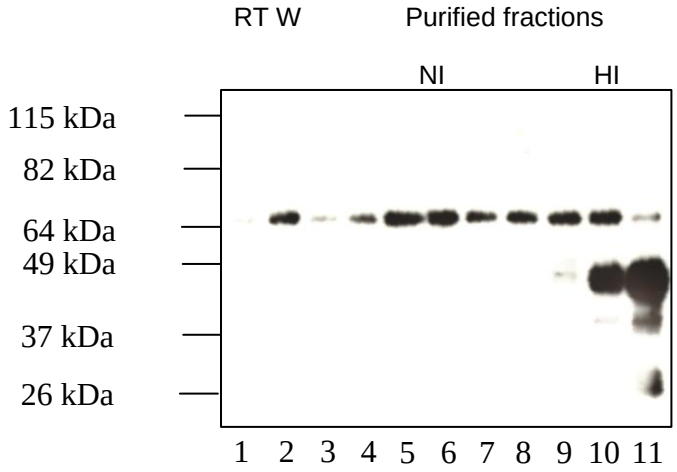

Protein of the predicted size purified at high concentration under elution conditions of high levels of imidazole (lanes 10 and 11). The protein showed mild levels of degradation, but these bands were less strong than the desired size of band. Subsequent to this first attempt, incubation with $MgSO_4$ for 30 min prior to application to the column prevented co-purification with the ~64 kDa protein, identified as DnaK, from co-purifying, although the transfer of this gel was compromised as above and so is not shown.

6.8.8 DG2N-HIS$_6$

DG2N-HIS$_6$ protein was generated by the transformation of DG2N-pET-28-c vector into BL21 (DE3) pLysS competent cells. DG2N-HIS$_6$ protein has an expected size of ~60 kDa. Purified fractions were analysed by western blotting (figure 6.10).

Figure 6.10: DG2N-HIS$_6$ purified protein. 10% SDS-PAGE gel. Lane 1: soluble lysate, lane 2: wash fraction, lanes 3-9: purified fractions, lanes 10 and 11: fractions purified at a higher imidazole concentration.

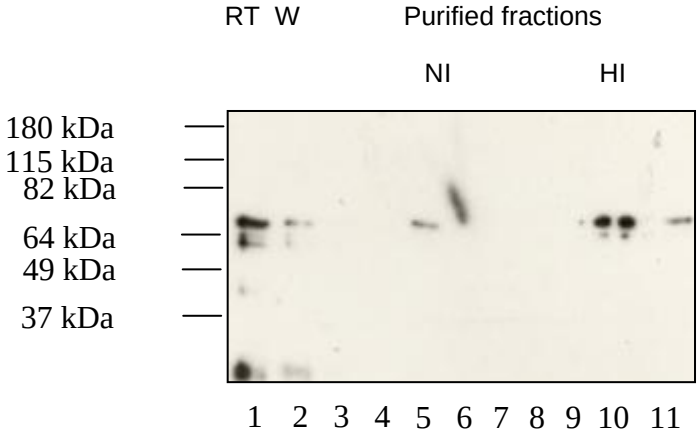

DG2N-HIS$_6$ purified protein ran as two bands, one of the expected size, and one ~5 kDa larger. Reasons for this are unknown; perhaps the protein was subjected to a post translational modification. Protein was recovered at a reasonable concentration where an increased concentration of imidazole was used, and showed no degradation, in lanes outside of the lysate and wash.

6.8.9 DG2C-HIS$_6$

DG2C-HIS$_6$ protein was generated by the transformation of DG2C-pET-28-c vector into BL21 (DE3) pLysS competent cells. DG2C-HIS$_6$ protein has an expected size of ~67 kDa. Purified fractions were analysed by western blotting (figure 6.11).

Figure 6.11: DG2C-HIS$_6$ purified protein. 10% SDS-PAGE gel. Lane 1: soluble lysate, lane 2: wash fraction, lanes 3-9: purified fractions, lanes 10 and 11: fractions purified at a higher imidazole concentration.

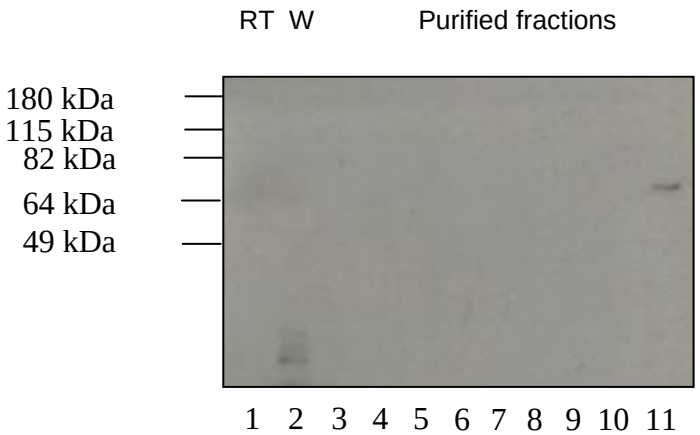

DG2C-HIS_6 purified protein was of the expected size, highly pure, recovered at a low concentration from elution conditions of increased imidazole concentration, and showed no discernable degradation outside of the wash fraction.

6.9 Screening of peptide libraries for direct interactions

In order to identify non-specific immunoreactive spots, each array was probed with purified HIS_6 protein at a concentration approximately equimolar to that of the purified gene – HIS_6 fusion protein subsequently applied, and detected with an anti-HIS_5 HRP conjugated monoclonal antibody, using several lengths of exposure. Arrays were then probed with a protein of interest fused to HIS_6 at 10 μg/ml, and probed with an anti-HIS_5 HRP conjugated monoclonal antibody as before. Putative direct interactions were identified by comparing control arrays with gene-HIS_6 probed arrays; where a spot is immunoreactive on the array probed with the gene-HIS_6 that is not immunoreactive on the control array, it is considered a putative interaction site. Arrays were stripped between probes. The technique is described in detail in materials and methods.

6.10 PDE11 Array

A peptide array representing the sequence of *Dm*PDE11, including sequence of the unique N-termini of the B and C isoforms, and the unique sequence of the short isoform C terminus, was produced in collaboration with Dr Allan Dunlop, and was probed with cGK fusion protein in order to detect putative interaction sites.

6.10.1 PDE11 array probed with HIS_6

As a control, the PDE11 array was probed with a control peptide, HIS_6, at a concentration approximately equimolar to that of the gene – HIS_6 fusion proteins that were subsequently applied, and non-specific spots were identified with an anti-HIS_5 HRP conjugated monoclonal antibody (figure 6.12).

Figure 6.12: PDE11 array probed with HIS_6. The DG2 array was probed with HIS_6 protein. Non-specific spots were identified by staining with an anti-HIS_5 HRP conjugated monoclonal antibody. Arrays exposed to film for 10 minutes.

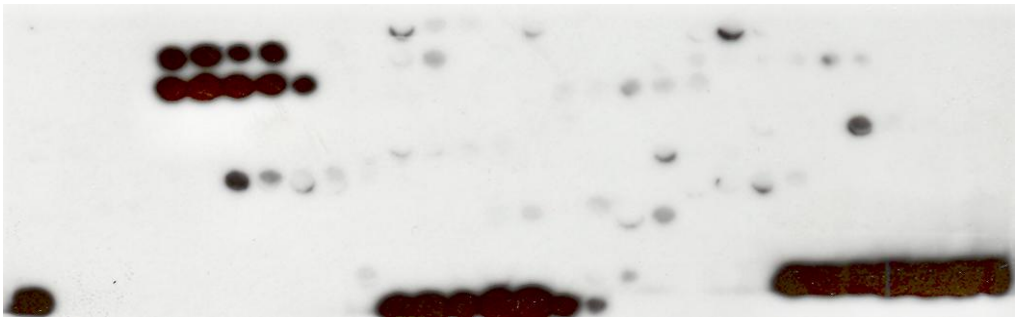

There is a large degree of background. Rows of immunoreactive spots contain either HIS_5mers, which matches the specificity of the αHIS_5 antibody used, or contain HIS_5mers with a single amino acid substitution (such as HHHNH, in the case of the two rows near the top left of the array), suggesting that conditions permit antibody binding to epitopes that are not 100% specific. The C terminal region of PDE11 has two histidine rich regions, which are represented in two strips of spots, 864-871, and 882-888.

6.10.2 PDE11 array probed with DG1C-HIS_6

The PDE11 array was probed with DG1C-HIS_6 protein. Specific interacting spots were identified by staining with an anti-HIS_5 HRP conjugated monoclonal antibody, and comparing these to a control exposed for 10 minutes (figure 6.13).

Figure 6.13: PDE11 array probed with DG1C-HIS$_6$, shown alongside HIS$_6$ control. The PDE11 array was probed with DG1C-HIS$_6$ protein. Interacting spots were identified by staining with an anti-HIS$_5$ HRP conjugated monoclonal antibody. Putative interaction sites are highlighted with a solid or dashed line. Array exposed to film for 1 minute.

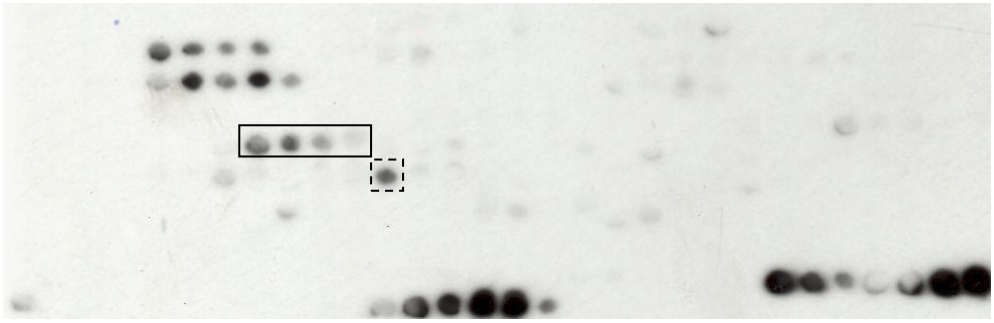

PDE11 array probed with HIS$_6$. Array exposed to film for 10 minutes.

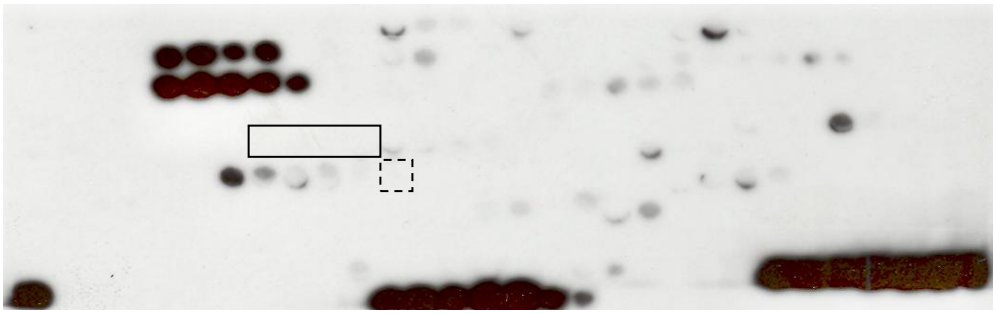

Spots 729 – 732 (highlighted with a solid line) and spot 763 (highlighted with a dashed line) are immunoreactive after a mere 30 seconds of exposure on the PDE11 array challenged with DG1C-HIS$_6$ and are negative on both HIS$_6$ controls, suggesting that these regions interact with the sequence of DG1 represented by DG1C-HIS$_6$, which consists of the final 341 amino acids of the protein, thus incorporating the kinase, and ATP binding domains. These spots correspond the sequence VHEADKGSFSRVFDFEANDLSEEEATSRTSPYESRFPINI (amino acids 630-669), and VHFRLHDFKFDDIHFEDDDTLKACL (amino acids 800 - 824) within *Dm*PDE11, using *Dm*PDE11 B long as a reference. These residues fall within the second GAF domain, and the region between the second GAF domain and the catalytic domain respectively, and as such both are found in the region of PDE11 shared by all four isoforms, and are included in Middle-HIS$_6$ (figure 6.14).

Figure 6.14: PDE 11, with putative regions of interaction with the C terminus of DG1. Exposures of equal time (5 minutes) shown. Top array control, bottom array probed with DG1C-HIS_6.

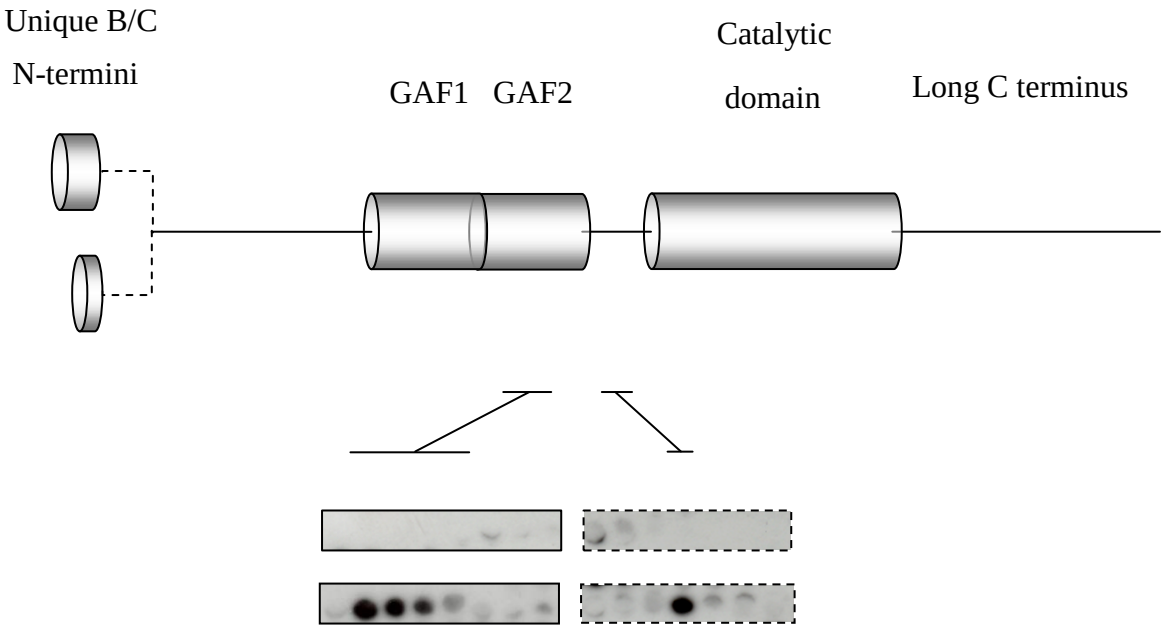

Analysis of both regions with NetPhosK predicts no putative cGK phosphorylation sites in either region of putative interaction. However, NetPhosK predicts serine 798 (of *Dm*PDE11B long) to be phosphorylated by cGK with a score of 0.68 (Blom et al., 2004), two amino acids immediately proximal to the 25mer of spot 763 showing strong immunoreactivity. Indeed this spot is immunoreactive in the DG1C-HIS_6 probed PDE11 array compared to control, but not to a convincing extent.

6.10.3 PDE11 array probed with DG2N-HIS_6

The *Dm*PDE11 peptide array was probed with DG2N-HIS_6 in order to detect any putative interaction sites. Specific interacting spots were identified by staining with an anti-HIS_5 HRP conjugated monoclonal antibody, and comparing these to a control exposed for 10 minutes, as this has similar background (figure 6.15).

Figure 6.15: PDE11 array probed with DG2N-HIS$_6$, shown alongside HIS$_6$ control. The PDE11 array was probed with DG2N-HIS$_6$ protein. Interacting spots were identified by staining with an anti-HIS$_5$ HRP conjugated monoclonal antibody. Array exposed to film for 1 min.

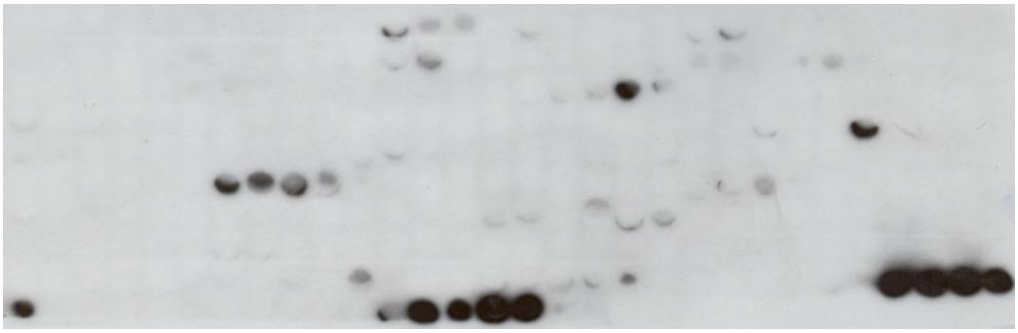

PDE11 array probed with HIS$_6$. Array exposed to film for 10 min.

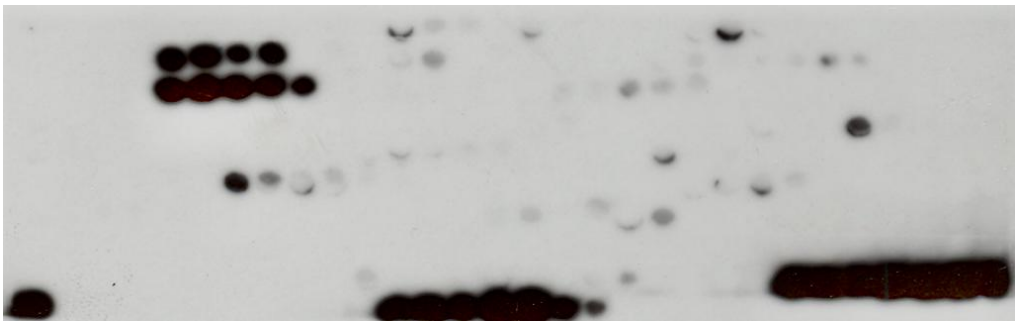

Compared to the HIS$_6$-probed control PDE11 array, the DG2N-HIS$_6$ probed PDE11 array showed a stronger average signal for each length of exposure, and as such the DG2N-HIS$_6$ probed array exposed for 1 min is compared to a HIS$_6$ control PDE11 array of ten minutes. Curiously, there are a number of spots positive in control blots that were not strongly immunoreactive in the DG2N-HIS$_6$ probed array even after a 20 min exposure. The reason for this is unknown. Comparison of the DG2N-HIS$_6$ probed PDE11 array with control does not show any novel spots. As such, there is no evidence of interaction. It does, however, merit further investigation. Use of a different anti-(poly)HIS antibody may reduce the non-specific immunoreactivity of non-specific immunoreactive spots, which would allow the array to be re-probed with DG2N-HIS$_6$. Alternatively, probing the array with GST-fused DG2N would give a different set of non-specific immunoreactive spots, and thus perhaps be more informative.

6.10.4 PDE11 array probed with DG2C-HIS$_6$

The *Dm*PDE11 peptide array was probed with DG2C-HIS$_6$ in order to detect any putative interaction sites. Specific interacting spots were identified by staining with an anti-HIS$_5$ HRP conjugated monoclonal antibody, and comparing these to a control exposed for 10 minutes, as this has similar background (figure 6.16).

Figure 6.16: PDE11 array probed with DG2C-HIS$_6$, shown alongside HIS$_6$ control. The DG2 array was probed with HIS$_6$ protein. Interacting spots were identified by staining with an anti-HIS$_5$ HRP conjugated monoclonal antibody. Array exposed to film for 5 min.

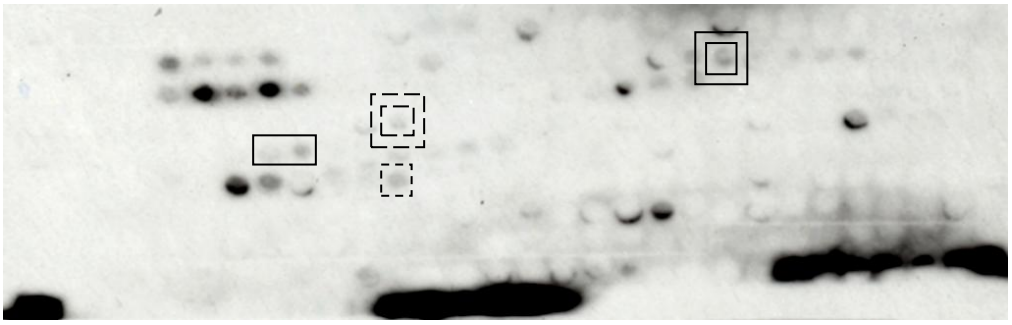

PDE11 array probed with HIS$_6$. Array exposed to film for 10 min.

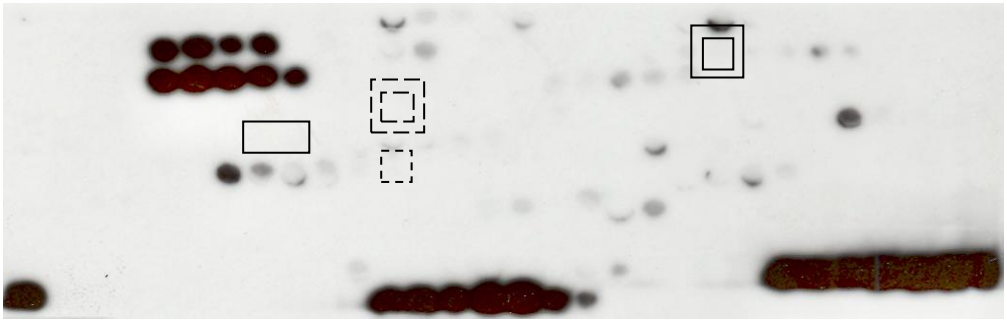

When the PDE11 array is probed with DG2C-HIS$_6$, spots 729-730, represented by a solid black line (VHEADKGSFSRVFDFEANDLSEEEATSRTS, amino acids 630-659) and 763, represented by a dashed line (VHFRLHDFKFDDIHFEDDDTLKACL, amino acids 800 - 824) are immunoreactive when compared to the HIS$_6$ probed control. These spots were also immunoreactive when overlaid with DG1C-HIS$_6$. However these spots are considerably weaker than those seen in the DG1C-HIS$_6$ probed PDE11 array, and as the DG2C-HIS$_6$ result was obtained subsequently to the DG1C-HIS$_6$ result, a stripping issue cannot be ruled out. A further two regions are immunoreactive in DG2-HIS$_6$ probed

PDE11 array, that show no detectable immunoreactivity on HIS_6 probed control PDE11 blots; spot 652, represented by a double solid line (THANGQTSSSRGGSGATTPVRKISA, amino acids 245-269) and 703, represented by a double dashed line (amino acids 500-524), are immunoreactive in the DG2C-HIS_6 probed blot. In all cases, "specific" immunoreactive spots do not display immunoreactivity comparable to putative positive spots returned by other arrays are, and as such it is desirable that the array be re-probed, or alanine substitution arrays generated representing these areas to verify the interaction. Certainly, these are not immunoreactive to an extent that they can be considered to constitute putative sites of interaction.

6.11 DG1 Array

A peptide array representing the sequence of DG1 was produced in collaboration with Dr Allan Dunlop, and was probed with Middle-HIS_6 protein, as a putative direct interaction was found when the PDE11 array was probed with DG1C-HIS_6 protein. Time did not permit the probing of the array with the other *Dm*PDE11 fusion proteins. One aspect of the protocol was changed for the DG1 arrays; *ECL Plus* Western Blotting Detection Reagent (Amersham) was used, which gives a wider dynamic range compared to *ECL* Western Blotting Detection Reagent. This had the effect of reducing the necessary time of exposure, and also had increased reactivity with the membrane itself. As such, blots of 5 minutes or over had overly high levels of background, and so these are not shown.

6.11.1 DG1 array probed with HIS_6

As a control, the DG1 array was probed with a control peptide, HIS_6, at a concentration approximately equimolar to that of the gene – HIS_6 fusion proteins that were subsequently applied, and non-specific spots were identified with an anti-HIS_5 HRP conjugated monoclonal antibody (figure 6.17).

Figure 6.17: DG1 array probed with HIS_6. The DG2 array was probed with HIS_6 protein. Non-specific spots were identified by staining with an anti-HIS_5 HRP conjugated monoclonal antibody. Array exposed to film for 2 min 30 s.

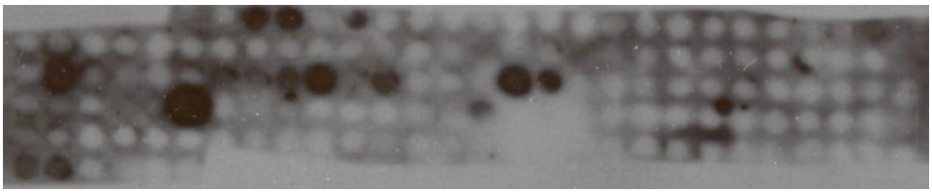

6.11.2 DG1 array probed with DmPDE11 Middle-HIS_6

The *DG1* peptide array was probed with Middle-HIS_6 in order to detect any putative interaction sites (figure 6.18).

Figure 6.18: DG1 array probed with Middle-HIS_6, shown alongside HIS_6 control. The DG2 array was probed with Middle-HIS_6 protein. Interacting spots were identified by staining with an anti-HIS_5 HRP conjugated monoclonal antibody. Array exposed to film for 1 min.

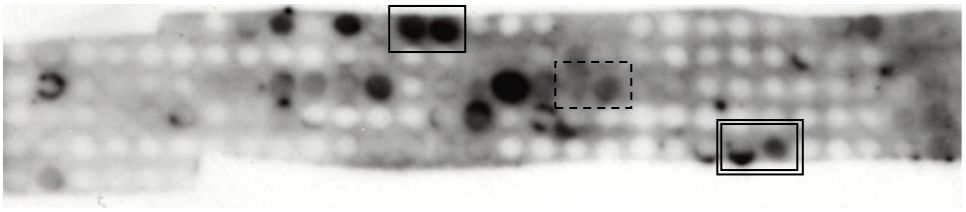

PDE11 array probed with HIS_6. Array exposed to film for 2 min 30 s.

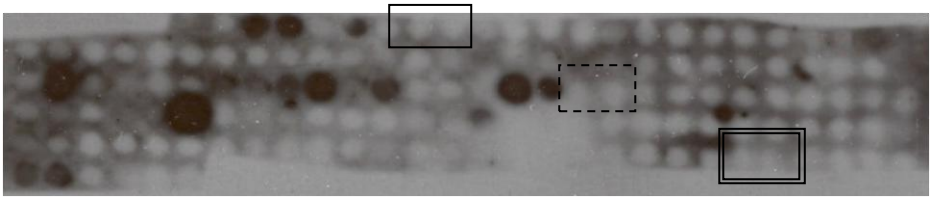

Spots 104-105, highlighted by a solid line, (LVKLHREIHKLKSVLQQTTNNLNVTREIHK, amino acids 60-90) are strongly immunoreactive compared to control probed arrays, and furthermore these spots give no immunofluorescence in a control exposed for 5 minutes (data not shown). There are two further spots that give immunofluorescence in the Middle-HIS_6 probed DG1 peptide array;

spots 169-170, highlighted by a dashed line (EETELRTLSRGDYFGEQALINEDKRTANII, amino acids 360-390), and spots 233-235 highlighted by a double solid line (ISRWAVQLIKRLCRDVPSERLGYQTGGIQDIKKHK, amino acids 680-715) (figure 6.19).

Figure 6.19: DG1, with putative regions of interaction with sequence represented by the Middle-HIS$_6$ fusion protein. Exposures of 1 min (Middle-HIS$_6$ probed) and 2 min 30 s (HIS$_6$ probed) shown. Top array control, bottom array probed with DG2C-HIS$_6$.

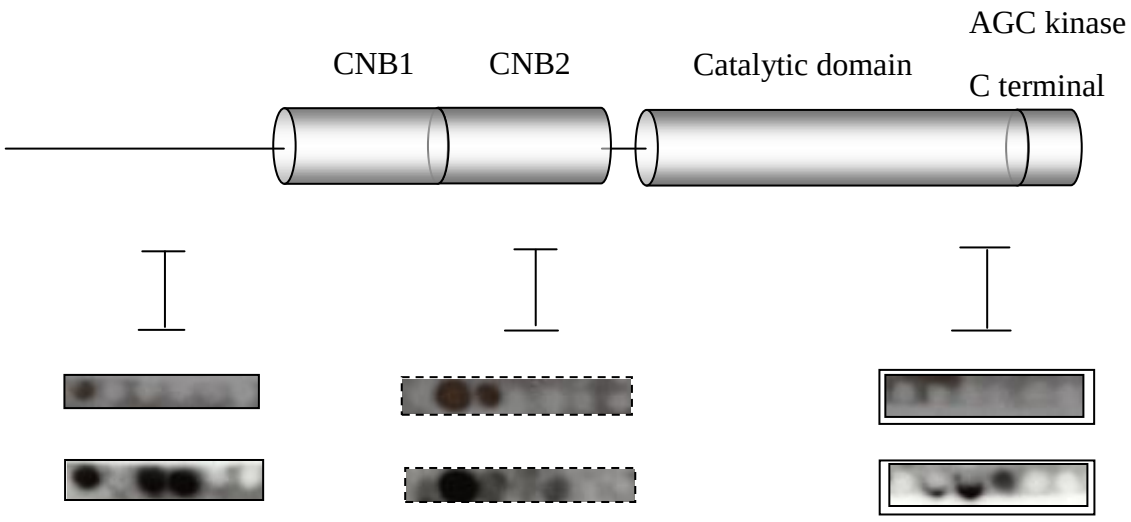

The first two putative regions of interaction identified in the Middle-HIS$_6$ probed DG1 array localise to a region of the N terminus not well characterised – the N terminus contains the dimerisation and regulatory domains, but the exact location of these is unknown - and to the second CNB domain. The third putative region of interaction falls within the catalytic domain of the enzyme, which is sequence represented by the DG1 C terminal truncate. DG1C-HIS$_6$ showed two putative regions of interaction within *Dm*DPE11 when applied to the PDE11 array. As two of the putative regions of interaction with PDE11 are represented by DG1N-HIS$_6$, it would be desirable to probe the PDE11 peptide array with this truncation in order to screen for a reciprocal interaction. Alanine substitution arrays would provide further proof that these regions interact, and identify individual amino acids within these regions vital to the interaction.

6.12 DG2 Array

A peptide array representing the sequence of DG2 P1, which incorporates the amino acid sequence of DG2 P2 in its entirety, was available from a collaboration between Dr Matt Macpherson and Dr George Baillie. As putative direct interactions were found when the PDE11 array was probed both DG2 HIS_6 fusion proteins, the DG2 array was probed with every HIS_6-tagged fragment of *Dm*PDE11, in order to detect any putative interaction sites.

6.12.1 HIS_6 Control

As a control, the DG2 array was probed with a control peptide, HIS_6, at a concentration approximately equimolar to that of the gene - HIS_6 fusion proteins that were subsequently applied, and non-specific spots were identified with an anti-HIS_5 HRP conjugated monoclonal antibody (figure 6.20).

Figure 6.20: DG2 array probed with HIS_6. The DG2 array was probed with HIS_6 protein. Non-specific spots were identified by staining with an anti-HIS_5 HRP conjugated monoclonal antibody. Array exposed to film for 15 min.

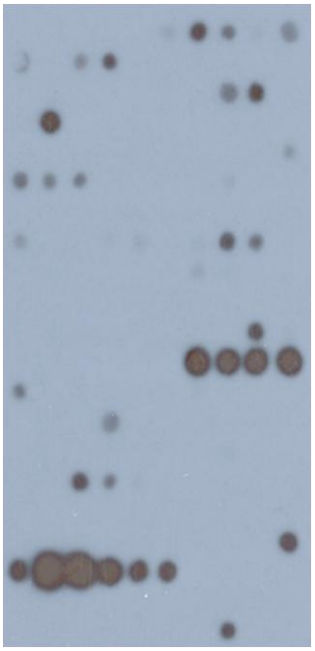

6.12.2 DG2 array probed with *Dm*PDE11-HIS$_6$

6.12.2.1 BN-HIS$_6$

The DG2 array was probed with BN-HIS$_6$ protein. Specific interacting spots were identified by staining with an anti-HIS$_5$ HRP conjugated monoclonal antibody, and comparing these to the equivalent control (figure 6.21).

Figure 6.21: DG2 array probed with BN-HIS$_6$, shown alongside HIS$_6$ control. The DG2 array was probed with BN-HIS$_6$ protein. Interacting spots were identified by staining with an anti-HIS$_5$ HRP conjugated monoclonal antibody. Array exposed to film for 15 min.

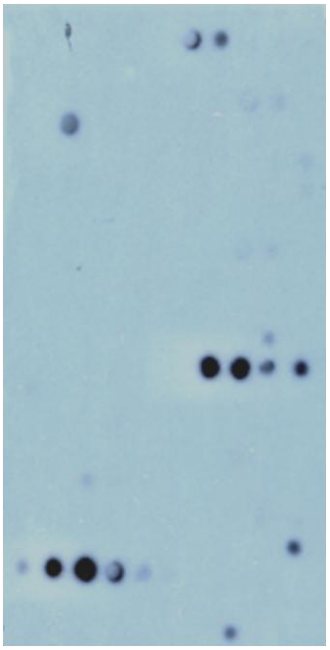

DG2 array probed with HIS_6. Array exposed to film for fifteen minutes.

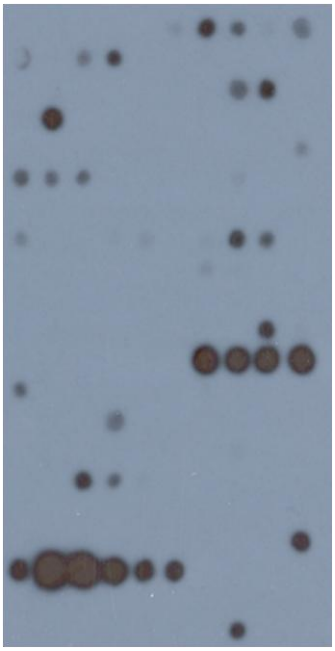

The BN-HIS_6 probed array showed a weaker signal than other DG2 array exposures; the reason for this is unknown. The BN-HIS_6 probed DG2 array show no novel spots when compared to the HIS_6 control DG2 array. This data suggests that there is no direct interaction between DG2, and the section of *Dm*PDE11B represented by BN-HIS_6, which incorporates from the unique B N-terminus until the end of the first GAF domain.

6.12.3 CN-HIS_6

The DG2 array was probed with CN-HIS_6 protein. Specific interacting spots were identified by staining with an anti-HIS_5 HRP conjugated monoclonal antibody, and comparing these to the equivalent control (figure 6.22).

Figure 6.22: DG2 array probed with CN-HIS$_6$, shown alongside HIS$_6$ control. The DG2 array was probed with CN-HIS$_6$ protein. Interacting spots were identified by staining with an anti-HIS$_5$ HRP conjugated monoclonal antibody. Array exposed to film for fifteen minutes.

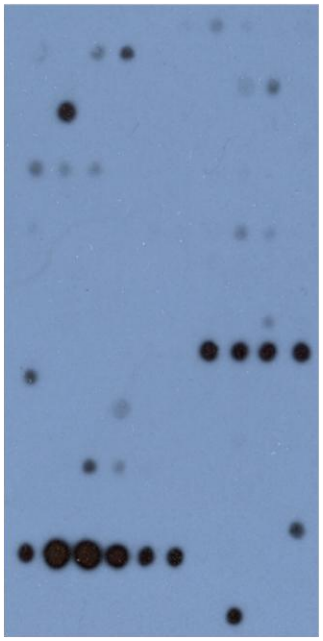

DG2 array probed with HIS$_6$. Array exposed to film for fifteen minutes.

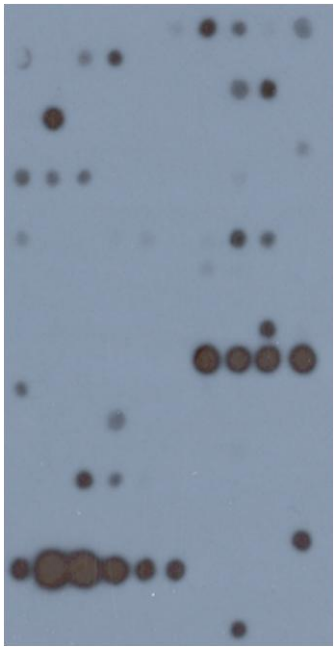

The CN-HIS$_6$ probed DG2 array shows no novel spots when compared to the HIS$_6$ control DG2 array. This data suggests that there is no direct interaction between DG2, and the

section of *Dm*PDE11C represented by CN-HIS_6, which incorporates from the unique C N-terminus until the end of the first GAF domain.

6.12.3.1 Middle-HIS_6

The DG2 array was probed with Middle-HIS_6 protein. Specific interacting spots were identified by staining with an anti-HIS_5 HRP conjugated monoclonal antibody, and comparing these to a control exposed for 15 min as this showed equivalent background (figure 6.23).

Figure 6.23: DG2 array probed with Middle-HIS_6, shown alongside HIS_6 control. The DG2 array was probed with Middle-HIS_6 protein. Interacting spots were identified by staining with an anti-HIS_5 HRP conjugated monoclonal antibody. Array exposed to film for 5 minutes.

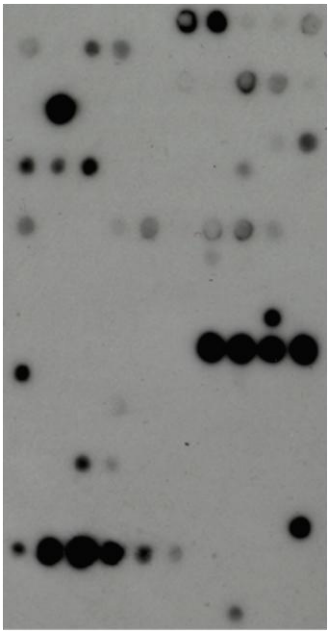

DG2 array probed with HIS_6. Array exposed to film for fifteen minutes.

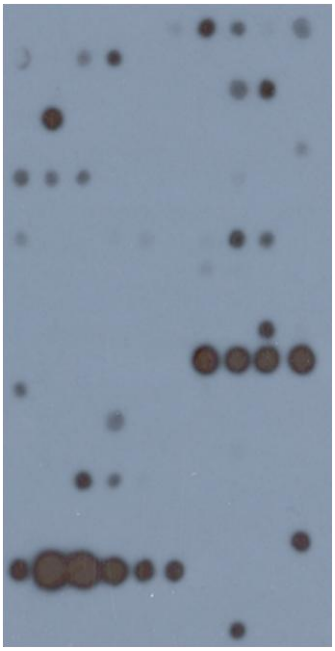

The Middle-HIS_6 probed DG2 array showed a strong signal after 5 min of exposure, and so this is compared to a HIS_6 control array exposed for 15 min. Comparison shows no novel spots when compared to the HIS_6 control DG2 array. There are two spots that appear after 5 min on the Middle-HIS_6 array that are barely visible after 15 min of exposure on the HIS_6 control blot. However, as background is higher on the Middle-HIS_6 probed DG2 array than control, it would be desirable to repeat the assay, using a different anti-(poly)HIS antibody, or a GST-tagged Middle fragment.

6.12.3.2 End-HIS_6

The DG2 array was probed with End-HIS_6 protein. Specific interacting spots were identified by staining with an anti-HIS_5 HRP conjugated monoclonal antibody, and comparing these to a control exposed for 15 min as this showed equivalent background (figure 6.24).

Figure 6.24: DG2 array probed with End-HIS_6, shown alongside HIS_6 control. The DG2 array was probed with End-HIS_6 protein. Interacting spots were identified by staining with an anti-HIS_5 HRP conjugated monoclonal antibody. Array exposed to film for two minutes thirty seconds.

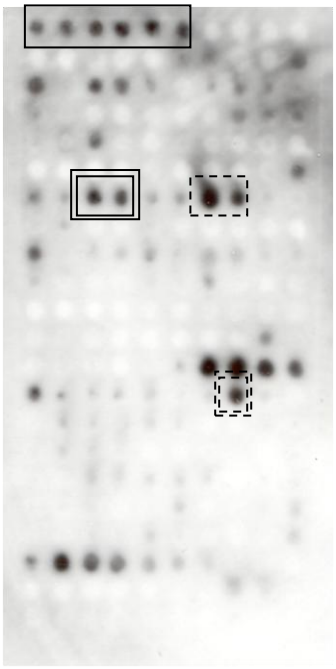

DG2 array probed with HIS_6. Array exposed to film for fifteen minutes.

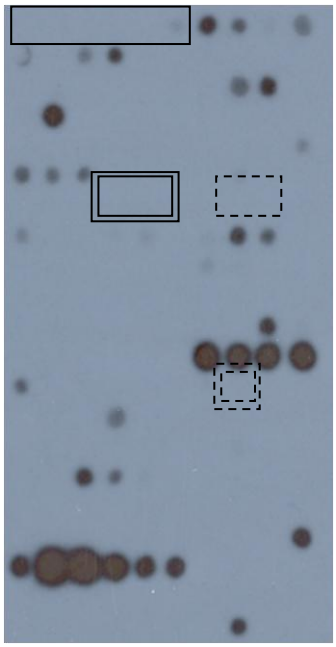

At an exposure time of 2 min 30 s, novel spots are seen at E22 – J22 (highlighted by a solid line), representing the sequence SNAPHSSTTVDAPPRPADVDVATVPVATPAPPPQQPVSNLFYADYQKLQP, C16 –

D16 (highlighted by a double solid line), representing the sequence YHQPSPGSSQPVAIPGATCHSPTQLQPPNT, G16 - H16 (highlighted with a dashed line), representing the sequence SPTQLQPPNTLNLQQQMQSLRISGCTPSGT, and C9 (highlighted by a double dashed line), representing the sequence RGDYIVRQGARGDTFFIISKGKVRV. However, multiple spots present as background on the control DG2 array are not immunoreactive on End-HIS_6 probed DG2 array. The reason for this is unknown. Furthermore, background was sufficient on the End-HIS_6 probed array at exposure times of five or more minutes to obscure previously clear spots. When purifying higher concentrations of End-HIS_6 protein, non-mobile, insoluble, immunoreactive protein transferred to the membrane in a manner that suggested it had not migrated from the wells; i.e., it had formed inclusion bodies, and so End-HIS_6 is partially insoluble, which most likely explains the high levels of background. The array was repeated with a different batch of purified protein in an attempt to reduce background, but as the DG2 array had been stripped twice, the exposures actually had more background and so again these results are omitted. These issues prevent these data from being taken to indicate a putative interaction. Were the experiment to be repeated, soluble protein would be necessary. Optimisation of growth conditions was attempted, but clearly optimum conditions were not achieved. The addition of Triton-X 100 when purifying the recombinant protein may render the protein soluble. Were this approach to fail, the generation of an N-and C-terminal tagged End-GST fusion protein may yield a more soluble protein. However, repeat of the experiment would also need a new DG2 array to be produced, as those used have been stripped numerous times.

6.13 Discussion

In this chapter, peptide arrays were used to determine whether the interaction between *Dm*PDE11 and the cGKs DG1, and the DG2 isoforms P1 and P2 are direct or indirect. A peptide array representing the sequence of *Dm*PDE11, including the novel N-termini of the B and C isoforms, and the novel sequence of the C-termini of the short isoforms was generated, and probed with HIS_6 fused cGK protein. While DG1N-HIS_6 was expressed at the predicted size, repeated attempts to affinity-purify the protein failed. The PDE11 array was probed with DG1C-HIS_6 peptide. Comparison of the control and DG1C-HIS_6 probed PDE11 arrays reveals two areas of putative interaction. The first occurs within the second of the GAF domains. GAF domains perform a multitude of roles, and are present in several classes of protein (Martinez et al., 2002a). They have been shown to modulate the function

of several mammalian PDEs. The GAF domains of PDE2, PDE5 (Zoraghi et al., 2004), and PDE11 have been shown to bind cGMP, and the GAF domain of PDE10 binds cAMP (Gross-Langenhoff et al., 2006). GAF domains have been shown to mediate oligomerisation in PDE2 (Martinez et al., 2002b), PDE5 (Zoraghi et al., 2005), PDE6αβ and PDE6α´α´ (Muradov et al., 2003), and PDE11A (Weeks et al., 2007), where phosphorylation of two cGK phosphorylation sites in the N terminus of the PDE11A modulates the process (Gross-Langenhoff et al., 2008). GAF domains function to relieve autoinhibition in PDE2 (Martinez et al., 2002b) and PDE5 (Rybalkin et al., 2003). GAF domains have also been implicated in protein-protein interaction, where binding of cGMP to the GAF domains of PDE6 R mediates the interaction of the catalytic domain with the inhibitory subunit Pγ (D'Amours and Cote, 1999). Within this context, a direct protein-protein interaction with DG1 at this site could have any number of implications. Were DG1 interaction at this site to affect any of these processes, this would modulate PDE11 activity, and therefore modulate the activity of the cGK itself. Within this region there are no cGK or PKA consensus phosphorylation sites. The second putative area of interaction lies between the second GAF domain and the catalytic site of *Dm*PDE11. Although this area contains no putative cGK phosphorylation sites, there is a putative cGK phosphorylated serine residue two amino acids proximal to the immunoreactive 25mer. Furthermore, this 25mer represents an entire putative phosphorylation site, and this spot is immunoreactive when compared to control. However, this spot was only mildly immunoreactive compared to its neighbour, visible after 5 minutes opposed to 10 seconds. This area of *Dm*PDE11A has had no function ascribed to it as yet; furthermore the putative phosphorylation site is not present in *Hs*PDE11A. As such the significance of this putative interaction is not clear. An *in vitro* or *in vivo* phosphorylation assay would show whether or not PDE11 is a *bona fide* phosphorylation target of DG1. These sites of interaction can only be considered putative; an alanine substitution array representing these spots would confirm whether the interaction is *bona fide*, and would identify essential residues in the region.

As both of the regions identified in the PDE11 array as putative regions of interaction with DG1C-HIS_6 fell within the PDE11 Middle-HIS_6 protein, and time remaining in the lab was short, the DG1 array was only overlaid with this *Dm*PDE11 fusion protein. Three putative regions of direct interaction were identified. The first putative region of interaction maps to the N-terminus of the DG1, which contains the dimerisation and regulatory domains. The second maps to the second CNB domain, and the third to the catalytic domain. The first two regions of interaction are incorporated within the DG1 N terminal truncate. As such it

is desirable that this protein is applied to the PDE11 array, in order to screen for a reciprocal interaction. The third putative region of interaction is represented within the DG1 C terminal truncate, which showed two putative regions of interaction within *Dm*DPE11 when applied to the PDE11 array. Again, alanine substitution arrays would provide further proof that these regions interact, and identify individual amino acids within these regions vital to the interaction. However, the putative data corresponds with the co-immunoprecipitation data presented in chapter 5. Further putative regions of interaction may be identified if the DG1 array is probed with the other *Dm*PDE11 truncations, and so it is desirable that these assays are performed. Importantly, such an interaction must be confirmed by two other methods; as an interaction has been shown using co-immunoprecipitation, yeast two hybrid or mutagenesis and subsequent co-immunoprecipitation would confirm the interaction as direct.

The PDE 11 array was probed with DG2N-HIS_6, which incorporates the dimerisation and regulatory domains, and DG2C-HIS_6, which incorporates the twin CNB, catalytic, and AGC kinase C terminal domains, in order to determine putative sites of protein-protein interaction. Two putative sites of interaction were identified when the PDE11 array was probed with DG2N-HIS_6, one immediately proximal to, and one immediately distal to the twin GAF domains. However, these spots were mildly immunoreactive in control arrays of equivalent background. Despite this, immunoreactivity of these spots on the DG2N-HIS_6 probed array was significantly, convincingly stronger. Repeat of the array using DG2N tagged with GST would clarify if the immunoreactivity was indeed due to bound, interacting protein, assuming these spots would not be immunoreactive in control blots. Alanine substitution arrays would likely suffer similar background if probed with DG2N-HIS_6 protein, and so these would also benefit from use with GST tagged DG2N protein. When probed with DG2C-HIS_6, four putative sites of interaction were identified, including two in common with the two identified in DG1C-HIS_6 probed PDE11 array, in the GAF-B domain, and immediately distal to this GAF domain. The two novel regions were found in GAF-A, and in the N terminus of PDE11. However, all four regions, although not at all immunoreactive in control blots, showed immunoreactivity at a lower intensity than on spots "positive" on other blots. As such none of these interactions are as convincing, and require further investigation; either a repeat of the assay, or use of GST tagged DG2C fragment.

The DG2 peptide array was probed with (*Dm*PDE11)BN-HIS_6, CN- HIS_6, Middle-HIS_6, and End-HIS_6 protein. Background for this array was higher than the other two arrays

probed, despite none of the 25mers containing 5x or 4xHISmers. The arrays were produced over a year before they was used; were new arrays to be generated background may be reduced. The two fusion proteins representing the N termini of *Dm*PDE11B and C showed no putative interactions with the DG2 array. When probed with Middle-HIS_6, a number of spots showed a higher intensity than on the control array, but no novel spots were identified. Probing with the End fragment identified two putative regions of interaction. However, there were a number of issues with this array, including apparent problems with the solubility of End-HIS_6, and as such the data cannot be taken to indicate a putative direct interaction. As the End fragment is small, tagging this fragment with N- and C-terminal GST tags would still result in a protein of a size that would facilitate expression in *E. coli*, and as the GST tag increases solubility, would hopefully prevent the formation of inclusion bodies, and reduce the background seen in the End-HIS_6 overlaid DG2 array.

Anti (poly)HIS antibodies recognise 4xHISmers or 5xHISmers. In the course of this study, an anti-HIS_5 monoclonal antibody was employed, which resulted in the unavoidable immunoreactivity of spots containing 5xHISmers, and thus "non-specific" interactions with antibody prevent the identification of a putative interaction with overlaid protein on any of these spots. The occurrence of these spots was unavoidable in the PDE11 array, as the C terminal of *Dm*PDE11 contains histidine-rich regions. However, the antibody also showed non-specific interaction with spots containing 4xHISmers, and indeed spots containing no HISmers, and so background levels were higher than anticipated. This would justify the additional probing of these arrays with GST (or other) tagged protein, as a higher number of non-immunoreactive spots would be probed with protein of interest, and thus the likelihood of false negative results would be lowered.

Chapter 7

Characterisation of the role of *Dm*PDE11 in immunity

7.1 Summary

This chapter describes work performed on *Dm*UAS-PDE11 RNAi and *Dm*PDE11 deletion lines to investigate the role of this phosphodiesterase in immunity. Data previously obtained suggested that cGMP and PDE11 may modulate diptericin levels in *Drosophila*. PDE11 has also been implicated in whole organism survival under septic immune challenge from *E. coli*. The role of PDE11 in immunity was investigated in flies with reduced PDE11 transcript levels, both in UAS-PDE11 RNAi flies, with expression driven either in Malpighian tubule principal cells or ubiquitously, and in the PDE11 deletion mutant PDE11▲121, by septic challenge with *E. coli*. The data suggests a role for PDE11 in immunity, but needs further investigation.

7.2 cGMP modulates innate immunity in *Drosophila*

As discussed in the introduction, NO has been shown to play an important role in *Drosophila* immunity. NOS modulates the immune response to lipopolysaccharides through the upregulation of diptericin (Foley and O'Farrell, 2003). In the Malpighian tubule, NOS has been shown to be upregulated following immune challenge, and has been shown to activate the IMD pathway (McGettigan et al., 2005). NO can activate cGMP signalling by the activation of sGC. Recent findings show that cGMP modulates expression of AMPs in the Malpighian tubule in a dose dependent manner. When tubules are incubated with nanomolar [cGMP], there is an increase in diptericin expression, whereas incubation with micromolar [cGMP] reduces diptericin transcription. This effect is not seen in the fat body (Aitcheson).

cGMP dependent protein kinases have been shown act as immune effector proteins. Diptericin expression is increased when DG1 is overexpressed in the principal cells of the tubule, whereas overexpression of DG2 P1 or P2 has the opposite effect, resulting in a reduction of diptericin expression (Aitcheson, 2009a). Furthermore, modulation of cGK expression in only the principal cells of the tubule is sufficient to modulate whole fly survival, when septically challenged with the gram-negative bacteria *E. coli* (Aitcheson, 2009e). In the Malpighian tubule, cGKs have been shown to affect the translocation of the transcription facor Relish, an NF-kappaB homologue (Dushay et al., 1996), to the nucleus, downstream of imd. This modulation of Relish localisation occurs in an antagonistic manner, via an unknown mechanism. DG1 appears to positively regulate the translocation

of Relish to the nucleus; overexpression of DG1 results in Relish translocation to the nucleus, even in the absence of immune challenge, whereas knockdown of DG1 via RNAi inhibits this translocation, even under immune challange. DG2, conversely, appears to inhibit Relish translocation to the nucleus. Overexpression of DG2 P1 or P2 inhibits Relish translocation to the nucleus, even under immune challenge (Aitcheson, 2009b). cGK function is tightly regluated by PDEs. The Malpighian tubule expresses all of the PDEs (Day et al, 2005), and so there are several candidates to modulate the immune function of the cGKs.

Data obtained by Aitcheson implicating PDE11 in the immune response against gram negative bacteria is summarised in appendix 5. Briefly, her findings were that increased cGMP in the Malpighian tubule decreases diptericin expression, and that this can be phenocopied by the reduction of PDE11 transcript levels in the principal cell. Furthermore, it was found that immune challenge of UAS-PDE11 RNAi/c42 progeny (thus PDE11 expression is reduced in tubule principal cells) results in reduced survivorship compared to UAS-PDE11 RNAi (line 1) parental control. As such, the role of PDE11 in immunity was investigated.

7.3 Immune challenge of UAS-PDE11 RNAi driven in tubule principal cells

I investigated the role of PDE11 in immunity using UAS-PDE11 RNAi line 9, as this line had been shown to give knock down of PDE11 expression by Q-PCR analysis, as detailed in chapter 3. These lines differ in the chromosomal localisation of the pWIZ-based UAS-PDE11 RNAi insertion. Thus, the two lines may achieve differing knockdowns, and any difference in results could be due to the extent of the knock down achieved by the RNAi.

E. coli was grown overnight to static phase, harvested by centrifugation, and the flies were stabbed with a 0.35mm bore needle dipped into the *E. coli* solution; mock stabbings were performed with a dry needle, as detailed in materials and methods. The experiment had an additional control to the experiment of Aitcheson presented in appendix 5, the addition of c42 mock- and *E. coli*-challenged survival assays. The below data represents the pooling of two survival experiments, with one set of controls (figure 7.1).

Figure 7.1: c42/UAS-PDE11 RNAi immune assay. No significant decrease in survival upon challenge with *E. coli* using a 0.35mm gauge needle was recorded when PDE11 expression was reduced via expression of PDE11 RNAi, driven in tubule principal cells. Error bars show standard error of the mean. Survivorship on Y axis shown between 50 – 100% for clarity.

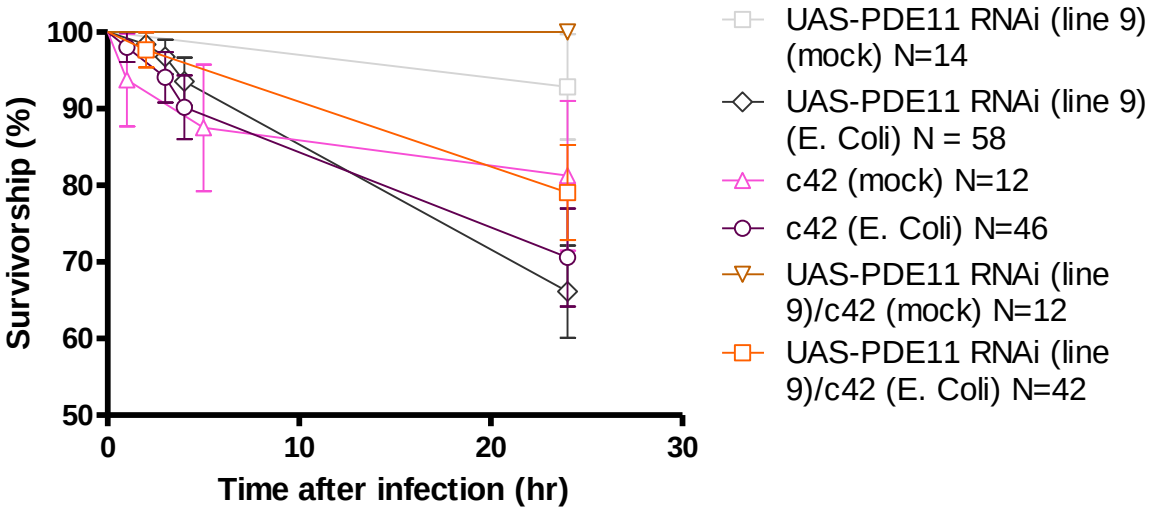

Although the number of mock controls was lacking, there was no decrease in survival in the c42/UAS-PDE11 RNAi (line 9) progeny when compared to survival of the parental strains under challenge of *E. coli*.

7.4 Immune challenge of UAS-PDE11 RNAi driven ubiquitously

It was reasoned that if PDE11 plays a vital immune role in barrier epithelia and perhaps other tissues, expression of UAS-PDE11 RNAi ubiquitously using the Act5C-GAL4/GFP CyO driver line would lead to an increased immune phenotype, were such a phenotype to exist. Although *Dm*UAS-PDE11 RNAi (line 9) is 90% lethal at the larval stage when driven ubiquitously by Act5C-GAL4, the cross is non-lethal at 18˚C, and the adults viable. Thus, UAS-PDE11 RNAi (line 9) parental flies were crossed with the Act5C-GAL4/GFP CyO driver line, and these flies were subjected to immune challenge with *E. coli* as above (figure 7.2). Negative control genotypes used were Canton S, and the other resultant progeny from the UAS-PDE11 RNAi (line 9) x Act5C-GAL4/GFP CyO cross, UAS-PDE11 RNAi (line 9)/GFP CyO. As a positive control, Relish e20, a complete Relish null

mutant (Hedengren et al., 1999), were also assayed. Relish is an NF-κB homologue found in the *imd* antimicrobial pathway. This data is excluded for clarity, but total death was seen within two days maximum in every assay performed

Figure 7.2: cAct5c-GAL4/UAS-PDE11 RNAi immune assay. Survival experiment showing no significant decrease in survival upon challenge with *E. coli* using a 0.35mm gauge needle when PDE11 expression is reduced via expression of UAS-PDE11 RNAi when driven ubiquitously. Error bars show standard error of the mean. Survivorship on Y axis shown between 60 – 100% for clarity.

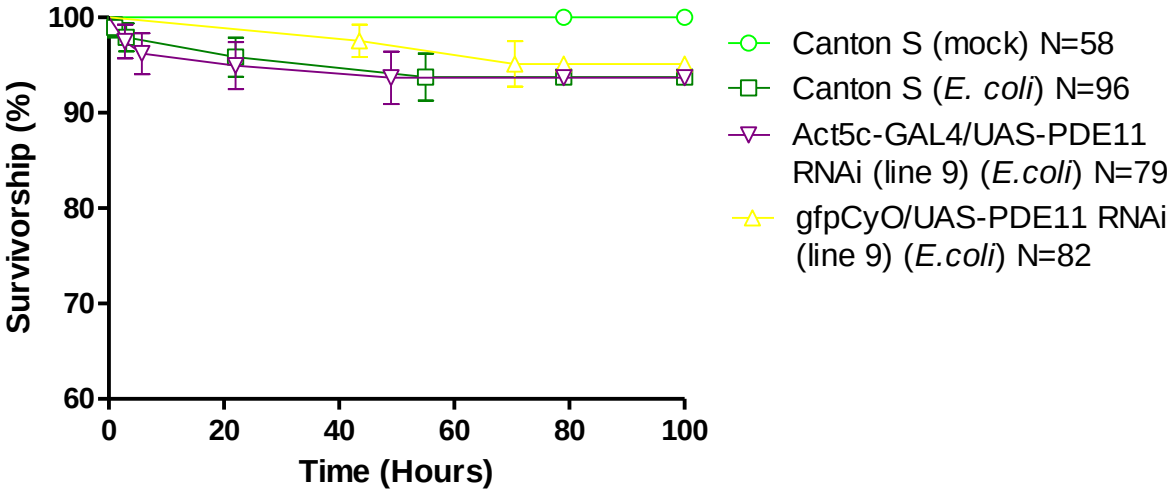

This experiment was performed in triplicate, and the data were merged. None of the experiments showed a significant, or even a qualitative reduction in survival in flies where PDE11 expression had been ubiquitously reduced, when analysed individually or when the data were pooled.

7.4.1 *Dm*PDE11 deletion line

The PDE11RB deletion line (courtesy of Prof. David Morton, Oregon), PDE11▲121, is balanced over the homozygous lethal balancer CyO. The existence of straight winged, red eyed flies demonstrates that the deletion is homozygous viable. The increased proportion of del/CyO flies suggests that the deletion has a lethality effect (table 7.1).

Table 7.1: PDE11▲121 produces viable homozygous flies when balanced with CyO. Heterozygous deletion flies were crossed and the progeny scored for the phenotypic marker CyO. Del/Del = PDE11▲121/ PDE11▲121, +/+, Del/CyO = PDE11▲121/CyO; +/+

	♂	♀
Del/Del	14	16
Del/CyO	30	26

However, Q-PCR with RB specific primers has not been performed, and so it is not clear if the deletion is a true null. Homozygous males have a deeper red eye colour than females; the reason for this is unknown; perhaps there is another insertion on the Y. Homozygous PDE11▲121 males are sterile, and this contributed to the fact that for individual experiments, a sufficient number of PDE11▲121 flies were not obtained to perform both an *E. coli* and a mock immune challenge, and as such flies were only challenged with *E. coli*, with the rationale that it would increase the chances of finding a significant phenotype, and that this could later be verified by the inclusion of mock-challenge controls. This lack of flies also dictated the pooling of homozygous and heterozygous flies; ideally, the two genotypes would be assayed separately within the same experiment. Pooled PDE11▲121/CyO and PDE11▲121/PDE11▲121 flies were assayed for an immune phenotype by septic challenge with *E. coli* as above, alongside the wild type fly Canton S, as a negative control, and Relish e20 deletion flies as a positive control (figure 7.3). This figure represents the pooling of 6 datasets.

Figure 7.3: *Dm*PDE11Δ121 immune assay. Survival experiment showing a significant decrease in survival upon challenge with *E. coli* using a 0.35mm gauge needle in PDE11 homozygous and heterozygous deletion flies (pooled) compared to controls. Error bars show standard error of the mean. Survivorship on Y axis shown between 60 – 100% for clarity.

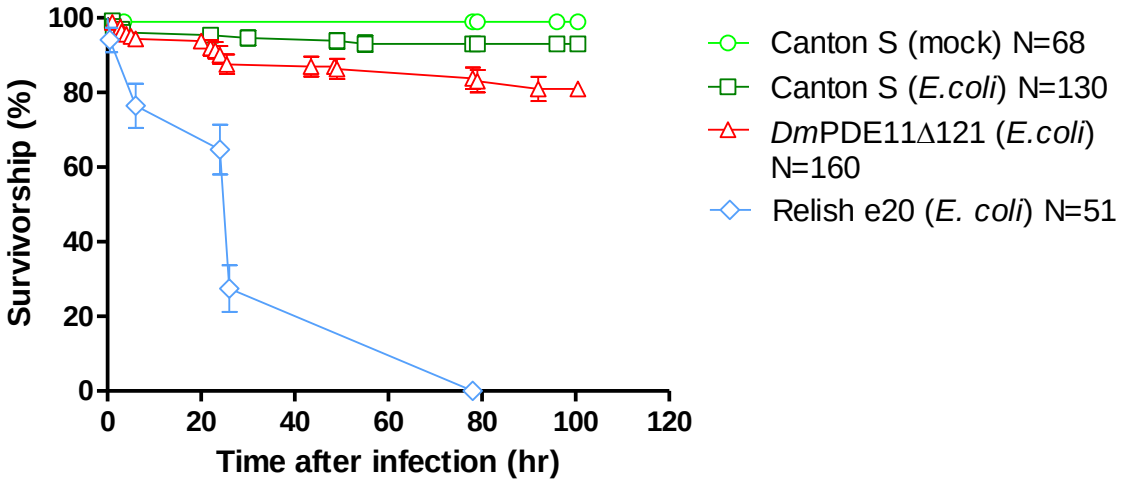

PDE11▲121 flies showed significantly lower survivorship than *E. coli* challenged Canton S flies, where P< 0.0001 using a Log-rank (Mantel-Cox) test.

The above assay was repeated with the appropriate mock stabbed controls, assaying homozygous and heterozygous deletion flies separately. Injections were performed using a Nanoject II Auto nanoliter injector, where *E. coli* was grown to an OD_{600} of 2.0 (which represents static phase), harvested by centrifugation, resuspended in an equal volume of PBS, and injected in a volume of 69nl just below the first abdominal turgite. This represents a lower dose than stabbing with a 0.35mm needle, although the difference cannot be quantified as the dose delivered with a 0.35mm needle is impossible to quantify. Mock stabbings were performed with PBS. The data presented represents the pooling of two immune assays (figure 7.4).

Figure 7.4: *Dm*PDE11Δ121 immune assay. Survival experiment showing no difference in survival upon challenge with *E. coli* using a Nanoject II Auto nanoliter injector between PDE11 homozygous or heterozygous deletion flies (pooled) and PBS injected controls. Error bars show standard error of the mean. Survivorship on Y axis shown between 80 – 100% for clarity.

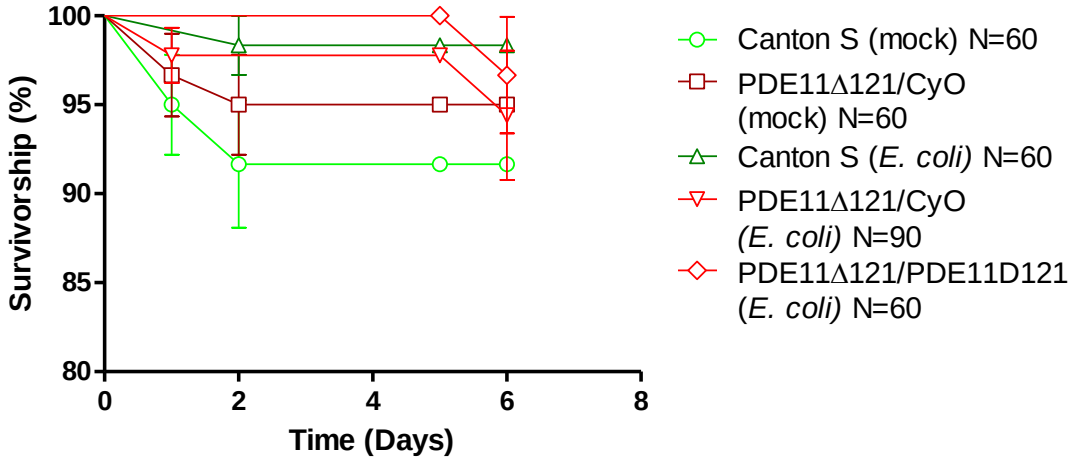

No difference in survival following immune challenge was seen between Canton S and homozygous or heterozygous PDE11▲121 flies.

7.5 Conclusion for the role of *Dm*PDE11 in immunity

Epithelial tissues have been shown to play a major role in immunity, expressing all of the known anti microbial peptides (Tzou et al., 2000), and the Malpighian tubule in particular has been shown to act as critical immune tissue, where NO and cGMP signalling play vital roles in the imd immune pathway (Aitcheson, 2009c; Davies and Dow, 2009; McGettigan et al., 2005). As a dual specificity PDE expressed in all epithelia (Chintapalli et al., 2007), *Dm*PDE11 is capable of modulating cGMP signalling, and thus the role of *Dm*PDE11 in immunity was investigated by subjecting flies with reduced PDE11 transcript levels to an immune challenge, and screening for a change in mortality. PDE11 deletion and UAS-PDE11 RNAi lines were used to reduce *Dm*PDE11 transcript levels both ubiquitously, and in a tissue specific manner.

UAS-PDE11 RNAi line 9 was crossed to the Malpighian tubule GAL4 driver line c42, and both parental lines and the resultant progeny were subjected to an *E. coli* stabbing assay. The progeny did not display an increase in mortality under immune challenge. If reduction

of *Dm*PDE11 transcript levels in the Malpighian tubule did not impact upon fly survival, then it was reasoned that a ubiquitous knock down of transcript levels may produce a phenotype. Thus, UAS-PDE11 RNAi (line 9) was crossed to the ubiquitous GAL4 driver line Act5C-GAL4. Progeny from this cross displayed no apparent increase in mortality when compared to parental controls. As the extent of the knockdown conferred by RNAi may not have been sufficient to confer a survival phenotype, the PDE11 deletion line PDE11▲121 was subjected to multiple *E. coli* stabbing assays, where a 0.35mm needle was dipped into an *E. coli* solution and survivorship recorded, and the data pooled. The data revealed a highly ($P< 0.0001$) significant reduction seen in PDE11▲121 line compared to Canton S under *E. coli* challenge. Where Canton S flies showed around 10% mortality after 100 h, PDE11▲121 showed around 20% mortality. However, homozygous and heterozygous flies were pooled in the above experiments, and a mock injection was not included, which is critical to proving that a reduction in survival is not due to increased susceptibility to the stab itself or a general reduction in the flies' viability.

As a lethality phenotype would be expected to be more pronounced in the homozygous null mutant that in the heterozygous, the experiment was repeated, with the genotypes assayed separately, using a new delivery system that permitted tighter control of the dose delivered, at the cost of having to reduce the dose of *E. coli*. Perhaps as a result of this reduced dose, no difference in survival was seen between Canton S controls and either homozygous or heterozygous PDE11 deletion flies. As such, a repeat of this experiment at the original dose would be desirable, including the mock stab controls. In addition to this, the extent of the deletion must be determined.

UAS-PDE11 RNAi line 9 did not show any immune phenotype when crossed to the GAL4 lines c42 and Act5c. Given that a reduction in survival was identified where UAS-PDE11 RNAi line 1 was crossed to c42 and the progeny subjected to immune assay alongside a parental control (Aitcheson, 2009e), as detailed in appendix 5, it may be that a higher knockdown was achieved with these flies. As such, Q-PCR using the primers used to screen line 9 should be used on line 1, and if a higher knockdown is achieved then that fly line should be employed. However, it is also possible that the apparent reduction in survival of the UAS-PDE11 RNAi (line 1) when crossed to c42 could be due to the low number of flies used for certain genotypes screened.

If PDE11 does indeed play a immune role, it is not a vital one; where a significant reduction in survivorship was achieved when assaying PDE11▲121, the increase in mortality was ~10% greater than controls after 100 hours at ~20% compared to ~10%,

whereas the Relish e20 deletion mutant showed 100% mortality after around a day. As the deletion has not been shown to be a true null, there may be sufficient expression of PDE11 to mask the phenotype to an extent.

If indeed it is shown that a reduction in PDE11 transcript levels reduces survival against *E. coli*, it may relate to the finding in the Malpighian tubule that expression of the antimicrobial peptide diptericin is modulated by cGMP. When tubules are incubated in cGMP, diptericin expression is reduced compared –cGMP incubated controls. Non cell-permeable extracellular cGMP is transported into the tubule (Riegel et al., 1998), and can induce cellular signalling events such as fluid transport (Davies et al., 1995). This suggests that the large decrease in diptericin expression induced by the incubation in 100μM cGMP is caused by transport of extracellular cGMP into the tubule, and by a subsequent increase of intracellular cGMP.

This increase in cGMP, and the subsequent reduction in diptericin expression, is phenocopied by reduction of PDE11 transcript levels in Malpighian tubule principal cells, as c42/UAS-PDE11 RNAi (line 1) tubules not incubated in cGMP display a similar level of diptericin expression to UAS-PDE11 RNAi (line 1) parental tubules incubated in cGMP. Furthermore, c42/UAS-PDE11 RNAi (line 1) incubation with cGMP does not further decrease diptericin expression. This data is presented in appendix 5 (Aitcheson, 2009c, d). This would suggest that PDE11 modulates an immune induced cGMP signal in a manner relevant to Diptericin expression, which directly affects *Drosophila* survival under immune challenge. This would be the first time a PDE had been shown to play an immune role. Taken together, the data in this chapter suggests that the role of *Dm*PDE11 in immunity deserves further investigation.

Chapter 8

A study of *H. Sapiens* PDE11A using the Malpighian tubule, a polarised epithelial tissue

8.1 Summary

The *Hs*PDE11A family has recently been characterised biochemically, but the physiological role it plays it not well understood. *Drosophila* PDE11 was first described in 2005, and has four splice variants. Using the powerful genetic model organism *Drosophila melanogaster,* we have further investigated this family of phosphodiesterases, both fly and human, in an organotypic context. *Hs*PDE11A3 expression is confined to testis in both rat and human (Yuasa et al., 2001), and has been shown to regulate spermatozoa physiology (Seftel, 2005). *Dm*PDE11 -/- null male mutants are infertile, and so function may be conserved.

The *Dm*PDE11 isoforms were aligned with all *Hs*PDE11A isoforms, compared with respect to sequence identity and homology, and were subjected to phylogenetic analysis. These results suggested that *Hs*PDE11A3 is a *Dm*PDE11 orthologue.

*Hs*PDE11A3 pP[UAST] constructs were generated, and the transgene expressed in S2 cells and fly. The protein showed predominantly nuclear localisation when expressed in S2 cells. In Malpighian tubule principal cells at low levels of expression, the protein localised predominantly to the nucleus, but was localised to the cytosol when the transgene was driven by stronger GAL4 expression.

8.2 Introduction

The Human phosphodiesterase-11A (PDE11) family consists of four splice variants *Hs*PDE11A1 (PDE11A 004), *Hs*PDE11A2 (PDE11A 003), *Hs*PDE11A3 (PDE11A 002), and *Hs*PDE11A4 (PDE11A 001) (Fawcett et al., 2000; Hetman et al., 2000; Yuasa et al., 2000). I will use the common nomenclature *Hs*PDE11A1-4 herein. *Hs*PDE11A isoforms hydrolyze cAMP and cGMP via a conserved carboxyl-terminal (C-terminal) catalytic domain. The amino-termini (N-termini) of the four isoforms vary in length and amino acid sequence. *Hs*PDE11A2, *Hs*PDE11A3, and *Hs*PDE11A4 contain one or more GAF (cGMP-binding phosphodiesterase, Anabaena adenylyl cyclase, and Escherichia coli FhlA) domains, which have been shown to affect oligomerisation, and affinity both for substrates as well as the structurally unrelated inhibitors vardenafil and tadalafil (Weeks et al., 2007). The structure of the four isoforms is shown in figure 8.1.

Figure 8.1: PDE11A1-4. Diagram shows the PDE11A isoforms. S = Serine, Black bar = catalytic domain, light blue bar = GAF-A domain, white bar = GAF-B domain, angled dashed bar = unique sequence. Modified from (Weeks et al., 2007).

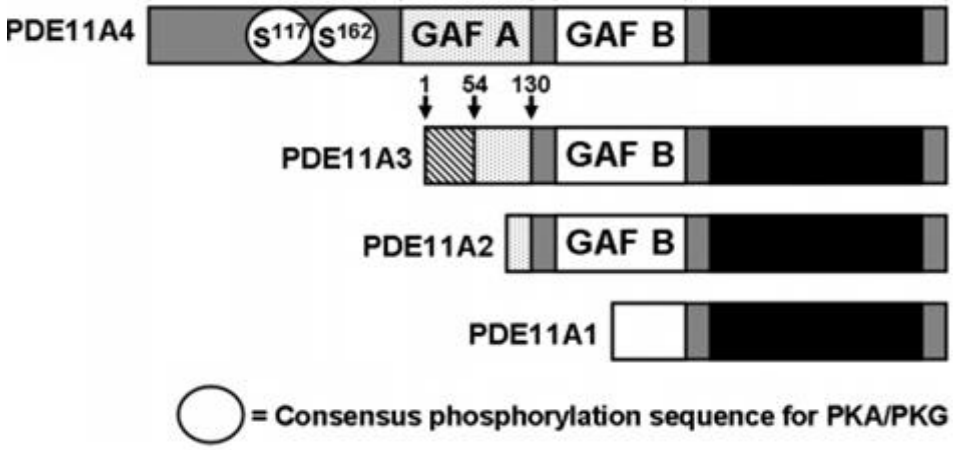

8.3 Alignment of *Dm*PDE11-B and -C protein against *Hs*PDE11A protein

Previous published work assigned *D. Melanogaster* PDE11 as a homologue of *H. sapiens* PDE11A3 or A4 (Day et al., 2005), due to high sequence similarity at the amino acid level, the dual-specificity PDE activity of the enzymes, and the twin GAF domains of these isoforms (figure 8.2).

Figure 8.2: *Dm*PDE11 contains twin GAF domains and a dual-specificity PDEase domain, in common with *Hs*PDE11A.

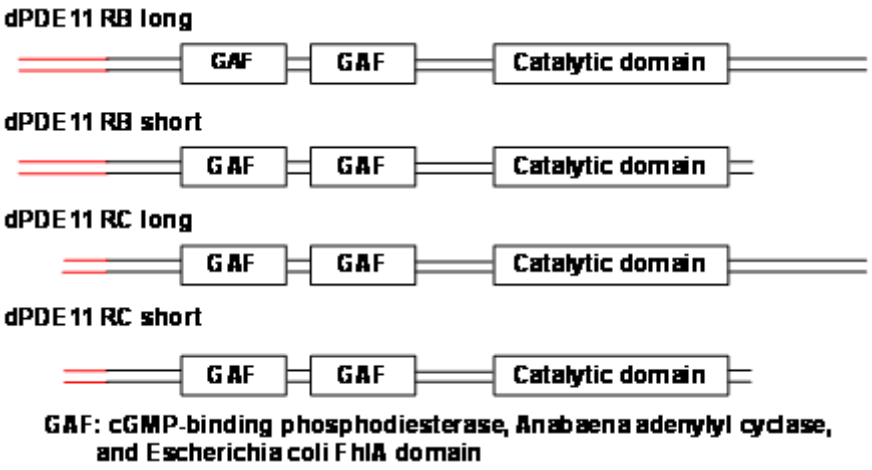

This analysis was performed with the amino acid sequence of *Dm*PDE11RA. This has been replaced on Flybase with two new isoforms, *Dm*PDE11RB and *Dm*PDE11RC; two novel short isoforms were cloned in the course of this study, so that both the *Dm*PDE11RB and *Dm*PDE11RC have long and short isoforms, as detailed in chapter 4. As such, further homology analysis was performed. Following alignment of protein sequence, (materials and methods 1.12), percentage identity/similarity was calculated following alignment of each of the *Dm*PDE11 isoforms with the *Hs*PDE11A gene family using ClustalW alignment (table 8.1).

Table 8.1: *Hs*PDE11A1-4 similarity/identity with *Dm*PDE11. Percentage similarities and identities of amino acid sequences between *Dm*PDE11 and each *Hs*PDE11A isoform were calculated using ClustalW alignment.

Dm PDE11RBl vs	Identity (%)	Similarity (%)
Hs PDE11A1 (004)	15.8	22
Hs PDE11A2 (003)	17.8	25.8
Hs PDE11A3 (002)	20.5	29.7
Hs PDE11A4 (001)	22.7	33.6
Dm PDE11RBs vs	Identity (%)	Similarity (%)
Hs PDE11A1 (004)	19.7	27.5
Hs PDE11A2 (003)	22.2	32.2
Hs PDE11A3 (002)	25.6	37.1
Hs PDE11A4 (001)	28.3	42
Dm PDE11RCl vs	Identity (%)	Similarity (%)
Hs PDE11A1 (004)	16.3	22.7
Hs PDE11A2 (003)	18.4	26.6
Hs PDE11A3 (002)	21.1	30.6
Hs PDE11A4 (001)	23.4	34.7
Dm PDE11RCs vs	Identity (%)	Similarity (%)
Hs PDE11A1 (004)	20.5	28.6
Hs PDE11A2 (003)	32.1	33.4
Hs PDE11A3 (002)	26.6	38.5
Hs PDE11A4 (001)	29.4	43.6

For each *Drosophila* PDE11 isoform, the order of highest – to – lowest sequence similarity and identity with the *Hs*PDE11A 1-4 isoforms, is *Hs*PDE11A4, *Hs*PDE11A3, *Hs*PDE11A2, *Hs*PDE11A1. Interestingly, it is apparent that between the four *Drosophila* PDE11 isoforms, the short isoforms of B and C have higher sequence similarity and identity to each *Hs*PDE11A isoform compared to their respective long isoforms, and that the long and short C isoforms have higher sequence similarity and identity to each

*Hs*PDE11A isoform, when compared to their respective B isoforms,. That the short C terminus isoforms are of higher homology than those with a long C terminus is not surprising, as the human isoforms do not have an extended C terminus. This may suggest that the C terminus evolved later, to perform some unknown function; as shown in chapter 4, it does not affect protein localisation.

The above analysis scores positively for identical or similar amino acids following sequence alignment. However, it does not negatively score for gaps, or highly dissimilar amino acids. Sequences were aligned with using a gonnet series matrix, and a best tree Phylogram was generated using neighbour-joining tree building and uncorrected "p" distance calculation. As a control, bootstrap analysis (1000 repetitions) was performed (materials and methods 1.12). Distance between nodes is presented in phylogenetic units, where a value of 0.1 corresponds to a difference of approximately 10% between two sequences. The data is presented in figure 8.3.

Figure 8.3: Phylogenetic analysis comparing *Dm*PDE11 with *Hs*PDE11A 1-4. Sequences were aligned using a gonnet series matrix, and a Phylogram was generated. Distances between nodes shown in phylogenetic units. Bootstrap analysis (1000 repetitions) was performed; numbers at branches refer to the % occurrence of the branch. Table shows distance between nodes in phylogenetic units. B long (A), B short (B), C long (C), C short (D). d = *D. melanogaster*, h = *H. sapiens*.

A

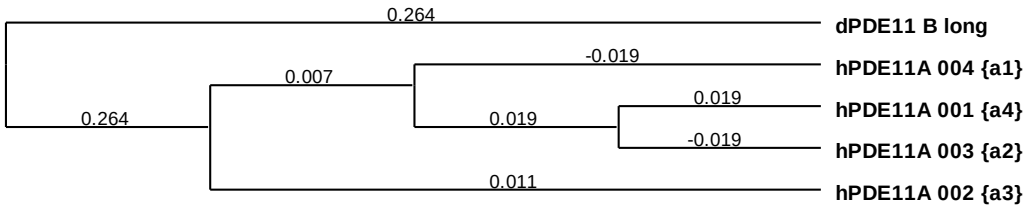

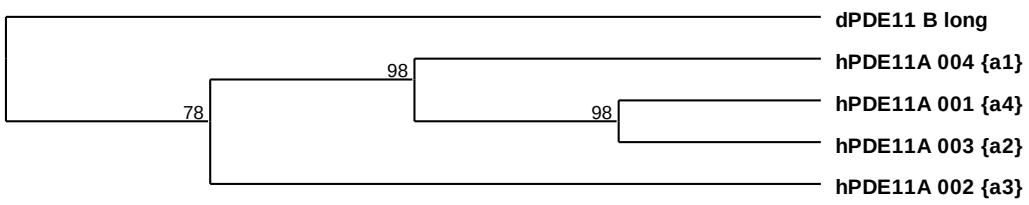

	hPDE11A001 {a4}	hPDE11A 002 {a3}	hPDE11A 003 {a2}	hPDE11A 004 {a1}
Dm PDE11 B long	0.5785	0.5385	0.5325	0.5134

B

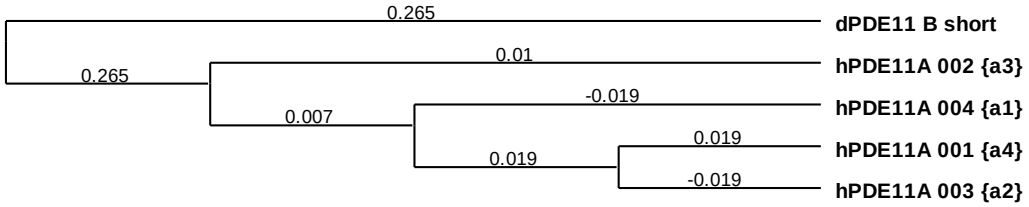

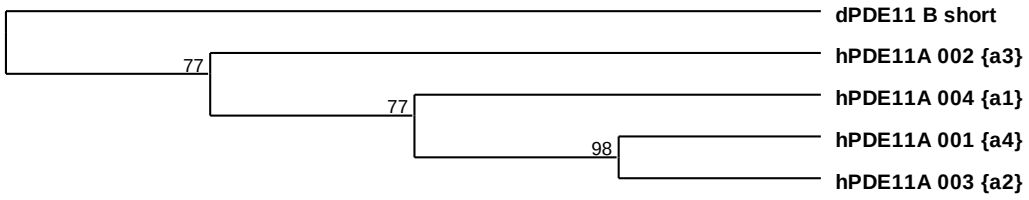

	hPDE11A001 {a4}	hPDE11A 002 {a3}	hPDE11A 003 {a2}	hPDE11A 004 {a1}
Dm PDE11 B short	0.5796	0.5399	0.5343	0.5155

C

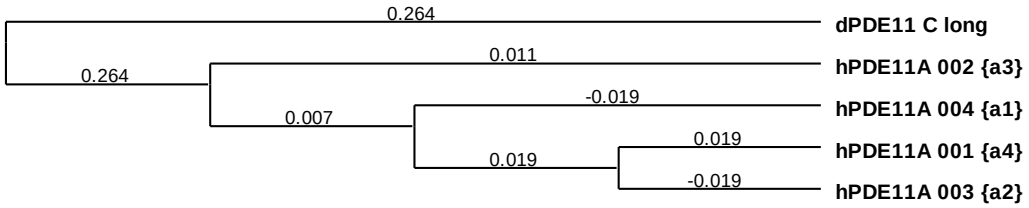

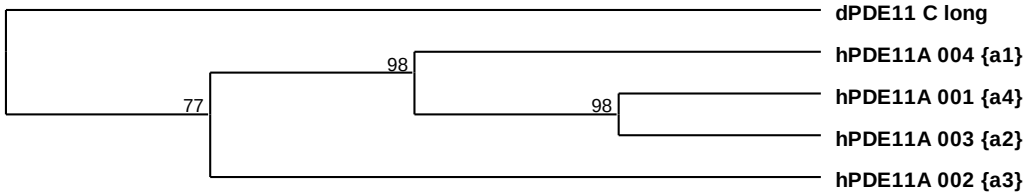

	hPDE11A 004 {a1}	hPDE11A 003 {a2}	hPDE11A 002 {a3}	hPDE11A 001 {a4}
Dm PDE11 C long	0.5785	0.5385	0.5325	0.5134

D

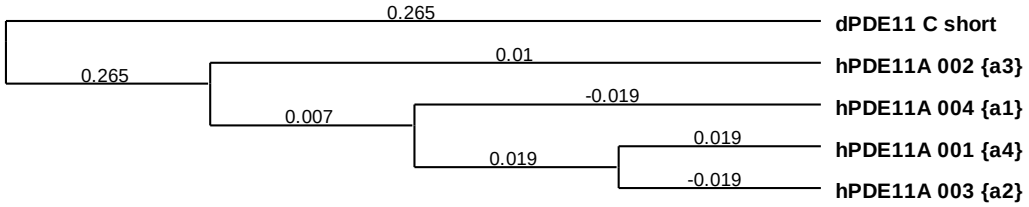

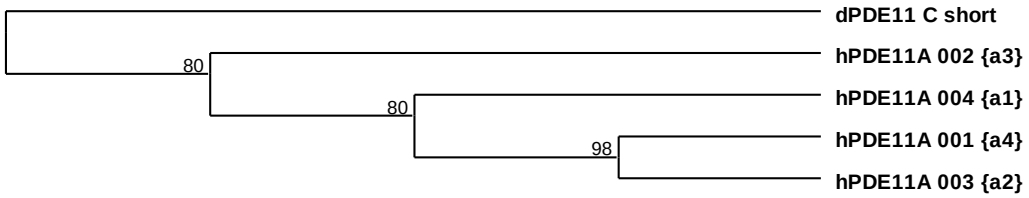

	hPDE11A001 {a4}	hPDE11A 002 {a3}	hPDE11A 003 {a2}	hPDE11A 004 {a1}
Dm PDE11 C short	0.5796	0.5399	0.5343	0.5155

In contrast to the above results, a ClustalW algorithm-generated phylogenetic tree shows that each *Drosophila* PDE11 isoform aligns in order of closest to furthest to *Hs*PDE11-A1, -A2, -A3, then -A4. For each *Dm*PDE11 isoform, *Hs*PDE11-A1 was assigned as the closest orthologue, scoring ~0.02 phylogenetic units (~2%) less than -A2. *Hs*PDE11-A2 and -A3 were typically separated by less than 0.05 phylogenetic units (~0.5%). Intriguingly, *Hs*PDE11A4, which scored highest for sequence similarity/identity with *Dm*PDE11, was designated the most distant of orthologues, 0.04 phylogenetic units (~4% distal). However, when bootstrap analysis is considered, it is notable that at the branchpoints separating *Hs*PDE11A3 from *Hs*PDE11-A1, -A2, and –A4, occur in ≤ 80% of the bootstrap replicates of each phylogenetic tree. Likewise, for the small isoforms of *Dm*PDE11 B and C, the branchpoint separating hPDE11-A2 and –A4 occurred in ≤80% of the bootstrap replicates of each phylogenetic tree. What is consistent is the occurrence of the branchpoint between *Hs*PDE11-A4 and -A2, at 98% for each phylogenetic tree, suggesting that the higher phylogenetic distance allocated to *Hs*PDE11A4 is perhaps the one significant finding of this analysis. Thus, as with the Day 2006 analysis of *Dm*PDE11A, *Dm*PDE11 B long, B short, C long, and C short isoforms were designated as *Hs*PDE11A3 orthologues. That *Hs*PDE11A4 shows the highest sequence similarity/identity with the *Dm*PDE11 isoforms, yet shows the highest phylogenetic distance from each of the *Dm*PDE11 isoforms when considering phylogenetic analysis, suggests that the N terminus of this protein may be of recent evolutionary origin. These are two Ser residues (S117 and S162) N terminal of the GAF-A and GAF-B domains of *Hs*PDE11A4 which have been shown to be phosphorylated by PKA and cGK, which reduce the EC_{50} for cGMP ~3 fold when phosphorylated (Gross-Langenhoff et al., 2008). Analysis of *Dm*PDE11 B and C for putative phosphorylation sites N terminal of the GAF domains returns three Ser residues that return a high score for either PKA or cGK phosphorylation, although only S268 (B isoform)/S224 (C isoform) is predicted as a putative phosphorylation site (threshold < 0.5 using the NetPhosK phosphorylation prediction tool (Blom et al., 2004)) for both cGK and PKA (figure 8.4).

Figure 8.4: Prediction of phosphorylation by PKA and cGK on residues N-terminal of the GAF domains of *Dm*PDE11. Sequences were analysed for putative PKA/cGK phosphorylation sites using the NetPhosK phosphorylation prediction tool (Blom et al., 2004).

S-258 (B isoform)/ S-214 (C isoform)	PKA	0.74 (TSSSRGGSGATTPUR)
S-268 (B isoform)/ S-224 (C isoform)	PKA	0.67 (TTPVRKISAHEFFRG)
S-268 (B isoform)/ S-224 (C isoform)	cGK	0.77 (TTPVRKISAHEFFRG)
S-306 (B isoform)/ S-262 (C isoform)	PKA	0.70 (NGSVGGSCSNLQNV)

Following this analysis, constructs to express *Hs*PDE11A3, with and without a YFP tag, were generated for expression in flies and S2 cells.

8.3.1 Generation of constructs

pP{UAST} and pP{YFP UAST} constructs for the expression of *Hs*PDE11A3 were generated for expression in flies and S2 cells, using a pcDNA3.1 *Hs*PDE11A3 plasmid as template, generously provided by Prof. Miles Houslay. Primers were designed to amplify the *Hs*PDE11A3 ORF with unique restriction sites at the 5' and 3' ends. Reverse primers with and without a stop codon were designed, to facilitate in-frame fusion to a YFP tag. The ORF was amplified with *Pfu* DNA polymerase, TOPO cloned into a TOPO vector to generate pMT/V5 TOPO *Hs*PDE11A3 (stop) and pMT/V5 TOPO *Hs*PDE11A3 (no stop), and sequenced for fidelity (data not shown). The ORF was digested from the TOPO vector, gel purified, and directionally ligated into digested pP{UAST} and pP{YFP UAST}.

8.3.2 Western blot to confirm expression of transgene

To confirm that *Hs*PDE11A3 will express in *Drosophila*, S2 cells were transiently transfected with pMT/V5 TOPO-*Hs*PDE11A3 (no stop), and the lysate subjected to western analysis (figure 8.5).

Figure 8.5: Western analysis of S2 cell lysate transiently transfected with (1) no plasmid control (2) pMT/V5 TOPO-*Hs*PDE11A3 (no stop). Equal amounts of protein (20 μg) were separated on a 10% SDS acrylamide gel, blotted and probed with anti-V5 mouse monoclonal primary antibody at 1:2000, anti-mouse HRP-conjugated secondary at 1:5000. Band sizes were calculated by comparison to Amersham Full-Range Rainbow™ Molecular Weight Markers.

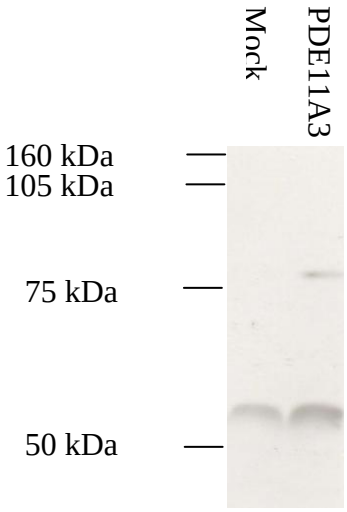

When fused in-frame with a V5 tag, the *Hs*PDE11A3 ORF encodes a protein of 79 KDa. S2 cell lysate produced a single immunoreactive band not present in the negative control, which runs to the expected size. An additional band at ~55 kDa was also present in mock-transfected S2 cell lysate, and so was non specific. As such it was accepted that YFP-*Hs*PDE11A3 is faithfully translated into a stable protein product in S2 cells.

8.3.3 Anti-*Hs*PDE11A polyclonal antibody design

Antibodies were designed against two epitopes, QRQTKTKDRRFNDE and SKGEYDWNIKNHRD, selected on the basis of antigenicity. The epitope sequences were screened for short near-exact matches against the *Drosophila* proteome using the BLASTP tool (http://www.ensembl.org/Multi/blastview), and returned no significant hits. QRQTKTKDRRFNDE is on the boundary between sequence unique to *Hs*PDE11A3, and sequence shared with *Hs*PDE11A4 within GAF-A. In future, were a *Hs*PDE11A3-specific polyclonal antibody required, an antibody-specific peptide QRQTKTKDRR would only purify antibody specific to *Hs*PDE11A3 by epitope purification. SKGEYDWNIKNHRD is

found in *Hs*PDE11A-002, -006, -203, 003, 004, 202, 204, 001. Antibodies were generated by Genososphere Biotech. Antibodies were IgG purified, and the purified IgG fraction was epitope purified (materials and method 1.7).

8.3.4 Antibody testing

Immunocytochemistry was performed on S2 cells transiently co-transfected with YFP-*Hs*PDE11A3 pP[UAST] and DES GAL4 as a GAL4 source, using pre- and post-immune serum at 1:100, 1:500, IgG purified antibody at 1:50, and epitope purified antibody at 1:2, staining with anti-rabbit TEXAS RED secondary antibody at a 1:500 dilution. For both antibodies, none of the YFP fluorescent cells displayed positive texas red staining above background staining, even using serum (data not shown). The antibody was not tested using western analysis.

8.3.5 Immunocytochemistry

8.3.5.1 Expression in S2 cells

*Hs*PDE11A3 protein subcellular localisation was determined in S2 cells. S2 cells were transiently transfected with YFP-*Hs*PDE11A3 pP{UAST}, using DES GAL4 as a GAL4 source. Cells were fixed, and DAPI stained to stain the nucleus (figure 8.6).

Figure 8.6: Localisation of YFP-*Hs*PDE11A3 in S2 cells. S2 cells were transiently transfected with pP{UAST} *Hs*PDE11A3 YFP, using DES GAL4 as a GAL4 source. Cells were fixed and stained with DAPI to visualise nuclei. YFP-*Hs*PDE11A3 (green), DAPI (blue).

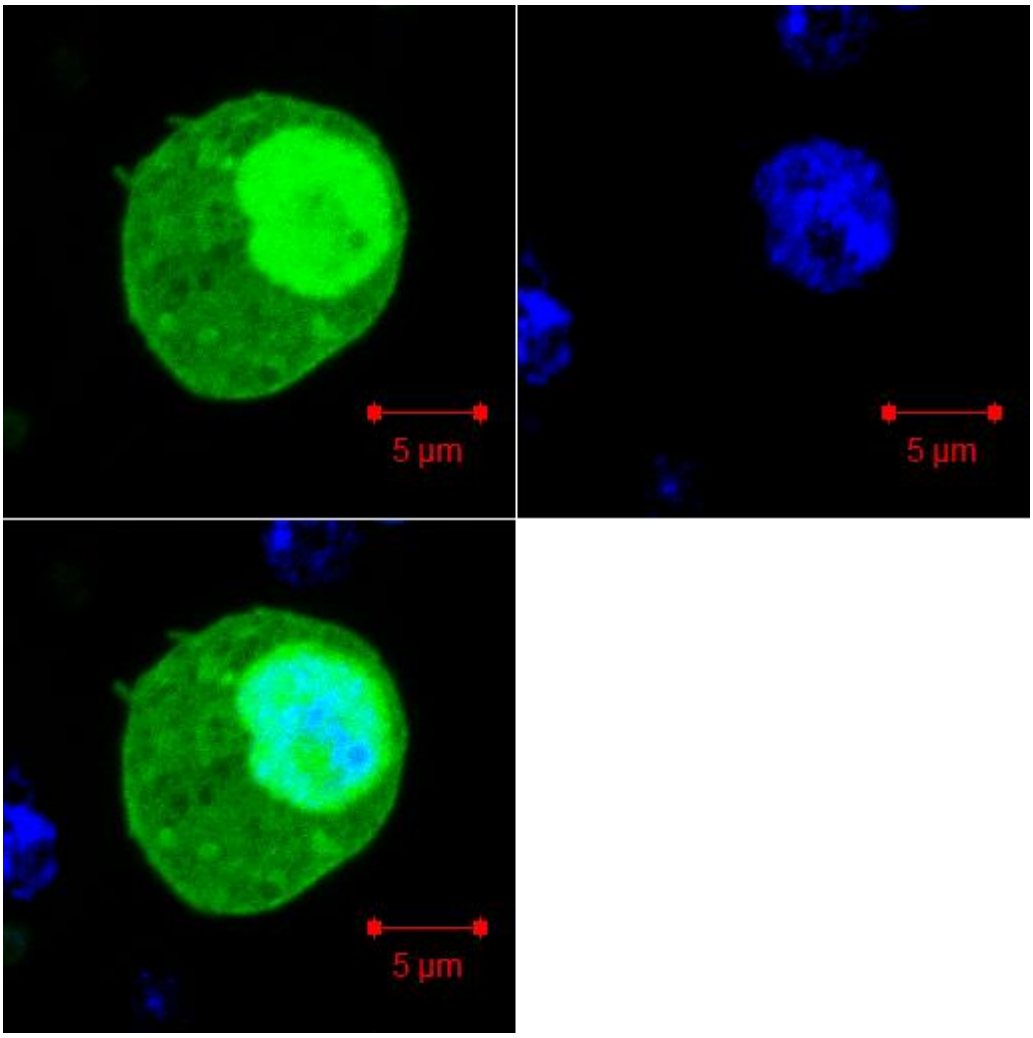

In S2 cells, YFP-*Hs*PDE11A3 is predominantly localised to the nucleus, and also shows cytoplasmic localisation, strongest at the membrane.

8.3.5.2 Localisation in Malpighian tubule

YFP-*Hs*PDE11A3 expression was driven in tubule principal cells by the c42 GAL4 driver line. Tubules were fixed, and YFP-*Hs*PDE11 expression visualised (figure 8.7).

Figure 8.7: Localisation of YFP-*Hs*PDE11A3 in the Malpighian tubule driven with c42 GAL4. UAS YFP-*Hs*PDE11A3 transgenic flies were crossed to c42 GAL4, a principal cell GAL4 driver line. The Malpighian tubules were dissected, fixed, and imaged using confocal microscopy. YFP-*Hs*PDE11A3 (green).

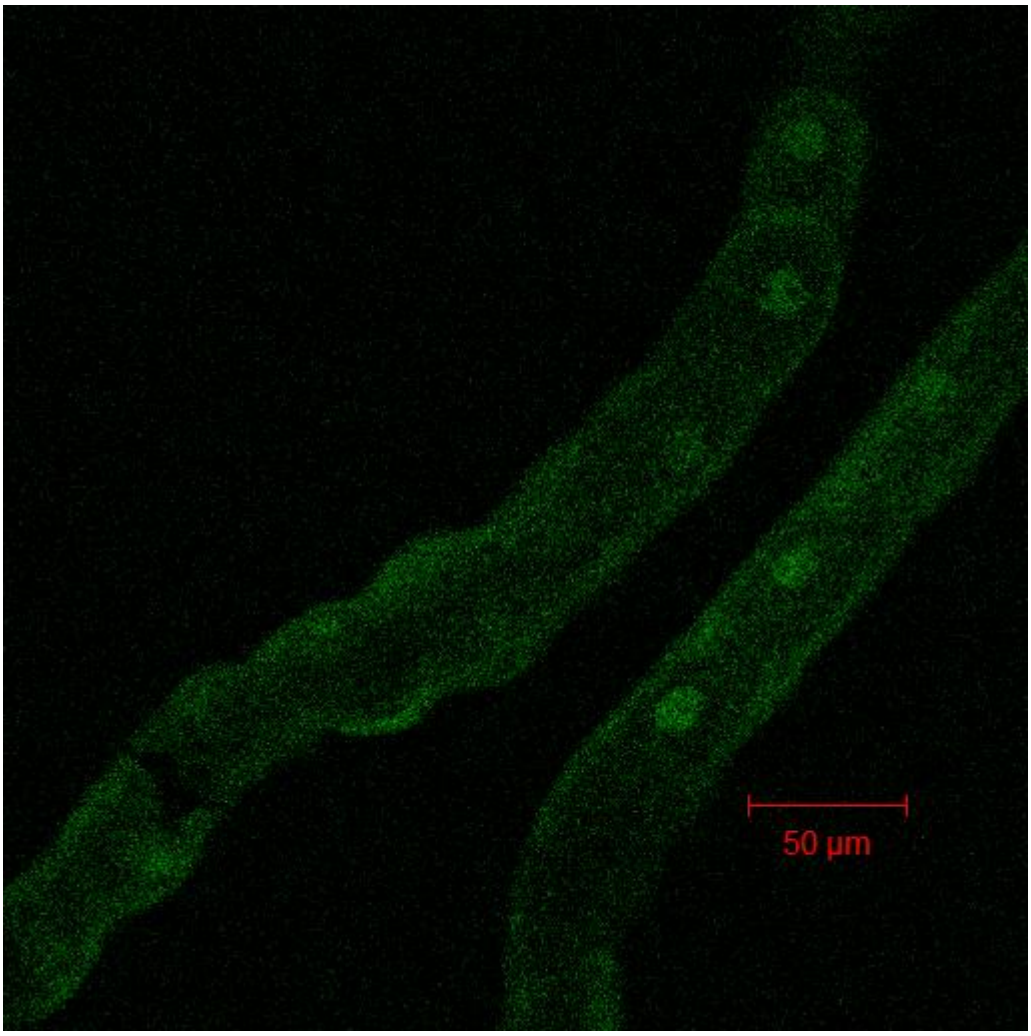

Expression of YFP-*Hs*PDE11A3 in c42 GAL4/YFP-*Hs*PDE11A3 progeny occurred at low levels, hence the high level of background noise in the confocal image. However, although DAPI staining was not employed, expression appears similar to that of S2 cells; predominantly nuclear, with some cytoplasmic (basolateral) expression. To drive expression levels to a higher level, UAS-YFP-*Hs*PDE11A3 flies were crossed to a heat shock GAL4 driver line. Following three thirty minute 37˚C heat shocks, expression levels were much higher, and the localisation of the protein changed (figure 8.8).

Figure 8.8: Localisation of YFP-*Hs*PDE11A3 in the Malpighian tubule driven with heat shock GAL4. UAS YFP-*Hs*PDE11A3 transgenic flies were crossed to heat shock GAL4, a ubiquitous GAL4 driver line. The Malpighian tubules were dissected, fixed, and the nuclei visualised by DAPI staining, and imaged using confocal microscopy. YFP-*Hs*PDE11A3 (green), DAPI (blue).

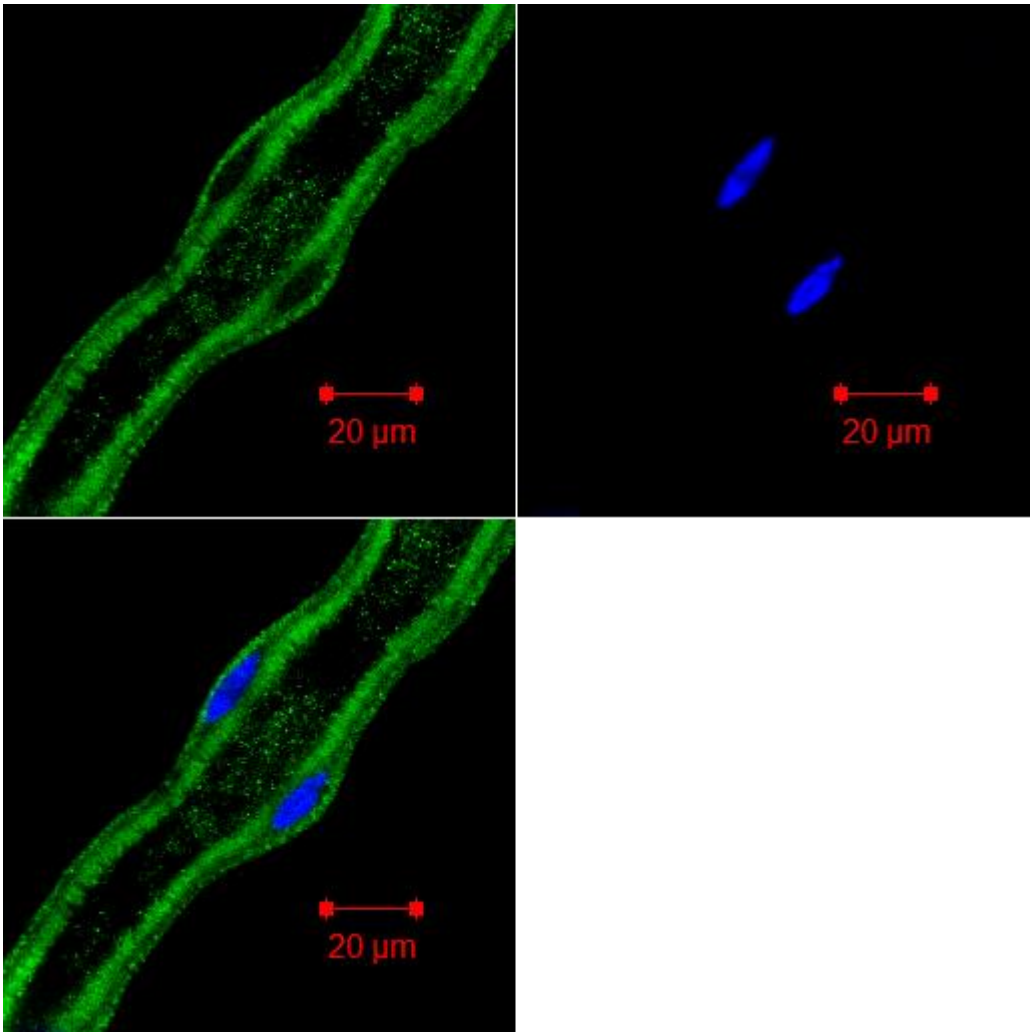

When YFP-*Hs*PDE11A3 expression is driven by heat shock GAL4, there is a dramatic change in protein subcellular localisation. The protein is now excluded from the nucleus, and shows localisation to the basolateral membrane, and the apical microvilli. It appears that localisation is dependent upon protein concentration. Imaging of Malpighian tubules from YFP-*Hs*PDE11A3/*HS*G4 exposed to varying lengths of heat shock would confirm this.

8.3.6 Update of gene model

The gene model for *Hs*PDE11A in the March 2009 release of Ensemble was as described above (http://mar2009.archive.ensembl.org/Homo_sapiens/Gene/Summary?g=ENSG00000128655). The June 2009 release (http://jul2009.archive.ensembl.org/Homo_sapiens/Gene/Summary?g=ENSG00000128655) contained several newly predicted transcripts, from the same gene (table 8.2).

Table 8.2: The newly predicted *Hs*PDE11A isoforms. Only protein coding isoforms shown (adapted from Ensemble).

Name	Transcript ID	Protein ID	Description
PDE11A4 (001)	ENST00000286063	ENSP00000286063	protein coding
PDE11A3 (002)	ENST00000358450	ENSP00000351232	protein coding
PDE11A2 (003)	ENST00000389683	ENSP00000374333	protein coding
PDE11A1 (004)	ENST00000409504	ENSP00000386539	protein coding
PDE11A-006	ENST00000433879	ENSP00000416884	protein coding
PDE11A-007	ENST00000436700	ENSP00000406922	protein coding
PDE11A-201	ENST00000431253	ENSP00000410190	protein coding
PDE11A-202	ENST00000449286	ENSP00000390599	protein coding
PDE11A-203	ENST00000450799	ENSP00000387964	protein coding
PDE11A-204	ENST00000457922	ENSP00000402534	protein coding

Beyond the isoforms listed in table 8.2, a further five transcripts, *Hs*PDE11A005, and *Hs*PDE11A009 – 012, are processed transcripts that are not translated into a protein product. The transcript and protein structure of these newly predicted *Hs*PDE11A isoforms are found in figure 8.9 (Ensemble).

Figure 8.9: Transcript and Protein structure (where translated) of all *Hs*PDE11A isoforms. From Ensemble, (http://www.ensembl.org/Homo_sapiens/Gene/Summary?g=ENSG00000128655). For protein structure, Yellow: low complexity region. Blue: superfamily domain. Green: SMART domain. Red: prints domain. Grey: Pfam domain. Orange: PROSITE patterns. Multiple colours: variations. Scale bar: amino acid position

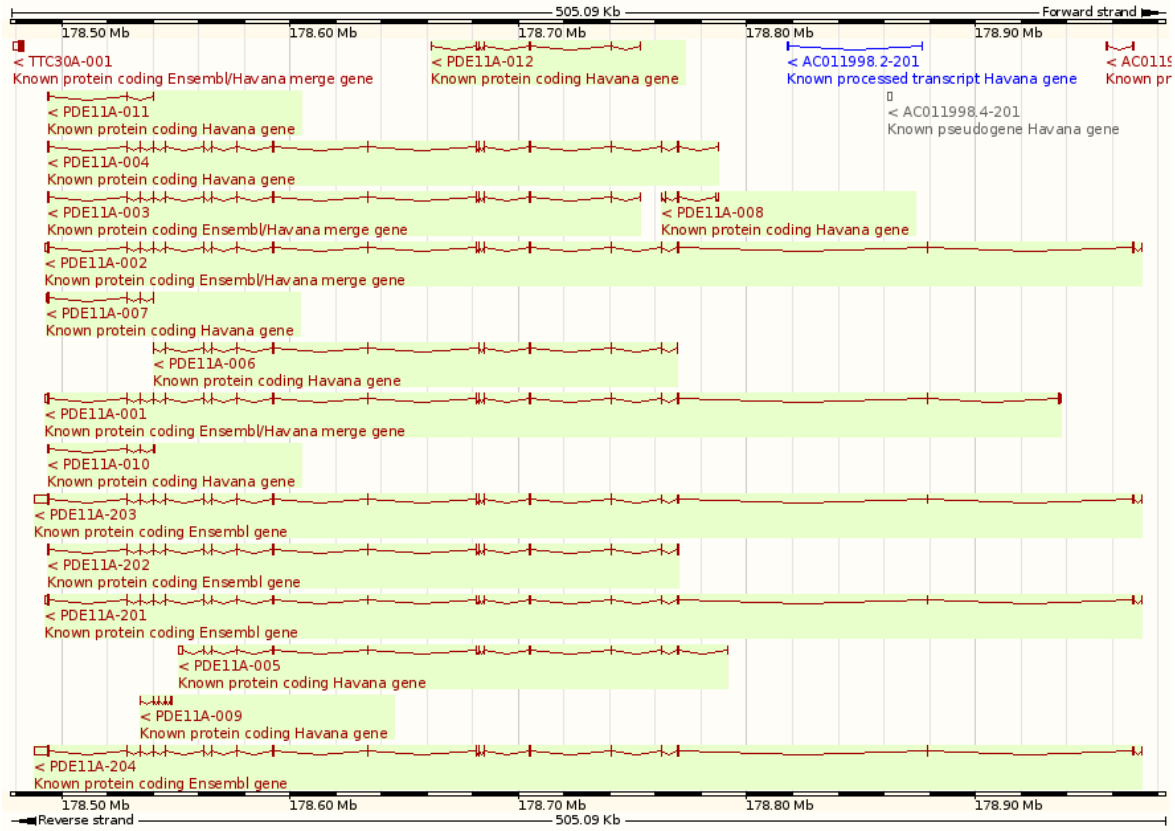

*Hs*PDE11A4 (001)

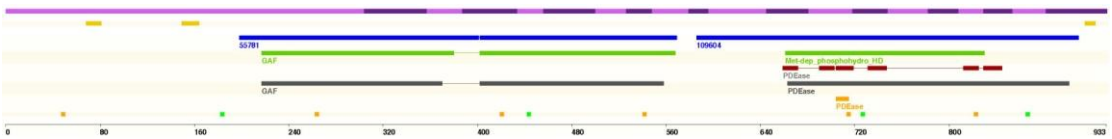

*Hs*PDE11A3 (002)

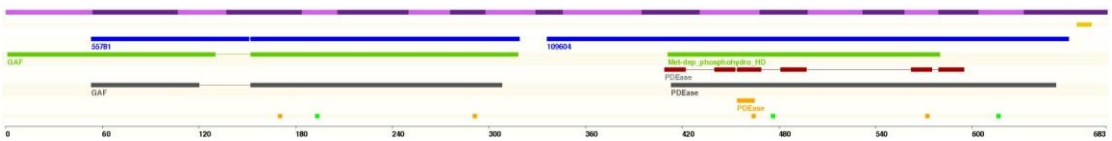

*Hs*PDE11A2 (003)

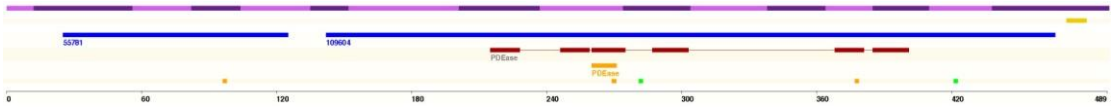

*Hs*PDE11A1 (004)

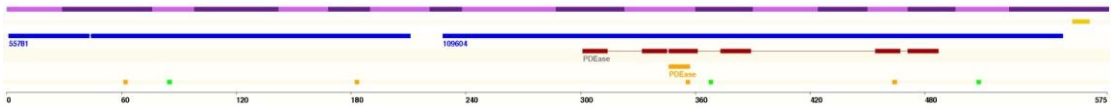

*Hs*PDE11006

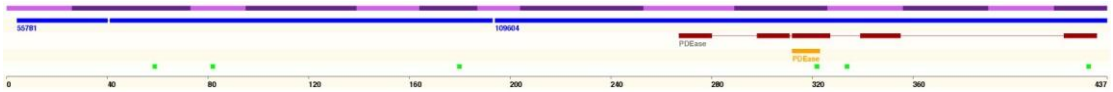

*Hs*PDE11007

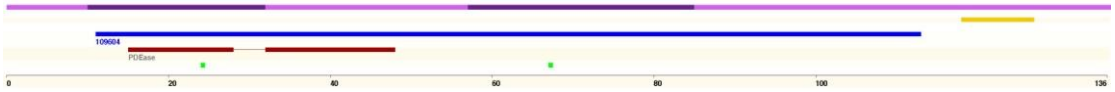

*Hs*PDE11A201

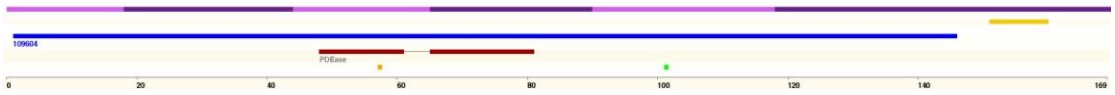

*Hs*PDE11A202

*Hs*PDE11A203

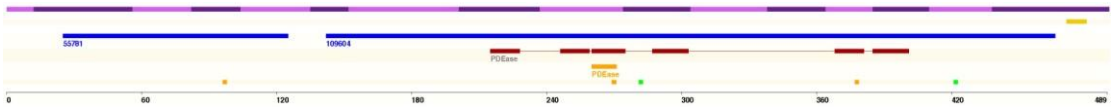

*Hs*PDE11A204

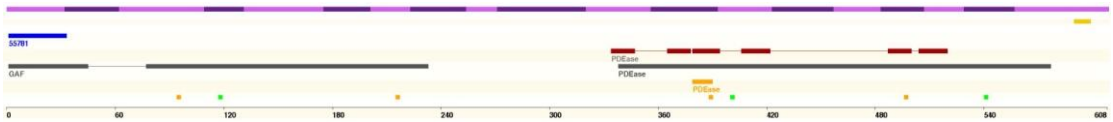

*Hs*PDE11A-006, -007, -201 and -203 are further truncations of the N terminus compared to the original *Hs*PDE11A1-A4 isoforms, truncated beyond the GAF domains to the catalytic domain. Of the newly predicted *Hs*PDE11A isoforms, only *Hs*PDE11A-202 and -204 contain a GAF domain.

In order to determine if any of these new isoforms were of higher sequence homology to *Dm*PDE11, sequence similarity/identity was calculated (tables 8.3 – 8.6). Phylogenetic analysis was performed as above between the two previously closest aligned, *Hs*PDE11A 001 {A4} and *Hs*PDE11A 002 {A3}, and the two newly predicted isoforms 202 and 204, as these contain GAF domains; *Hs*PDE11A 202 contains one GAF domain, and *Hs*PDE11 204 contains one whole and one partial GAF domain (figure 8.10).

Table 8.3: *Dm*PDE11 B long similarity/identity with the *Hs*PDE11A gene family. Percentage similarities and identities of amino acid sequences between *Dm*PDE11 B long and all the *Hs*PDE11A isoforms were calculated using ClustalW alignment.

Dm PDE11RBl vs	Identity (%)	Similarity (%)
hPDE11A1 (004)	15.8	22
hPDE11A2 (003)	17.8	25.8
hPDE11A3 (002)	20.5	29.7
hPDE11A4 (001)	22.7	33.6
hPDE11 006	13.7	19.9
hPDE11 007	1.7	4
hPDE11A 201	4.8	7.1
hPDE11A 202	17.8	25.8
hPDE11A 203	15.8	22.1
hPDE11A 204	19	27.4

Figure 8.10: Phylogenetic analysis comparing *Dm*PDE11 B long with *Hs*PDE11A-001 (A4), -002 (A3), -202, -204. Sequences were aligned using a gonnet series matrix, and a Phylogram was generated. Distances between nodes shown in phylogenetic units. Bootstrap analysis (1000 repetitions) was performed; numbers at branches refer to the % occurrence of the branch. Table shows distance between nodes in phylogenetic units.

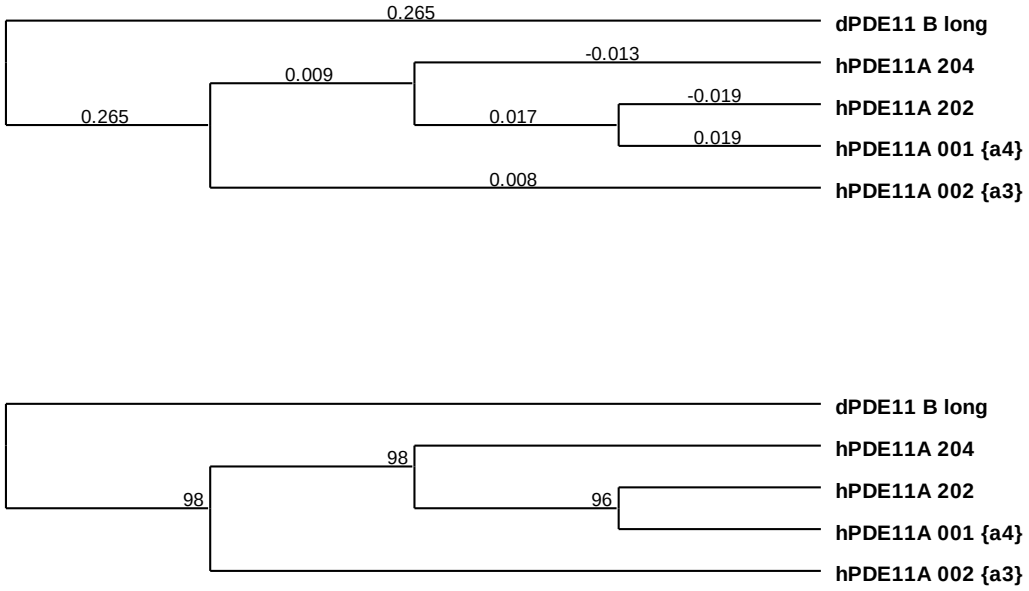

	hPDE11A 001 {A4}	hPDE11A {002 A3}	hPDE11A 202	hPDE11A 204
Dm PDE11 B long	0.5785	0.5385	0.5317	0.5267

Table 8.4: *Dm*PDE11 B short similarity/identity with the *Hs*PDE11A gene family. Percentage similarities and identities of amino acid sequences between *Dm*PDE11 B short and all the *Hs*PDE11A isoforms were calculated using ClustalW alignment.

Dm PDE11RBs vs	Identity (%)	Similarity (%)
hPDE11A1 (004)	19.7	27.5
hPDE11A2 (003)	22.2	32.2
hPDE11A3 (002)	25.6	37.1
hPDE11A4 (001)	28.3	42
hPDE11 006	17.1	24.9
hPDE11 007	2.1	5
hPDE11A 201	6	8.9
hPDE11A 202	22.2	32.2
hPDE11A 203	19.7	27.6
hPDE11A 204	23.7	34.2

Figure 8.11: Phylogenetic analysis comparing *Dm*PDE11 B short with *Hs*PDE11A-001 (A4), -002 (A3), -202, -204. Sequences were aligned using a gonnet series matrix, and a Phylogram was generated. Distances between nodes shown in phylogenetic units. Bootstrap analysis (1000 repetitions) was performed; numbers at branches refer to the % occurrence of the branch. Table shows distance between nodes in phylogenetic units.

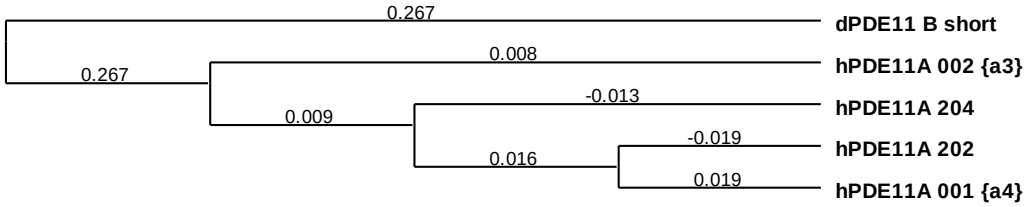

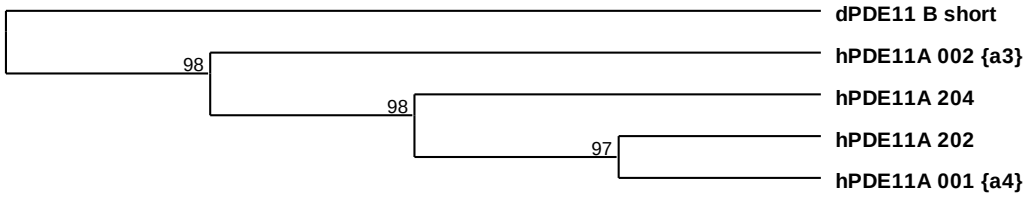

	hPDE11A 001 {A4}	hPDE11A 002 {A3}	hPDE11A 202	hPDE11A 204
Dm PDE11 B short	0.5818	0.5429	0.537	0.5317

Table 8.5: *Dm*PDE11 C long similarity/identity with the *Hs*PDE11A gene family. Percentage similarities and identities of amino acid sequences of *Dm*PDE11 C long and all the *Hs*PDE11A isoforms were calculated using ClustalW alignment.

Dm PDE11RCl vs	Identity (%)	Similarity (%)
hPDE11A1 (004)	16.3	22.7
hPDE11A2 (003)	18.4	26.6
hPDE11A3 (002)	21.1	30.6
hPDE11A4 (001)	23.4	34.7
hPDE11 006	14.1	20.6
hPDE11 007	1.8	4.1
hPDE11A 201	5	7.3
hPDE11A 202	18.4	26.6
hPDE11A 203	16.3	22.8
hPDE11A 204	19.6	28.2

Figure 8.12: Phylogenetic analysis comparing *Dm*PDE11 C long with *Hs*PDE11A-001 (A4), -002 (A3), -202, -204. Sequences were aligned using a gonnet series matrix, and a Phylogram was generated. Distances between nodes shown in phylogenetic units. Bootstrap analysis (1000 repetitions) was performed; numbers at branches refer to the % occurrence of the branch. Table shows distance between nodes in phylogenetic units.

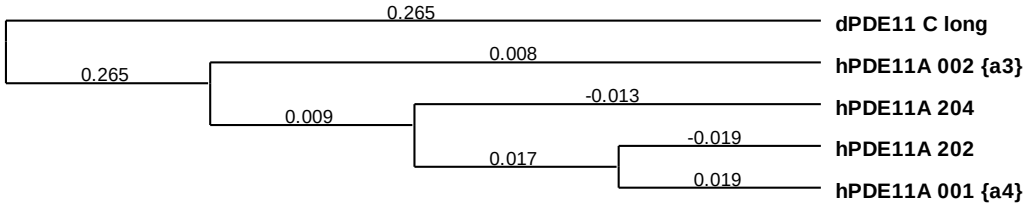

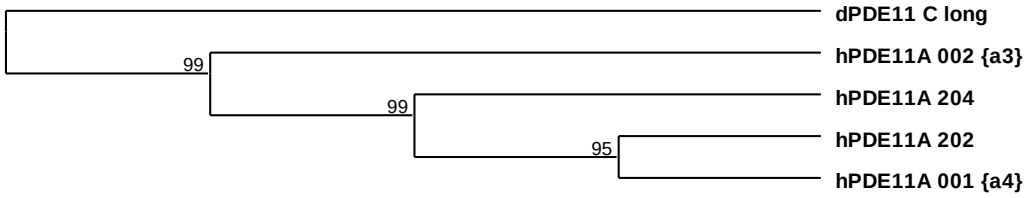

	hPDE11A 001 {A4}	hPDE11A 002 {A3}	hPDE11A 202	hPDE11A 204
Dm PDE11 C long	0.5785	0.5385	0.5317	0.5267

Table 8.6: *Dm*PDE11 C short similarity/identity with the *Hs*PDE11A gene family. Percentage similarities and identities of amino acid sequences between *Dm*PDE11 C short, and all the *Hs*PDE11A isoforms were calculated using ClustalW alignment.

Dm PDE11RCs vs	Identity (%)	Similarity (%)
hPDE11A1 (004)	20.5	28.6
hPDE11A2 (003)	32.1	33.4
hPDE11A3 (002)	26.6	38.5
hPDE11A4 (001)	29.4	43.6
hPDE11 006	17.8	25.9
hPDE11 007	2.2	5.2
hPDE11A 201	6.3	9.2
hPDE11A 202	23.1	33.5
hPDE11A 203	20.5	28.7
hPDE11A 204	24.6	35.5

Figure 8.13: Phylogenetic analysis comparing *Dm*PDE11 C short with *Hs*PDE11A-001 (A4), -002 (A3), -202, -204. Sequences were aligned using a gonnet series matrix, and a Phylogram was generated. Distances between nodes shown in phylogenetic units. Bootstrap analysis (1000 repetitions) was performed; numbers at branches refer to the % occurrence of the branch. Table shows distance between nodes in phylogenetic units.

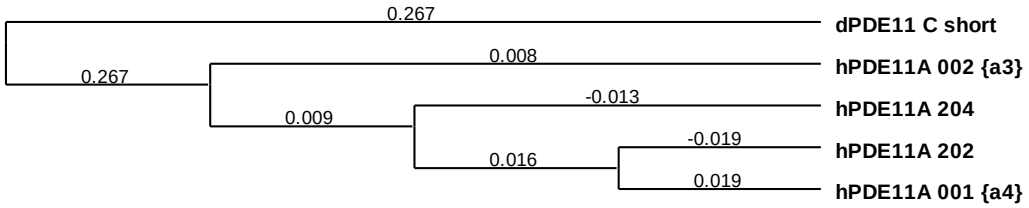

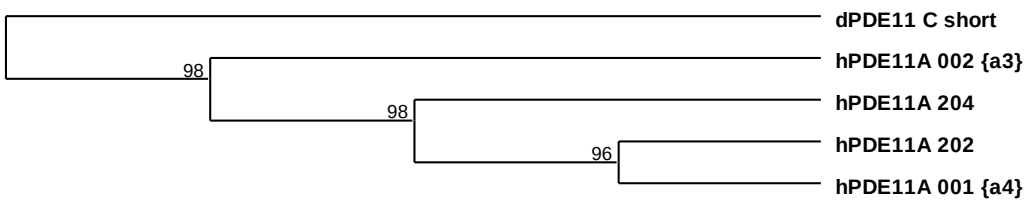

	hPDE11A 001 {A4}	hPDE11A 002 {A3}	hPDE11A 202	hPDE11A 204
Dm PDE11 C short	0.5818	0.5429	0.537	0.5317

When sequence similarity/identity is considered, *Hs*PDE11A3 has the highest homology to each *Dm*PDE11 isoform compared to *Hs*PDE11A4, *Hs*PDE11202, and *Hs*PDE11204. Phylogenetic analysis was again employed. However, bootstrap analysis this time returned no lower than 95% at any branch of the phylogenetic tree, suggesting that this data is of greater significance. Figures 8.10 – 8.13 suggests that amino acid sequence specific to *Hs*PDE11A4 is of furthest phylogenetic distance from the *Dm*PDE11 isoforms, although this branchpoint is of the lowest % score when considering bootstrap analysis. *Hs*PDE11A3 is of around 0.01 phylogenetic units more distal than 202 and 204 to the *Dm*PDE11 isoforms in each phylogenetic tree, which equates to around 1% lower homology. The bootstrap analysis assigns 98% or 99% to the branchpoint separating *Hs*PDE11A3 from the other isoforms, and so a difference in phylogenetic units of ~0.01 may not be significant. *Hs*PDE11A204 is virtually identical to *Hs*PDE11A3, except for the unique N terminus of *Hs*PDE11A3, two adjacent, changed amino acids, and a single amino acid deletion. As such, the unique N terminus of *Hs*PDE11A3 should be used to determine which is closer. The unique N terminus of *Hs*PDE11A3 was aligned with *Dm*PDE11 B long using ClustalW analysis (figure 8.14).

Figure 8.14: The unique N-terminus of *Hs*PDE11A002 (A3) aligns with *Dm*PDE11 B long from amino acid ~435 of *Dm*PDE11 B long to amino acid ~530.

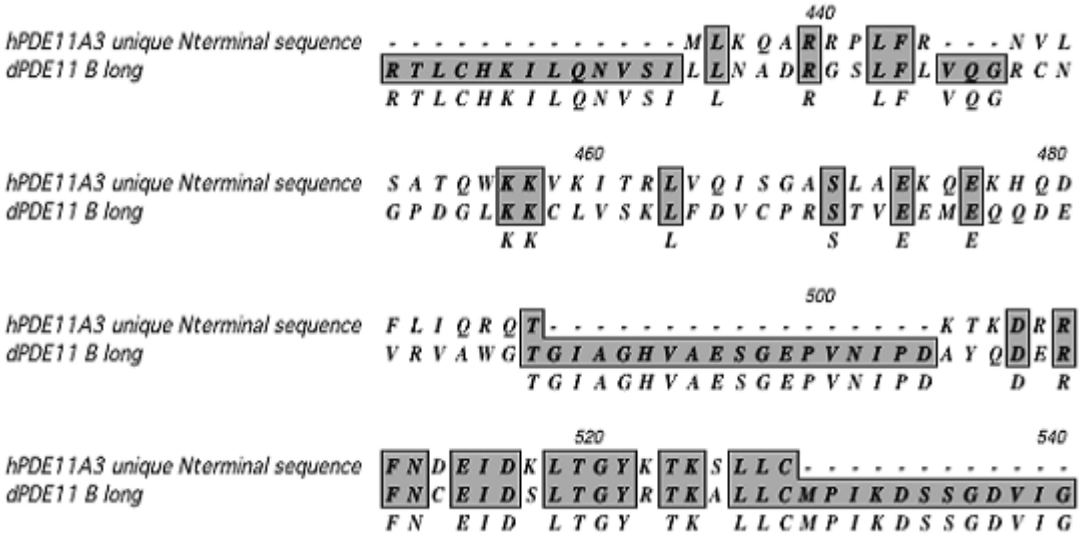

The unique sequence of the N terminus of *Hs*PDE11A3 was found to align between amino acids 435 – 530, sequence common to both the B and C *Dm*PDE11 isoforms. Alignment of *Hs*PDE11A 204 with *Dm*PDE11 B long revealed an alignment from amino acid 530 onwards (figure 8.15).

Figure 8.15: *Hs*PDE11A 204 aligns with *Dm*PDE11 B long from amino acid 530 of B long onwards. First ~400 amino acids of ClustalW alignment shown.

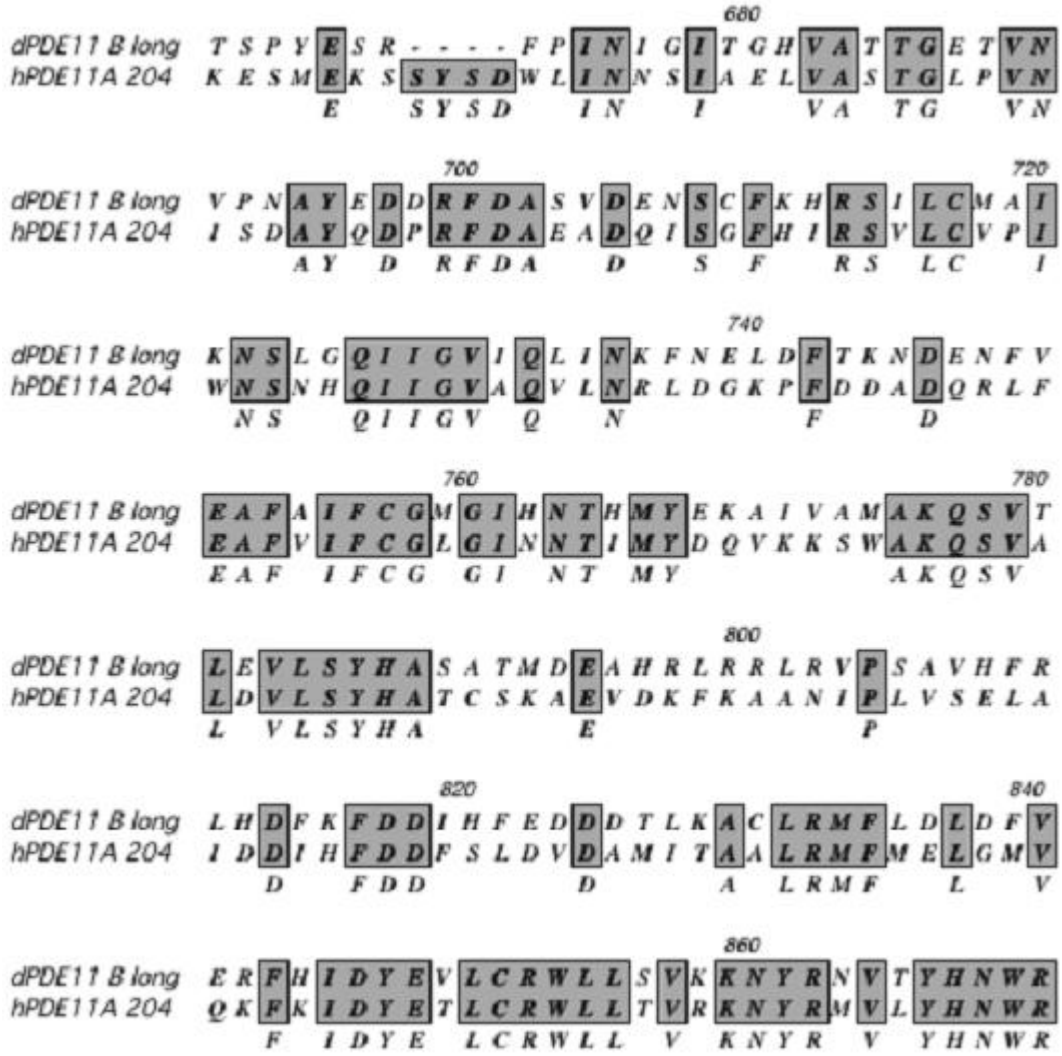

Multiple methods of sequence analysis designate amino acids 420 to 750 (using B long as a reference) of *Dm*PDE11 as encoding twin GAF domains (figure 8.16).

Figure 8.16: *Dm*PDE11 (B long shown) has twin GAF domains between amino acids 420 to 750. From Ensemble.

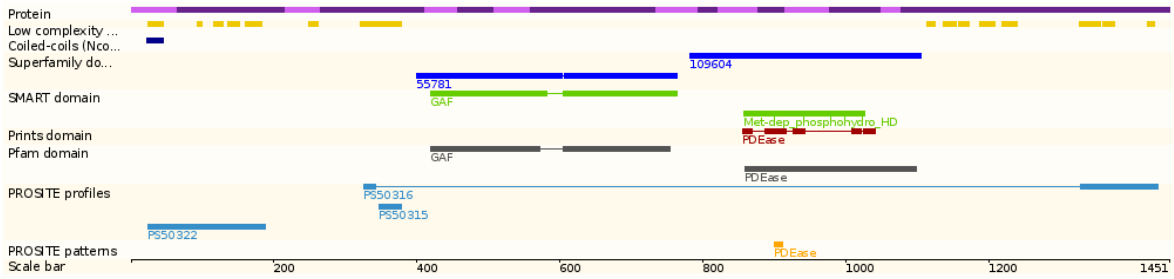

As the unique N terminus of *Hs*PDE11A3 aligns within this region, and furthermore aligns to sequence just adjacent to the region of GAF-A that *Hs*PDE11204 aligns to, it would appear that this sequence constitutes novel GAF-A sequence, and thus forms a novel GAF-A. As such, it was considered that the designation of *Hs*PDE11A3 as the closest *Dm*PDE11 homologue/orthologue remains valid.

8.4 Conclusions and future work

Using *Drosophila melanogaster* to study the *in vivo* function of vertebrate PDEs has been shown to be worthwhile in previous studies. The vertebrate PDE11A family has been characterised biochemically, but the physiological role it plays it not well understood, with the only role so far assigned is a role in spermatogenesis. *Drosophila* PDE11 was first described in 2005, which also has four splice variants. The four isoforms of *Dm*PDE11 were aligned with the *Hs*PDE11A isoforms, and compared in terms of sequence identity and homology, and were subjected to phylogenetic analysis. These results, when considered alongside the strong homology between the unique N terminus of *Hs*PDE11A3 and GAF-A of *Dm*PDE11, suggest that *Hs*PDE11A3 is the closest orthologue to *Dm*PDE11 of the *Hs*PDE11A isoforms.

*Hs*PDE11A3 pP[UAST] and *Hs*PDE11A3pP [YFP UAST] constructs were generated, and the transgene expressed in S2 cells and fly. The protein showed predominantly nuclear localisation when expressed in S2 cells, and the principal cells of the Malpighian tubule at low levels of expression, but was localised to the cytosol when the transgene was driven by stronger GAL4 expression. Analysis of *Hs*PDE11A3 using the PREDICTNLS nuclear localisation signal prediction tool shows that the protein does not contain a nuclear localisation signal (Cokol et al., 2000). Therefore, it must be piggybacking its way into the

nucleus with another protein. As for the change in localisation at higher concentration, reasons for this are unknown. Immunohistochemical studies concerning *Hs*PDE11A have tended to focus on the distribution among tissues (D'Andrea et al., 2005; Loughney et al., 2005); one study looked at the subcellular localisation of *Hs*PDE11A, which was shown to localise to the cytosol of nerve cell bodies of the trigeminal ganglion (Kruse et al., 2009). The nuclear localisation of two PDEs has been investigated; PDE1A localises to the nucleus in neointimal synthetic vascular smooth muscle cells, but localises to the cytoplasm in contractile vascular smooth muscle cells. The basis for this change in localisation is not currently understood (Nagel et al., 2006). Certain PDE9A isoforms localise to the nucleus, but this is due to a nuclear localisation signal (Wang et al., 2003). Thus, the mechanism of translocation of *Hs*PDE11A3 to the nucleus is unknown, but appears to be dependent of the concentration of protein.

Transgenic expression in *Drosophila* of *Hs*PDE11A3 gives a protein of the predicted size, which shows a distinct subcellular localisation. Time did not permit to perform PDE assays, and so it is unknown whether the PDE is active in *Drosophila*. PDE11 -/- mice display reduced sperm concentration, rate of forward progression, and percentage of live spermatozoa (Wayman et al., 2005), and inhibition of *Hs*PDE11A has also been shown to negatively impact spermatozoa quality (Pomara and Morelli, 2005), as *Hs*PDE11A regulates spermatozoa physiology (Seftel, 2005). *Dm*PDE11 -/- null mutant males are infertile, as detailed in chapter 4, and so function may be conserved. Spermatogenesis in *Drosophila* is highly analogous to mammalian spermatogenesis (White-Cooper, 2009), and so *Drosophila* could be used to delineate the role of *Hs*PDE11A in spermatogenesis.

Chapter 9

Summary and further work

9.1 Summary

Initial attempts to characterise *Dm*PDE11 focused on two resources; the *Dm*PDE11RA ORF, and UAS-PDE11 RNAi flies. While work performed on the ORF of *Dm*PDE11RA ultimately proved to be void, due to the replacement of the gene model with two newly predicted ORFs, B and C, which encoded two novel polypeptides, work performed on the RNAi line is fortunately still valid, due to the targeted sequence being conserved in the B and C isoforms. The role of *Dm*PDE11 in the Ca^{2+} response to capa-1 was investigated, as Ca^{2+} and cGMP crosstalk occurs in non-excitable cells (Bruce et al., 2003). No difference in the cytoplasmic calcium response was seen in tubules with reduced *Dm*PDE11 transcript levels compared to control. Treatment of tubules with cGMP induces fluid transport (Dow et al., 1994), and the possible involvement of *Dm*PDE11 in modulation of this cGMP signal and therefore fluid secretion was investigated by driving *Dm*PDE11 RNAi in the principal cells of the Malpighian tubule and comparing the cG-induced fluid secretion of these to parental control, where no difference was seen.

Flybase release 5.2 predicted that the previously predicted gene model for CG34341 was incorrect. The previously predicted transcript, *Dm*PDE11RA, was replaced by two transcripts, *Dm*PDE11RB and *Dm*PDE11RC. These transcripts were shown to be transcribed *in vivo* by a combination of RT-PCR from cDNA from several tissue sources, and by the analysis of EST databases not used in the Flybase analysis. In the course of this analysis, a novel exon/exon boundary was identified within exon 17, where the novel exon 18 encodes 4 amino acids, followed by a stop codon. This results in a truncated polypeptide. RT-PCR analysis demonstrated that both *Dm*PDE11RB and RC were transcribed with both full length and a truncated isoforms. The generation of transgenic flies expressing these isoforms tagged with YFP allowed the verification of these isoforms as *bona fide* dual specificity PDEs. Importantly, the RNAi lines generated against *Dm*PDE11RA targeted a region unchanged in the new isoforms, and so work done with these lines remained valid.

Analysis of the subcellular localisation of these isoforms showed that *Dm*PDE11B and C display markedly different subcellular localisation, and that the long and short isoforms of these do not show distinct subcellular localisation. *Dm*PDE11B localises predominantly to the apical and basolateral membranes of the Malpighian tubule, and *Dm*PDE11C localises to an unknown organelle or vesicles.

As *Dm*PDE11B and C only differ in the sequence of the first exon, this must encode protein sequence that influences the subcellular localisation of the protein. Indeed, analysis of the protein sequence of *Dm*PDE11B with the coiled coil prediction software COILS (Lupas et al., 1991) predicts a coiled coil in the unique N terminus. Coiled coils facilitate the formation of homo- and heteromeric protein-protein interactions (Strauss and Keller, 2008), and thus protein complexes (Langosch and Heringa, 1998). The subcellular localisation of this isoform to the membrane suggests that this region may be responsible for an interaction with a protein that tethers *Dm*PDE11 to the membrane. The differing subcellular localisation of the B and C isoforms will lead the isoforms to sample and modulate different pools of cyclic nucleotides, and thus they may modulate different aspects of the cyclic nucleotide signalling pathway (Omori and Kotera, 2007).

*Dm*PDE11 was shown to co-localise with the cGKs DG1 and DG2. This may be of extreme importance, since phosphorylation of PDE11A4 and PDE5A by cGKs has been shown to modulate catalytic function (Corbin et al., 2000; Gross-Langenhoff et al., 2008; Turko et al., 1998; Yuasa et al., 2000), and the co-localisation and mutual modulation of function of PDE5 and cGK1β in platelets is essential in modulating IP_3R mediated Ca^{2+} release from the ER (Wilson et al., 2008). DG2 modulates the cG-PDE activity of an unidentified PDE in the Malpighian tubule (MacPherson et al., 2004), and so demonstrating that the subcellular localisation of these overlap renders any interaction worthy of further investigation.

Peptide arrays were used to show whether any interaction between these proteins may be direct. A *Dm*PDE11 array probed with the C-terminal half of DG1 (from the end of the second nucleotide binding domain onwards) tagged with HIS_6 gave a number of positive spots compared to control, and the reciprocal assay, where a DG1 array was probed with a HIS_6 tagged fragment representing the middle of *Dm*PDE11 (from the second GAF domain to the end of the catalytic domain) also gave positive spots. However, this data must be considered preliminary, as alanine substitution arrays have not been performed, and peptide arrays must be validated by a further two pieces of interaction data such as co-IP and Y2H analysis, and in this case only co-IP data has been obtained. Peptide arrays investigating a putative DG2/*Dm*PDE11 interaction were non-informative, and unfortunately N-terminal DG1 truncate could not be successfully purified and so was not applied to the *Dm*PDE11 array.

Previous findings by Lorraine Aitcheson suggested that *Dm*PDE11 may modulate expression of the anti-microbial peptide diptericin, and that a reduction in *Dm*PDE11

expression in principal cells of the Malpighian tubule affects survival upon immune challenge with *E. coli*. The possibility that flies with reduced *Dm*PDE11 transcript levels may be immunocompromised was investigated by delivering a septic challenge with *E. coli* to a *Dm*PDE11 deletion line, *Dm*PDE11Δ121, and UAS-*Dm*PDE11 RNAi flies crossed to GAL4 driver lines. UAS-*Dm*PDE11 RNAi was crossed to Act5c GAL4 and c42 driver lines, which drive expression ubiquitously, and in the principal cells of the Malpighian tubule respectively. The progeny of these crosses did not display a reduction in survivorship when compared to controls. *Dm*PDE11Δ121 flies showed a highly significant reduction in survivorship following immune challenge, although 100 hours following septic challenge, these flies only displayed survivorship ~13% lower than Canton S *E. coli* stabbed control. This is a fairly modest, although significant, reduction in survivorship, which suggests that the immune role played by *Dm*PDE11 is not a vital one.

*Hs*PDE11A is the most recently characterised PDE family (Fawcett et al., 2000; Yuasa et al., 2000). Phylogenetic analysis of the *Hs*PDE11A gene family suggests that the closest homologue to *Dm*PDE11 is *Hs*PDE11A3, which is expressed exclusively in testis in both rat and human (Yuasa et al., 2001), and regulates spermatozoa physiology (Seftel, 2005). As *Dm*PDE11 -/- males are infertile, function may be conserved. As the physiological role of PDE11 is not well understood, *Hs*PDE11A3 pP[UAST] constructs were generated, and the transgene expressed in S2 cells and fly. The protein showed predominantly nuclear localisation with lower levels of protein in the cytoplasm when expressed in S2 cells. In Malpighian tubule principal cells, *Hs*PDE11A3 localised to the nucleus at low levels of expression, but was excluded from the nucleus when the transgene was driven by stronger GAL4 expression. Such a change to the subcellular localisation may be crucial to its function, and so further study of *Hs*PDE11A3 in *Drosophila* would be worthwhile.

9.2 Future work

cA- and cG-PDE assays of *Hs*PDE11A3

Time did not permit the verification of *Hs*PDE11A3 cA- and cG- PDE activity when transgenically expressed in *Drosophila*. This would be necessary to demonstrate that the enzyme is functional when heterologously expressed, and would justify the use of these flies to characterise a role for *Hs*PDE11A3 *in vivo*.

*Dm*PDE11C localisation

As YFP-tagged *Dm*PDE11C transgenic flies were generated, the identification of the unknown organelle could be identified by either co-staining of each organelle using specific antibodies, or by the crossing of these flies to GFP tagged proteins known to localise to a particular organelle, and screening for co-localisation. If the localisation is to vesicles, these could be purified, and this fraction subjected to western blotting to confirm the presence or absence of *Dm*PDE11C.

*Hs*PDE11A3 localisation

*Hs*PDE11 localisation appeared to be dependent upon levels of protein, where at lower concentrations the protein localises to the nucleus, and at high concentration, the protein is excluded from the nucleus. Truncation mutants could be assayed for subcellular localisation, in an effort to identify the sequence that modulates this shift in localisation.

Identification of proteins that interact with *Dm*PDE11

Although this assay has been performed, the availability of a new polyclonal antibody against *Dm*PDE11 would allow the immunoprecipitation of the enzyme, and the identification of any putative interactors by analysis of the immunoprecipitate by MALTI-TOF mass spectrometry.

Co-immunoprecipitation of *Dm*PDE11 and the cGKs using specific antisera

Specific antisera against *Dm*PDE11, and the cGKs DG1 and DG2 were generated during the course of this study, but unfortunately were produced after my time in the laboratory had finished. Upon verification that these antibodies can recognise their antigens both in immunoprecipitation and western blot, co-immunoprecipitations could be performed against fly lysate. Co-immunoprecipitation from tissue using specific antisera is considered the gold standard in co-immunoprecipitation, and would provide evidence of an interaction *in vivo*.

Screen for co-localisation of *Dm*PDE11 and the cGKs *in vivo*

In order for a putative protein-protein interaction to be relevant, proteins must occupy an overlapping subcellular localisation. During the course of this study it was ascertained that *Dm*PDE11B long and short localise to the apical and basolateral membranes of the Malpighian tubule, whereas *Dm*PDE11C long and short localised to an unidentified organelle, or to vesicles. DG1 localises to the basolateral membrane and to the cytosol, DG2P1 localises to the apical and basolateral membranes, and DG2P2 localises to the apical membrane. Of these, only DG1 could potentially interact with *Dm*PDE11C, which is wholly localised within the cytosol.

Modulation of PDEs by DG2

When compared to control, *Dm*PDE11 RA overexpressing S2 cells showed no significant increase in either cA-, or cG-PDE activity. Co-expression of either DG2P1 or DG2P2 with *Dm*PDE11RA further reduced both cA- and cG-PDE activity. Although N=1 for each condition, this suggests that over-expressed cGK modulates phosphodiesterase activity or protein levels. The experiment mirrors a finding in flies overexpressing DG2P1 and DG2P2 in tubule principal cells, the tubules of which show a drastic reduction in endogenous PDE activity (Macpherson and Day, 2005). The Malpighian tubule could be used to further investigate this. Q-PCR of each PDE gene in DG2 overexpressing tubules would reveal whether DG2 modulated PDE activity by a reduction in transcript levels. The availability of GST- and HIS_6 tagged cGK and *Dm*PDE11 raises the possibility of *in vitro* phosphorylation assays; if *Dm*PDE11 is found to be phosphorylated, the targeted mutagenesis of residues predicted as cGK substrates would allow the identification of each phosphorylation site.

Confirmation of *Dm*PDE11 role in immunity

Assay of an increased number of *Dm*PDE11Δ121 and other *Dm*PDE11 deletion mutants, alongside the appropriate controls, would confirm whether *Dm*PDE11 has a role in immunity. As *Dm*PDE11Δ121 showed only a modest, but significant, reduction in survivorship, it may be that multiple phosphodiesterases modulate the immune response, and this redundancy leads a knock-down of *Dm*PDE11 transcript levels to have a modest

effect. Immune challenge of flies treated with a broad-spectrum phosphodiesterase inhibitor may reveal whether this is the case.

Repeat of DG2 probed *Dm*PDE11 peptide arrays

Although several putative sites of protein-protein interaction were identified on the PDE11 array, when probed with both the N- and C-terminal HIS_6 tagged DG2 proteins, there was non-specific immunoreactivity at each of these sites on the control PDE11 array. Repeat using GST-tagged protein would potentially give different background, and so the putative interaction at these sites could be confirmed, in which case an alanine array would be generated and overlaid.

Repeat of *Dm*PDE11 probed DG2 peptide arrays

Middle-HIS_6 and End-HIS_6 probed DG2 arrays were compromised; Middle-HIS_6 overlaid DG2 array showed higher levels of background staining, and so putative spots could not be taken as evidence of an interaction, while End-HIS_6 overlaid arrays showed staining significantly dissimilar to control blots, and so novel immunoreactive spots could not be taken as putative interaction sites. Repeat of these assays with GST-tagged protein would again give a different background, and hopefully allow the identification of putative interaction sites.

Confirmation of direct *Dm*PDE11-DG1 interaction

Several sites were determined on *Dm*PDE11 and DG1 which may be regions of direct protein-protein interaction. Alanine substitution arrays would confirm whether these regions are indeed sites of protein-protein interaction, and furthermore would identify those key amino acids within these regions vital for the interaction. As peptide array data must be verified by a further two methods, yeast two hybrid and co-IP of deletion mutants would confirm the interaction.

DG1N probed *Dm*PDE11 array

*Dm*PDE11 and DG1 showed several putative interaction sites on both proteins. Three sites were identified within DG1, two of which corresponded to the N terminal fusion protein. This fusion protein gave protein of the predicted size at the analytical stage, but failed to yield protein following immunoprecipitation. Use of a GST-tagged DG1N terminal fusion

protein would hopefully allow the affinity purification of the protein, and subsequently the probing of the *Dm*PDE11 array, in order to identify additional putative regions of interaction.

This work has confirmed that *Dm*PDE11RB and RC are transcribed *in vivo*, and that RB and RC each have a short isoform. These show closest homology with *Hs*PDE11A3 in terms of sequence. Transgenic *Drosophila melanogaster* were generated which express each of these proteins, and it is hoped that these tools will be used to further characterise these biomedically relevant enzymes. Furthermore, the identification of a putative direct interaction between *Dm*PDE11 and the cGKs needs to be explored further, as this raises the possibility of a new level of feedback in cGMP signalling between the main effectors of the pathway, cGMP-dependent protein kinases, and the main regulator of the pathway, phosphodiesterases.

Appendices

Appendix 1: Projects undertaken that were halted when the new *Dm*PDE11 sequence predictions were released

Yeast Two Hybrid

In order to investigate whether the interaction between *Dm*PDE11A and the cGKs was direct, a Yeast Two Hybrid screen was undertaken. The N and C termini of *Dm*PDE11RA, and the complete ORFs of DG2P1 and P2 were amplified with proofreading polymerase, sequenced for fidelity (data not shown), digested, and cloned into pACT2 AD, an activation domain vector, and pGBKT7, a DNA binding domain vector. The cloning for this was completed, and the constructs were transformed and screened for expression. However this approach was abandoned in favour of peptide arrays, which not only show whether an interaction is direct, but show the peptides responsible for the interaction. This data was presented in chapter six.

Yeast and expertise kindly supplied by Dr. Joe Gray.

TAP-tagging

Retrieval of multi-subunit protein complexes utilising tandem affinity purification, and their subsequent purification via -mass spectrometry (TAP-tagging) is a technique that was pioneered in Yeast (Riguat et al, 1999,) and first used in *Drosophila* in 2004 (Veraska, 2004.) TAP-tagging is similar to epitope tagging, except multiple tags are used instead of one. The technique involves the cloning of a protein of interest, fused in-frame to a "tap-tag" at either the C or N terminus. The "tap tag" in our possession consists of two IgG binding domains of Protein A from *Staphylococcus aureus* and a calmodulin binding peptide, which are separated by a TEV protease cleavage site (Rigaut et al, 1999). The TEV protease site allows the release of the protA units from the matrix-bound IgG under native conditions, which should keep native interactions intact, and thus permit the purification of interacting protein complexes. Following the elution of these proteins, mass spectrometry is used to identify each individual protein. The presence of two tags allows a two-step purification process, which provides a reduction in protein background, while the native conditions should not inhibit protein binding, thus preventing the loss of proteins from the complex.

The tap-tag can be combined with the UAS/GAL4 binary expression system. This allows a cell-specific identification of any interactors, at specific points in the fly's development,

and to a tissue specific level if the daunting number of dissections could be overcome. When this process is coupled to mass spectrometry, proteins at the sub-picomolar range are readily identifiable (Bauer and Kuster, 2003).

The aim of the TAP tagging project was to identify any proteins that interact with *Dm*PDE11 and DG2P1. Stable S2 cell lines expressing the TAP-tagged *Dm*PDE11RA, DG1, DG2P1 and DG2P2 were generated by co-transfection with a pCoHygro plasmid, and selection with hygromycin-B. However these were not validated for expression, as this coincided with the release of Flybase release 5.2. The stock was immortalised.

Appendix 2: Data pertaining to *Dm*PDE11 catalytic activity in S2 cells and fly

Analysis of PDE (and PDE truncate) catalytic activity in S2 cells

Attempts to express full length *Dm*PDE11 in S2 cells failed (Day, 2005). As such the catalytic domain was cloned into pMT/V5-His-TOPO, again in frame with the C-terminal V5 tag, and subjected to cA- and cG-PDE assays alongside *Dm*PDE6 and *Dm*PDE8 (figure A2.1) (Day, 2005).

Figure A2.1: PDE activity of *Dm*PDE6, *Dm*PDE8 and *Dm*PDE11 catalytic domain constructs. S2 cell lysate was assayed for cG and cA-specific PDE activity at a spread of substrate concentrations. Activities represent PDE-transfected activity minus mock transfected activity. Specific PDE activity expressed as pmol cGMP or cAMP/mg/min.

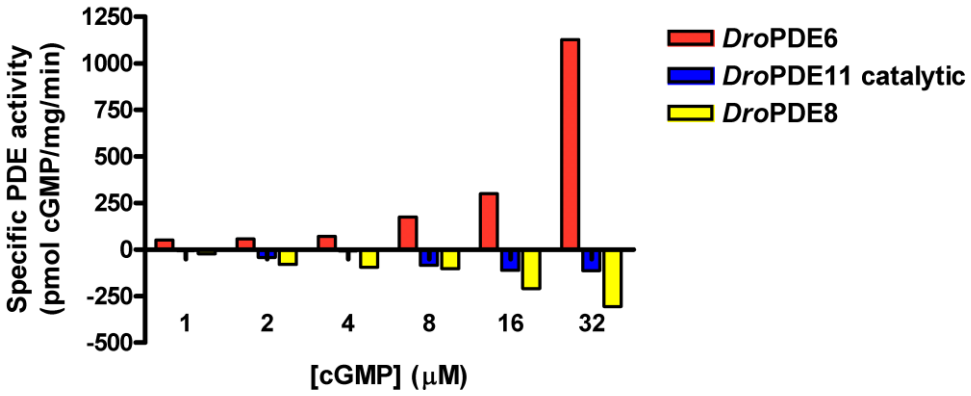

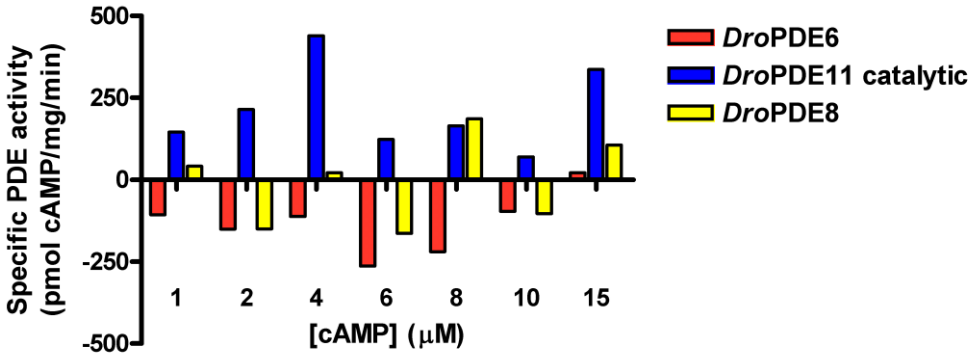

Analysis of *Dm*PDE11 immunoprecipitate by PDE assays

*Dm*PDE11 was verified as a dual specificity PDE by immunoprecipitation using specific polyclonal antisera from head lysate, and subjecting this IP to cA- and cG-PDE assays (figure A2.2) (Day et al., 2005)

Figure A2.2: *Dm*PDE11A shows significant cA- and cG-PDE activity when immunoprecipitated, and subjected to cN-PDE assays. Immunoprecipitate of *Dm*PDE11 using specific antisera from head lysate yields significant cA- and cG-PDE activity when compared to pre-immune control. N=3. Error bars represent standard error of the mean.

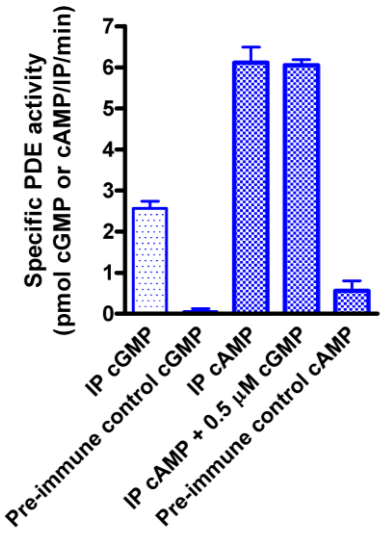

Appendix 3: *Dm*PDE11B and C isoforms are expressed in hindgut and head

PCR analysis of *Dm*PDE11 expression in hindgut and head

PCR using primers specific to isoforms B and C was performed on hindgut and head cDNA to determine if RB and RC were expressed in each (figure A3.1) (Day and Sebastian, unpublished observations, 2007).

Figure A3.1: *Dm*PDE11 RB and RC are expressed in head and hindgut. PCR (30 cycles) was performed using primers specific to the N termini of *Dm*PDE11 RB and RC using head (A; expected product 315 bp) and hindgut (B; expected product 183bp) cDNA, and the products verified by agarose electrophoresis. Band size identified using 100bp ladder. For both gels: Lane 1: *Dm*PDE11-RB N-termini, lane 2: *Dm*PDE11-RC N-termini.

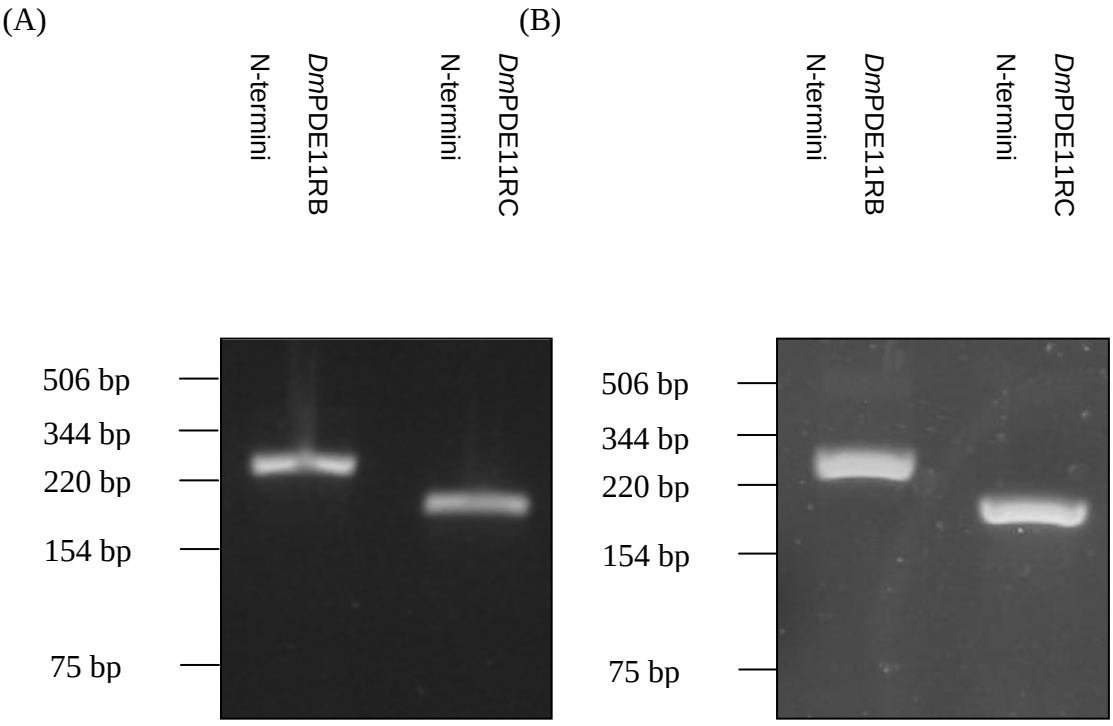

Appendix 4: Data pertaining to an interaction between *Dm*PDE11 and cGKs

*Dm*PDE1, *Dm*PDE6 and *Dm*PDE11 co-immunoprecipitate with cGK activity

Immunoprecipitates of PDE 1, 6 and 11 using specific IgG purified antisera from *Drosophila* head lysate were assayed for cGK activity (figure A4.1) (Day and Sebastian).

Figure A4.1: Immunoprecipitation from fly head lysate using *Drosophila* anti-*Dm*PDE1, anti-*Dm*PDE6, and anti-*Dm*PDE11 polyclonal antibodies yields significant cGK activity. PDE was immunoprecipitated from fly head lysate using IgG purified anti-*Dm*PDE1, anti-*Dm*PDE6, and anti-*Dm*PDE11 specific antisera, and IgG purified pre-immune serum ("IgG"), and the immunoprecipitate subjected to a kinase assay against a "glasstide" cGK substrate. * denotes significant difference of mean P <0.05 against pre-immune IgG control.

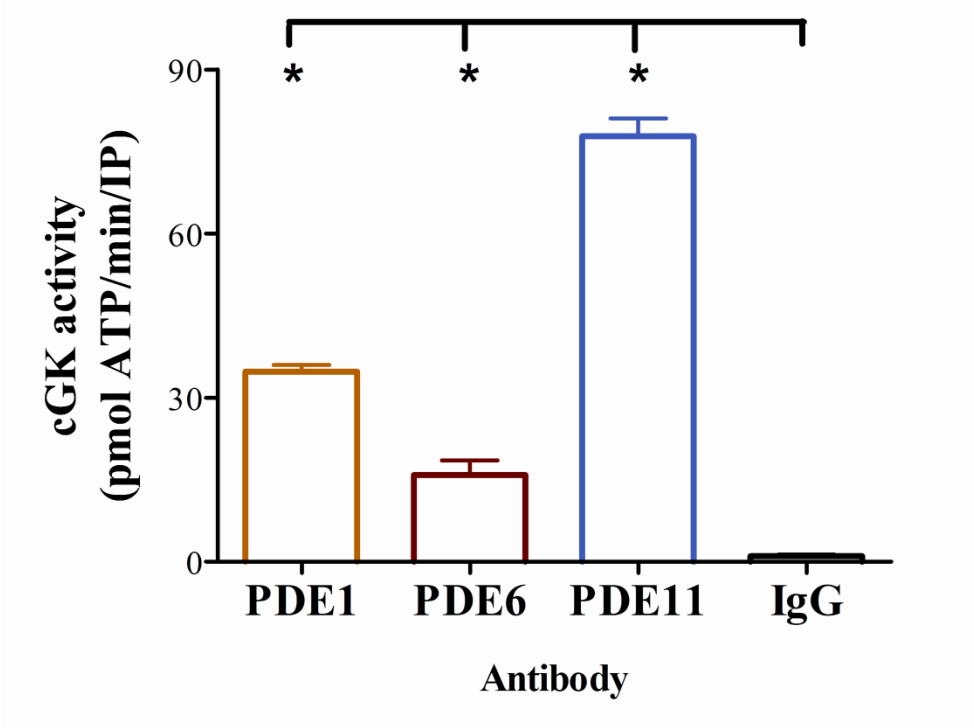

Immunoprecipitation of *Dm*PDE1, *Dm*PDE6, and *Dm*PDE11 each yielded a significant amount of cGK activity when compared to pre-immune control (Day and Sebastian), suggesting that each *Dm*PDE interacts with cGK(s).

DG1 or DG2 co-immunoprecipitate with cG-PDE activity

DG1 and DG2 were immunoprecipitated using IgG purified specific polyclonal antisera from head lysate, and the immunoprecipitate subjected to cG-PDE assay (figure A4.2) (Day and Sebastian).

Figure A4.2: Immunoprecipitation from fly head lysate using *Drosophila* anti-DG1 and anti-DG2 polyclonal antibodies yields significant cG-PDE activity. DG1 and DG2 were immunoprecipitated from fly head lysate using IgG purified anti-DG1 and anti-DG2 specific antisera, and IgG purified pre-immune serum ("Pre-Im"), and the IP subjected to a cG-PDE assay. * denotes significant difference of mean P <0.05 against pre-immune control.

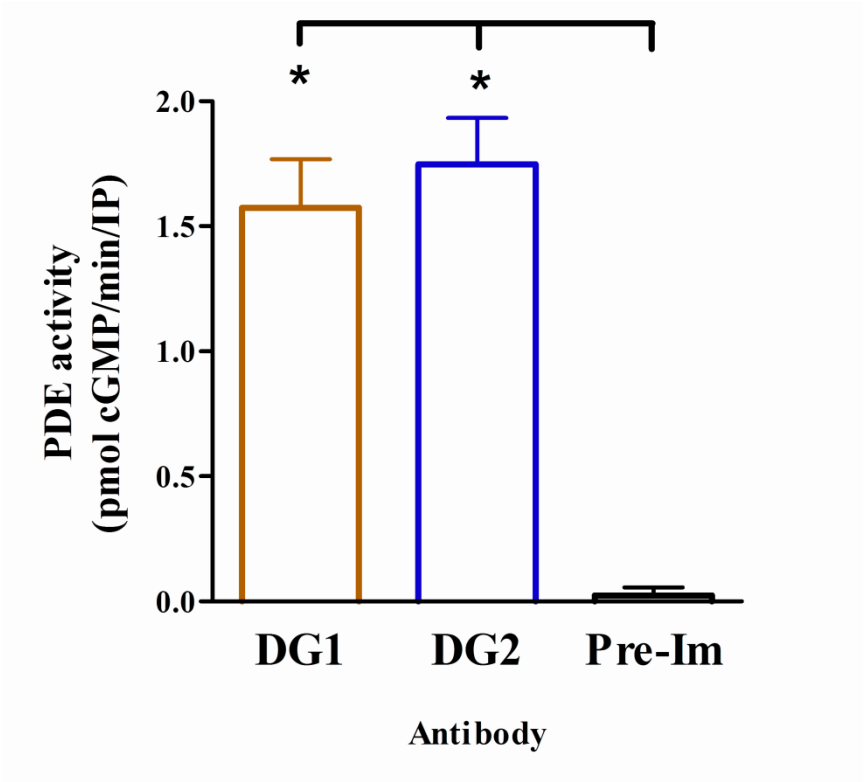

Both the DG1 and DG2 immunoprecipitates yielded significant cG-PDE activity when compared to pre-immune controls (Day and Sebastian), suggesting that both DG1 and DG2 interact with at least one unidentified cG-PDE.

DmPDE11 co-immunoprecipitates with DG2P2

Wild-type canton S flies were homogenised and subjected to immunoprecipitation with an anti-*Dm*PDE11 polyclonal antibody which recognises all four isoforms. The immunoprecipitate was resolved on an SDS-PAGE gel, and individual bands were excised and sequenced using Matrix-assisted laser desorption/ionisation-time of flight mass spectrometry (MALDI-TOF MS). One band yielded several stretches of amino acids corresponding to DG2P2 sequence, that have no significant homology to any other *Drosophila* protein when BlastP analysis is performed against the *Drosophila* proteome (Day).

Appendix 5: Previously obtained data implicates *Dm*PDE11 in the gram negative immune response

Diptericin expression is modulated by a pool of cGMP that is in turn modulated by PDE11

When UAS-PDE11 RNAi (line 1) expression is driven in the Malpighian tubule principal cell with the GAL4 driver c42, there is a significant reduction in diptericin expression. While parental tubules incubated in Schneider's solution for three hours, either with or without 100μM cGMP, show a significant reduction of diptericin expression in the plus cGMP condition, c42/UAS-PDE11 RNAi (line 1) flies show a significantly lower level of diptericin expression in both conditions, where the addition of cGMP does not result in a further reduction of diptericin expression (figure A5.1) (Aitcheson, 2009a).

Figure A5.1: Q-PCR analysis of the affect of cGMP on diptericin expression in the Malpighian tubule. Q-PCR for diptericin expression in the Malpighian tubule, where tubules were incubated in Schneider's solution for three hours, in the presence or absence of 100µM cGMP. Error bars show standard error of the mean (courtesy of Lorraine Aitcheson.)

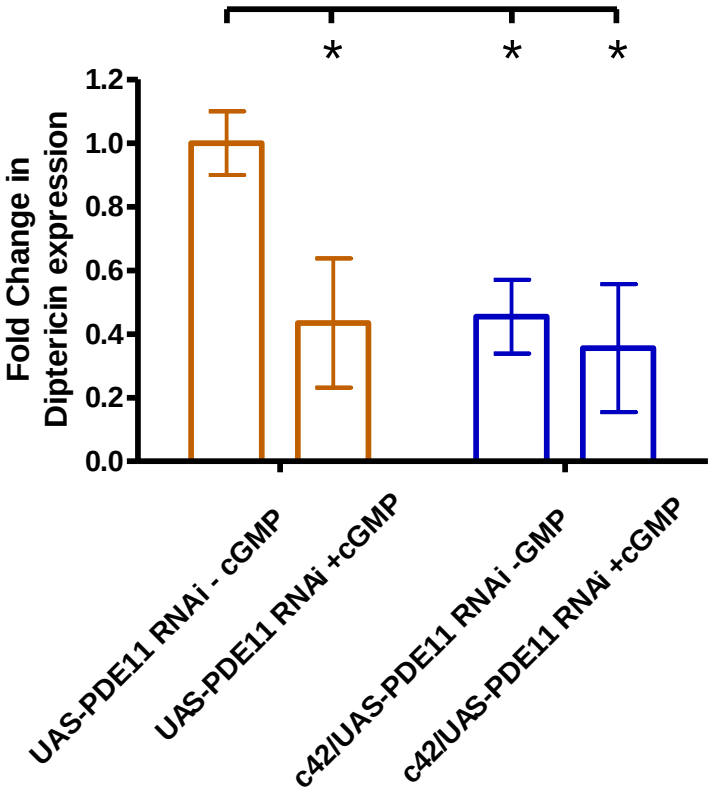

Reduction of PDE11 transcript levels in Malpighian tubule principal cells affects whole fly survival in response to a septic challenge with *E. coli*

UAS-PDE11 RNAi (line 1) flies were crossed to c42 GAL4. UAS-PDE11 RNAi (line 1), and c42/UAS-PDE11 RNAi (line 1) flies were either "mock" stabbed with a dry 0.35mm needle, or stabbed with a 0.35 gauge needle dipped in an *E. coli* solution (at static phase) in the abdomen, and survival was monitored for 24 hours (figure A5.2), as detailed in materials and methods (Aitcheson, 2009b).

Figure A5.2: Preliminary data showing a reduction in survivorship in c42/UAS-PDE11 RNAi compared to controls when septically challenged with *E. coli*. Survival experiment showing a significant decrease in survival upon challenge with *E. coli* using a 0.35mm gauge needle when PDE11 expression is reduced via expression of a PDE11 RNAi transgene, driven in tubule principal cells. Error bars show standard error of the mean (courtesy of Lorraine Aitcheson.)

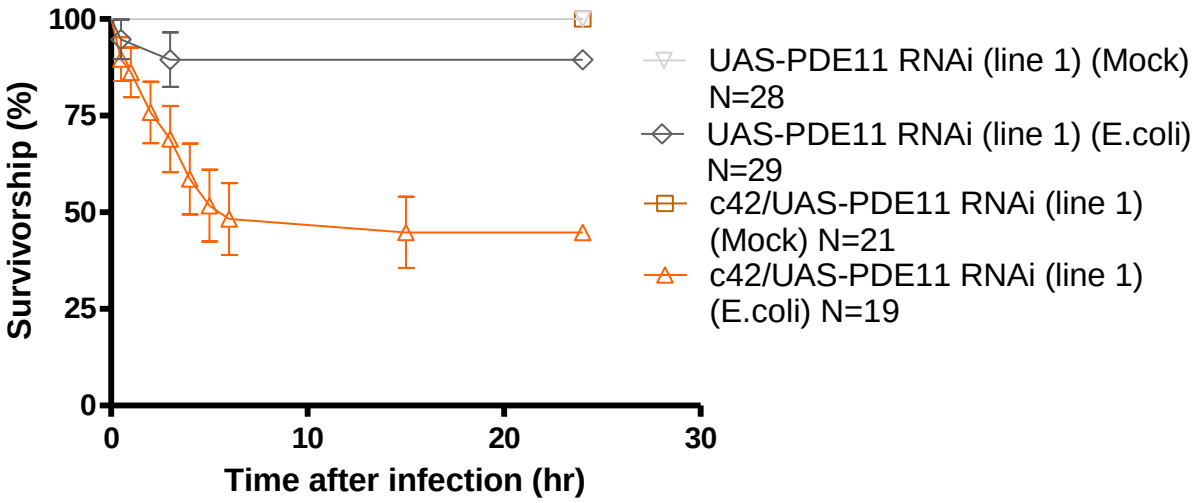

Following septic challenge with *E. coli*, c42/UAS-PDE11 RNAi (line 1) flies displayed a lower level of survival compared to the negative controls. This experiment was performed to N=1, using between 19 to 29 flies for each genotype, where N=3 replicates of 30 flies per genotype is necessary to perform statistical analysis.

Appendix 6: *Drosophila* Media

Standard growth media per litre of water	10 g agar
	15 g sucrose
	30 g glucose
	35 g dried yeast
	15 g maize meal

	10 g wheat germ
	30 g treacle
	10 g soya flour
Grape-juice agar	per litre of water
	40 g agar
	52 g glucose
	26 g sucrose
	15 g dried yeast
	50 % (v/v) blackcurrant diluting juice
	1 % (v/v) Nipagin

Appendix 7: *Escherichia coli* growth media and selective agents

L-broth per litre of water	10 g Bacto-tryptone
	5 g dried yeast
	10 g NaCl
L-agar per litre of water	10 g Bacto-tryptone
	5 g dried yeast
	10 g NaCl
	15 g Bacto-agar
SOC broth	2 % (w/v) Bacto-tryptone

0.5 % (w/v) dried yeast

10 mM NaCl

2.5 mM KCl

10 mM $MgCl_2$

10 mM $MgSO_4$

20 mM glucose

Selective agents

Ampicillin: 100-200 μg/ml ampicillin when being grown on L-Agar or in L-Broth.

100 mg/ml stock solution (w/v) in 50% H_2O, 50% ethanol and stored at -20°C.

Kanamycin: 50 mg/ml solution (Sigma) and stored at 4°C. Selection for kanamycin resistance was performed by the presence of 50 μg/ml kanamycin on L-Agar or in L-Broth.

Appendix 8: SDS-PAGE and Western blotting solutions

6 x SDS-PAGE Loading buffer	0.35 M Tris HCl, pH6.8
	10.28 % (w/v) SDS
	36 % v/v glycerol
	5 % v/v β-mercaptoethanol
	0.012 % w/v bromophenol blue
	in 0.5 ml aliquots stored at –20°C
Tris-Glycine Running Buffer	per 500 ml of H_2O
	7.2 g Glycine

	1.5 g Tris Base
	6 ml 10% (w/v) SDS
Staining Solution	465 ml Brilliant blue R concentrate (Sigma)
	535 ml H_2O
Destaining Solution	10 % (v/v) Acetic Acid
	45% (v/v) Methanol
	in H_2O
Poncau S Staining Solution	per 500 ml of H_2O
	1.5 g TCA
	0.5 g Poncau S stain
Transfer Buffer	per litre of H_2O
	20 % (v/v) Methanol
	14.4 g Glycine
	3 g Tris Base
1 x PBS	137 mM NaCl
	2.7 mM KCl
	10 mM Na_3PO_4
	2 mM KH_2PO_4, pH 7.4

From (Sambrook and Russell, 2001)

Appendix 9: Resolving and Stacking gels for SDS-PAGE

Each solution is sufficient to prepare 2 x 5ml gels

<u>6 % gel</u>

H_2O	5.3 ml

30 % acrylamide mix	2.0
1.5 M Tris (pH 8.8)	2.5
10 % (v/v) SDS	0.1
10 % (v/v) APS	0.1
TEMED	0.008

7 % gel

H_2O	5ml
30 % acrylamide mix	2.3
1.5 M Tris (pH 8.8)	2.5
10 % (v/v) SDS	0.1
10 % (v./v) APS	0.1
TEMED	0.007

10 % gel

H_2O	4.0
30 % acrylamide mix	3.3
1.5 M Tris (pH 8.8)	2.5
10 % (v/v) SDS	0.1
10 % (v/v) APS	0.1
TEMED	0.004

Sufficient to prepare 2 x 5% 1.5ml stacking gels

H_2O	2.1 ml
30 % acrylamide mix	0.5
1.0 M Tris (pH 6.8)	0.38

10 % (v/v) SDS	0.03
10 % (v/v) APS	0.03
TEMED	0.003

From (Sambrook and Russell, 2001)

References

Adams, M.D., Celni. http://fb2007_01.flybase.org/reports/FBgn0085370.html.

. http://flybase.bio.indiana.edu/reports/FBgn0085370.html.

. http://flybase.org/.

. http://flybase.org/reports/FBgn0000721.html.

. http://www.biochemj.org/bj/388/bj3880333add.htm.

. http://www.ensembl.org/*Drosophila*_melanogaster/geneview?gene=CG34341.

Adams, M.D., Celniker, S.E., Holt, R.A., Evans, C.A., Gocayne, J.D., Amanatides, P.G., Scherer, S.E., Li, P.W., Hoskins, R.A., Galle, R.F., *et al.* (2000). The genome sequence of Drosophila melanogaster. Science *287*, 2185-2195.

Ahumada, A., Slusarski, D.C., Liu, X., Moon, R.T., Malbon, C.C., and Wang, H.Y. (2002). Signaling of rat Frizzled-2 through phosphodiesterase and cyclic GMP. Science *298*, 2006-2010.

Airhart, N., Yang, Y.F., Roberts, C.T., Jr., and Silberbach, M. (2003). Atrial natriuretic peptide induces natriuretic peptide receptor-cGMP-dependent protein kinase interaction. J Biol Chem *278*, 38693-38698.

Aitcheson, L. (2006). c42/*Dm*PDE11 RNAi line 1 progeny tubule cDNA and parental strains were subjected to Q-PCR analysis. Progeny showed a knockdown of 69% compared to parental controls

Aitcheson, L. (2009a). cGKs modulate Relish translocation to the nucleus.

Aitcheson, L. (2009b). cGMP modulates expression of AMPs in the Malpighian tubule in a dose dependent manner.

Aitcheson, L. (2009c). *Dm*PDE11 transcript levels affect diptericin expression.

Aitcheson, L. (2009d). modulation of cGK expression in only the principal cells of the tubule is sufficient to modulate whole fly survival, when septically challenged with the gram-negative bacteria *E. coli*.

Aitchison, L. (2008). Modulation of innate immunity by the cGMP signalling pathway in the drosophila malpighian tubule (University of Glasgow).

Ally, S., Larson, A.G., Barlan, K., Rice, S.E., and Gelfand, V.I. (2009). Opposite-polarity motors activate one another to trigger cargo transport in live cells. J Cell Biol *187*, 1071-1082.

Anant, J.S., Ong, O.C., Xie, H.Y., Clarke, S., O'Brien, P.J., and Fung, B.K. (1992). In vivo differential prenylation of retinal cyclic GMP phosphodiesterase catalytic subunits. J Biol Chem *267*, 687-690.

Arnold, W.P., Mittal, C.K., Katsuki, S., and Murad, F. (1977). Nitric oxide activates guanylate cyclase and increases guanosine 3':5'-cyclic monophosphate levels in various tissue preparations. Proc Natl Acad Sci U S A *74*, 3203-3207.

Artemyev, N.O., Surendran, R., Lee, J.C., and Hamm, H.E. (1996). Subunit structure of rod cGMP-phosphodiesterase. J Biol Chem *271*, 25382-25388.

Ashman, D.F., Lipton, R., Melicow, M.M., and Price, T.D. (1963). Isolation of adenosine 3', 5'-monophosphate and guanosine 3', 5'-monophosphate from rat urine. Biochem Biophys Res Commun *11*, 330-334.

Asirvatham, A., Galligan, S., Schillace, R., Davey, M., Vasta, V., Beavo, J., and Carr, D. (2004). A-kinase anchoring proteins interact with phosphodiesterases in T lymphocyte cell lines. J Immunol *173*, 4806-4814.

Attwood, T., Bradley, P., Flower, D., Gaulton, A., Maudling, N., Mitchell, A., Moulton, G., Nordle, A., Paine, K., Taylor, P., *et al.* (2003). PRINTS and its automatic supplement, prePRINTS. Nucleic Acids Res *31*, 400-402.

Ayoob, J., Yu, H., Terman, J., and Kolodkin, A. (2004). The Drosophila receptor guanylyl cyclase Gyc76C is required for semaphorin-1a-plexin A-mediated axonal repulsion. J Neurosci, 6639-6649.

Baehr, W., Devlin, M.J., and Applebury, M.L. (1979). Isolation and characterization of cGMP phosphodiesterase from bovine rod outer segments. J Biol Chem *254*, 11669-11677.

Baillie, G., Huston, E., Scotland, G., Hodgkin, M., Gall, I., Peden, A., MacKenzie, C., Houslay, E., Currie, R., Pettitt, T., *et al.* (2002). TAPAS-1, a novel microdomain within the unique N-terminal region of the PDE4A1 cAMP-specific phosphodiesterase that allows

rapid, Ca2+-triggered membrane association with selectivity for interaction with phosphatidic acid. J Biol Chem *277*, 28298-28309.

Baillie, G.S. (2009). Compartmentalized signalling: spatial regulation of cAMP by the action of compartmentalized phosphodiesterases. FEBS J *276*, 1790-1799.

Baillie, G.S., MacKenzie, S.J., McPhee, I., and Houslay, M.D. (2000). Sub-family selective actions in the ability of Erk2 MAP kinase to phosphorylate and regulate the activity of PDE4 cyclic AMP-specific phosphodiesterases. Br J Pharmacol *131*, 811-819.

Baruscotti, M., Bucchi, A., and Difrancesco, D. (2005). Physiology and pharmacology of the cardiac pacemaker ("funny") current. Pharmacol Ther *107*, 59-79.

Basset, A., Khush, R.S., Braun, A., Gardan, L., Boccard, F., Hoffmann, J.A., and Lemaitre, B. (2000). The phytopathogenic bacteria Erwinia carotovora infects Drosophila and activates an immune response. Proc Natl Acad Sci U S A *97*, 3376-3381.

Bateman, A., Coin, L., Durbin, R., Finn, R., Hollich, V., Griffiths-Jones, S., Khanna, A., Marshall, M., Moxon, S., Sonnhammer, E., *et al.* (2004). The Pfam protein families database. Nucleic Acids Res *32*, D138-141.

Bauer, A., and Kuster, B. (2003). Affinity purification-mass spectrometry. Powerful tools for the characterization of protein complexes. Eur J Biochem *270*, 570-578.

Bauman, A.L., Soughayer, J., Nguyen, B.T., Willoughby, D., Carnegie, G.K., Wong, W., Hoshi, N., Langeberg, L.K., Cooper, D.M., Dessauer, C.W., *et al.* (2006). Dynamic regulation of cAMP synthesis through anchored PKA-adenylyl cyclase V/VI complexes. Mol Cell *23*, 925-931.

Baumann, A., Frings, S., Godde, M., Seifert, R., and Kaupp, U.B. (1994). Primary structure and functional expression of a Drosophila cyclic nucleotide-gated channel present in eyes and antennae. Embo J *13*, 5040-5050.

Beavo, Conti, and Joseph (2007). Biochemistry and Physiology of Cyclic Nucleotide Phosphodiesterases: Essential Components In Cyclic Nucleotide Signaling. Annu Rev Biochem, 76:481–511.

Beavo, J., and Brunton, L. (2002). Cyclic nucleotide research – still expanding after half a century. Nat Rev Mol Cell Biol, 3, 710–718.

Beavo, J., Hardman, J., and Sutherland, E. (1971a). Stimulation of Adenosine 3', 5'-Monophosphate Hydrolysis by Guanosine 3', 5'-Monophosphate. J Biol Chem, 246: 3841 - 3846.

Beavo, J.A., Hardman, J.G., and Sutherland, E.W. (1970). Hydrolysis of cyclic guanosine and adenosine 3',5'-monophosphates by rat and bovine tissues. J Biol Chem *245*, 5649-5655.

Beavo, J.A., Hardman, J.G., and Sutherland, E.W. (1971b). Stimulation of adenosine 3',5'-monophosphate hydrolysis by guanosine 3',5'-monophosphate. J Biol Chem *246*, 3841-3846.

Beavo, J.A., Rogers, N.L., Crofford, O.B., Baird, C.E., Hardman, J.G., Sutherland, E.W., and Newman, E.V. (1971c). Effects of phosphodiesterase inhibitors on cyclic AMP levels and on lipolysis. Ann N Y Acad Sci *185*, 129-136.

Bechtel, P.J., Beavo, J.A., and Krebs, E.G. (1977). Purification and characterization of catalytic subunit of skeletal muscle adenosine 3':5'-monophosphate-dependent protein kinase. J Biol Chem *252*, 2691-2697.

Bellen, H.J., and Kiger, J.A., Jr. (1987). Sexual hyperactivity and reduced longevity of dunce females of Drosophila melanogaster. Genetics *115*, 153-160.

Bessay, E., Blount, M., Zoraghi, R., Beasley, A., Grimes, K., Francis, S., and Corbin, J. (2008). Phosphorylation increases affinity of the phosphodiesterase-5 catalytic site for tadalafil. J Pharmacol Exp Ther *325*, 62-68.

Bicker, G. (1998). NO news from insect brains. Trends Neurosci, (8):349-355.

Bicker, G. (2005). STOP and GO with NO: nitric oxide as a regulator of cell motility in simple brains. Bioessays *27*, 495-505.

Biel, M., and Michalakis, S. (2009). Cyclic nucleotide-gated channels. Handb Exp Pharmacol, 111-136.

Blom, N., Sicheritz-Ponten, T., Gupta, R., Gammeltoft, S., and Brunak, S. (2004). Prediction of post-translational glycosylation and phosphorylation of proteins from the amino acid sequence. Proteomics *4*, 1633-1649.

Bogdan, C. (2001). Nitric oxide and the immune response. Nat Immunol *2*, 907-916.

Bolger, G.B., Baillie, G.S., Li, X., Lynch, M.J., Herzyk, P., Mohamed, A., Mitchell, L.H., McCahill, A., Hundsrucker, C., Klussmann, E., *et al.* (2006). Scanning peptide array analyses identify overlapping binding sites for the signalling scaffold proteins, beta-arrestin and RACK1, in cAMP-specific phosphodiesterase PDE4D5. Biochem J *398*, 23-36.

Bonfini, L., Karlovich, C., Dasgupta, C., and Banerjee, U. (1992). The Son of sevenless gene product: a putative activator of Ras. Science, 31;255(5044):5603-5046.

Bos, J. (2006). Epac proteins: multi-purpose cAMP targets. Trends Biochem Sci *31*, 680-686.

Bowman, B.J., Dschida, W.J., and Bowman, E.J. (1992). Vacuolar ATPase of Neurospora crassa: electron microscopy, gene characterization and gene inactivation/mutation. J Exp Biol *172*, 57-66.

Brand, A.H., and Perrimon, N. (1993). Targeted gene expression as a means of altering cell fates and generating dominant phenotypes. Development *118*, 401-415.

Breer, H., Boekhoff, I., and Tareilus, E. (1990). Rapid kinetics of second messenger formation in olfactory transduction. Nature *345*, 65-68.

Bregman, D.B., Bhattacharyya, N., and Rubin, C.S. (1989). High affinity binding protein for the regulatory subunit of cAMP-dependent protein kinase II-B. Cloning, characterization, and expression of cDNAs for rat brain P150. J Biol Chem *264*, 4648-4656.

Bregman, D.B., Hirsch, A.H., and Rubin, C.S. (1991). Molecular characterization of bovine brain P75, a high affinity binding protein for the regulatory subunit of cAMP-dependent protein kinase II beta. J Biol Chem *266*, 7207-7213.

Broderick, K., Kean, L., Dow, J., Pyne, N., and Davies, S. (2004). Ectopic expression of bovine type 5 phosphodiesterase confers a renal phenotype in Drosophila. J Biol Chem *279*, 8159-8168.

Broderick, K.E., MacPherson, M.R., Regulski, M., Tully, T., Dow, J.A., and Davies, S.A. (2003). Interactions between epithelial nitric oxide signaling and phosphodiesterase activity in Drosophila. Am J Physiol Cell Physiol *285*, C1207-1218.

Bruce, J.I., Straub, S.V., and Yule, D.I. (2003). Crosstalk between cAMP and Ca2+ signaling in non-excitable cells. Cell Calcium *34*, 431-444.

Brunton, L., Hayes, J., and Mayer, S. (1981). Functional compartmentation of cyclic AMP and protein kinase in heart. Adv Cyclic Nucleotide Res, 14, 391–397.

Butcher, R., and Sutherland, E. (1962a). Adenosine-3prime,5prime-phosphate in biological materials. J Biol Chem, 237, 1244 - 1250.

Butcher, R.W., and Sutherland, E.W. (1962b). Adenosine 3',5'-phosphate in biological materials. I. Purification and properties of cyclic 3',5'-nucleotide phosphodiesterase and use of this enzyme to characterize adenosine 3',5'-phosphate in human urine. J Biol Chem *237*, 1244-1250.

Button, D., and Eidsath, A. (1996). Aequorin targeted to the endoplasmic reticulum reveals heterogeneity in luminal Ca++ concentration and reports agonist- or IP3-induced release of Ca++. Mol Biol Cell *7*, 419-434.

Byers, D., Davis, R.L., and Kiger, J.A., Jr. (1981). Defect in cyclic AMP phosphodiesterase due to the dunce mutation of learning in Drosophila melanogaster. Nature *289*, 79-81.

Cabrero, P., Radford, J.C., Broderick, K.E., Costes, L., Veenstra, J.A., Spana, E.P., Davies, S.A., and Dow, J.A. (2002). The Dh gene of Drosophila melanogaster encodes a diuretic peptide that acts through cyclic AMP. J Exp Biol *205*, 3799-3807.

Carnegie, G.K., and Scott, J.D. (2003). A-kinase anchoring proteins and neuronal signaling mechanisms. Genes Dev *17*, 1557-1568.

Cassel, D., and Selinger, Z. (1978a). Mechanism of adenylate cyclase activation through the beta-adrenergic receptor: catecholamine-induced displacement of bound GDP by GTP. Proc Natl Acad Sci U S A *75*, 4155-4159.

Cassel, D., and Selinger, Z. (1978b). Mechanism of adenylate cyclase activation through the beta-adrenergic receptor: catecholamine-induced displacement of bound GDP by GTP. Proc Natl Acad Sci U S A *75*, 4155-4159.

Castro, L.R., Verde, I., Cooper, D.M., and Fischmeister, R. (2006). Cyclic guanosine monophosphate compartmentation in rat cardiac myocytes. Circulation *113*, 2221-2228.

Cawley, S., Sawyer, C., Brunelle, K., van der Vliet, A., and Dostmann, W. (2007). Nitric oxide-evoked transient kinetics of cyclic GMP in vascular smooth muscle cells. Cell Signal *19*, 1023-1033.

Chappe, V., Hinkson, D.A., Howell, L.D., Evagelidis, A., Liao, J., Chang, X.B., Riordan, J.R., and Hanrahan, J.W. (2004). Stimulatory and inhibitory protein kinase C consensus sequences regulate the cystic fibrosis transmembrane conductance regulator. Proc Natl Acad Sci U S A *101*, 390-395.

Charbonneau, H., Beier, N., Walsh, K.A., and Beavo, J.A. (1986). Identification of a conserved domain among cyclic nucleotide phosphodiesterases from diverse species. Proc Natl Acad Sci U S A *83*, 9308-9312.

Charbonneau, H., Prusti, R.K., LeTrong, H., Sonnenburg, W.K., Mullaney, P.J., Walsh, K.A., and Beavo, J.A. (1990). Identification of a noncatalytic cGMP-binding domain conserved in both the cGMP-stimulated and photoreceptor cyclic nucleotide phosphodiesterases. Proc Natl Acad Sci U S A *87*, 288-292.

Charroux, B., and Royet, J. (2009). Elimination of plasmatocytes by targeted apoptosis reveals their role in multiple aspects of the Drosophila immune response. Proc Natl Acad Sci U S A *106*, 9797-9802.

Chen, C.N., Denome, S., and Davis, R.L. (1986). Molecular analysis of cDNA clones and the corresponding genomic coding sequences of the Drosophila dunce+ gene, the structural gene for cAMP phosphodiesterase. Proc Natl Acad Sci U S A *83*, 9313-9317.

Chen, L.J., and Walsh, D.A. (1971). Multiple forms of hepatic adenosine 3':5'-monophosphate dependent protein kinase. Biochemistry *10*, 3614-3621.

Chen, Z., Otto, J.C., Bergo, M.O., Young, S.G., and Casey, P.J. (2000). The C-terminal polylysine region and methylation of K-Ras are critical for the interaction between K-Ras and microtubules. J Biol Chem *275*, 41251-41257.

Cheng, H.F., Wang, J.L., Zhang, M.Z., McKanna, J.A., and Harris, R.C. (2000). Nitric oxide regulates renal cortical cyclooxygenase-2 expression. Am J Physiol Renal Physiol *279*, F122-129.

Cherry, S., and Silverman, N. (2006). Host-pathogen interactions in drosophila: new tricks from an old friend. Nat Immunol *7*, 911-917.

Cheung, W.Y. (1970). Cyclic 3',5'-nucleotide phosphodiesterase. Demonstration of an activator. Biochem Biophys Res Commun *38*, 533-538.

Chinkers, M., Garbers, D.L., Chang, M.S., Lowe, D.G., Chin, H.M., Goeddel, D.V., and Schulz, S. (1989). A membrane form of guanylate cyclase is an atrial natriuretic peptide receptor. Nature *338*, 78-83.

Chintapalli, V., Wang, J., and Dow, J. (2007). Using FlyAtlas to identify better Drosophila melanogaster models of human disease. Nat Genet, 39(36):715-720.

Clack, J.W., Oakley, B., 2nd, and Stein, P.J. (1983). Injection of GTP-binding protein or cyclic GMP phosphodiesterase hyperpolarizes retinal rods. Nature *305*, 50-52.

Cokol, M., Nair, R., and Rost, B. (2000). Finding nuclear localization signals. EMBO Rep *1*, 411-415.

Colicelli, J., Birchmeier, C., Michaeli, T., O'Neill, K., Riggs, M., and Wigler, M. (1989a). Isolation and characterization of a mammalian gene encoding a high-affinity cAMP phosphodiesterase. Proc Natl Acad Sci U S A *86*, 3599-3603.

Colicelli, J., Birchmeier, C., Michaeli, T., O'Neill, K., Riggs, M., and Wigler, M. (1989b). Isolation and characterization of a mammalian gene encoding a high-affinity cAMP phosphodiesterase. Proc Natl Acad Sci U S A *86*, 3599-3603.

Conti, M., and Beavo, J. (2007). Biochemistry and physiology of cyclic nucleotide phosphodiesterases: essential components in cyclic nucleotide signaling. Annu Rev Biochem *76*, 481-511.

Conti, M., Richter, W., Mehats, C., Livera, G., Park, J.Y., and Jin, C. (2003). Cyclic AMP-specific PDE4 phosphodiesterases as critical components of cyclic AMP signaling. J Biol Chem *278*, 5493-5496.

Cook, T.A., Ghomashchi, F., Gelb, M.H., Florio, S.K., and Beavo, J.A. (2000). Binding of the delta subunit to rod phosphodiesterase catalytic subunits requires methylated, prenylated C-termini of the catalytic subunits. Biochemistry *39*, 13516-13523.

Cook, T.A., Ghomashchi, F., Gelb, M.H., Florio, S.K., and Beavo, J.A. (2001). The delta subunit of type 6 phosphodiesterase reduces light-induced cGMP hydrolysis in rod outer segments. J Biol Chem *276*, 5248-5255.

Cook, W.H., Lipkin, D., and Markham, R. (1957). The formation of cyclic dianhydrodiadenylic acid by the alkaline degradation of adenosine-5'-triphosphoric acid. J Am Chem Soc *79*, 3607-3608.

Cooper, D.M. (2003). Regulation and organization of adenylyl cyclases and cAMP. Biochem J *375*, 517-529.

Corbin, J.D., Turko, I.V., Beasley, A., and Francis, S.H. (2000). Phosphorylation of phosphodiesterase-5 by cyclic nucleotide-dependent protein kinase alters its catalytic and allosteric cGMP-binding activities. Eur J Biochem *267*, 2760-2767.

Corfas, G., and Dudai, Y. (1990). Adaptation and fatigue of a mechanosensory neuron in wild-type Drosophila and in memory mutants. J Neurosci *10*, 491-499.

Cox, A.D., and Der, C.J. (1992). Protein prenylation: more than just glue? Curr Opin Cell Biol *4*, 1008-1016.

Craven, P.A., DeRubertis, F.R., and Pratt, D.W. (1979). Electron spin resonance study of the role of NO . catalase in the activation of guanylate cyclase by NaN3 and NH2OH. Modulation of enzyme responses by heme proteins and their nitrosyl derivatives. J Biol Chem *254*, 8213-8222.

Cropp, C.D., Komori, T., Shima, J.E., Urban, T.J., Yee, S.W., More, S.S., and Giacomini, K.M. (2008). Organic anion transporter 2 (SLC22A7) is a facilitative transporter of cGMP. Mol Pharmacol *73*, 1151-1158.

D'Amours, M.R., and Cote, R.H. (1999). Regulation of photoreceptor phosphodiesterase catalysis by its non-catalytic cGMP-binding sites. Biochem J *340 (Pt 3)*, 863-869.

D'Andrea, M.R., Qiu, Y., Haynes-Johnson, D., Bhattacharjee, S., Kraft, P., and Lundeen, S. (2005). Expression of PDE11A in normal and malignant human tissues. J Histochem Cytochem *53*, 895-903.

Dagger, Z., LeeDagger, K., and Kruh, G. (2001). Transport of Cyclic Nucleotides and Estradiol 17-B-D-Glucuronide by Multidrug Resistance Protein 4. J Biol Chem, 276: 33747-33754.

Dahan, D., Evagelidis, A., Hanrahan, J.W., Hinkson, D.A., Jia, Y., Luo, J., and Zhu, T. (2001). Regulation of the CFTR channel by phosphorylation. Pflugers Arch *443 Suppl 1*, S92-96.

Daugan, A., Grondin, P., Ruault, C., Le Monnier de Gouville, A.C., Coste, H., Linget, J.M., Kirilovsky, J., Hyafil, F., and Labaudiniere, R. (2003). The discovery of tadalafil: a novel and highly selective PDE5 inhibitor. 2: 2,3,6,7,12,12a-

hexahydropyrazino[1',2':1,6]pyrido[3,4-b]indole-1,4-dione analogues. J Med Chem *46*, 4533-4542.

Dauwalder, B., and Davis, R.L. (1995). Conditional rescue of the dunce learning/memory and female fertility defects with Drosophila or rat transgenes. J Neurosci *15*, 3490-3499.

Davies, S. (2000). Nitric oxide signalling in insects. Insect Biochem Mol Biol *30*, 1123-1138.

Davies, S., and Dow, J. (2009a). Modulation of epithelial innate immunity by autocrine production of nitric oxide. Gen Comp Endocrinol *162*, 113-121.

DAVIES, S., HUESMANN, G., MADDRELL, S., O'DONNELL, M., DOW, J., and TUBLITZ, N. (1995). CAP2b, a cardioacceleratory peptide, is present in Drosophila and stimulates tubule fluid secretion via cGMP. AmJ Physiol, 269, R1321-R1326.

Davies, S.A. (2006). Signalling via cGMP: lessons from Drosophila. Cell Signal *18*, 409-421.

Davies, S.A., and Dow, J.A. (2009b). Modulation of epithelial innate immunity by autocrine production of nitric oxide. Gen Comp Endocrinol *162*, 113-121.

Davies, S.A., Huesmann, G.R., Maddrell, S.H., O'Donnell, M.J., Skaer, N.J., Dow, J.A., and Tublitz, N.J. (1995). CAP2b, a cardioacceleratory peptide, is present in Drosophila and stimulates tubule fluid secretion via cGMP. Am J Physiol *269*, R1321-1326.

Davies, S.A., Stewart, E.J., Huesmann, G.R., Skaer, N.J., Maddrell, S.H., Tublitz, N.J., and Dow, J.A. (1997). Neuropeptide stimulation of the nitric oxide signaling pathway in Drosophila melanogaster Malpighian tubules. Am J Physiol *273*, R823-827.

Davis, R., Takayasu, H., Eberwine, M., and Myres, J. (1989a). Cloning and characterization of mammalian homologs of the Drosophila dunce+ gene. Proc Natl Acad Sci U S A *86*, 3604-3608.

Davis, R.L., and Kiger, J.A., Jr. (1980). A partial characterization of the cyclic nucleotide phosphodiesterases of Drosophila melanogaster. Arch Biochem Biophys *203*, 412-421.

Davis, R.L., and Kiger, J.A., Jr. (1981). Dunce mutants of Drosophila melanogaster: mutants defective in the cyclic AMP phosphodiesterase enzyme system. J Cell Biol *90*, 101-107.

Davis, R.L., Takayasu, H., Eberwine, M., and Myres, J. (1989b). Cloning and characterization of mammalian homologs of the Drosophila dunce+ gene. Proc Natl Acad Sci U S A *86*, 3604-3608.

Day, J. Seperation of an anti-*Dm*PDE11 immunoprecipitation from wild-type canton S homogenate by SDS-PAGE gel, and MALDI-TOF MS of each band reveals several stretches of amino acids corresponding to DG2P2 sequence, that have no significant homology to any other *Drosophila* protein when BlastP analysis is performed against the *D*rosophila proteome.

Day, J. (2005). Novel phosphodiesterases in the Drosophila melanogaster Malpighian tubule (Glasgow University).

Day, J., Houslay, M., and Davies, S. (2006). A novel role for a Drosophila homologue of cGMP-specific phosphodiesterase in the active transport of cGMP. Biochem J, 393, 481–488.

Day, J., and Sebastian, S. PDEs and cGKs co-immunoprecipitate.

Day, J., and Sebastian, S. (2007). PCR using primers specific to isoforms B and C was performed on hindgut and head cDNA shows that RB and RC are expressed in each.

Day, J.P., Cleghon, V., Houslay, M.D., and Davies, S.A. (2008). Regulation of a Drosophila melanogaster cGMP-specific phosphodiesterase by prenylation and interaction with a prenyl-binding protein. Biochem J *414*, 363-374.

Day, J.P., Dow, J.A., Houslay, M.D., and Davies, S.A. (2005). Cyclic nucleotide phosphodiesterases in Drosophila melanogaster. Biochem J *388*, 333-342.

Day, P. PDE assays on S2 cells transfected with sub-cloned *Dm*PDE11RA catalytic domain yields slight cA-PDE activity over untransfected S2 cells.

Day, P. S2 cells transiently transfected with *Dm*PDE11RA fail to generate expressed protein

Day, P. The EST SD13096 gives a band of approximately 5.8kb on a Northern blot, which matches the size of *Dm*PDE11RA.

de Belle, J.S., Hilliker, A.J., and Sokolowski, M.B. (1989). Genetic localization of foraging (for): a major gene for larval behavior in Drosophila melanogaster. Genetics *123*, 157-163.

de Rooij, J., Rehmann, H., van Triest, M., Cool, R.H., Wittinghofer, A., and Bos, J.L. (2000). Mechanism of regulation of the Epac family of cAMP-dependent RapGEFs. J Biol Chem *275*, 20829-20836.

de Rooij, J., Zwartkruis, F.J., Verheijen, M.H., Cool, R.H., Nijman, S.M., Wittinghofer, A., and Bos, J.L. (1998). Epac is a Rap1 guanine-nucleotide-exchange factor directly activated by cyclic AMP. Nature *396*, 474-477.

Deschenes, R.J., Resh, M.D., and Broach, J.R. (1990). Acylation and prenylation of proteins. Curr Opin Cell Biol *2*, 1108-1113.

Deterre, P., Bigay, J., Forquet, F., Robert, M., and Chabre, M. (1988). cGMP phosphodiesterase of retinal rods is regulated by two inhibitory subunits. Proc Natl Acad Sci U S A *85*, 2424-2428.

Di Benedetto, G., Zoccarato, A., Lissandron, V., Terrin, A., Li, X., Houslay, M.D., Baillie, G.S., and Zaccolo, M. (2008). Protein kinase A type I and type II define distinct intracellular signaling compartments. Circ Res *103*, 836-844.

Dijkers, P., and O'Farrell, P. (2009). Dissection of a Hypoxia-induced, Nitric Oxide-mediated Signaling Cascade. Mol Biol Cell, [epub].

Dimarcq, J.L., Imler, J.L., Lanot, R., Ezekowitz, R.A., Hoffmann, J.A., Janeway, C.A., and Lagueux, M. (1997). Treatment of l(2)mbn Drosophila tumorous blood cells with the steroid hormone ecdysone amplifies the inducibility of antimicrobial peptide gene expression. Insect Biochem Mol Biol *27*, 877-886.

Dodge, K.L., Khouangsathiene, S., Kapiloff, M.S., Mouton, R., Hill, E.V., Houslay, M.D., Langeberg, L.K., and Scott, J.D. (2001). mAKAP assembles a protein kinase A/PDE4 phosphodiesterase cAMP signaling module. Embo J *20*, 1921-1930.

Dodge-Kafka, K., Bauman, A., and Kapiloff, M. (2008). A-kinase anchoring proteins as the basis for cAMP signaling. Handb Exp Pharmacol, 3-14.

Dodge-Kafka, K.L., and Kapiloff, M.S. (2006). The mAKAP signaling complex: integration of cAMP, calcium, and MAP kinase signaling pathways. Eur J Cell Biol *85*, 593-602.

Dodge-Kafka, K.L., Soughayer, J., Pare, G.C., Carlisle Michel, J.J., Langeberg, L.K., Kapiloff, M.S., and Scott, J.D. (2005). The protein kinase A anchoring protein mAKAP coordinates two integrated cAMP effector pathways. Nature *437*, 574-578.

Dogan, R., Getoor, L., Wilbur, W., and Mount, S. (2007). SplicePort--an interactive splice-site analysis tool (Nucleic Acids Res).

Dolci, S., Belmonte, A., Santone, R., Giorgi, M., Pellegrini, M., Carosa, E., Piccione, E., Lenzi, A., and Jannini, E. (2006a). Subcellular localization and regulation of type-1C and type-5 phosphodiesterases. Biochem Biophys Res Commun *341*, 837-846.

Dolci, S., Belmonte, A., Santone, R., Giorgi, M., Pellegrini, M., Carosa, E., Piccione, E., Lenzi, A., and Jannini, E.A. (2006b). Subcellular localization and regulation of type-1C and type-5 phosphodiesterases. Biochem Biophys Res Commun *341*, 837-846.

Dong, C.J., and Liu, J.Y. (2010). The Arabidopsis EAR-motif-containing protein RAP2.1 functions as an active transcriptional repressor to keep stress responses under tight control. BMC Plant Biol *10*, 47.

Dow, J., and Davies, S. (2003a). Integrative physiology and functional genomics of epithelial function in a genetic model organism. Physiol Rev *83*, 687-729.

Dow, J.A., Maddrell, S.H., Davies, S.A., Skaer, N.J., and Kaiser, K. (1994a). A novel role for the nitric oxide-cGMP signaling pathway: the control of epithelial function in Drosophila. Am J Physiol *266*, R1716-1719.

Dow, J.A., Maddrell, S.H., Gortz, A., Skaer, N.J., Brogan, S., and Kaiser, K. (1994b). The malpighian tubules of Drosophila melanogaster: a novel phenotype for studies of fluid secretion and its control. J Exp Biol *197*, 421-428.

Dow, J.D., and Wang, J. (2009). Solexa Illumina EST sequencing runs from poly-A primed mRNA generated from head and Malpighian tubule RNA.

Dow, J.T., and Davies, S.A. (2003b). Integrative physiology and functional genomics of epithelial function in a genetic model organism. Physiol Rev *83*, 687-729.

Drain, P., Folkers, E., and Quinn, W.G. (1991). cAMP-dependent protein kinase and the disruption of learning in transgenic flies. Neuron *6*, 71-82.

Dudai, Y., Jan, Y.N., Byers, D., Quinn, W.G., and Benzer, S. (1976). dunce, a mutant of Drosophila deficient in learning. Proc Natl Acad Sci U S A *73*, 1684-1688.

Dushay, M.S., Asling, B., and Hultmark, D. (1996). Origins of immunity: Relish, a compound Rel-like gene in the antibacterial defense of Drosophila. Proc Natl Acad Sci U S A *93*, 10343-10347.

Evans, J., Day, J., Cabrero, P., JAT, D., and Davies, S. (2008). A new role for a classical gene: White transports cyclic GMP. The Journal of Experimental Biology, 211, 890-899.

Farazi, T.A., Waksman, G., and Gordon, J.I. (2001). The biology and enzymology of protein N-myristoylation. J Biol Chem *276*, 39501-39504.

Fawcett, L., Baxendale, R., Stacey, P., McGrouther, C., Harrow, I., Soderling, S., Hetman, J., Beavo, J., and Phillips, S. (2000). Molecular cloning and characterization of a distinct human phosphodiesterase gene family: PDE11A. PNAS, vol. 97, no. 97, 3702–3707.

Feany, M.B. (1990). Rescue of the learning defect in dunce, a Drosophila learning mutant, by an allele of rutabaga, a second learning mutant. Proc Natl Acad Sci U S A *87*, 2795-2799.

Feron, O., Dessy, C., Opel, D.J., Arstall, M.A., Kelly, R.A., and Michel, T. (1998). Modulation of the endothelial nitric-oxide synthase-caveolin interaction in cardiac myocytes. Implications for the autonomic regulation of heart rate. J Biol Chem *273*, 30249-30254.

Fesenko, E.E., Kolesnikov, S.S., and Lyubarsky, A.L. (1985). Induction by cyclic GMP of cationic conductance in plasma membrane of retinal rod outer segment. Nature *313*, 310-313.

Fink, T.L., Francis, S.H., Beasley, A., Grimes, K.A., and Corbin, J.D. (1999). Expression of an active, monomeric catalytic domain of the cGMP-binding cGMP-specific phosphodiesterase (PDE5). J Biol Chem *274*, 34613-34620.

Firestein, S., Zufall, F., and Shepherd, G.M. (1991). Single odor-sensitive channels in olfactory receptor neurons are also gated by cyclic nucleotides. J Neurosci *11*, 3565-3572.

Florio, S.K., Prusti, R.K., and Beavo, J.A. (1996). Solubilization of membrane-bound rod phosphodiesterase by the rod phosphodiesterase recombinant delta subunit. J Biol Chem *271*, 24036-24047.

Foley, E., and O'Farrell, P.H. (2003). Nitric oxide contributes to induction of innate immune responses to gram-negative bacteria in Drosophila. Genes Dev *17*, 115-125.

Forte, L.R., London, R.M., Freeman, R.H., and Krause, W.J. (2000). Guanylin peptides: renal actions mediated by cyclic GMP. Am J Physiol Renal Physiol *278*, F180-191.

Foster, J., Higgins, G., and Jackson, F. (1996a). Biochemical properties and cellular localization of the Drosophila DG1 cGMP-dependent protein kinase. J Biol Chem *271*, 23322-23328.

Foster, J.L., Higgins, G.C., and Jackson, F.R. (1996b). Biochemical properties and cellular localization of the Drosophila DG1 cGMP-dependent protein kinase. J Biol Chem *271*, 23322-23328.

Frame, M., Wan, K.F., Tate, R., Vandenabeele, P., and Pyne, N.J. (2001). The gamma subunit of the rod photoreceptor cGMP phosphodiesterase can modulate the proteolysis of two cGMP binding cGMP-specific phosphodiesterases (PDE6 and PDE5) by caspase-3. Cell Signal *13*, 735-741.

Francis, S.H., Turko, I.V., and Corbin, J.D. (2001). Cyclic nucleotide phosphodiesterases: relating structure and function. Prog Nucleic Acid Res Mol Biol *65*, 1-52.

Gamm, D.M., Francis, S.H., Angelotti, T.P., Corbin, J.D., and Uhler, M.D. (1995). The type II isoform of cGMP-dependent protein kinase is dimeric and possesses regulatory and catalytic properties distinct from the type I isoforms. J Biol Chem *270*, 27380-27388.

Giannakou, M.E., and Dow, J.A. (2001). Characterization of the Drosophila melanogaster alkali-metal/proton exchanger (NHE) gene family. J Exp Biol *204*, 3703-3716.

Gibbs, C., and Zoller, M. (1991). Rational scanning mutagenesis of a protein kinase identifies functional regions involved in catalysis and substrateinteractions. J Biol Chem *266*, 8923-8931.

Gibbs, S.M., Becker, A., Hardy, R.W., and Truman, J.W. (2001). Soluble guanylate cyclase is required during development for visual system function in Drosophila. J Neurosci *21*, 7705-7714.

Gillespie, P.G., and Beavo, J.A. (1988). Characterization of a bovine cone photoreceptor phosphodiesterase purified by cyclic GMP-sepharose chromatography. J Biol Chem *263*, 8133-8141.

Gillespie, P.G., Prusti, R.K., Apel, E.D., and Beavo, J.A. (1989). A soluble form of bovine rod photoreceptor phosphodiesterase has a novel 15-kDa subunit. J Biol Chem *264*, 12187-12193.

Giot, L., Bader, J., Brouwer, C., Chaudhuri, A., B, K., Y, L., YL, H., CE, O., B, G., E, V., *et al.* (2003). A protein interaction map of Drosophila melanogaster. Science *302*, 1727-1736.

Gomez-Diaz, C., Martin, F., and Alcorta, E. (2004). The cAMP transduction cascade mediates olfactory reception in Drosophila melanogaster. Behav Genet *34*, 395-406.

Gray, J.M., Karow, D.S., Lu, H., Chang, A.J., Chang, J.S., Ellis, R.E., Marletta, M.A., and Bargmann, C.I. (2004). Oxygen sensation and social feeding mediated by a C. elegans guanylate cyclase homologue. Nature *430*, 317-322.

Gross-Langenhoff, M., Hofbauer, J., Weber, J., Schultz, A., and Schultz, J. (2006). cAMP Is a Ligand for the Tandem GAF Domain of Human Phosphodiesterase 10 and cGMP for the Tandem GAF Domain of Phosphodiesterase 11. THE JOURNAL OF BIOLOGICAL CHEMISTRY, VOL. 281, NO. 285, pp. 2841–2846.

Gross-Langenhoff, M., Stenzl A, A.F., Schultz, A., and Schultz, J. (2008). The properties of phosphodiesterase 11A4 GAF domains are regulated by modifications in its N-terminal domain. FEBS *275*, 1643-1650.

Guo, Day, and Davies (2007). In situ hybridisation localises multiple rCGs to the main segment of the Malpighian tubule.

Guo, Y., Kotova, E., Chen, Z.S., Lee, K., Hopper-Borge, E., Belinsky, M.G., and Kruh, G.D. (2003). MRP8, ATP-binding cassette C11 (ABCC11), is a cyclic nucleotide efflux pump and a resistance factor for fluoropyrimidines 2',3'-dideoxycytidine and 9'-(2'-phosphonylmethoxyethyl)adenine. J Biol Chem *278*, 29509-29514.

Ha, E.M., Oh, C.T., Bae, Y.S., and Lee, W.J. (2005). A direct role for dual oxidase in Drosophila gut immunity. Science *310*, 847-850.

Hagiwara, M., Alberts, A., Brindle, P., Meinkoth, J., Feramisco, J., Deng, T., Karin, M., Shenolikar, S., and Montminy, M. (1992). Transcriptional attenuation following cAMP induction requires PP-1-mediated dephosphorylation of CREB. Cell *70*, 105-113.

Hancock, J.F., Cadwaller, K., Paterson, H., and Marshall, C.J. (1992). A CAAX or a CAAL motif and a second signal are sufficient for plasma membrane targeting of ras proteins. EMBO J. 10, 4033-4039. Trends Cell Biol *2*, 73.

Hancock, J.F., Magee, A.I., Childs, J.E., and Marshall, C.J. (1989). All ras proteins are polyisoprenylated but only some are palmitoylated. Cell *57*, 1167-1177.

Hancock, J.F., Paterson, H., and Marshall, C.J. (1990). A polybasic domain or palmitoylation is required in addition to the CAAX motif to localize p21ras to the plasma membrane. Cell *63*, 133-139.

Hanzal-Bayer, M., Renault, L., Roversi, P., Wittinghofer, A., and Hillig, R.C. (2002). The complex of Arl2-GTP and PDE delta: from structure to function. Embo J *21*, 2095-2106.

Hardman, J., and Sutherland, E. (1969a). Guanyl cyclase, an enzyme catalysing the formation of guanosine 3',5'-monophosphate from guanosine triphosphate. J Biol Chem, 244: 6368 - 6370.

Hardman, J.G., and Sutherland, E.W. (1969b). Guanyl cyclase, an enzyme catalyzing the formation of guanosine 3',5'-monophosphate from guanosine trihosphate. J Biol Chem *244*, 6363-6370.

Hata, Y., Kaibuchi, K., Kawamura, S., Hiroyoshi, M., Shirataki, H., and Takai, Y. (1991). Enhancement of the actions of smg p21 GDP/GTP exchange protein by the protein kinase A-catalyzed phosphorylation of smg p21. J Biol Chem *266*, 6571-6577.

Havel, C.M., Fisher, P., and Watson, J.A. (1992). Isopentenoid synthesis in embryonic Drosophila cells: prenylated protein profile and prenyl group usage. Arch Biochem Biophys *295*, 410-420.

Hayashi, M., Matsushima, K., Ohashi, H., Tsunoda, H., Murase, S., Kawarada, Y., and Tanaka, T. (1998). Molecular cloning and characterization of human PDE8B, a novel thyroid-specific isozyme of 3',5'-cyclic nucleotide phosphodiesterase. Biochem Biophys Res Commun *250*, 751-756.

Hayashi, M., Shimada, Y., Nishimura, Y., Hama, T., and Tanaka, T. (2002). Genomic organization, chromosomal localization, and alternative splicing of the human phosphodiesterase 8B gene. Biochem Biophys Res Commun *297*, 1253-1258.

Hayes, J., and Brunton, L. (1982). Functional compartments in cyclic nucleotide action. J Cyclic Nucleotide Res, 8, 1–16.

Hayes, J., Brunton, L., and Mayer, S. (1980). Selective activation of particulate cAMP-dependent protein kinase by isoproterenol and prostaglandin E1. J Biol Chem, 255, 5113–5119.

Hazelrigg, T., Levis, R., and Rubin, G.M. (1984). Transformation of white locus DNA in drosophila: dosage compensation, zeste interaction, and position effects. Cell *36*, 469-481.

Heath, C.M., Stahl, P.D., and Barbieri, M.A. (2003). Lipid kinases play crucial and multiple roles in membrane trafficking and signaling. Histol Histopathol *18*, 989-998.

Hedengren, M., Asling, B., Dushay, M.S., Ando, I., Ekengren, S., Wihlborg, M., and Hultmark, D. (1999). Relish, a central factor in the control of humoral but not cellular immunity in Drosophila. Mol Cell *4*, 827-837.

Heil, W.G., Landgraf, W., and Hofmann, F. (1987). A catalytically active fragment of cGMP-dependent protein kinase. Occupation of its cGMP-binding sites does not affect its phosphotransferase activity. Eur J Biochem *168*, 117-121.

Heine, H., and Lien, E. (2003). Toll-like receptors and their function in innate and adaptive immunity. Int Arch Allergy Immunol *130*, 180-192.

Herberg, F.W., Maleszka, A., Eide, T., Vossebein, L., and Tasken, K. (2000). Analysis of A-kinase anchoring protein (AKAP) interaction with protein kinase A (PKA) regulatory subunits: PKA isoform specificity in AKAP binding. J Mol Biol *298*, 329-339.

Hetman, J., Robas, N., Baxendale, R., Fidock, M., Phillips, S., Soderling, S., and Beavo, J. (2000a). Cloning and characterization of two splice variants of human phosphodiesterase 11A. PNAS, vol. 97 no. 23 12891-12895.

Hetman, J.M., Soderling, S.H., Glavas, N.A., and Beavo, J.A. (2000b). Cloning and characterization of PDE7B, a cAMP-specific phosphodiesterase. Proc Natl Acad Sci U S A *97*, 472-476.

Hingorani, V.N., Tobias, D.T., Henderson, J.T., and Ho, Y.K. (1988). Chemical cross-linking of bovine retinal transducin and cGMP phosphodiesterase. J Biol Chem *263*, 6916-6926.

Hinton, R., and Mullock, B. (1996). Isolation of subcellular fractions. In Subcellular fractionation: A practical approach, J. Graham, and D. Rickwood, eds. (IRL Press), pp. 31-69.

Hirose, T., Nakano, Y., Nagamatsu, Y., Misumi, T., Ohta, H., and Ohshima, Y. (2003). Cyclic GMP-dependent protein kinase EGL-4 controls body size and lifespan in C elegans. Development *130*, 1089-1099.

Ho, Y.S., Burden, L.M., and Hurley, J.H. (2000). Structure of the GAF domain, a ubiquitous signaling motif and a new class of cyclic GMP receptor. Embo J *19*, 5288-5299.

Hoffmann, R., Baillie, G.S., MacKenzie, S.J., Yarwood, S.J., and Houslay, M.D. (1999). The MAP kinase ERK2 inhibits the cyclic AMP-specific phosphodiesterase HSPDE4D3 by phosphorylating it at Ser579. EMBO J *18*, 893-903.

Hofmann, F., Bechtel, P.J., and Krebs, E.G. (1977). Concentrations of cyclic AMP-dependent protein kinase subunits in various tissues. J Biol Chem *252*, 1441-1447.

Hofmann, F., Bernhard, D., Lukowski, R., and Weinmeister, P. (2009). cGMP Regulated Protein Kinases (cGK). In cGMP: Generators, Effectors and therapeutic implications (Springer Berlin Heidelberg), pp. 137-162.

Hofmann, F., Feil, R., Kleppisch, T., and Schlossmann, J. (2006). Function of cGMP-dependent protein kinases as revealed by gene deletion. Physiol Rev *1*, 1-23.

Honda, A., Adams, S., Sawyer, C., Lev-Ram, V., Tsien, R., and Dostmann, W. (2001). Spatiotemporal dynamics of guanosine 3',5'-cyclic monophosphate revealed by a genetically encoded, fluorescent indicator. Proc Natl Acad Sci U S A *98*, 2437-2442.

Honda, A., Moosmeier, M., and Dostmann, W. (2005). Membrane-permeable cygnets: rapid cellular internalization of fluorescent cGMP-indicators. Front Biosci *10*, 1290-1301.

Horiuchi, J., Yamazaki, D., Naganos, S., Aigaki, T., and Saitoe, M. (2008). Protein kinase A inhibits a consolidated form of memory in Drosophila. Proc Natl Acad Sci U S A *105*, 20976-20981.

Horvath, A., Giatzakis, C., Robinson-White, A., Boikos, S., Levine, E., Griffin, K., Stein, E., Kamvissi, V., Soni, P, Bossis, I., de Herder, W., *et al.* (2006). Adrenal Hyperplasia and Adenomas Are Associated with Inhibition of Phosphodiesterase 11A in Carriers of PDE11A Sequence Variants That Are Frequent in the Population. Cancer Research, 66, 11571.

Horvath, A., Korde, L., Greene, M.H., Libe, R., Osorio, P., Faucz, F.R., Raffin-Sanson, M.L., Tsang, K.M., Drori-Herishanu, L., Patronas, Y., *et al.* (2009). Functional phosphodiesterase 11A mutations may modify the risk of familial and bilateral testicular germ cell tumors. Cancer Res *69*, 5301-5306.

Houslay, M.D. (2001). PDE4 cAMP-specific phosphodiesterases. Prog Nucleic Acid Res Mol Biol *69*, 249-315.

Houslay, M.D., and Milligan, G. (1997). Tailoring cAMP-signalling responses through isoform multiplicity. Trends Biochem Sci *22*, 217-224.

Huai, Q., Liu, Y., Francis, S.H., Corbin, J.D., and Ke, H. (2004a). Crystal structures of phosphodiesterases 4 and 5 in complex with inhibitor 3-isobutyl-1-methylxanthine suggest a conformation determinant of inhibitor selectivity. J Biol Chem *279*, 13095-13101.

Huai, Q., Wang, H., Zhang, W., Colman, R.W., Robinson, H., and Ke, H. (2004b). Crystal structure of phosphodiesterase 9 shows orientation variation of inhibitor 3-isobutyl-1-methylxanthine binding. Proc Natl Acad Sci U S A *101*, 9624-9629.

Huang, S.H., Rio, D.C., and Marletta, M.A. (2007). Ligand binding and inhibition of an oxygen-sensitive soluble guanylate cyclase, Gyc-88E, from Drosophila. Biochemistry *46*, 15115-15122.

Iversen, A., Cazzamali, G., Williamson, M., Hauser, F., and Grimmelikhuijzen, C.J. (2002). Molecular cloning and functional expression of a Drosophila receptor for the neuropeptides capa-1 and -2. Biochem Biophys Res Commun *299*, 628-633.

Janeway, C.A., Jr. (1989). Approaching the asymptote? Evolution and revolution in immunology. Cold Spring Harb Symp Quant Biol *54 Pt 1*, 1-13.

Jarchau, T., Hausler, C., Markert, T., Pohler, D., Vanderkerckhove, J., De Jonge, H.R., Lohmann, S.M., and Walter, U. (1994). Cloning, expression, and in situ localization of rat intestinal cGMP-dependent protein kinase II. Proc Natl Acad Sci U S A *91*, 9426-9430.

Jedlitschky, G., Burchell, B., and Keppler, D. (2000). The Multidrug Resistance Protein 5 (MRP5) Functions as an ATP-dependent Export Pump for Cyclic Nucleotides. J Biol Chem, 275, 30069-30074.

JL., B. (2006). Epac proteins: multi-purpose cAMP targets. Trends Biochem Sci *31*, 680-686.

Jordan, J.D., Landau, E.M., and Iyengar, R. (2000). Signaling networks: the origins of cellular multitasking. Cell *103*, 193-200.

Kalderon, D., and Rubin, G.M. (1989). cGMP-dependent protein kinase genes in Drosophila. J Biol Chem *264*, 10738-10748.

Kalidas, S., and Smith, D.P. (2002). Novel genomic cDNA hybrids produce effective RNA interference in adult Drosophila. Neuron *33*, 177-184.

Kannan, N., Haste, N., Taylor, S.S., and Neuwald, A.F. (2007). The hallmark of AGC kinase functional divergence is its C-terminal tail, a cis-acting regulatory module. Proc Natl Acad Sci U S A *104*, 1272-1277.

Kaupp, B., and Seifert, R. (2002a). Cyclic Nucleotide-Gated Ion Channels. Physiol Rev, 82: 769–824.

Kaupp, U.B., Niidome, T., Tanabe, T., Terada, S., Bonigk, W., Stuhmer, W., Cook, N.J., Kangawa, K., Matsuo, H., Hirose, T., *et al.* (1989). Primary structure and functional expression from complementary DNA of the rod photoreceptor cyclic GMP-gated channel. Nature *342*, 762-766.

Kaupp, U.B., and Seifert, R. (2002b). Cyclic nucleotide-gated ion channels. Physiol Rev *82*, 769-824.

Kawasaki, H., Springett, G.M., Mochizuki, N., Toki, S., Nakaya, M., Matsuda, M., Housman, D.E., and Graybiel, A.M. (1998). A family of cAMP-binding proteins that directly activate Rap1. Science *282*, 2275-2279.

Kean, L., Cazenave, W., Costes, L., Broderick, K., S, G., Pollock, V., Davies, S., Veenstra, J., and Dow, J. (2002a). Two nitridergic peptides are encoded by the gene capability in Drosophila melanogaster. Am J Physiol Regul Integr Comp Physiol *282*, 1297-1307.

Kean, L., Cazenave, W., Costes, L., Broderick, K.E., Graham, S., Pollock, V.P., Davies, S.A., Veenstra, J.A., and Dow, J.A. (2002b). Two nitridergic peptides are encoded by the gene capability in Drosophila melanogaster. Am J Physiol Regul Integr Comp Physiol *282*, R1297-1307.

Kennerdell, J.R., and Carthew, R.W. (2000). Heritable gene silencing in Drosophila using double-stranded RNA. Nat Biotechnol *18*, 896-898.

Kerr, M., Davies, S.A., and Dow, J.A. (2004). Cell-specific manipulation of second messengers; a toolbox for integrative physiology in Drosophila. Curr Biol *14*, 1468-1474.

Kiger, J.A., Jr., Davis, R.L., Salz, H., Fletcher, T., and Bowling, M. (1981). Genetic analysis of cyclic nucleotide phosphodiesterases in Drosophila melanogaster. Adv Cyclic Nucleotide Res *14*, 273-288.

Kiger, J.A., Jr., and Golanty, E. (1977). A cytogenetic analysis of cyclic nucleotide phosphodiesterase activities in Drosophila. Genetics *85*, 609-622.

Kiger, J.A., Jr., and Golanty, E. (1979). A genetically distinct form of cyclic AMP phosphodiesterase associated with chromomere 3D4 in Drosophila melanogaster. Genetics *91*, 521-535.

Kitayama, H., Sugimoto, Y., Matsuzaki, T., Ikawa, Y., and Noda, M. (1989). A ras-related gene with transformation suppressor activity. Cell *56*, 77-84.

Kleppisch, T., and Feil, R. (2009). cGMP signalling in the mammalian brain: role in synaptic plasticity and behaviour. Handb Exp Pharmacol, 549-579.

Kobayashi, T., Gamanuma, M., Sasaki, T., Yamashita, Y., Yuasa, K., Kotera, J., and Omori, K. (2003). Molecular comparison of rat cyclic nucleotide phosphodiesterase 8 family: unique expression of PDE8B in rat brain. Gene *319*, 21-31.

Kobialka, M., and Gorczyca, W.A. (2000). Particulate guanylyl cyclases: multiple mechanisms of activation. Acta Biochim Pol *47*, 517-528.

Koglin, M., Vehse, K., Budaeus, L., H, S., and Behrends, S. (2001). Nitric oxide activates the beta 2 subunit of soluble guanylyl cyclase in the absence of a second subunit. J Biol Chem *276*, 30737-30743.

Kotera, J., Sasaki, T., Kobayashi, T., Fujishige, K., Yamashita, Y., and Omori, K. (2004). Subcellular localization of cyclic nucleotide phosphodiesterase type 10A variants, and alteration of the localization by cAMP-dependent protein kinase-dependent phosphorylation. J Biol Chem *279*, 4366-4375.

Kramer, A., Volkmer-Engert, R., Malin, R., Reineke, U., and Schneider-Mergener, J. (1993). Simultaneous synthesis of peptide libraries on single resin and continuous cellulose membrane supports: examples for the identification of protein, metal and DNA binding peptide mixtures. Pept Res *Nov-Dec;6(6)*, 314-319.

Krause, M., Dent, E.W., Bear, J.E., Loureiro, J.J., and Gertler, F.B. (2003). Ena/VASP proteins: regulators of the actin cytoskeleton and cell migration. Annu Rev Cell Dev Biol *19*, 541-564.

Kruse, L., Møller, M., Tibaek, M., Gammeltoft, S., Olesen, J., and Kruuse, C. (2009). PDE9A, PDE10A, and PDE11A expression in rat trigeminovascular pain signalling system. Brain Res *1281*, 25-34.

Kuhn, M. (2004). Molecular physiology of natriuretic peptide signalling. Basic Res Cardiol *99*, 76-82.

Kuo, J., and Greengard, P. (1970). Cyclic nucleotide-dependent protein kinases. VI. Isolation and partial purification of a protein kinase activated by guanosine 3',5'-monophosphate. J Biol Chem, 245;2493-2498.

Kuo, J.F. (1974). Guanosine 3':5'-monophosphate-dependent protein kinases in mammalian tissues. Proc Natl Acad Sci U S A *71*, 4037-4041.

Kuzin, B., Roberts, I., Peunova, N., and Enikolopov, G. (1996). Nitric oxide regulates cell proliferation during Drosophila development. Cell *87*, 639-649.

Körschen, H., Beyermann, M., Müller, F., Heck, M., Vantler, M., Koch, K., Kellner, R., Wolfrum, U., Bode, C., Hofmann, K., *et al.* (1999). Interaction of glutamic-acid-rich proteins with the cGMP signalling pathway in rod photoreceptors. Nature *400*, 761-766.

Langosch, D., and Heringa, J. (1998). Interaction of transmembrane helices by a knobs-into-holes packing characteristic of soluble coiled coils. Proteins *31*, 150-159.

Lanning, C.C., Daddona, J.L., Ruiz-Velasco, R., Shafer, S.H., and Williams, C.L. (2004). The Rac1 C-terminal polybasic region regulates the nuclear localization and protein degradation of Rac1. J Biol Chem *279*, 44197-44210.

Lannutti, B.J., and Schneider, L.E. (2001). Gprk2 controls cAMP levels in Drosophila development. Dev Biol *233*, 174-185.

Lemaitre, B., Kromer-Metzger, E., Michaut, L., Nicolas, E., Meister, M., Georgel, P., Reichhart, J.M., and Hoffmann, J.A. (1995a). A recessive mutation, immune deficiency (imd), defines two distinct control pathways in the Drosophila host defense. Proc Natl Acad Sci U S A *92*, 9465-9469.

Lemaitre, B., Meister, M., Govind, S., Georgel, P., Steward, R., Reichhart, J.M., and Hoffmann, J.A. (1995b). Functional analysis and regulation of nuclear import of dorsal during the immune response in Drosophila. EMBO J *14*, 536-545.

Lerner, E.C., Qian, Y., Hamilton, A.D., and Sebti, S.M. (1995). Disruption of oncogenic K-Ras4B processing and signaling by a potent geranylgeranyltransferase I inhibitor. J Biol Chem *270*, 26770-26773.

Letunic, I., Copley, R., Pils, B., Pinkert, S., Schultz, J., and Bork, P. (2006). SMART 5: domains in the context of genomes and networks. Nucleic Acids Res *34*, D257-260.

Levine, J.D., Casey, C.I., Kalderon, D.D., and Jackson, F.R. (1994). Altered circadian pacemaker functions and cyclic AMP rhythms in the Drosophila learning mutant dunce. Neuron *13*, 967-974.

Li, W., Tully, T., and Kalderon, D. (1996). Effects of a conditional Drosophila PKA mutant on olfactory learning and memory. Learn Mem *2*, 320-333.

Libe, R., Fratticci, A., Coste, J., Tissier, F., Horvath, A., Ragazzon, B., Rene-Corail, F., Groussin, L., Bertagna, X., Raffin-Sanson, M.L., *et al.* (2008). Phosphodiesterase 11A (PDE11A) and genetic predisposition to adrenocortical tumors. Clin Cancer Res *14*, 4016-4024.

Limbird, L.E., and Lefkowitz, R.J. (1977). Resolution of beta-adrenergic receptor binding and adenylate cyclase activity by gel exclusion chromatography. J Biol Chem *252*, 799-802.

Lincoln, T.M., Cornwell, T.L., and Taylor, A.E. (1990). cGMP-dependent protein kinase mediates the reduction of Ca2+ by cAMP in vascular smooth muscle cells. Am J Physiol *258*, C399-407.

Lincoln, T.M., Komalavilas, P., and Cornwell, T.L. (1994). Pleiotropic regulation of vascular smooth muscle tone by cyclic GMP-dependent protein kinase. Hypertension *23*, 1141-1147.

Lipkin, D., Cook, W.H., and Markham, R. (1959). Adenosine-3':5'-phosphoric acid: A proof of structure. J Am Chem Soc *81*, 6198-6203.

Littleton, J.T., and Ganetzky, B. (2000). Ion channels and synaptic organization: analysis of the Drosophila genome. Neuron *26*, 35-43.

Liu, C., Ding, J.M., Faiman, L.E., and Gillette, M.U. (1997). Coupling of muscarinic cholinergic receptors and cGMP in nocturnal regulation of the suprachiasmatic circadian clock. J Neurosci *17*, 659-666.

Lohmann, S.M., Vaandrager, A.B., Smolenski, A., Walter, U., and De Jonge, H.R. (1997). Distinct and specific functions of cGMP-dependent protein kinases. Trends Biochem Sci *22*, 307-312.

Lohse, M., Bünemann, M., Hoffmann, C., Vilardaga, J., and Nikolaev, V. (2007). Monitoring receptor signaling by intramolecular FRET. Curr Opin Pharmacol *7*, 547-553.

Lopez, M., Garbers, D., and Kuhn, M. (1997). The guanylyl cyclase-deficient mouse defines differential pathways of natriuretic peptide signaling. J Biol Chem, 23064-23068.

Loughney, K., Martins, T.J., Harris, E.A., Sadhu, K., Hicks, J.B., Sonnenburg, W.K., Beavo, J.A., and Ferguson, K. (1996). Isolation and characterization of cDNAs corresponding to two human calcium, calmodulin-regulated, 3',5'-cyclic nucleotide phosphodiesterases. J Biol Chem *271*, 796-806.

Loughney, K., Taylor, J., and Florio, V.A. (2005). 3',5'-cyclic nucleotide phosphodiesterase 11A: localization in human tissues. Int J Impot Res *17*, 320-325.

Lucas, K.A., Pitari, G.M., Kazerounian, S., Ruiz-Stewart, I., Park, J., Schulz, S., Chepenik, K.P., and Waldman, S.A. (2000). Guanylyl cyclases and signaling by cyclic GMP. Pharmacol Rev *52*, 375-414.

Luo, H.R., Wu, G.S., Dong, C., Arcos-Burgos, M., Ribeiro, L., Licinio, J., and Wong, M.L. (2009). Association of PDE11A global haplotype with major depression and antidepressant drug response. Neuropsychiatr Dis Treat *5*, 163-170.

Lupas, A. (1997). Predicting coiled-coil regions in proteins. Curr Opin Struct Biol *7*, 388-393.

Lupas, A., Van Dyke, M., and Stock, J. (1991). Predicting coiled coils from protein sequences. Science *252*, 1162-1164.

M, A., Shah, and MacCarthy, P.A. (2000). Paracrine and autocrine effects of nitric oxide on myocardial function. Pharmacology & Therapeutics, 86, 49–86.

MacKenzie, S.J., Baillie, G.S., McPhee, I., Bolger, G.B., and Houslay, M.D. (2000). ERK2 mitogen-activated protein kinase binding, phosphorylation, and regulation of the PDE4D cAMP-specific phosphodiesterases. The involvement of COOH-terminal docking sites and NH2-terminal UCR regions. J Biol Chem *275*, 16609-16617.

MacKenzie, S.J., Baillie, G.S., McPhee, I., MacKenzie, C., Seamons, R., McSorley, T., Millen, J., Beard, M.B., van Heeke, G., and Houslay, M.D. (2002). Long PDE4 cAMP specific phosphodiesterases are activated by protein kinase A-mediated phosphorylation of a single serine residue in Upstream Conserved Region 1 (UCR1). Br J Pharmacol *136*, 421-433.

MacMillan-Crow, L.A., and Lincoln, T.M. (1994). High-affinity binding and localization of the cyclic GMP-dependent protein kinase with the intermediate filament protein vimentin. Biochemistry *33*, 8035-8043.

MacPherson, Davies, and Nimmo (2004a). DG2 purifies as a dimer under gel filtration.

Macpherson, M., and Day, J. (2004). DG2P1 and DG2P2 overexpression in tubule principal cells causes a significant reduction in endogenous PDE activity

Macpherson, M., and Day, J. (2005). flies overexpressing DG2P1 and DG2P2 in tubule principal cells show a drastic reduction in endogenous tubule PDE activity.

MacPherson, M.R., Broderick, K.E., Graham, S., Day, J.P., Houslay, M.D., Dow, J.A., and Davies, S.A. (2004b). The dg2 (for) gene confers a renal phenotype in Drosophila by modulation of cGMP-specific phosphodiesterase. J Exp Biol *207*, 2769-2776.

MacPherson, M.R., Lohmann, S.M., and Davies, S.A. (2004c). Analysis of Drosophila cGMP-dependent protein kinases and assessment of their in vivo roles by targetted expression in a renal transporting epithelium. J Biol Chem.

MacPherson, M.R., Pollock, V.P., Broderick, K.E., Kean, L., O'Connell, F.C., Dow, J.A., and Davies, S.A. (2001). Model organisms: new insights into ion channel and transporter function. L-type calcium channels regulate epithelial fluid transport in Drosophila melanogaster. Am J Physiol Cell Physiol *280*, C394-407.

Malva, C., Graziani, F., Gargiulo, G., and Manzi, A. (1994). Cell functions in Drosophila oogenesis. Genetica *94*, 115-126.

Manganiello, V.C., Murata, T., Taira, M., Belfrage, P., and Degerman, E. (1995). Diversity in cyclic nucleotide phosphodiesterase isoenzyme families. Arch Biochem Biophys *322*, 1-13.

Manthorpe, M., and McConnell, D.G. (1975). Cyclic nucleotide phosphodiesterases associated with bovine retinal outer-segment fragments. Biochim Biophys Acta *403*, 438-445.

Marchmont, R.J., and Houslay, M.D. (1980). Insulin trigger, cyclic AMP-dependent activation and phosphorylation of a plasma membrane cyclic AMP phosphodiesterase. Nature *286*, 904-906.

Markert, T., Vaandrager, A., Gambaryan, S., Pöhler, D., Häusler, C., Walter, U., De Jonge, H., Jarchau, T., and Lohmann, S. (1995). Endogenous expression of type II cGMP-dependent protein kinase mRNA and protein in rat intestine. Implications for cystic fibrosis transmembrane conductance regulator. J Clin Invest *96*, 822-830.

Marletta, M.A., and Spiering, M.M. (2003). Trace elements and nitric oxide function. J Nutr *133*, 1431S-1433S.

Martinez, S.E., Beavo, J.A., and Hol, W.G. (2002a). GAF domains: two-billion-year-old molecular switches that bind cyclic nucleotides. Mol Interv *2*, 317-323.

Martinez, S.E., Wu, A.Y., Glavas, N.A., Tang, X.B., Turley, S., Hol, W.G., and Beavo, J.A. (2002b). The two GAF domains in phosphodiesterase 2A have distinct roles in dimerization and in cGMP binding. Proc Natl Acad Sci U S A *99*, 13260-13265.

Martins, T.J., Mumby, M.C., and Beavo, J.A. (1982). Purification and characterization of a cyclic GMP-stimulated cyclic nucleotide phosphodiesterase from bovine tissues. J Biol Chem *257*, 1973-1979.

Mashimo, H., and Goyal, R.K. (1999). Lessons from genetically engineered animal models. IV. Nitric oxide synthase gene knockout mice. Am J Physiol *277*, G745-750.

Matthiesen, K., and Nielsen, J. (2009). Binding of cyclic nucleotides to phosphodiesterase 10A and 11A GAF domains does not stimulate catalytic activity. Biochem J *423*, 401-409.

McGettigan, J., McLennan, R.K., Broderick, K.E., Kean, L., Allan, A.K., Cabrero, P., Regulski, M.R., Pollock, V.P., Gould, G.W., Davies, S.A., *et al.* (2005). Insect renal tubules constitute a cell-autonomous immune system that protects the organism against bacterial infection. Insect Biochem Mol Biol *35*, 741-754.

McNeil, L., Chinkers, M., and Forte, M. (1995). Identification, characterization, and developmental regulation of a receptor guanylyl cyclase expressed during early stages of Drosophila development. J Biol Chem *270*, 7189-7196.

McSorley, T., Stefan, E., Henn, V., Wiesner, B., Baillie, G.S., Houslay, M.D., Rosenthal, W., and Klussmann, E. (2006). Spatial organisation of AKAP18 and PDE4 isoforms in renal collecting duct principal cells. Eur J Cell Biol *85*, 673-678.

Meister, M. (2004). Blood cells of Drosophila: cell lineages and role in host defence. Curr Opin Immunol *16*, 10-15.

Miki, N., Baraban, J., Keirns, J., Boyce, J., and and Bitensky, M. (1975a). Purification and properties of the light-activated cyclic nucleotide phosphodiesterase of rod outer segments. J Biol Chem, 250: 6320 - 6372.

Miki, N., Baraban, J.M., Keirns, J.J., Boyce, J.J., and Bitensky, M.W. (1975b). Purification and properties of the light-activated cyclic nucleotide phosphodiesterase of rod outer segments. J Biol Chem *250*, 6320-6327.

Millul, V., Prié, D., Géniteau-Legendre, M., Verpont, M., Baudouin, B., and Ronco, P. (1996). ANP-stimulated cGMP egression in renal principal cells: abrogation of polarity by SV40 large T. Am J Physiol, 270(274 Pt 271):C1051-1060.

Miyazu, M., Tanimura, T., and Sokabe, M. (2000). Molecular cloning and characterization of a putative cyclic nucleotide-gated channel from Drosophila melanogaster. Insect Mol Biol *9*, 283-292.

Mizuno, T., Kaibuchi, K., Yamamoto, T., Kawamura, M., Sakoda, T., Fujioka, H., Matsuura, Y., and Takai, Y. (1991). A stimulatory GDP/GTP exchange protein for smg p21 is active on the post-translationally processed form of c-Ki-ras p21 and rhoA p21. Proc Natl Acad Sci U S A *88*, 6442-6446.

Monken, C., and Gill, G. (1985). A comparison of the cyclic nucleotide-dependent protein kinases using chemical cleavage at tryptophan and cysteine. Arch Biochem Biophys, Aug 1;240(242):888-903.

Morgan, T.H. (1910). SEX LIMITED INHERITANCE IN DROSOPHILA. Science *32*, 120-122.

Morin, F., Lugnier, C., Kameni, J., and Voisin, P. (2001). Expression and role of phosphodiesterase 6 in the chicken pineal gland. J Neurochem *78*, 88-99.

Morton, D., and Hudson, M. (2002). Cyclic GMP regulation and function in insects. Advances in Insect Physiology *29*, 1–54.

Morton, D., Langlais, K., Stewart, J., and Vermehren, A. (2005). Comparison of the properties of the five soluble guanylyl cyclase subunits in Drosophila melanogaster. J Insect Sci *5*, 12.

Morton, D., Stewart, J., Langlais, K., Clemens-Grisham, R., and Vermehren, A. (2008). Synaptic transmission in neurons that express the Drosophila atypical soluble guanylyl

cyclases, Gyc-89Da and Gyc-89Db, is necessary for the successful completion of larval and adult ecdysis. J Exp Biol *211*, 1645-1656.

Morton, D.B. (2004). Atypical soluble guanylyl cyclases in Drosophila can function as molecular oxygen sensors. J Biol Chem *279*, 50651-50653.

Mou, H., Grazio, H.J., 3rd, Cook, T.A., Beavo, J.A., and Cote, R.H. (1999). cGMP binding to noncatalytic sites on mammalian rod photoreceptor phosphodiesterase is regulated by binding of its gamma and delta subunits. J Biol Chem *274*, 18813-18820.

Muradov, K.G., Boyd, K.K., Martinez, S.E., Beavo, J.A., and Artemyev, N.O. (2003). The GAFa domains of rod cGMP-phosphodiesterase 6 determine the selectivity of the enzyme dimerization. J Biol Chem *278*, 10594-10601.

Muta, T., and Iwanaga, S. (1996). The role of hemolymph coagulation in innate immunity. Curr Opin Immunol *8*, 41-47.

Nagel, D., Aizawa, T., Jeon, K., Liu, W., Mohan, A., Wei, H., Miano, J., Florio, V., Gao, P., Korshunov, V., *et al.* (2006). Role of nuclear Ca2+/calmodulin-stimulated phosphodiesterase 1A in vascular smooth muscle cell growth and survival. Circ Res *98*, 777-784.

Nakamura, T., and Gold, G.H. (1987). A cyclic nucleotide-gated conductance in olfactory receptor cilia. Nature *325*, 442-444.

Nakane, M., Arai, K., Saheki, S., Kuno, T., Buechler, W., and Murad, F. (1990). Molecular cloning and expression of cDNAs coding for soluble guanylate cyclase from rat lung. J Biol Chem *265*, 16841-16845.

Nancy, V., Callebaut, I., El Marjou, A., and de Gunzburg, J. (2002). The delta subunit of retinal rod cGMP phosphodiesterase regulates the membrane association of Ras and Rap GTPases. J Biol Chem *277*, 15076-15084.

Nappi, A.J., and Vass, E. (1993). Melanogenesis and the generation of cytotoxic molecules during insect cellular immune reactions. Pigment Cell Res *6*, 117-126.

Nappi, A.J., Vass, E., Frey, F., and Carton, Y. (2000). Nitric oxide involvement in Drosophila immunity. Nitric Oxide *4*, 423-430.

Nausch, L., Ledoux, J., Bonev, A., Nelson, M., and Dostmann, W. (2008). Differential patterning of cGMP in vascular smooth muscle cells revealed by single GFP-linked biosensors. Proc Natl Acad Sci U S A *105*, 365-370.

Netherton, S.J., Sutton, J.A., Wilson, L.S., Carter, R.L., and Maurice, D.H. (2007). Both protein kinase A and exchange protein activated by cAMP coordinate adhesion of human vascular endothelial cells. Circ Res *101*, 768-776.

Nighorn, A., Healy, M.J., and Davis, R.L. (1991). The cyclic AMP phosphodiesterase encoded by the Drosophila dunce gene is concentrated in the mushroom body neuropil. Neuron *6*, 455-467.

Nikolaev, V., Gambaryan, S., and Lohse, M. (2006). Fluorescent sensors for rapid monitoring of intracellular cGMP. Nat Methods *3*, 23-25.

Nomura, K., Kanemura, H., Satoh, T., and Kataoka, T. (2004). Identification of a novel domain of Ras and Rap1 that directs their differential subcellular localizations. J Biol Chem *279*, 22664-22673.

Norton, A.W., D'Amours, M.R., Grazio, H.J., Hebert, T.L., and Cote, R.H. (2000). Mechanism of transducin activation of frog rod photoreceptor phosphodiesterase. Allosteric interactiona between the inhibitory gamma subunit and the noncatalytic cGMP-binding sites. J Biol Chem *275*, 38611-38619.

Norton, A.W., Hosier, S., Terew, J., Li, N., Dhingra, A., Vardi, N., Baehr, W., and Cote, R. (2004). Evaluation of the 17 kDa prenyl binding protein as a regulatory protein for phototransduction in retinal photoreceptors. J Biol Chem, M410475200.

O'Donnell, M.J., and Maddrell, S.H. (1995). Fluid reabsorption and ion transport by the lower Malpighian tubules of adult female Drosophila. J Exp Biol *198 (Pt 8)*, 1647-1653.

O'Donnell, M.J., Rheault, M.R., Davies, S.A., Rosay, P., Harvey, B.J., Maddrell, S.H., Kaiser, K., and Dow, J.A. (1998). Hormonally controlled chloride movement across Drosophila tubules is via ion channels in stellate cells. Am J Physiol *274*, R1039-1049.

O'Kane, C.J., and Gehring, W.J. (1987). Detection in situ of genomic regulatory elements in Drosophila. Proc Natl Acad Sci U S A *84*, 9123-9127.

Omori, K., and Kotera, J. (2007). Overview of PDEs and their regulation. Circ Res *100*, 309-327.

Ong, O.C., Ota, I.M., Clarke, S., and Fung, B.K. (1989). The membrane binding domain of rod cGMP phosphodiesterase is posttranslationally modified by methyl esterification at a C-terminal cysteine. Proc Natl Acad Sci U S A *86*, 9238-9242.

Osborne, K., Robichon, A., Burgess, E., Butland RA, S, S., Coulthard, A., Pereira, H., Greenspan, R., and Sokolowski, M. (1997a). Natural Behavior Polymorphism Due to a cGMP-Dependent Protein Kinase of Drosophila. Science, Vol. 277. no. 5327, pp. 5834 - 5836.

Osborne, K.A., Robichon, A., Burgess, E., Butland, S., Shaw, R.A., Coulthard, A., Pereira, H.S., Greenspan, R.J., and Sokolowski, M.B. (1997b). Natural behavior polymorphism due to a cGMP-dependent protein kinase of Drosophila. Science *277*, 834-836.

Oster, H., Werner, C., Magnone, M.C., Mayser, H., Feil, R., Seeliger, M.W., Hofmann, F., and Albrecht, U. (2003). cGMP-dependent protein kinase II modulates mPer1 and mPer2 gene induction and influences phase shifts of the circadian clock. Curr Biol *13*, 725-733.

Patel, M., Wypij, D., Rose, D., Rimele, T., and Wiseman, J. (1995). Secretion of cyclic GMP by cultured epithelial and fibroblast cell lines in response to nitric oxide. J Pharmacol Exp Ther, 273(271):216-225.

Pawson, T., and Nash, P. (2003). Assembly of cell regulatory systems through protein interaction domains. Science *300*, 445-452.

Pawson, T., and Scott, J.D. (1997). Signaling through scaffold, anchoring, and adaptor proteins. Science *278*, 2075-2080.

Pereira, H.S., and Sokolowski, M.B. (1993). Mutations in the larval foraging gene affect adult locomotory behavior after feeding in Drosophila melanogaster. Proc Natl Acad Sci U S A *90*, 5044-5046.

Perez-Sala, D., Cernuda-Morollon, E., Diaz-Cazorla, M., Rodriguez-Pascual, F., and Lamas, S. (2001). Posttranscriptional regulation of human iNOS by the NO/cGMP pathway. Am J Physiol Renal Physiol *280*, F466-473.

Piggott, L.A., Hassell, K.A., Berkova, Z., Morris, A.P., Silberbach, M., and Rich, T.C. (2006). Natriuretic peptides and nitric oxide stimulate cGMP synthesis in different cellular compartments. J Gen Physiol *128*, 3-14.

Pollock, V.P., McGettigan, J., Cabrero, P., Maudlin, I.M., Dow, J.A., and Davies, S.A. (2004). Conservation of capa peptide-induced nitric oxide signalling in Diptera. J Exp Biol *207*, 4135-4145.

Pomara, G., and Morelli, G. (2005). Inhibition of phosphodiesterase 11 (PDE11) impacts on sperm quality. Int J Impot Res *17*, 385-386; author reply 387.

Ponting, C.P., and Aravind, L. (1997). PAS: a multifunctional domain family comes to light. Curr Biol *7*, R674-677.

Prickaerts, J., de Vente, J., Honig, W., Steinbusch, H.W., and Blokland, A. (2002). cGMP, but not cAMP, in rat hippocampus is involved in early stages of object memory consolidation. Eur J Pharmacol *436*, 83-87.

Puig, O., Caspary, F., Rigaut, G., Rutz, B., Bouveret, E., Bragado-Nilsson, E., Wilm, M., and Seraphin, B. (2001). The tandem affinity purification (TAP) method: a general procedure of protein complex purification. Methods *24*, 218-229.

Qin, N., and Baehr, W. (1994). Expression and mutagenesis of mouse rod photoreceptor cGMP phosphodiesterase. J Biol Chem *269*, 3265-3271.

Qin, N., Pittler, S.J., and Baehr, W. (1992). In vitro isoprenylation and membrane association of mouse rod photoreceptor cGMP phosphodiesterase alpha and beta subunits expressed in bacteria. J Biol Chem *267*, 8458-8463.

Qiu, Y.H., Chen, C.N., Malone, T., Richter, L., Beckendorf, S.K., and Davis, R.L. (1991). Characterization of the memory gene dunce of Drosophila melanogaster. J Mol Biol *222*, 553-565.

Quevillon, E., Silventoinen, V., Pillai, S., Harte, N., Mulder, N., Apweiler, R., and Lopez, R. (2005). InterProScan: protein domains identifier. Nucleic Acids Res *33*, W116-120.

Radford, J.C., Davies, S.A., and Dow, J.A. (2002). Systematic G-protein-coupled receptor analysis in Drosophila melanogaster identifies a leucokinin receptor with novel roles. J Biol Chem *277*, 38810-38817.

Rall, T.W., and Sutherland, E.W. (1958). Formation of a cyclic adenine ribonucleotide by tissue particles. J Biol Chem *232*, 1065-1076.

Rall, T.W., and Sutherland, E.W. (1962). Adenyl cyclase. II. The enzymatically catalyzed formation of adenosine 3',5'-phosphate and inorganic pyrophosphate from adenosine triphosphate. J Biol Chem *237*, 1228-1232.

Rall, T.W., Sutherland, E.W., and Wosilait, W.D. (1956). The relationship of epinephrine and glucagon to liver phosphorylase. III. Reactivation of liver phosphorylase in slices and in extracts. J Biol Chem *218*, 483-495.

Raymond, D.R., Carter, R.L., Ward, C.A., and Maurice, D.H. (2009). Distinct phosphodiesterase-4D variants integrate into protein kinase A-based signaling complexes in cardiac and vascular myocytes. Am J Physiol Heart Circ Physiol *296*, H263-271.

Raymond, D.R., Wilson, L.S., Carter, R.L., and Maurice, D.H. (2007). Numerous distinct PKA-, or EPAC-based, signalling complexes allow selective phosphodiesterase 3 and phosphodiesterase 4 coordination of cell adhesion. Cell Signal *19*, 2507-2518.

Regulski, M., Stasiv, Y., Tully, T., and Enikolopov, G. (2004). Essential function of nitric oxide synthase in Drosophila. Curr Biol *14*, R881-882.

Regulski, M., and Tully, T. (1995). Molecular and biochemical characterization of dNOS: a Drosophila Ca2+/calmodulin-dependent nitric oxide synthase. Proc Natl Acad Sci U S A *92*, 9072-9076.

Reimann, E.M., Walsh, D.A., and Krebs, E.G. (1971). Purification and properties of rabbit skeletal muscle adenosine 3',5'-monophosphate-dependent protein kinases. J Biol Chem *246*, 1986-1995.

Reineke, U., Sabat, R., Kramer, A., Stigler, R.D., Seifert, M., Michel, T., Volk, H.D., and Schneider-Mergener, J. (1996). Mapping protein-protein contact sites using cellulose-bound peptide scans. Mol Divers *1*, 141-148.

Resh, M.D. (1999). Fatty acylation of proteins: new insights into membrane targeting of myristoylated and palmitoylated proteins. Biochim Biophys Acta *1451*, 1-16.

Riegel, J.A., Maddrell, S.H., Farndale, R.W., and and Caldwell, F.M. (1998a). Stimulation of fluid secretion of malpighian tubules of Drosophila melanogaster Meig by cyclic nucleotides of inosine, cytidine, thymidine and uridine. J Exp Bio, 201: 3411-3418.

Riegel, J.A., Maddrell, S.H., Farndale, R.W., and Caldwell, F.M. (1998b). Stimulation of fluid secretion of malpighian tubules of drosophila melanogaster meig. by cyclic nucleotides of inosine, cytidine, thymidine and uridine. J Exp Biol *201 (Pt 24)*, 3411-3418.

Roegiers, F., and Jan, Y.N. (2004). Asymmetric cell division. Curr Opin Cell Biol *16*, 195-205.

Romorini, S., Piccoli, G., Jiang, M., Grossano, P., Tonna, N., Passafaro, M., Zhang, M., and Sala, C. (2004). A functional role of postsynaptic density-95-guanylate kinase-associated protein complex in regulating Shank assembly and stability to synapses. J Neurosci *24*, 9391-9404.

Ronnett, G.V., and Moon, C. (2002). G proteins and olfactory signal transduction. Annu Rev Physiol *64*, 189-222.

Rorth, P. (1996). A modular misexpression screen in Drosophila detecting tissue-specific phenotypes. Proc Natl Acad Sci U S A *93*, 12418-12422.

Rorth, P., Szabo, K., Bailey, A., Laverty, T., Rehm, J., Rubin, G.M., Weigmann, K., Milan, M., Benes, V., Ansorge, W., *et al.* (1998). Systematic gain-of-function genetics in Drosophila. Development *125*, 1049-1057.

Rosay, P., Davies, S.A., Yu, Y., Sozen, A., Kaiser, K., and Dow, J.A. (1997). Cell-type specific calcium signalling in a Drosophila epithelium. J Cell Sci *110 (Pt 15)*, 1683-1692.

Rosman, G., Martins, T., Sonnenburg, W., Beavo, J., Ferguson, K., and Loughney, K. (1997). Isolation and characterization of human cDNAs encoding a cGMP-stimulated 3',5'-cyclic nucleotide phosphodiesterase. Gene *191*, 89-95.

Rubin, G.M., and Spradling, A.C. (1983). Vectors for P element-mediated gene transfer in Drosophila. Nucleic Acids Res *11*, 6341-6351.

Russwurm, C., Zoidl, G., Koesling, D., and Russwurm, M. (2009). Dual acylation of PDE2A splice variant 3: targeting to synaptic membranes. J Biol Chem *284*, 25782-25790.

Russwurm, M., Mullershausen, F., Friebe, A., Jäger, R., Russwurm, C., and Koesling, D. (2007). Design of fluorescence resonance energy transfer (FRET)-based cGMP indicators: a systematic approach. Biochem J *407*, 69-77.

Rybalkin, S.D., Rybalkina, I.G., Feil, R., Hofmann, F., and Beavo, J.A. (2002). Regulation of cGMP-specific phosphodiesterase (PDE5) phosphorylation in smooth muscle cells. J Biol Chem *277*, 3310-3317.

Rybalkin, S.D., Rybalkina, I.G., Shimizu-Albergine, M., Tang, X.B., and Beavo, J.A. (2003). PDE5 is converted to an activated state upon cGMP binding to the GAF A domain. Embo J *22*, 469-478.

Rybin, V., Xu, X., Lisanti, M., and Steinberg, S. (2000). Differential targeting of beta-adrenergic receptor subtypes and adenylyl cyclase to cardiomyocyte caveolae. A mechanism to functionally regulate the cAMP signaling pathway. J Biol Chem, 275:41447– 41457.

Sager, G. (2004). Cyclic GMP transporters. Neurochem Int *45*, 865-873.

Sambrook, J., and Russell, D. (2001a). Molecular Cloning: A Laboratory Manual(Third Edition). In.

Sambrook, J., and Russell, D. (2001b). Molecular Cloning: A Laboratory Manual(Third Edition).

Sarkar, D., Erlichman, J., and Rubin, C.S. (1984). Identification of a calmodulin-binding protein that co-purifies with the regulatory subunit of brain protein kinase II. J Biol Chem *259*, 9840-9846.

Sato, M., Hida, N., Ozawa, T., and Umezawa, Y. (2000). Fluorescent indicators for cyclic GMP based on cyclic GMP-dependent protein kinase Ialpha and green fluorescent proteins. Anal Chem *72*, 5918-5924.

Scapin, G., Patel, S.B., Chung, C., Varnerin, J.P., Edmondson, S.D., Mastracchio, A., Parmee, E.R., Singh, S.B., Becker, J.W., Van der Ploeg, L.H., *et al.* (2004). Crystal structure of human phosphodiesterase 3B: atomic basis for substrate and inhibitor specificity. Biochemistry *43*, 6091-6100.

Schlossmann, J., Ammendola, A., Ashman, K., Zong, X., Huber, A., Neubauer, G., Wang, G.X., Allescher, H.D., Korth, M., Wilm, M., *et al.* (2000). Regulation of intracellular calcium by a signalling complex of IRAG, IP3 receptor and cGMP kinase Ibeta. Nature *404*, 197-201.

Schlossmann, J., and Desch, M. (2009). cGK substrates. Handb Exp Pharmacol, 163-193.

Schmidt, R.A., Glomset, J.A., Wight, T.N., Habenicht, A.J., and Ross, R. (1982). A study of the Influence of mevalonic acid and its metabolites on the morphology of swiss 3T3 cells. J Cell Biol *95*, 144-153.

Schmidt, R.A., Schneider, C.J., and Glomset, J.A. (1984). Evidence for post-translational incorporation of a product of mevalonic acid into Swiss 3T3 cell proteins. J Biol Chem *259*, 10175-10180.

Schulz, S., Green, C.K., Yuen, P.S., and Garbers, D.L. (1990). Guanylyl cyclase is a heat-stable enterotoxin receptor. Cell *63*, 941-948.

Schulz, S., Singh, S., Bellet, R.A., Singh, G., Tubb, D.J., Chin, H., and Garbers, D.L. (1989). The primary structure of a plasma membrane guanylate cyclase demonstrates diversity within this new receptor family. Cell *58*, 1155-1162.

Schwarz, U.R., Walter, U., and Eigenthaler, M. (2001). Taming platelets with cyclic nucleotides. Biochem Pharmacol *62*, 1153-1161.

Sebastian, S. (2009a). *Dm*PDE11Δ121 gives no significant change in cA-PDE activity when midgut is excised and assayed. cG-PDE assays reveal a large reduction in cG-PDE activity when head lysate is assayed.

Sebastian, S. (2009b). *Dm*PDE11Δ121 displays no significant change in cA-PDE activity in comparison with wild type controls when midgut is excised and assayed. cG-PDE assays of *Dm*PDE11Δ121 head lysate give a large reduction in activity compared to wild type controls

Seftel, A. (2005a). 3′,5′-Cyclic Nucleotide Phosphodiesterase 11A: Localization in Human Tissues. Journal of Urology, The, Volume 174, Issue 173, 1044.

Seftel, A.D. (2005b). Phosphodiesterase 11 (PDE11) regulation of spermatozoa physiology. J Urol *174*, 1043-1044.

Sekine, T., Watanabe, N., Hosoyamada, M., Kanai, Y., and Endou, H. (1997). Expression cloning and characterization of a novel multispecific organic anion transporter. J Biol Chem *272*, 18526-18529.

Sellak, H., Yang, X., Cao, X., Cornwell, T., Soff, G.A., and Lincoln, T. (2002). Sp1 transcription factor as a molecular target for nitric oxide-- and cyclic nucleotide--mediated suppression of cGMP-dependent protein kinase-Ialpha expression in vascular smooth muscle cells. Circ Res *90*, 405-412.

Sette, C., and Conti, M. (1996). Phosphorylation and activation of a cAMP-specific phosphodiesterase by the cAMP-dependent protein kinase. Involvement of serine 54 in the enzyme activation. J Biol Chem *271*, 16526-16534.

Shah, A.M., and MacCarthy, P.A. (2000). Paracrine and autocrine effects of nitric oxide on myocardial function. Pharmacol Ther *86*, 49-86.

Shah, S., and Hyde, D.R. (1995). Two Drosophila genes that encode the alpha and beta subunits of the brain soluble guanylyl cyclase. J Biol Chem *270*, 15368-15376.

Shakur, Y., Holst, L.S., Landstrom, T.R., Movsesian, M., Degerman, E., and Manganiello, V. (2001). Regulation and function of the cyclic nucleotide phosphodiesterase (PDE3) gene family. Prog Nucleic Acid Res Mol Biol *66*, 241-277.

Shevchuk, N.A., Bryksin, A.V., Nusinovich, Y.A., Cabello, F.C., Sutherland, M., and Ladisch, S. (2004). Construction of long DNA molecules using long PCR-based fusion of several fragments simultaneously. Nucleic Acids Res *32*, e19.

Siegfried, G., Vrtovsnik, F., Prié, D., Amiel, C., and Friedlander, G. (1995). Parathyroid hormone stimulates ecto-5'-nucleotidase activity in renal epithelial cells: role of protein kinase-C. Endocrinology, 136(133):1267-1275.

Silverman, N. (2003). Flies kNOw how to signal. Dev Cell *4*, 5-6.

Silverman, N., and Maniatis, T. (2001). NF-kappaB signaling pathways in mammalian and insect innate immunity. Genes Dev *15*, 2321-2342.

Skoulakis, E.M., Kalderon, D., and Davis, R.L. (1993). Preferential expression in mushroom bodies of the catalytic subunit of protein kinase A and its role in learning and memory. Neuron *11*, 197-208.

Soderling, S.H., Bayuga, S.J., and Beavo, J.A. (1998a). Cloning and characterization of a cAMP-specific cyclic nucleotide phosphodiesterase. Proc Natl Acad Sci U S A *95*, 8991-8996.

Soderling, S.H., Bayuga, S.J., and Beavo, J.A. (1998b). Identification and characterization of a novel family of cyclic nucleotide phosphodiesterases. J Biol Chem *273*, 15553-15558.

Sokolowski, M.B. (1980). Foraging strategies of Drosophila melanogaster: a chromosomal analysis. Behav Genet *10*, 291-302.

Sonnenburg, W.K., and Beavo, J.A. (1994). Cyclic GMP and regulation of cyclic nucleotide hydrolysis. Adv Pharmacol *26*, 87-114.

Sonnenburg, W.K., Seger, D., Kwak, K.S., Huang, J., Charbonneau, H., and Beavo, J.A. (1995). Identification of inhibitory and calmodulin-binding domains of the PDE1A1 and

PDE1A2 calmodulin-stimulated cyclic nucleotide phosphodiesterases. J Biol Chem *270*, 30989-31000.

Sorbera, L.A., and Morad, M. (1991). Modulation of cardiac sodium channels by cAMP receptors on the myocyte surface. Science *253*, 1286-1289.

Southall, T.D., Terhzaz, S., Cabrero, P., Chintapalli, V.R., Evans, J.M., Dow, J.A., and Davies, S.A. (2006). Novel subcellular locations and functions for secretory pathway Ca2+/Mn2+-ATPases. Physiol Genomics *26*, 35-45.

Sozen, M.A., Armstrong, J.D., Yang, M., Kaiser, K., and Dow, J.A. (1997). Functional domains are specified to single-cell resolution in a Drosophila epithelium. Proc Natl Acad Sci U S A *94*, 5207-5212.

Spradling, A.C., and Rubin, G.M. (1982). Transposition of cloned P elements into Drosophila germ line chromosomes. Science *218*, 341-347.

Stefan, E., Wiesner, B., Baillie, G.S., Mollajew, R., Henn, V., Lorenz, D., Furkert, J., Santamaria, K., Nedvetsky, P., Hundsrucker, C., *et al.* (2007). Compartmentalization of cAMP-dependent signaling by phosphodiesterase-4D is involved in the regulation of vasopressin-mediated water reabsorption in renal principal cells. J Am Soc Nephrol *18*, 199-212.

Stone, J.R., and Marletta, M.A. (1996). Spectral and kinetic studies on the activation of soluble guanylate cyclase by nitric oxide. Biochemistry *35*, 1093-1099.

Strauss, H.M., and Keller, S. (2008). Pharmacological interference with protein-protein interactions mediated by coiled-coil motifs. Handb Exp Pharmacol, 461-482.

Sutherland, E., and Rall, T. (1957a). The isolation and characterisation of a cyclic adenine ribonucleotide formed by tissue particles. The Journal of Biologocal Chemistry, 232 (232): 1077.

Sutherland, E.W., Jr., and Wosilait, W.D. (1955). Inactivation and activation of liver phosphorylase. Nature *175*, 169-170.

Sutherland, E.W., and Rall, T.W. (1957b). The properties of an adenine ribonucleotide produced with cellular particles, ATP, Mg++ and epinephrine or glucagon. J Am Chem Soc *79*, 3608.

Sutherland, E.W., and Rall, T.W. (1958). Fractionation and characterization of a cyclic adenine ribonucleotide formed by tissue particles. J Biol Chem *232*, 1077-1091.

Sutherland, E.W., Rall, T.W., and Menon, T. (1962). Adenyl cylase. I. Distribution, preparation, and properties. J Biol Chem *237*, 1220-1227.

Swinnen, J.V., Joseph, D.R., and Conti, M. (1989). Molecular cloning of rat homologues of the Drosophila melanogaster dunce cAMP phosphodiesterase: evidence for a family of genes. Proc Natl Acad Sci U S A *86*, 5325-5329.

Takimoto, E., Champion, H.C., Li, M., Belardi, D., Ren, S., Rodriguez, E.R., Bedja, D., Gabrielson, K.L., Wang, Y., and Kass, D.A. (2005). Chronic inhibition of cyclic GMP phosphodiesterase 5A prevents and reverses cardiac hypertrophy. Nat Med *11*, 214-222.

Takio, K., Smith, S.B., Krebs, E.G., Walsh, K.A., and Titani, K. (1984). Amino acid sequence of the regulatory subunit of bovine type II adenosine cyclic 3',5'-phosphate dependent protein kinase. Biochemistry *23*, 4200-4206.

Terhzaz, S., O'Connell, F.C., Pollock, V.P., Kean, L., Davies, S.A., Veenstra, J.A., and Dow, J.A. (1999). Isolation and characterization of a leucokinin-like peptide of Drosophila melanogaster. J Exp Biol *202 Pt 24*, 3667-3676.

Thomas, M.K., Francis, S.H., and Corbin, J.D. (1990). Substrate- and kinase-directed regulation of phosphorylation of a cGMP-binding phosphodiesterase by cGMP. J Biol Chem *265*, 14971-14978.

Thomason, P.A., Traynor, D., Cavet, G., Chang, W.T., Harwood, A.J., and Kay, R.R. (1998). An intersection of the cAMP/PKA and two-component signal transduction systems in Dictyostelium. Embo J *17*, 2838-2845.

Thomason, P.A., Traynor, D., Stock, J.B., and Kay, R.R. (1999). The RdeA-RegA system, a eukaryotic phospho-relay controlling cAMP breakdown. J Biol Chem *274*, 27379-27384.

Thompson, W.J., and Appleman, M.M. (1971). Multiple cyclic nucleotide phosphodiesterase activities from rat brain. Biochemistry *10*, 311-316.

Torrie, L.S., Radford, J.C., Southall, T.D., Kean, L., Dinsmore, A.J., Davies, S.A., and Dow, J.A. (2004). Resolution of the insect ouabain paradox. Proc Natl Acad Sci U S A.

Touhara, K. (2002). Odor discrimination by G protein-coupled olfactory receptors. Microsc Res Tech *58*, 135-141.

Tsruya, R., Schlesinger, A., Reich, A., Gabay, L., Sapir, A., and Shilo, B. (2002). Intracellular trafficking by Star regulates cleavage of the Drosophila EGF receptor ligand Spitz. Genes Dev *16*, 222-234.

Turko, I.V., Francis, S.H., and Corbin, J.D. (1998). Binding of cGMP to both allosteric sites of cGMP-binding cGMP-specific phosphodiesterase (PDE5) is required for its phosphorylation. Biochem J *329 (Pt 3)*, 505-510.

Tzou, P., Ohresser, S., Ferrandon, D., Capovilla, M., Reichhart, J.M., Lemaitre, B., Hoffmann, J.A., and Imler, J.L. (2000). Tissue-specific inducible expression of antimicrobial peptide genes in Drosophila surface epithelia. Immunity *13*, 737-748.

Uttamchandani, M., Chan, E.W., Chen, G.Y., and Yao, S.Q. (2003). Combinatorial peptide microarrays for the rapid determination of kinase specificity. Bioorg Med Chem Lett *13*, 2997-3000.

Vaandrager, A.B., Hogema, B.M., Edixhoven, M., van den Burg, C.M., Bot, A.G., Klatt, P., Ruth, P., Hofmann, F., Van Damme, J., Vandekerckhove, J., *et al.* (2003). Autophosphorylation of cGMP-dependent protein kinase type II. J Biol Chem *278*, 28651-28658.

Vaandrager, A.B., Smolenski, A., Tilly, B.C., Houtsmuller, A.B., Ehlert, E.M., Bot, A.G., Edixhoven, M., Boomaars, W.E., Lohmann, S.M., and de Jonge, H.R. (1998). Membrane targeting of cGMP-dependent protein kinase is required for cystic fibrosis transmembrane conductance regulator Cl- channel activation. Proc Natl Acad Sci U S A *95*, 1466-1471.

Valeyev, N.V., Heslop-Harrison, P., Postlethwaite, I., Gizatullina, A.N., Kotov, N.V., and Bates, D.G. (2009). Crosstalk between G-protein and Ca2+ pathways switches intracellular cAMP levels. Mol Biosyst *5*, 43-51.

Vani, K., Yang, G., and Mohler, J. (1997). Isolation and cloning of a Drosophila homolog to the mammalian RACK1 gene, implicated in PKC-mediated signalling. Biochim Biophys Acta *1358*, 67-71.

Verde, I., Pahlke, G., Salanova, M., Zhang, G., Wang, S., Coletti, D., Onuffer, J., Jin, S., and Conti, M. (2001). Myomegalin is a novel protein of the golgi/centrosome that interacts with a cyclic nucleotide phosphodiesterase. J Biol Chem *276*, 11189-11198.

Vermehren, A., Langlais, K., and Morton, D. (2006). Oxygen-sensitive guanylyl cyclases in insects and their potential roles in oxygen detection and in feeding behaviors. J Insect Physiol, 52(54):340-348.

Villalonga, P., Lopez-Alcala, C., Chiloeches, A., Gil, J., Marais, R., Bachs, O., and Agell, N. (2002). Calmodulin prevents activation of Ras by PKC in 3T3 fibroblasts. J Biol Chem *277*, 37929-37935.

Vo, N.K., Gettemy, J.M., and Coghlan, V.M. (1998). Identification of cGMP-dependent protein kinase anchoring proteins (GKAPs). Biochem Biophys Res Commun *246*, 831-835.

W, W., and JD., S. (2004). AKAP signalling complexes: focal points in space and time. Nat Rev Mol Cell Biol *5*, 959-970.

Walsh, D., Perkins, J., and Krebs, E. (1968a). An Adenosine 5',3'-monophosphate-dependent protein kinase from rat skeletal muscle. J Biol Chem, 243: 3763 - 3675.

Walsh, D.A., Ashby, C.D., Gonzalez, C., Calkins, D., and Fischer, E.H. (1971). Krebs EG: Purification and characterization of a protein inhibitor of adenosine 3',5'-monophosphate-dependent protein kinases. J Biol Chem *246*, 1977-1985.

Walsh, D.A., Perkins, J.P., and Krebs, E.G. (1968b). An adenosine 3',5'-monophosphate-dependant protein kinase from rabbit skeletal muscle. J Biol Chem *243*, 3763-3765.

Walter, M.F., and Kiger, J.A., Jr. (1984). The Dunce gene of Drosophila: roles of Ca2+ and calmodulin in adenosine 3':5'-cyclic monophosphate-specific phosphodiesterase activity. J Neurosci *4*, 495-501.

Wang, B., Goode, J., Best, J., Meltzer, J., Schilman, P.E., Chen, J., Garza, D., Thomas, J.B., and Montminy, M. (2008). The insulin-regulated CREB coactivator TORC promotes stress resistance in Drosophila. Cell Metab *7*, 434-444.

Wang, J., Kean, L., Yang, J., Allan, A.K., Davies, S.A., Herzyk, P., and Dow, J.A. (2004). Function-informed transcriptome analysis of Drosophila renal tubule. Genome Biol *5*, R69.

Wang, J., Lindholm, J.R., Willis, D.K., Orth, A., and Goodman, W.G. (2009). Juvenile hormone regulation of Drosophila Epac--a guanine nucleotide exchange factor. Mol Cell Endocrinol *305*, 30-37.

Wang, L., and Ligoxygakis, P. (2006). Pathogen recognition and signalling in the Drosophila innate immune response. Immunobiology *211*, 251-261.

Wang, P., Wu, P., Egan, R., and Billah, M. (2003a). Identification and characterization of a new human type 9 cGMP-specific phosphodiesterase splice variant (PDE9A5). Differential tissue distribution and subcellular localization of PDE9A variants. Gene *314*, 15-27.

Wang, P., Wu, P., Egan, R.W., and Billah, M.M. (2001). Human phosphodiesterase 8A splice variants: cloning, gene organization, and tissue distribution. Gene *280*, 183-194.

Wang, P., Wu, P., Egan, R.W., and Billah, M.M. (2003b). Identification and characterization of a new human type 9 cGMP-specific phosphodiesterase splice variant (PDE9A5). Differential tissue distribution and subcellular localization of PDE9A variants. Gene *314*, 15-27.

Wastila, W.B., Stull, J.T., Mayer, S.E., and Walsh, D.A. (1971). Measurement of cyclic 3',5'-denosine monophosphate by the activation of skeletal muscle protein kinase. J Biol Chem *246*, 1996-2003.

Wayman, C., Phillips, S., Lunny, C., Webb, T., Fawcett, L., Baxendale, R., and Burgess, G. (2005). Phosphodiesterase 11 (PDE11) regulation of spermatozoa physiology. Int J Impot Res *17*, 216-223.

Wechsler, J., Choi, Y.H., Krall, J., Ahmad, F., Manganiello, V.C., and Movsesian, M.A. (2002). Isoforms of cyclic nucleotide phosphodiesterase PDE3A in cardiac myocytes. J Biol Chem *277*, 38072-38078.

Weeks, J., Zoraghi, R., Francis, S., and Corbin, J. (2007). N-Terminal Domain of Phosphodiesterase-11A4 (PDE11A4) Decreases Affinity of the Catalytic Site for Substrates and Tadalafil, and is Involved in Oligomerization. Biochemistry, 46, 10353-10364.

Wen, J.F., Cui, X., Jin, J.Y., Kim, S.M., Kim, S.Z., Kim, S.H., Lee, H.S., and Cho, K.W. (2004). Distinct roles for particulate GC- and soluble GC-cGMP-PDE3 signaling in rabbit atria. Circ Res *94*, 936-943.

Wessing , A., and Eichelberg, D. (1978). Malpighian tubules, rectal papillae and excretion. In The genetics and biology of Drosophila, M. Ashburner, and T.R.F. Wright, eds. (London and New York, Academic Press), pp. 1-42.

White-Cooper, H. (2009). Studying how flies make sperm--investigating gene function in Drosophila testes. Mol Cell Endocrinol *306*, 66-74.

Wicher, D., Schafer, R., Bauernfeind, R., Stensmyr, M.C., Heller, R., Heinemann, S.H., and Hansson, B.S. (2008). Drosophila odorant receptors are both ligand-gated and cyclic-nucleotide-activated cation channels. Nature *452*, 1007-1011.

Wieczorek, H. (1992). The insect V-ATPase, a plasma membrane proton pump energizing secondary active transport: molecular analysis of electrogenic potassium transport in the tobacco hornworm midgut. J Exp Biol *172*, 335-343.

Wieczorek, H., Putzenlechner, M., Zeiske, W., and Klein, U. (1991). A vacuolar-type proton pump energizes K+/H+ antiport in an animal plasma membrane. J Biol Chem *266*, 15340-15347.

Wildemann, B., and Bicker, G. (1999a). Developmental expression of nitric oxide/cyclic GMP synthesizing cells in the nervous system of Drosophila melanogaster. J Neurobiol *38*, 1-15.

Wildemann, B., and Bicker, G. (1999b). Nitric oxide and cyclic GMP induce vesicle release at Drosophila neuromuscular junction. J Neurobiol *39*, 337-346.

Willoughby, D., and Cooper, D.M. (2007). Organization and Ca2+ regulation of adenylyl cyclases in cAMP microdomains. Physiol Rev *87*, 965-1010.

Willumsen, B.M., Christensen, A., Hubbert, N.L., Papageorge, A.G., and Lowy, D.R. (1984). The p21 ras C-terminus is required for transformation and membrane association. Nature *310*, 583-586.

Wilson, L., Elbatarny, H., Crawley, S., Bennett, B., and Maurice, D. (2008a). Compartmentation and compartment-specific regulation of PDE5 by protein kinase G allows selective cGMP-mediated regulation of platelet functions. Proc Natl Acad Sci U S A *105*, 13650-13655.

Wilson, L.S., Elbatarny, H.S., Crawley, S.W., Bennett, B.M., and Maurice, D.H. (2008b). Compartmentation and compartment-specific regulation of PDE5 by protein kinase G allows selective cGMP-mediated regulation of platelet functions. Proc Natl Acad Sci U S A *105*, 13650-13655.

Witczak, O., Orstavik, S., Natarajan, V., Frengen, E., Jahnsen, T., and Sandberg, M. (1998). Characterization of the gene encoding the human type II cGMP-dependent protein kinase. Biochem Biophys Res Commun *245*, 113-119.

Wong, M., Whelan, F., Deloukas, P, Whittaker, P., Delgado, M., Cantor, R., McCann, S., and Licinio, J. (2006). Phosphodiesterase genes are associated with susceptibility to major depression and antidepressant treatment response. PNAS, vol. 103 no. 141 15124-15129.

Wong, W., and Scott, J.D. (2004). AKAP signalling complexes: focal points in space and time. Nat Rev Mol Cell Biol *5*, 959-970.

Wosilait, W., and Sutherland, E. (1957). The relationship of epinephrine and glucagon to liver phosphorylase. II. Enzymatic inactivation of liver phosphorylase. J Biol Chem, 218: 469 - 481.

Wyatt, T.A., Naftilan, A.J., Francis, S.H., and Corbin, J.D. (1998). ANF elicits phosphorylation of the cGMP phosphodiesterase in vascular smooth muscle cells. Am J Physiol *274*, H448-455.

Xu, R.X., Hassell, A.M., Vanderwall, D., Lambert, M.H., Holmes, W.D., Luther, M.A., Rocque, W.J., Milburn, M.V., Zhao, Y., Ke, H., *et al.* (2000). Atomic structure of PDE4: insights into phosphodiesterase mechanism and specificity. Science *288*, 1822-1825.

Xu, R.X., Rocque, W.J., Lambert, M.H., Vanderwall, D.E., Luther, M.A., and Nolte, R.T. (2004). Crystal structures of the catalytic domain of phosphodiesterase 4B complexed with AMP, 8-Br-AMP, and rolipram. J Mol Biol *337*, 355-365.

Yamazaki, D., Horiuchi, J., Nakagami, Y., Nagano, S., Tamura, T., and Saitoe, M. (2007). The Drosophila DCO mutation suppresses age-related memory impairment without affecting lifespan. Nat Neurosci *10*, 478-484.

Yan, C., Zhao, A.Z., Bentley, J.K., and Beavo, J.A. (1996). The calmodulin-dependent phosphodiesterase gene PDE1C encodes several functionally different splice variants in a tissue-specific manner. J Biol Chem *271*, 25699-25706.

Yan, C., Zhao, A.Z., Bentley, J.K., Loughney, K., Ferguson, K., and Beavo, J.A. (1995). Molecular cloning and characterization of a calmodulin-dependent phosphodiesterase enriched in olfactory sensory neurons. Proc Natl Acad Sci U S A *92*, 9677-9681.

Yuasa, K., Kotera, J., Fujishige, K., Michibata, H., Sasaki, T., and Omori, K. (2000a). Isolation and characterization of two novel phosphodiesterase PDE11A variants showing unique structure and tissue-specific expression. J Biol Chem *275*, 31469-31479.

Yuasa, K., Kotera, J., Fujishige, K., Michibata, H., Sasaki, T., and Omori, K. (2000b). Isolation and Characterization of Two Novel Phosphodiesterase PDE11A Variants Showing Unique Structure and Tissue-specific Expression. THE JOURNAL OF BIOLOGICAL CHEMISTRY, Vol. 275, No. 240, 31469–31479.

Yuasa, K., Ohgaru, T., Asahina, M., and Omori, K. (2001). Identification of rat cyclic nucleotide phosphodiesterase 11A (PDE11A): comparison of rat and human PDE11A splicing variants. Eur J Biochem *268*, 4440-4448.

Yuasa, K., Omori, K., and Yanaka, N. (2000c). Binding and phosphorylation of a novel male germ cell-specific cGMP-dependent protein kinase-anchoring protein by cGMP-dependent protein kinase Ialpha. J Biol Chem *275*, 4897-4905.

Zabel, U., Kleinschnitz, C., Oh, P., Nedvetsky, P., Smolenski, A., Muller, H., Kronich, P., Kugler, P., Walter, U., Schnitzer, J.E., *et al.* (2002). Calcium-dependent membrane association sensitizes soluble guanylyl cyclase to nitric oxide. Nat Cell Biol *4*, 307-311.

Zaccolo, M. (2006). Phosphodiesterases and compartmentalized cAMP signalling in the heart. Eur J Cell Biol *85*, 693-697.

Zaccolo, M., and Movsesian, M. (2007a). Role of Phosphodiesterases and Implications for Cardiac Pathophysiology. Circulation Research, 100; 1569-1578.

Zaccolo, M., and Movsesian, M.A. (2007b). cAMP and cGMP signaling cross-talk: role of phosphodiesterases and implications for cardiac pathophysiology. Circ Res *100*, 1569-1578.

Zaccolo, M., and Pozzan, T. (2002). Discrete microdomains with high concentration of cAMP in stimulated rat neonatal cardiac myocytes. Science *295*, 1711-1715.

Zdobnov, E.M., and Apweiler, R. (2001). InterProScan--an integration platform for the signature-recognition methods in InterPro. Bioinformatics *17*, 847-848.

Zhang, H., Liu, X.H., Zhang, K., Chen, C.K., Frederick, J.M., Prestwich, G.D., and Baehr, W. (2004a). Photoreceptor cGMP phosphodiesterase delta subunit (PDEdelta) functions as a prenyl-binding protein. J Biol Chem *279*, 407-413.

Zhang, J., Kuvelkar, R., Wu, P., Egan, R.W., Billah, M.M., and Wang, P. (2004b). Differential inhibitor sensitivity between human recombinant and native photoreceptor cGMP-phosphodiesterases (PDE6s). Biochem Pharmacol *68*, 867-873.

Zhang, K.Y., Card, G.L., Suzuki, Y., Artis, D.R., Fong, D., Gillette, S., Hsieh, D., Neiman, J., West, B.L., Zhang, C., *et al.* (2004c). A glutamine switch mechanism for nucleotide selectivity by phosphodiesterases. Mol Cell *15*, 279-286.

Zhang, K.Y., Card, G.L., Suzuki, Y., Artis, D.R., Fong, D., Gillette, S., Hsieh, D., Neiman, J., West, B.L., Zhang, C., *et al.* (2004d). cA Glutamine Switch Mechanism for Nucleotide Selectivity by Phosphodiesterases. Mol Cell *15*, 279-286.

Zhong, Y., Budnik, V., and Wu, C.F. (1992). Synaptic plasticity in Drosophila memory and hyperexcitable mutants: role of cAMP cascade. J Neurosci *12*, 644-651.

Zhong, Y., and Wu, C.F. (1991). Altered synaptic plasticity in Drosophila memory mutants with a defective cyclic AMP cascade. Science *251*, 198-201.

Zimmerman, A.L., Yamanaka, G., Eckstein, F., Baylor, D.A., and Stryer, L. (1985). Interaction of hydrolysis-resistant analogs of cyclic GMP with the phosphodiesterase and light-sensitive channel of retinal rod outer segments. Proc Natl Acad Sci U S A *82*, 8813-8817.

Zoraghi, R., Bessay, E.P., Corbin, J.D., and Francis, S.H. (2005). Structural and functional features in human PDE5A1 regulatory domain that provide for allosteric cGMP binding, dimerization, and regulation. J Biol Chem *280*, 12051-12063.

Zoraghi, R., Corbin, J.D., and Francis, S.H. (2004). Properties and functions of GAF domains in cyclic nucleotide phosphodiesterases and other proteins. Mol Pharmacol *65*, 267-278.